Alaska Department of Transportation & Public Facilities

Alaska University Transportation Center

# Study to Compare the Performance of Two Designs to Prevent River Bend Erosion in Arctic Environments


**Prepared By:**
Horacio Toniolo
Paul Duvoy


September 2010

**Prepared For :**


**Alaska University Transportation Center**
**Duckering Building Room 245**
**P.O. Box 755900**
**Fairbanks, AK 99775-5900**

**Alaska Department of Transportation**
**Research, Development, and Technology Transfer**
**2301 Peger Road**
**Fairbanks, AK 99709-5399**



**INE/ AUTC# 10.02**

**DOT # FHWA-AK-RD-12-11**

# REPORT DOCUMENTATION PAGE

Form approved OMB No.



| 1. AGENCY USE ONLY (LEAVE BLANK) | 2. REPORT DATE | 3. REPORT TYPE AND DATES COVERED |
|---|---|---|
| FHWA-AK-RD-12-11 | September 2010 | Final Report (07/01/09-09/30/10) |

**4. TITLE AND SUBTITLE**
Study to Compare the Performance of Two Designs to Prevent River Bend Erosion in Arctic Environments

**5. FUNDING NUMBERS**
AUTC #309009
DTRT06-G-0011
T2-09-07

**6. AUTHOR(S)**
Horacio Toniolo
Paul Duvoy

**7. PERFORMING ORGANIZATION NAME(S) AND ADDRESS(ES)**
Alaska University Transportation Center
P.O. Box 755900
Fairbanks, AK 99775-5900

**8. PERFORMING ORGANIZATION REPORT NUMBER**
INE/AUTC 10.02

**9. SPONSORING/MONITORING AGENCY NAME(S) AND ADDRESS(ES)**
Alaska Department of Transportation
Research, Development, and Technology Transfer
2301 Peger Road
Fairbanks, AK 99709-5399

**10. SPONSORING/MONITORING AGENCY REPORT NUMBER**
FHWA-AK-RD-12-11

**11. SUPPLENMENTARY NOTES**
This project was also conducted with the support of WERC, the Water and Environmental Research Center, College of Engineering and Mines, at University of Alaska Fairbanks.

**12a. DISTRIBUTION / AVAILABILITY STATEMENT**
No restrictions

**12b. DISTRIBUTION CODE**

**13. ABSTRACT (Maximum 200 words)**

Messing with Mother Nature takes knowledge and work, and she is hard to outfox, especially when it comes to redirecting rivers. To protect infrastructure, however, sometimes river flow must be altered. This study focuses on two erosion-control projects built in Alaska using different design criteria. One was constructed by ADOT&PF at the Sagavanirktok River to protect the Dalton Highway; the other was built by Alyeska Pipeline Service Company at Hess Creek to protect the trans-Alaska pipeline. Though bank erosion along river bends is a natural process, lateral erosion, which causes streams to shift laterally, can expose infrastructure to serious risk. To avoid damaging or destroying the transportation system, researchers and engineers have developed several types of strategies to prevent streambank erosion, including watercourse realignment, that is, moving water away from the bank. Project researchers gathered hydraulic data, including continuous velocity measurements, at selected points in both streams. The project took an unexpected turn when the research team decided to include a hydraulic numerical model. This model is capable of simulating different flow conditions, calculates shear stress, velocity and Froude number, among other hydraulic parameters. Different scenarios were simulated by the model, showing how the river might behave under different flow conditions at different seasons .

14- KEYWORDS: Erosion control, Protection against environmental damage, Scour, Erosion, Materials and structures protection

**15. NUMBER OF PAGES**
201

**16. PRICE CODE**
N/A

| 17. SECURITY CLASSIFICATION OF REPORT | 18. SECURITY CLASSIFICATION OF THIS PAGE | 19. SECURITY CLASSIFICATION OF ABSTRACT | 20. LIMITATION OF ABSTRACT |
|---|---|---|---|
| Unclassified | Unclassified | Unclassified | N/A |

**Notice**

This document is disseminated under the sponsorship of the U.S. Department of Transportation in the interest of information exchange. The U.S. Government assumes no liability for the use of the information contained in this document.

The U.S. Government does not endorse products or manufacturers. Trademarks or manufacturers' names appear in this report only because they are considered essential to the objective of the document.

**Quality Assurance Statement**

The Federal Highway Administration (FHWA) provides high-quality information to serve Government, industry, and the public in a manner that promotes public understanding. Standards and policies are used to ensure and maximize the quality, objectivity, utility, and integrity of its information. FHWA periodically reviews quality issues and adjusts its programs and processes to ensure continuous quality improvement.

**Author's Disclaimer**

Opinions and conclusions expressed or implied in the report are those of the author. They are not necessarily those of the Alaska DOT&PF or funding agencies.

# SI* (MODERN METRIC) CONVERSION FACTORS

## APPROXIMATE CONVERSIONS TO SI UNITS

| Symbol | When You Know | Multiply By | To Find | Symbol |
|---|---|---|---|---|
| | | **LENGTH** | | |
| in | inches | 25.4 | millimeters | mm |
| ft | feet | 0.305 | meters | m |
| yd | yards | 0.914 | meters | m |
| mi | miles | 1.61 | kilometers | km |
| | | **AREA** | | |
| $in^2$ | square inches | 645.2 | square millimeters | $mm^2$ |
| $ft^2$ | square feet | 0.093 | square meters | $m^2$ |
| $yd^2$ | square yard | 0.836 | square meters | $m^2$ |
| ac | acres | 0.405 | hectares | ha |
| $mi^2$ | square miles | 2.59 | square kilometers | $km^2$ |
| | | **VOLUME** | | |
| fl oz | fluid ounces | 29.57 | milliliters | mL |
| gal | gallons | 3.785 | liters | L |
| $ft^3$ | cubic feet | 0.028 | cubic meters | $m^3$ |
| $yd^3$ | cubic yards | 0.765 | cubic meters | $m^3$ |
| | NOTE: volumes greater than 1000 L shall be shown in $m^3$ | | | |
| | | **MASS** | | |
| oz | ounces | 28.35 | grams | g |
| lb | pounds | 0.454 | kilograms | kg |
| T | short tons (2000 lb) | 0.907 | megagrams (or "metric ton") | Mg (or "t") |
| | | **TEMPERATURE (exact degrees)** | | |
| $^oF$ | Fahrenheit | 5 (F-32)/9<br>or (F-32)/1.8 | Celsius | $^oC$ |
| | | **ILLUMINATION** | | |
| fc | foot-candles | 10.76 | lux | lx |
| fl | foot-Lamberts | 3.426 | $candela/m^2$ | $cd/m^2$ |
| | | **FORCE and PRESSURE or STRESS** | | |
| lbf | poundforce | 4.45 | newtons | N |
| $lbf/in^2$ | poundforce per square inch | 6.89 | kilopascals | kPa |

## APPROXIMATE CONVERSIONS FROM SI UNITS

| Symbol | When You Know | Multiply By | To Find | Symbol |
|---|---|---|---|---|
| | | **LENGTH** | | |
| mm | millimeters | 0.039 | inches | in |
| m | meters | 3.28 | feet | ft |
| m | meters | 1.09 | yards | yd |
| km | kilometers | 0.621 | miles | mi |
| | | **AREA** | | |
| $mm^2$ | square millimeters | 0.0016 | square inches | $in^2$ |
| $m^2$ | square meters | 10.764 | square feet | $ft^2$ |
| $m^2$ | square meters | 1.195 | square yards | $yd^2$ |
| ha | hectares | 2.47 | acres | ac |
| $km^2$ | square kilometers | 0.386 | square miles | $mi^2$ |
| | | **VOLUME** | | |
| mL | milliliters | 0.034 | fluid ounces | fl oz |
| L | liters | 0.264 | gallons | gal |
| $m^3$ | cubic meters | 35.314 | cubic feet | $ft^3$ |
| $m^3$ | cubic meters | 1.307 | cubic yards | $yd^3$ |
| | | **MASS** | | |
| g | grams | 0.035 | ounces | oz |
| kg | kilograms | 2.202 | pounds | lb |
| Mg (or "t") | megagrams (or "metric ton") | 1.103 | short tons (2000 lb) | T |
| | | **TEMPERATURE (exact degrees)** | | |
| $^oC$ | Celsius | 1.8C+32 | Fahrenheit | $^oF$ |
| | | **ILLUMINATION** | | |
| lx | lux | 0.0929 | foot-candles | fc |
| $cd/m^2$ | $candela/m^2$ | 0.2919 | foot-Lamberts | fl |
| | | **FORCE and PRESSURE or STRESS** | | |
| N | newtons | 0.225 | poundforce | lbf |
| kPa | kilopascals | 0.145 | poundforce per square inch | $lbf/in^2$ |

*SI is the symbol for the International System of Units. Appropriate rounding should be made to comply with Section 4 of ASTM E380.
(Revised March 2003)

**Table of Contents**

## Acknowledgments

This project was funded by grants from Alaska Department of Transportation and Public Facilities (AKDOT&PF), Alaska University Transportation Center (AUTC), and Alyeska Pipeline Service Company (Alyeska). Data collected on other research projects and by other governmental agencies are included or used in this report for comparison/analyses purposes.

## Summary

This research focuses on the evaluation of the performance of two different designs to prevent river bend erosion in arctic environments. The river training structures considered are barbs and vanes, which are oriented upstream and downstream respectively. The study sites were located on the Sagavanirktok River near Deadhorse and Hess Creek near the pipeline crossing. Field work, numerical modeling and analysis were performed. As a result of these tasks, it was found that both structures displaced the thalweg from the river bank. Numerical results indicate that first and second barbs are critical for the entire river reach. Significant scour was detected at the tip of these barbs, which in turn could be beneficial for fish.

**Keywords**: river training structures, barbs, vanes, numerical modeling, channel bends, turbulence.

# 1. Introduction

This report presents an evaluation of the performance of two different river training structures to prevent river bend erosion in arctic environments. These structures are located on the Sagavanirktok (referred to as Sag) River on the Dalton Highway (also known as the Haul Road) at Milepost 414 and on Hess Creek. The conceptual design of these river training configurations is diametrically opposed. Structures are facing upstream in the Sag River and downstream in Hess Creek.

For this study, both fieldwork and a numerical model were employed. Fieldwork consisted of velocity measurements and bathymetric surveys with an Acoustic Doppler Current Profiler (ADCP) and a Global Positioning System (GPS) device with real-time kinematic (RTK) correction. In addition, breakup on the Sag River was monitored. Numerical work consisted of simulation of different flow and bathymetric configurations during the open-channel season. Results from a physical model built at laboratory scale were used to validate the numerical model.

Additional simulations were performed on the Sag River. These simulations analyzed several theoretical scenarios with different structure settings. The objective of this work was to assess the river reach response in terms of flow velocity, Froude number, and specific discharge to changes in the number of barbs and the corresponding modifications in terms of shear stress on the existing barbs.

# 2. Sites Description

## 2.1 Sag River at Dalton MP 414

The Dalton 414 Erosion Control Project was constructed in 2006 to prevent further displacement of the Sagavanirktok River near the Haul Road at Deadhorse. Eight bendaway weirs (stream barbs) oriented upstream were installed along the reach (Figure 1). Barbs were oriented at 70 degrees from the riverbank. The separation between barbs was two times the barb's length.


Figure 1 – Aerial View of Sag River near Deadhorse

## 2.2 Hess Creek

Hess Creek (Figure 2) is located 85 miles north of Fairbanks and 32 miles south of the Yukon River. The trans-Alaska pipeline crosses Hess Creek on a 180 ft steel plate girder bridge. Erosion altered the stream pattern, creating a meander bend upstream of the bridge. To prevent additional erosion along the riverbank, a new floodplain was established in 2005 and ten riprap directional flow vanes were installed along the 800 ft meander bend. The vanes manipulate flow direction, forcing the stream into a shallower curvature prior to its entering the pipeline bridge opening (Lai and Gaboury, 2008). Vanes are oriented downstream.

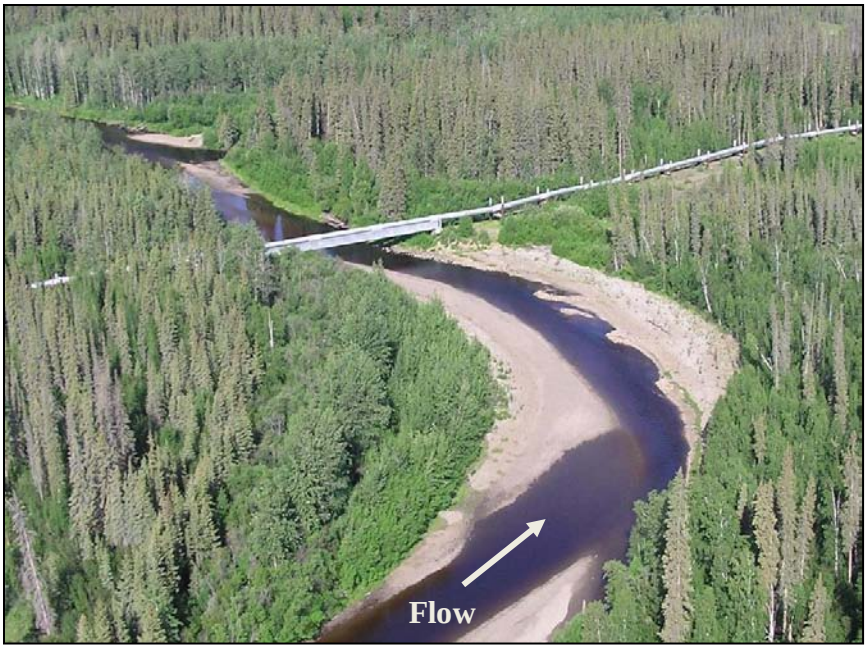


Figure 2 – Aerial View of Hess Creek

### 2.3 Differences and Similarities between River Training Structures

Although stream barbs are similar to submerged vanes, the most distinct feature of barbs is their trapezoidal shape with inclined sides and wide-sloped crest; hence, the barb acts as a partially submerged structure in low flow conditions and as a fully submerged structure in bankfull conditions. The submerged section of the upstream-pointed barb forces the water to flow over it into a hydraulic jump, promoting the formation of eddies and sediment deposition on the lee side of the barb. Other significant features of stream barbs are their riprap structure composition and fixed angle with respect to the bank (Kjos, 2003). All the barbs are designed to change the flow direction markedly. This generates an abrupt flow separation at the tip of the barb, which in turn causes important scour holes near the tip of the barb. These holes could be beneficial for fish during winter months in cold environments. However, the scour holes could pose stability issues on the tip.

Submerged vanes, which are pointed downstream, are constructed along an eroding bank to direct flow away from the bank to the center of the channel. Sediment is deposited at the base of the eroding bank and the bank can be revegetated (Water and Rivers Commission, 2001). Vanes are designed to align the riverward tip of the upstream vane to the base of the next consecutive vane downstream to avoid direct exposure to critical lines of attack (conceptual lines of maximum stream velocity) to the eroding bank during floods (Lai and Gaboury, 2008). This design does not significantly change the flow direction. As a consequence, flow separation and scour on the tip are reduced in this configuration.

The objective of these structures is to move the main current away from the riverbank. It should be pointed out that extensive research has been conducted on river training structures. A detailed work was recently presented by Odgaard (2009).

# 3. Fieldwork

## 3.1 Fall 2009 Survey

Bathymetric surveys were carried out by Alyeska personnel on the Sag River and Hess Creek. Work was conducted on the Sag River in early August and on Hess Creek in mid-September. An airboat and a tethered boat were used in the Sag and in Hess Creek, respectively. In both streams, an Acoustic Doppler Current Profiler (ADCP) Rio Grande 1200 KHz and a GPS with continuous real-time kinematic correction were used. In addition to the survey, velocity measurements at selected points were performed to describe main turbulence characteristics in both streams. Flow condition in both streams was defined as "clear water" at the time of fieldwork; thus, no sediment samples were taken.

Surveys were used in the numerical model, which is described later in the text as input for the condition named "2009." The maps are shown in Section 5.

## 3.2 Spring 2010 Breakup Monitoring

### 3.2.1 Physical Breakup Process

Before the beginning or during the early stages of breakup, after the initial snowmelt period and initiation of ice decay, further snowmelt at low elevations in the basin cause runoff to flow onto the ice. Continued increasing flow in the channel generates greater pressure underneath the ice.

Additional pressure on the undersurface of the ice due to increasing flow, as well as weakening of the ice near the edges, causes the ice that is frozen to the banks to break free or the ice sheet to break away from the bank ice. The ice sheet floats on the rising water. Since water levels during the fall freeze-up period are usually low, rising water levels in the spring result in a wider channel with a relatively narrow strip of main-channel ice floating above the deeper portion of the channel. Subsequent undermining of the ice and the sustained force of the river current on the sheet will eventually cause the ice sheet to fracture along the banks, float on the rising water, and shift in the open water, originating the first movement of ice.

The size of moving ice sheets is reduced mainly by physical impact, even though ice continues to melt as it moves downstream. Ice sheets break into smaller ice pans that impact each other as they flow downstream, reducing their size to chunks (http://aprfc.arh.noaa.gov/resources/docs/brkup.html). Thus, it is important for river engineers to predict ice loads on river structures (Tuthill, 2008).

### 3.2.2 Breakup Monitoring

Breakup in Alaskan streams is a phenomenon that is very difficult to predict. The specific breakup day responds to a combination of multiple factors, which include but are not limited to air temperature, cumulative freezing degree-days, snow accumulation in the watershed, wind, and solar radiation. It was proposed that breakup would be monitored in both streams; however, Hess Creek had an unusually early breakup this year (Lai, personal communication) and monitoring was not done. The purpose of this monitoring was to document through observations main flow configuration (i.e., water flow over barbs, ice displacement downstream).

Project team members Paul Duvoy and Peter Prokein monitored the Spring 2010 breakup on the Sag River from May 16 to June 8. The field crew used four specialty time-lapse cameras (Plantcam, http://www.wingscapes.com/productdetail.aspx?id=WSCA04), which were set to take a picture every minute (Figure 3 and Table 1). For each camera, a time-lapse movie was then built with the collected pictures using VirtualDub, an open source video-processing application (http://www.virtualdub.org). Comparison of the four movies shows that the flow is diverted downstream from the left bank; for example, the first barb cannot be seen, while the eighth barb is clearly visible. Videos can be located at http://ine.uaf.edu/autc


**Figure 3 – Location of Each Camera at Sag River. Image © 2010 Google**

Table 1 – Geographical Coordinates of each Camera Location

| Camera | Latitude (° N) | Longitude (° W) |
|---|---|---|
| SAG1 | 70.19402 | 148.42737 |
| SAG2 | 70.19589 | 148.42029 |
| SAG3 | 70.19654 | 148.41487 |
| SAG4 | 70.19656 | 148.41101 |

The breakup event was recorded on the videos during the morning of May 25. Table 2 shows a partial list of previous breakup dates for the Sag River at Deadhorse/Prudhoe Bay (River Forecast Center, Alaska – Pacific, National Weather Service, http://aprfc.arh.noaa.gov/php/brkup/getbrkup.php?riverbasin=Arctic&river=Sagavanirktok+River).

From October 1, 2009, to May 31, 2010, the Accumulated Freezing Degree Day index (AFFD) for Deadhorse Airport reached a value of 7615 °F-days (National Climatic Data Center, http://lwf.ncdc.noaa.gov/oa/ncdc.html). Using the proposed formula by the Cold Regions Research and Engineering Laboratory (White, 2004) for estimating ice thickness of an average river, with snow, yields an approximate maximum ice thickness of 10.5 to 13.1 in. (26.7 to 33.3 cm), with the coefficient ranging from 0.12 to 0.15.

Table 2 – Recorded Breakup Date for Sag River at Deadhorse/Prudhoe Bay

| RIVER | BREAKUP DATE | BREAKUP YEAR |
|---|---|---|
| Sagavanirktok River | 05-29 | 1983 |
| Sagavanirktok River | 05-23 | 1984 |
| Sagavanirktok River | 05-28 | 1989 |
| Sagavanirktok River | 05-04 | 1995 |
| Sagavanirktok River | 05-25 | 1996 |

Table 3 lists the series of events registered during the Sag River breakup monitoring. Figures 4 and 5 show a downstream and upstream panoramic view, respectively, from barb #5 on May 16. Figure 6 to 13 show for each barb the evolution from ice cover to open-channel conditions through four composite pictures taken on May 17, 23, 25 (breakup), and 29, respectively.

Figure 6 indicates high water levels in the proximity of barb 1, which is totally submerged. Thus, the barb's performance was similar to a submerged dam during the breakup. Figure 13 shows that part of barb 8 was visible during breakup. Thus, the main flow was diverted from the bank (out of the barbs); consequently, water level dropped

**Table 3 – List of Recorded Events during the Sag River Monitoring**

| Date | Description |
|---|---|
| May 15th and 16th | Overcast sky. Some openings in the channel. |
| 17th | Windier, blowing snow, some ice forming in the channel openings (similar to frazil ice). |
| 18th and 19th | Overall ice cover is visually getting thinner. |
| 20th | Some direct sunlight before midnight. |
| 21st | Snow melting at the left bank. Temperatures close to 0°C. Less windy than previous days. Some direct sunlight. |
| 22nd | More snow melting. Windy. Openings are increasing in size. At 5 P.M. there is a wide opening with small chunks of ice flowing. Slight increase in water level height. |
| 23rd | Windy. Ice cover reduced, especially close to the last and middle barbs. |
| 24th | Ice cover opening bigger and wider. |
| 25th | Breakup during the morning. Ice chunks coming upstream at intervals. Maximum water level height around 1 P.M., slight decrease around 3 P.M. |
| 26th to 28th | Some slush flowing. |
| 31st | Decreasing water level height. |

**Figure 4 – Downstream Panoramic View from Barb #5, May 16, 2010**

**Figure 5 - Upstream Panoramic View from Barb #5, May 16, 2010**


Figure 6 – View from Barb #1 for May 17, 23, 25 (Breakup), and 29, 2010

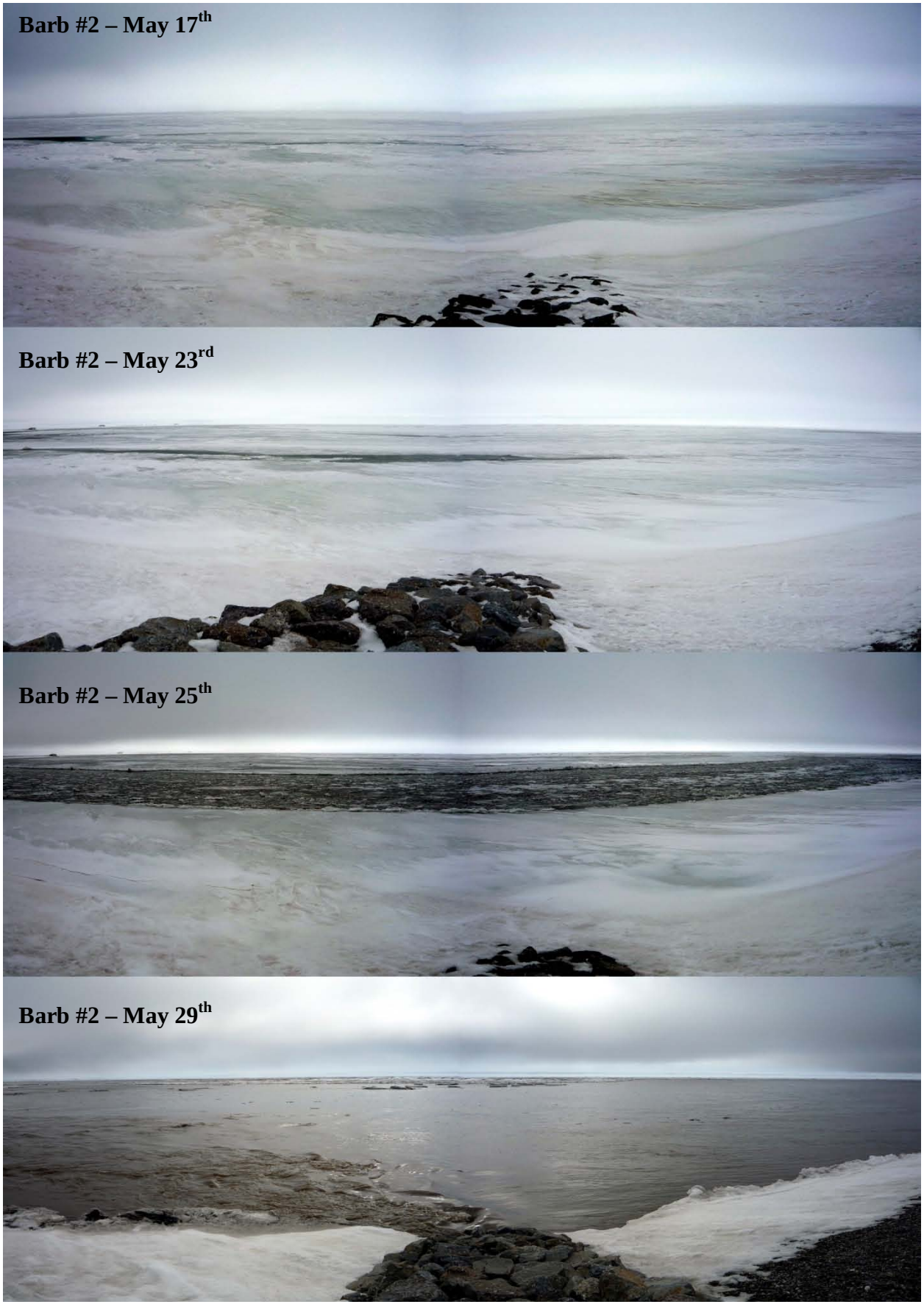


Figure 7 – View from Barb #2 for May 17, 23, 25 (Breakup), and 29, 2010

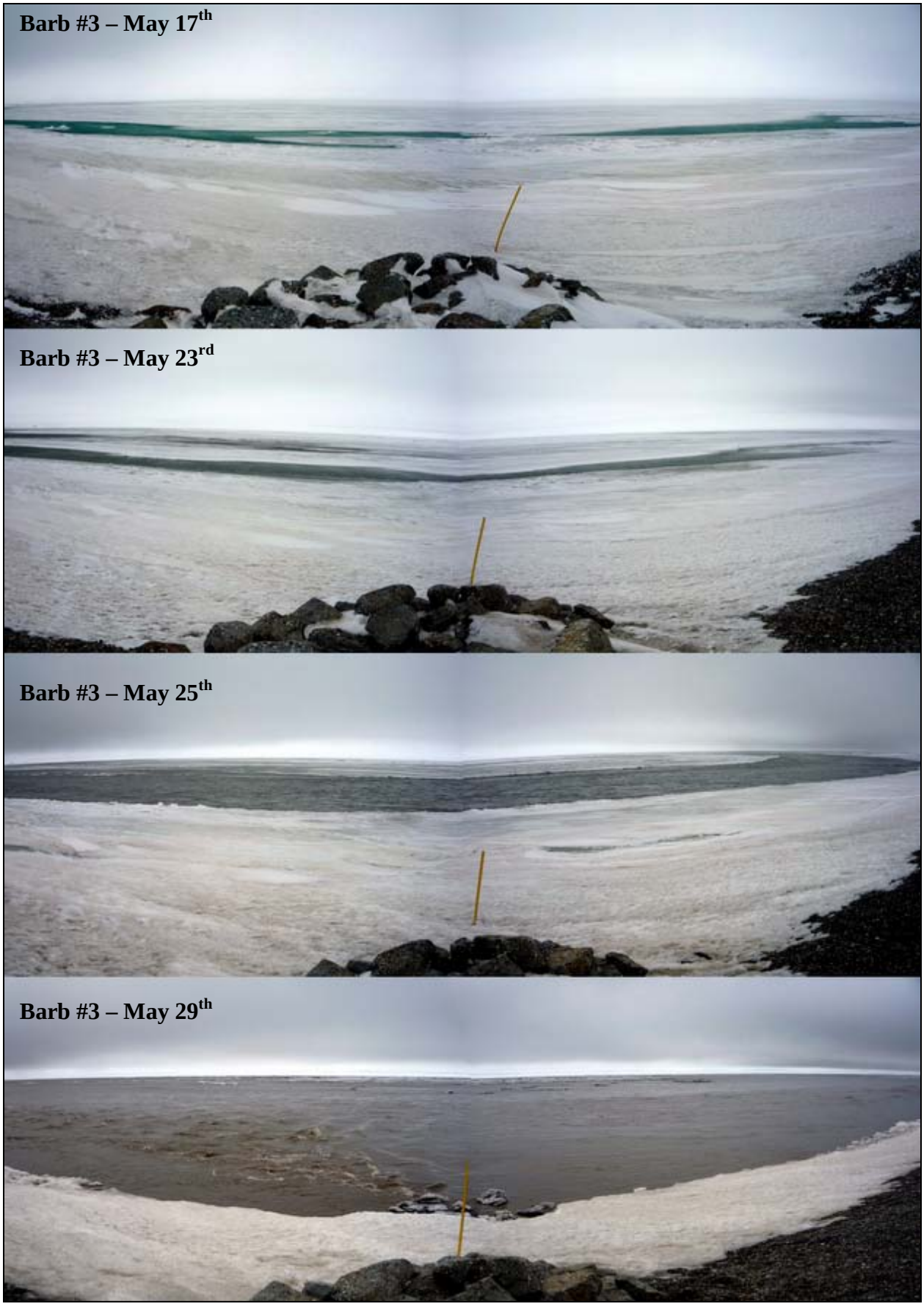


Figure 8 – View from Barb #3 for May 17, 23, 25 (Breakup), and 29, 2010


Figure 9 – View from Barb #4 for May 17, 23, 25 (Breakup), and 29, 2010


Figure 10 – View from Barb #5 for May 17, 23, 25 (Breakup), and 29, 2010


Figure 11 – View from Barb #6 for May 17, 23, 25 (Breakup), and 29, 2010

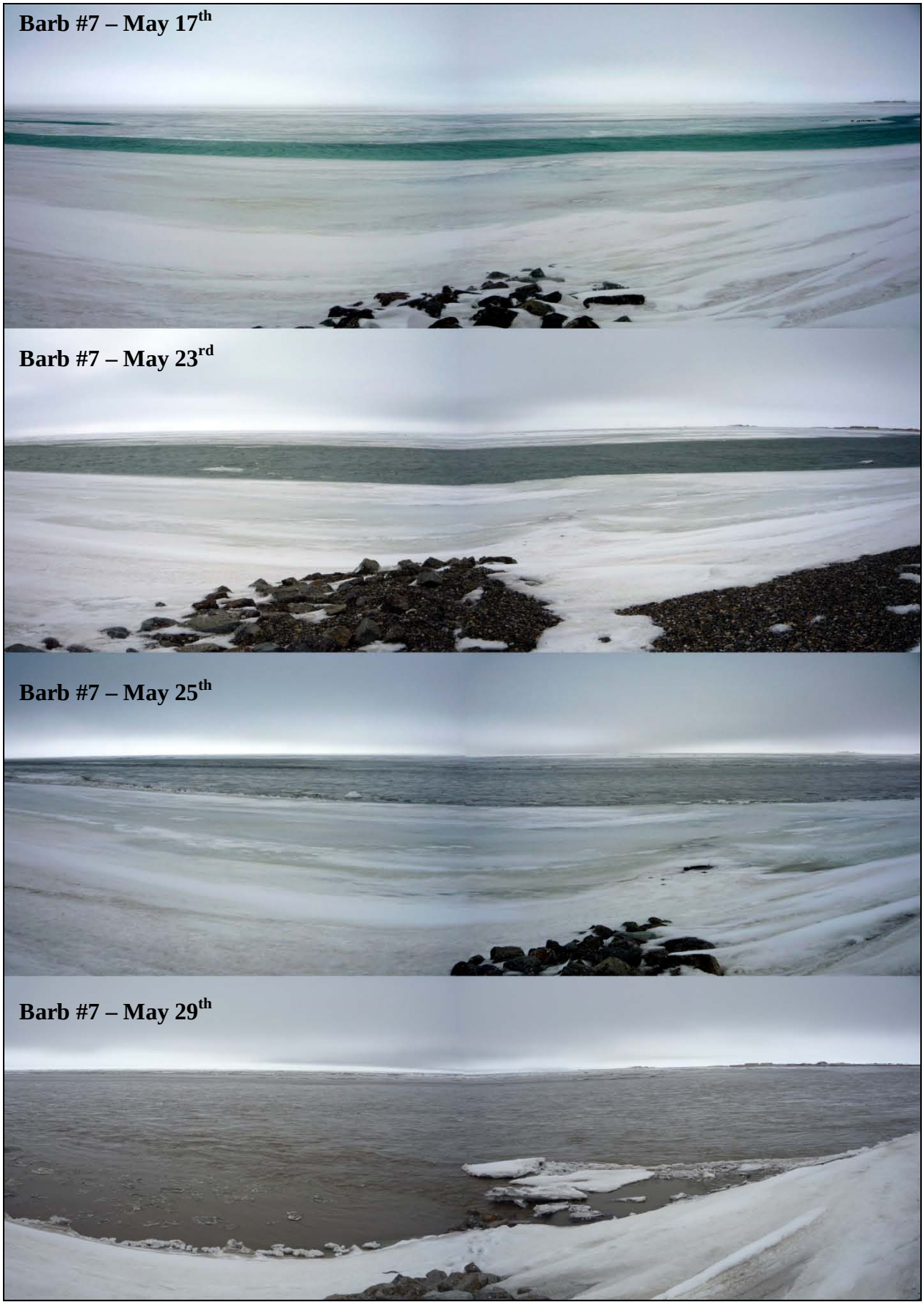


Figure 12 – View from Barb #7 for May 17, 23, 25 (Breakup), and 29, 2010


Figure 13 – View from Barb #8 for May 17, 23, 25 (Breakup), and 29, 2010

Figure 14 to Figure 23 show the water level height evolution as registered on the time-lapse movies. The water level heights were estimated around 1.40 m (4.5 ft) on May 16, 3.3 m to 3.5 m (10.8 ft to 11.5 ft) on May 25 during breakup, and 2.10 m (7 ft) on June 8. Note that 0 m corresponds to the lowest point of the thalweg in 2006.


Figure 14 – Upstream View from Camera #2 on May 16, 2010


Figure 15 – Upstream View from Camera #2 on May 21, 2010


Figure 16 – Upstream View from Camera #2 on May 22, 2010


Figure 17 – Upstream View from Camera #2 on May 25, 2010


Figure 18 – Upstream View from Camera #2 on May 25, 2010


Figure 19 – Upstream View from Camera #2 on May 25, 2010


Figure 20 – Upstream View from Camera #2 on May 25, 2010

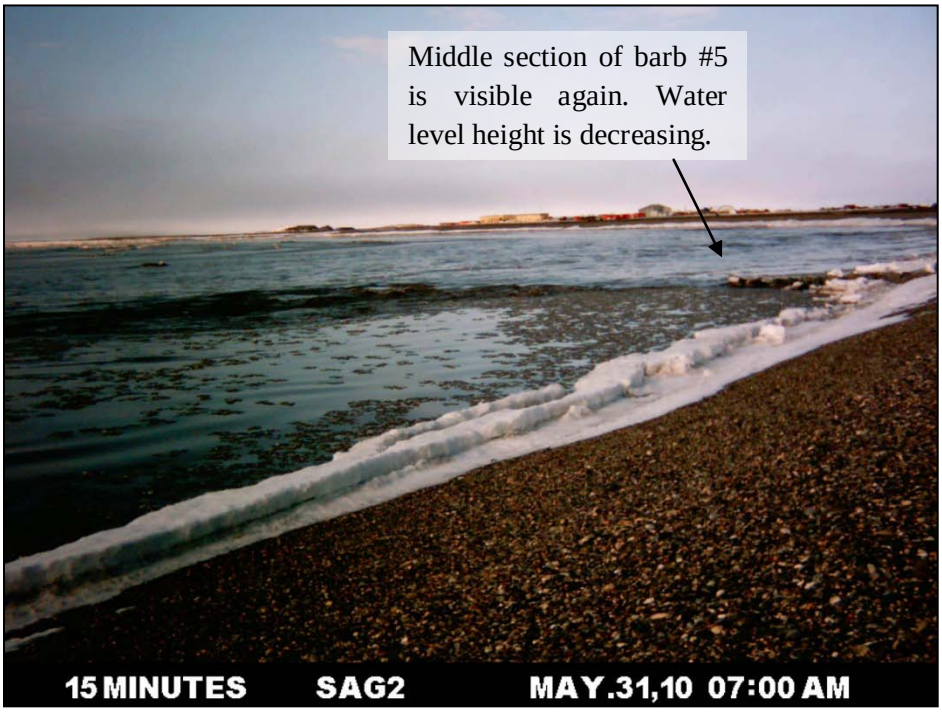


Figure 21 – Upstream View from Camera #2 on May 31, 2010

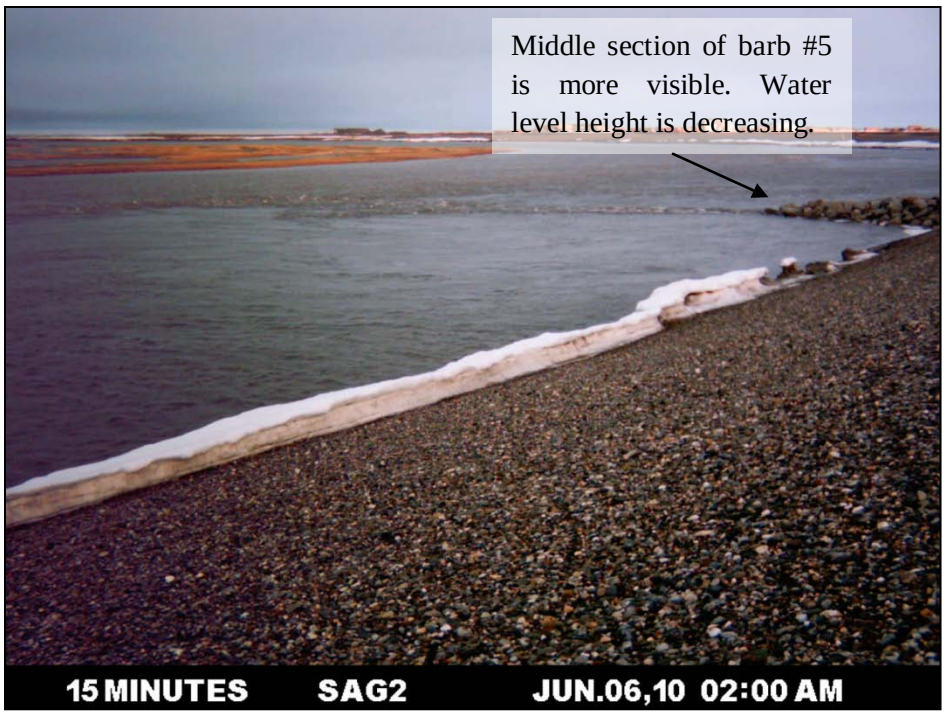


**Figure 22 – Upstream View from Camera #2 on June 6, 2010**


**Figure 23 – Upstream View from Camera #2 on June 8, 2010**

Summarizing, field observations indicate that flow was dammed (high water elevation) by barb 1 and effectively diverted to the center of the channel.

# 4. Turbulence Analysis

As mentioned before, the ADCP was configured to measure velocity on selected locations along the Sag River (Figure 24) and Hess Creek (Figure 25). The instrument was running for 15 minutes, collecting data at a high frequency rate and minimal averaging, following the procedure described by Muste et al. (2004).

A complex numerical code was developed to extract and calculate main turbulent characteristics of velocity measurements. The analysis is based on the pioneer work conducted by Tennekes and Lumley (1972). Additional information related to the methodology applied to the turbulence analysis is presented in Toniolo et al. (in press 2010).

Corresponding graphs (see Appendix A) show that turbulence is relatively high in the upstream area (barb #1) and generally decreases in the downstream direction in the Sag River. In addition, data show downward currents (points 2 and 3) upstream of the scour holes located near the end of each barb, and upward currents near the end of each scour hole (points 1 and 4).

There is no clear pattern of turbulence in Hess Creek. However, the dimensionless graph (Figure 26) seems to indicate that velocity profiles are similar along the river reach where vanes were installed (points 3 to 6). Thus, it can be argued that the river reach was in equilibrium at the time the survey was conducted.

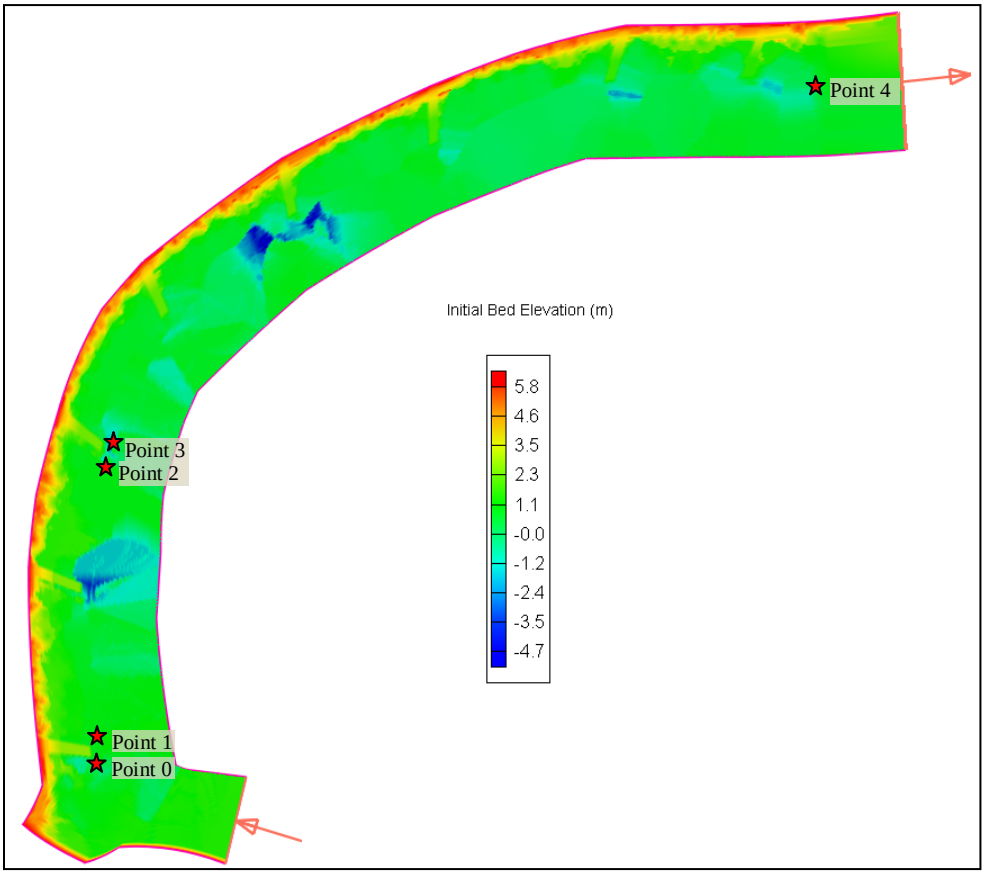


Figure 24 – Location of Turbulence Measurements at Sag River

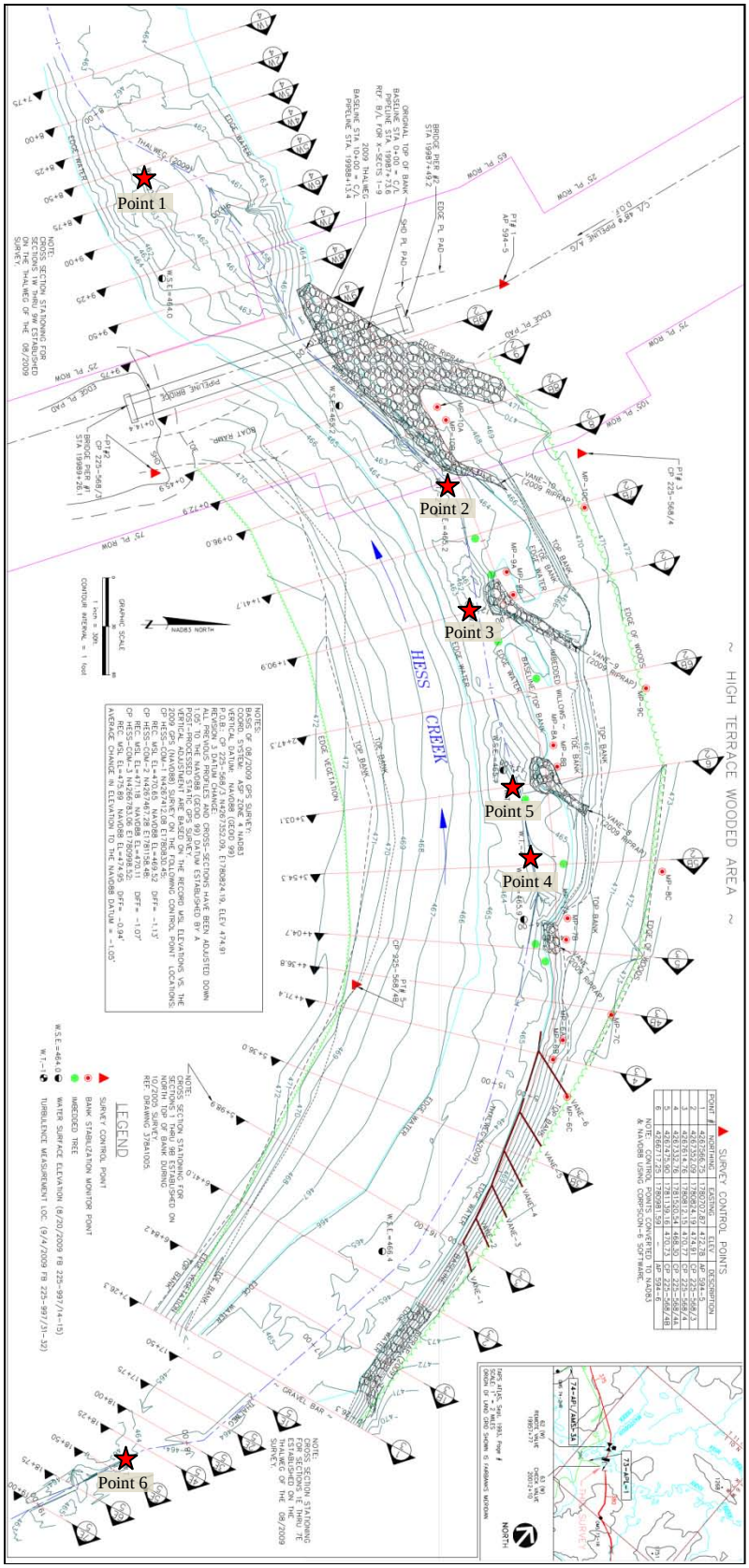


**Figure 25 –Location of Turbulence Measurements at Hess Creek**

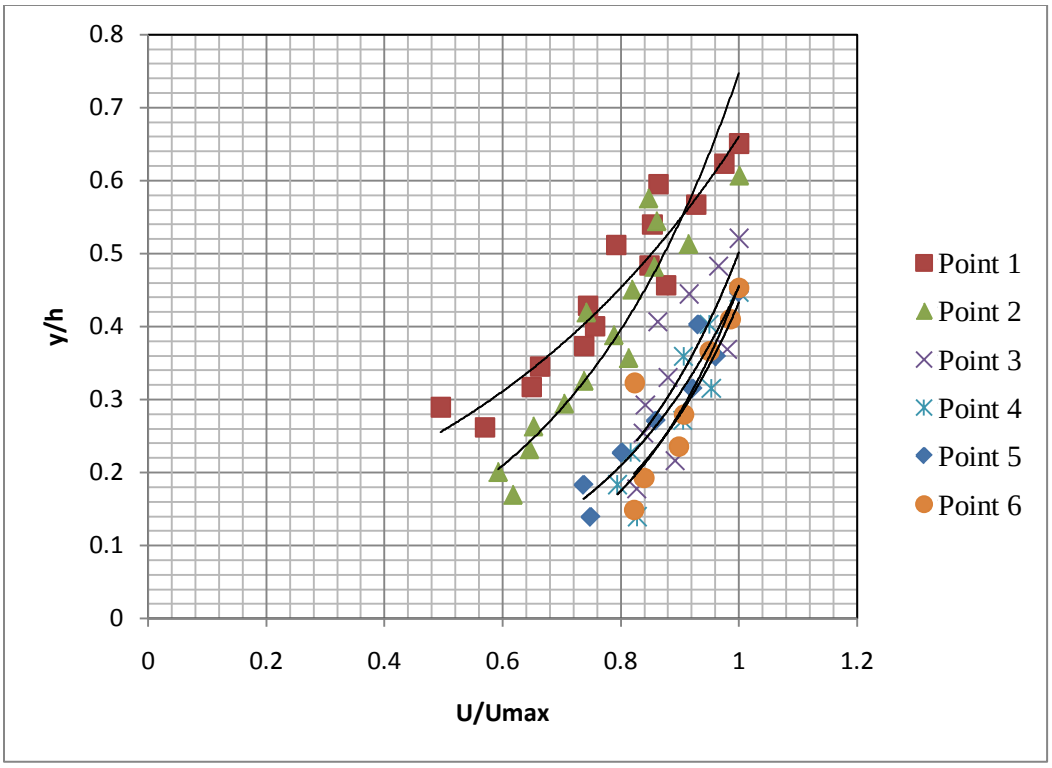


Figure 26 – Dimensionless Velocity Profiles at Different Points of Hess Creek

# 5. CCHE2D Numerical Model

## 5.1 Introduction to Numerical Modeling

River flow and sediment transport are complex processes in nature, and it is difficult and tedious to find analytical solutions to problems related to them. For this reason, many river engineering problems are suitable for solving with the aid of numerical models (Wu, 2007).

One-dimensional models are useful for short- and long-term modeling of flow and sediment-transport processes of an entire river reach, while two- and three-dimensional models are frequently used for a more detailed analysis of morphodynamic processes in a particular sub-reach under complex flow conditions of bends and hydraulic structures (Wu, 2007).

Most cases of open-channel flows in nature can be treated in a manner similar to shallow water cases, because the effect of vertical motion is generally insignificant. Thus, a depth-integrated two-dimensional model is usually accepted for studying open-channel hydraulics, with reasonable accuracy and efficiency (Jia and Wang, 1999).

Langendoen (2001) has analyzed several two-dimensional models—for example, CCHE2D, Delft2D-Rivers, MIKE21C, TABS-MD, and TELEMAC—for free surface flow and sediment-transport capabilities to predict the effect of hydraulic structures on river morphology.

Conclusions of this study are summarized in Table 4. Note that the only free software applications listed in this table are CCHE2D (http://www.ncche.olemiss.edu/software) and TELEMAC (http://www.telemacsystem.com/images/licence/Licence_Telemac.pdf).

**Table 4 – Comparison of Free Surface Flow and Sediment-transport Capabilities of Selected Two-dimensional Models. Langendoen (2001).**

| Feature | CCHE2D | Delft2D-Rivers | MIKE21C | TABS-MD | TELEMAC |
|---|---|---|---|---|---|
| Schematization of physical domain | X | X | X | X | X |
| Flow description and simulation: | | | | | |
| Unsteady Flow | X | X | X | X | X |
| Sub- and supercritical flow | X | N/A | N/A | N/A | X |
| Wetting and drying | X | X | X | X | X |
| Turbulence model | X | X | X | X | X |
| Secondary flow effects | N/A | X | X | X | N/A |
| Solution method | X | X | X | X | X |
| Sediment transport description and simulation: | | | | | |
| Cohesionless and cohesive | X | X | X | X | X |
| Bed-material load description | X | X | X | X | X |
| Graded sediments | X | X | X | N/A | N/A |
| Secondary flow effects | X | X | X | N/A | N/A |
| Solution method | X | X | X | X | X |
| Streambank erosion | N/A | N/A | X | N/A | N/A |
| Long-term simulation capability | X | X | X | X | X |
| Integrated coupling of processes and efficiency | X | X | X | N/A | X |
| Integrated model documentation | X | X | X | X | X |
| Pre- and post-processors | X | X | X | X | X |
| Known, documented application to similar problem | X | X | X | X | X |

X: Implemented; N/A: Not available

## 5.2 Model Description

The CCHE2D is a depth-integrated two-dimensional hydrodynamic model for studying steady and unsteady free surface open-channel flow and sediment transport in channels with irregular topography and bank protection structures (Jia and Wang, 2001a; Jia et al., 2002). The model is capable of simulating subcritical, supercritical, and transitional flows (Jia and Wang, 2001b). Developed by researchers at the National Center for Computational Hydroscience and Engineering, University of Mississippi, the CCHE2D software is free but a closed source.

The CCHE2D model is based on a mixed finite element and finite volume method to solve the continuity equation on a staggered grid and the momentum equations on a collocated grid (Figure 27). This partially staggered arrangement prevents oscillation caused by a collocated grid

where the velocity and pressure fields are decoupled (Jia et al, 2002). The model is targeted for evaluating the effects of hydraulic structures on river morphology and for predicting riverbed erosion (Zhang, 2006).

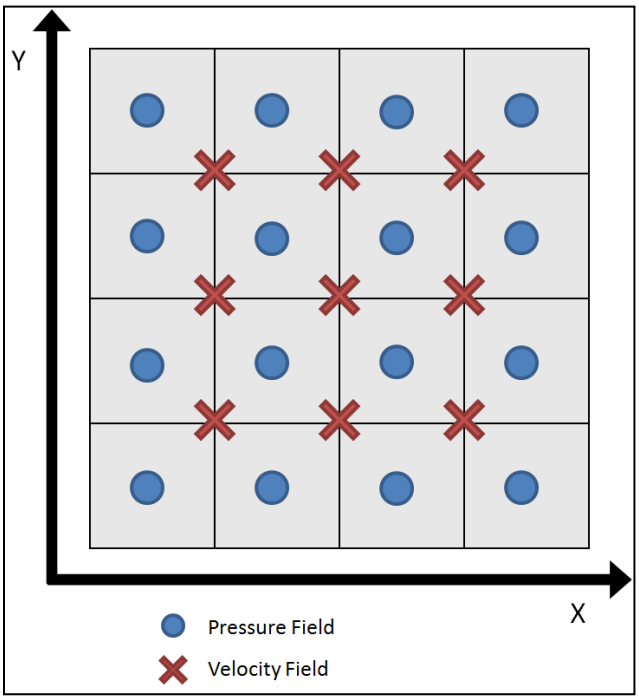


Figure 27 – Partially Staggered Grid Used by the CCHE2D Model

The CCHE2D model is composed of CCHE-MESH, the Mesh Generation Software, and CCHE-GUI, the Graphical User Interface to the numerical model. Software versions utilized for this project were 3.0 and 3.26, respectively.

## 5.3 Governing Equations

### 5.3.1 Continuity and Momentum

The governing equations for two-dimensional modeling are obtained by depth integrating of the original three-dimensional equations (Spasojevic and Holly, 2008; Wu, 2007):

$$\tilde{\phi} = \frac{1}{h}\int_{h} \phi \, dz \qquad (1)$$

where $\tilde{\phi}$ is the depth-integrated variable of $\phi$, h is the local water depth, and z is the

Cartesian coordinate direction.

Free surface elevation is calculated by the continuity equation (Zhang, 2006)

$$\frac{\partial Z}{\partial t} + \frac{\partial (hu)}{\partial x} + \frac{\partial (hv)}{\partial y} = 0 \tag{2}$$

where Z is the water surface elevation; t is time; and u,v are the depth-integrated velocity components in the *x* and *y* directions, respectively.

The momentum equations for depth-integrated two-dimensional turbulent flows are (Zhang, 2006)

$$\frac{\partial u}{\partial t} + u\frac{\partial u}{\partial x} + v\frac{\partial u}{\partial y} = -g\frac{\partial Z}{\partial x} + \frac{1}{h}\left[\frac{\partial (h\tau_{xx})}{\partial x} + \frac{\partial (h\tau_{xy})}{\partial y}\right] - \frac{\tau_{bx}}{\rho h} + f_{cor}v \tag{3}$$

$$\frac{\partial v}{\partial t} + u\frac{\partial v}{\partial x} + v\frac{\partial v}{\partial y} = -g\frac{\partial Z}{\partial y} + \frac{1}{h}\left[\frac{\partial (h\tau_{yx})}{\partial x} + \frac{\partial (h\tau_{yy})}{\partial y}\right] - \frac{\tau_{by}}{\rho h} - f_{cor}u \tag{4}$$

where $g$ is the gravitational acceleration; $\tau_{xx}, \tau_{xy}, \tau_{yx}, \tau_{yy}$ are the depth-integrated Reynolds stresses; $\tau_{bx}$,$\tau_{by}$ are shear stresses on the bed surface; and $f_{cor}$ is the Coriolis parameter.

Turbulence Reynolds stresses in equations (3) and (4) are approximated, based on the Boussinesq assumption (Zhang, 2006):

$$\tau_{xx} = 2v_t\frac{\partial u}{\partial x} \tag{5}$$

$$\tau_{xy} = \tau_{yx} = v_t\left(\frac{\partial u}{\partial y} + \frac{\partial v}{\partial x}\right) \tag{6}$$

$$\tau_{yy} = 2v_t\frac{\partial v}{\partial y} \tag{7}$$

where $v_t$ is the eddy viscosity.

### 5.3.2 Turbulence Models

There are three turbulence models available in the CCHE2D model: two eddy viscosity models and one two-dimensional k – ε. The first eddy viscosity $v_t$ is calculated by the following formula using a depth-integrated parabolic model (Zhang, 2006):

$$v_t = \frac{A_{xy}}{6}KU^*h \tag{8}$$

where $A_{xy}$ is an adjustable coefficient of eddy viscosity with a default value of 1; $K$ is the von Karman constant (0.41); and $U^*$ is the shear velocity.

The second eddy viscosity model uses a depth-integrated mixing length model, where $\nu_t$ is calculated by the following (Zhang, 2006):

$$v_t = \bar{l}^2 \sqrt{2\left(\frac{\partial u}{\partial x}\right)^2 + 2\left(\frac{\partial v}{\partial x}\right)^2 + 2\left(\frac{\partial u}{\partial x} + \frac{\partial v}{\partial x}\right)^2 + \left(\frac{\partial \bar{U}}{\partial z}\right)^2} \tag{9}$$

$$\bar{l} = \frac{1}{h}\int KZ\sqrt{\left(1 - \frac{Z}{h}\right)}\,dZ \tag{10}$$

$$\frac{\partial \bar{U}}{\partial z} = C_m \frac{U^*}{Kh} \tag{11}$$

where $\bar{l}$ is the mixing length, $\frac{\partial \bar{U}}{\partial z}$ is the depth integrated velocity gradient along the vertical coordinate to account for the effect of bed surface turbulence, and $C_m$ is a coefficient equal to 2.34375 (Jia and Wang, 2001a).

In the two-dimensional $k$ – ε model, differential equations are used for the turbulent kinetic energy $k$, and for the rate of dissipation of turbulent energy ε (Jia and Wang, 2001a):

$$\frac{\partial k}{\partial t} + u\frac{\partial k}{\partial x} + v\frac{\partial k}{\partial y} - \frac{\partial}{\partial x}\left[\frac{v_t}{\sigma_k}\frac{\partial k}{\partial x}\right] - \frac{\partial}{\partial y}\left[\frac{v_t}{\sigma_k}\frac{\partial k}{\partial y}\right] = P - \varepsilon + P_{kv} \tag{12}$$

$$\frac{\partial \varepsilon}{\partial t} + u\frac{\partial \varepsilon}{\partial x} + v\frac{\partial \varepsilon}{\partial y} - \frac{\partial}{\partial x}\left[\frac{v_t}{\sigma_\varepsilon}\frac{\partial \varepsilon}{\partial x}\right] - \frac{\partial}{\partial y}\left[\frac{v_t}{\sigma_\varepsilon}\frac{\partial \varepsilon}{\partial y}\right] = c_{1\varepsilon}\frac{\varepsilon}{k}P - c_{2\varepsilon}\frac{\varepsilon^2}{k} + P_{\varepsilon v} \tag{13}$$

where

$$P = -\overline{u_i' u_j'}u_i u_j = v_t\left[2\left(\frac{\partial u}{\partial x}\right)^2 + 2\left(\frac{\partial v}{\partial y}\right)^2 + \left(\frac{\partial u}{\partial y} + \frac{\partial v}{\partial x}\right)^2\right] \tag{14}$$

$$P_{kv} = C_k \frac{{U_*}^3}{h} \tag{15}$$

$$P_{\varepsilon v} = C_\varepsilon \frac{{U_*}^4}{h^2} \tag{16}$$

and

$$U_* = \sqrt{C_f\,(u^2 + v^2)} \tag{17}$$

$$C_k = \frac{1}{\sqrt{C_f}} \tag{18}$$

$$C_\varepsilon = 3.6 \frac{C_{2\varepsilon}}{C_f^{3/4}} \sqrt{C_\mu} \tag{19}$$

where the following are empirical variables: $C_\mu = 0.09$, $\sigma_k = 1$, $\sigma_\varepsilon = 1.3$, $c_{1\varepsilon} = 1.44$, $c_{2\varepsilon} = 1.92$. The terms $P_{kv}$ and $P_{\varepsilon v}$ account for the generation of energy and dissipation due to bed friction in the event of uniform flow (Jia and Wang, 2001a).

The local eddy viscosity is then evaluated by solving the *k-e* model:

$$v_t = \frac{C_\mu k^2}{\varepsilon} \tag{20}$$

The depth-integrated parabolic model (8) was selected for the simulations, as it proved to be the most stable turbulent model for the runs to complete successfully.

### 5.3.3 Bed-Shear Stress

The CCHE2D model utilizes two approaches to calculate bed-shear velocity: a depth-integrated logarithmic law and a Manning's coefficient method. The following formulas describe the depth-integrated logarithmic law (Jia and Wang, 2001a):

$$\frac{U}{U^*} = \frac{1}{z}\left[\frac{z_0}{h} - 1 + \ln\left(\frac{h}{z_0}\right)\right] \tag{21}$$

where

$$U = \sqrt{u^2 + v^2} \tag{22}$$

and $z_0$ is the zero-velocity level ($u$ = 0 at $z = z_0$) and is calculated with the following formulas for smooth, rough, and transition flow conditions:

$$z_0 = 0.11 \frac{\nu}{U^*} \qquad \frac{U^* k_s}{\nu} \le 5 \tag{23}$$

$$z_0 = 0.0333\, k_s \qquad \frac{U^* k_s}{\nu} \ge 70 \tag{24}$$

$$z_0 = 0.11 \frac{\nu}{U^*} + 0.0333\, k_s \qquad 5 < \frac{U^* k_s}{\nu} < 70 \tag{25}$$

where $\nu$ is the fluid kinematic viscosity, and $k_s$ is the roughness height of the bed surface. Equation 21 is solved iteratively. Once $U^*$ has been calculated, the friction factor $f_c$ is obtained by the following formulas (Jia and Wang, 2001a):

$$\left(\frac{f_c}{8}\right)^{-0.5} = 3 + 2.5 \cdot ln\left(\frac{U^* h}{\nu}\right) \qquad \frac{U^* k_s}{\nu} \leq 5 \tag{26}$$

$$\left(\frac{f_c}{8}\right)^{-0.5} = 6 + 2.5 \cdot ln\left(\frac{h}{k_s}\right) \qquad \frac{U^* k_s}{\nu} \geq 70 \tag{27}$$

$$\left(\frac{f_c}{8}\right)^{-0.5} = 6 + 2.5 \cdot ln\left(\frac{h}{k_s + 3.3\frac{\nu}{U^*}}\right) \qquad 5 < \frac{U^* k_s}{\nu} < 70 \tag{28}$$

The shear stress components are then calculated:

$$\tau_{bx} = \frac{1}{8}\rho f_c u U \tag{29}$$

$$\tau_{by} = \frac{1}{8}\rho f_c u U \tag{30}$$

The second method uses the Manning's coefficient method to calculate the shear stress components and the shear velocity (Jia and Wang, 2001a):

$$\tau_{bx} = \frac{1}{h^{1/3}}\rho g n^2 u U \tag{31}$$

$$\tau_{by} = \frac{1}{h^{1/3}}\rho g n^2 v U \tag{32}$$

$$U^{*2} = \frac{1}{\rho}\sqrt{\tau_{bx}{}^2 + \tau_{by}{}^2} \tag{33}$$

where *n* is the Manning's coefficient.

### 5.4 Setting of Model Parameters

The following flow parameters control the simulation process: simulation time, number of time steps, turbulence model option, bed roughness type (Manning's number, *n*; or roughness height, *Ks*), and the setting of advanced parameters (Coriolis force coefficient, gravity, von Karman constant, fluid kinematic viscosity). Appendix B lists screenshots with the default values used in the simulations.

### 5.5 Mesh Generation

A mesh is the computational domain where the governing equations are discretized, and a reliable simulation depends on the following characteristics: sufficient resolution; mesh inlet and outlet that is distant enough from the study zone; and mesh that is as orthogonal and smooth as possible (Zhang, 2006). The CCHE-GUI software and the CCHE2D model require a mesh file with a .geo extension, which can be built by the CCHE-MESH generator.

## 5.6 Specification of Initial Conditions

The initial conditions that must be specified with the CCHE2D software are the mesh, the initial bed elevation (see Appendix C for detailed steps for mesh and bathymetric settings), the initial water surface, and bed roughness.

Table 5 and Table 6 summarize the settings for each run:

**Table 5 – Initial Conditions for Sag River Simulation**

| Model | Initial Water Surface (m)* | | Roughness, Ks (m) | |
|---|---|---|---|---|
| | | | Bed | Barbs |
| 2006 – As Built | 1.5 | 3.3 | 0.025 | 0.45 |
| 2006 – No 1st Barb | 1.5 | 3.3 | 0.025 | 0.45 |
| 2006 – No 2nd Barb | 1.5 | 3.3 | 0.025 | 0.45 |
| 2006 – No 3rd Barb | 1.5 | 3.3 | 0.025 | 0.45 |
| 2006 – No 4th Barb | 1.5 | 3.3 | 0.025 | 0.45 |
| 2006 – No 5th Barb | 1.5 | 3.3 | 0.025 | 0.45 |
| 2006 – No 6th Barb | 1.5 | 3.3 | 0.025 | 0.45 |
| 2006 – No 7th Barb | 1.5 | 3.3 | 0.025 | 0.45 |
| 2006 – No 8th Barb | 1.5 | 3.3 | 0.025 | 0.45 |
| 2006 – 5 Barbs | 1.5 | 3.3 | 0.025 | 0.45 |
| 2006 – 4 Barbs | 1.5 | 3.3 | 0.025 | 0.45 |
| 2009 – All Barbs | 1.5 | 3.3 | 0.025 | 0.45 |

* 0 m. is an arbitrary datum and corresponds to the lowest point of the thalweg in 2006.

**Table 6 - Initial Conditions for Hess River Simulation**

| Model | Initial Water Surface (NAVD88, m) | | Roughness (Manning's n) | |
|---|---|---|---|---|
| | | | Bed | Vanes |
| 2004 | 142.9 | 144.78 | 0.035 | 0.065 |
| 2009 | 142.9 | 144.78 | 0.035 | 0.065 |

## 5.7 Specification of Boundary Conditions

Boundary conditions constitute the forcing mechanism for free surface flow in the simulated area, thus they should be as close as possible as the physics being represented (Zhang, 2006). The inlet and outlet boundary conditions are analogous to the headgate and tailgate requirements of a physical model, respectively, where the headgate regulates the inflow water discharge and the tailgate determines the tailwater elevation (Thomas and Chang, 2008).

The boundaries are indicated in the domain graphs with an ingoing arrow for the inlet and an outgoing arrow for the outlet. See Appendix D for screenshots of the settings. Table 7 and Table 8 show the boundary conditions set for Sag River and Hess River simulations, respectively.

**Table 7 - Boundary Conditions for Sag River Simulation**

| Run | Inlet (Discharge, $m^3/s$) | Outlet (Water Level Height, m) | Observations |
|---|---|---|---|
| 1 | 40 | 1.5 | Observed conditions during fieldwork conducted in August 2009. |
| 2 | 300 | 3.3 | Probable bankfull conditions – No data available. |

**Table 8 - Boundary Conditions for Hess River Simulation**

| Run | Inlet (Discharge, $m^3/s$) | Outlet (Water Level Height, m) | Observations |
|---|---|---|---|
| 1 | 95.57 | 142.9 | Bankfull conditions. |

## 5.8 Simulations

Once the mesh is built and both the boundary conditions and parameters are set, the simulation is ready to be run (Figure 28). The time step should be small enough for the simulation to complete without interruptions due to instability of the numerical model; otherwise, the simulation has to be restarted with a lower time step until stable solutions are reached (Zhang, 2006). Another condition that will cause the simulation to stop prematurely is the existence of too many dry nodes in the domain at the beginning of the simulation. This condition can be overridden by running a new simulation with a higher initial water surface to reduce the number of dry nodes.

To ensure reliability of model results, they must be validated if possible with field data. If the model results do not match the available field data, or if field data are insufficient, the model has to be calibrated until the calculated results agree with the available field data. The calibration process includes any representative data of the area in study, model parameters, and roughness coefficients (Pizzuto et al., 2008).

After the model is validated, running it by varying the parameters may assist the modeler in the study of different river flow conditions (Zhang, 2006).

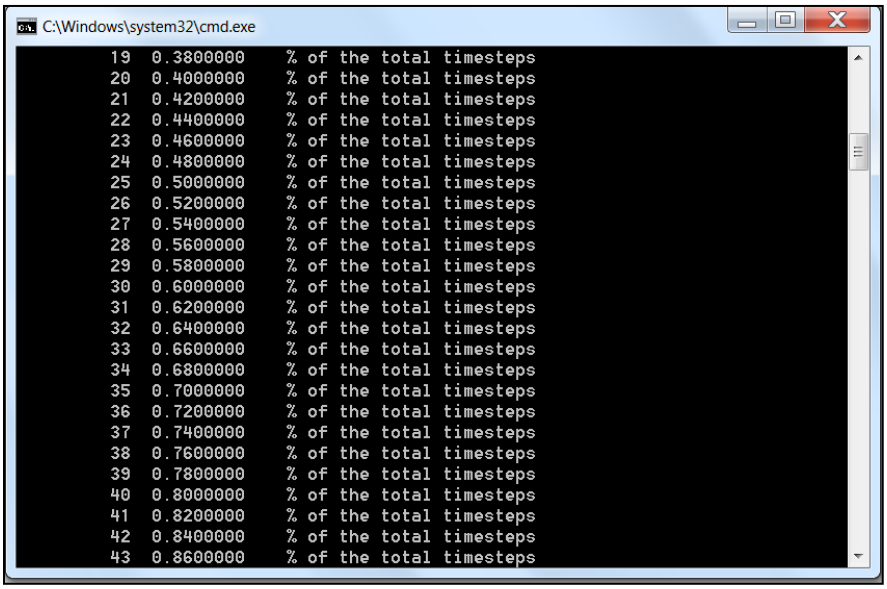


Figure 28 - Example of Running Simulation Indicating % of Completion for Each Simulation Step

## 5.9 Result Visualization

Once the simulation has completed, results are available from the CCHE-GUI Interface. To load the results, the proper run has to be selected (Figure 29). Then the list of final flow results is displayed for the selected run (Figure 30 and Figure 31):

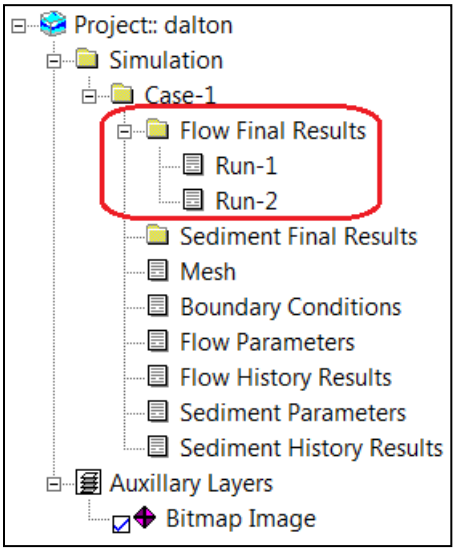


Figure 29 – List of Runs

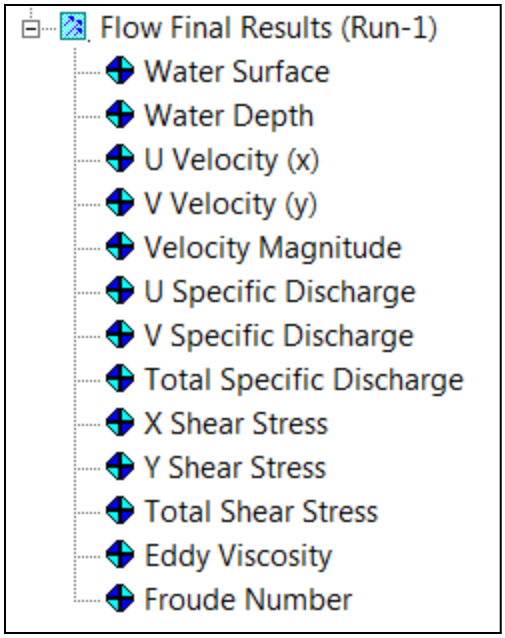


**Figure 30 - Flow Final Results**

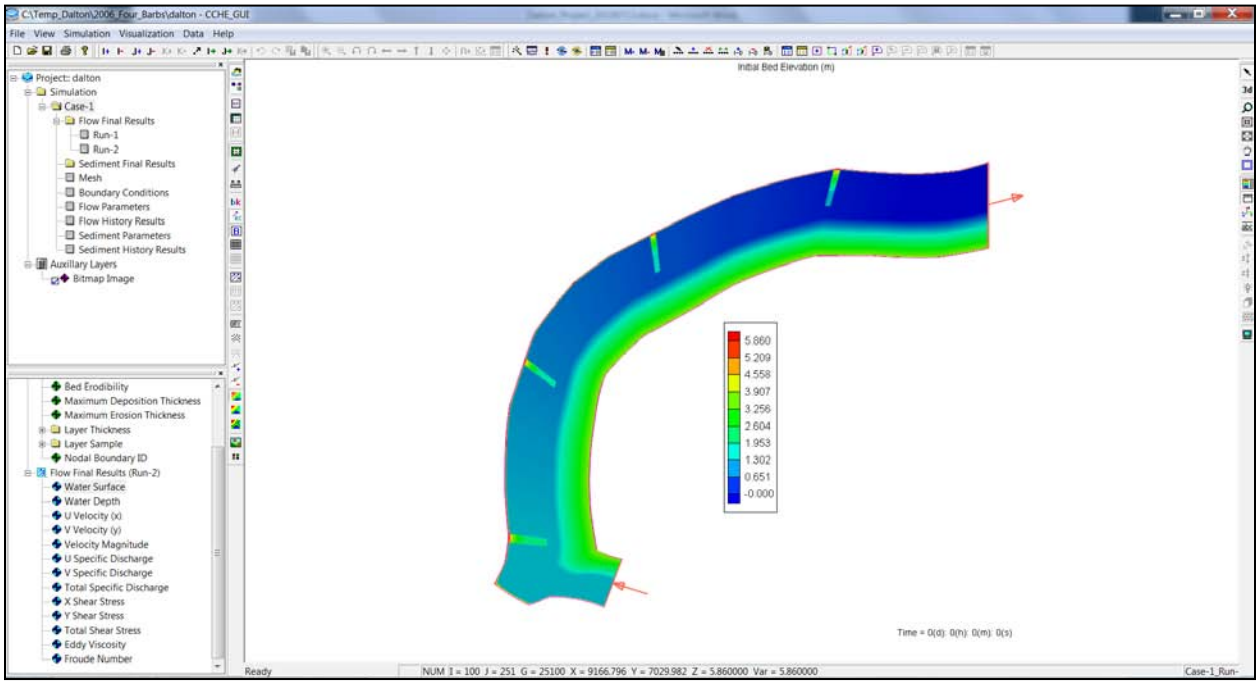


**Figure 31 – Sag River Modeled with Four Barbs**

Numerical results can also be visualized in tabulated rows and/or exported to a delimited text file (Figure 32).

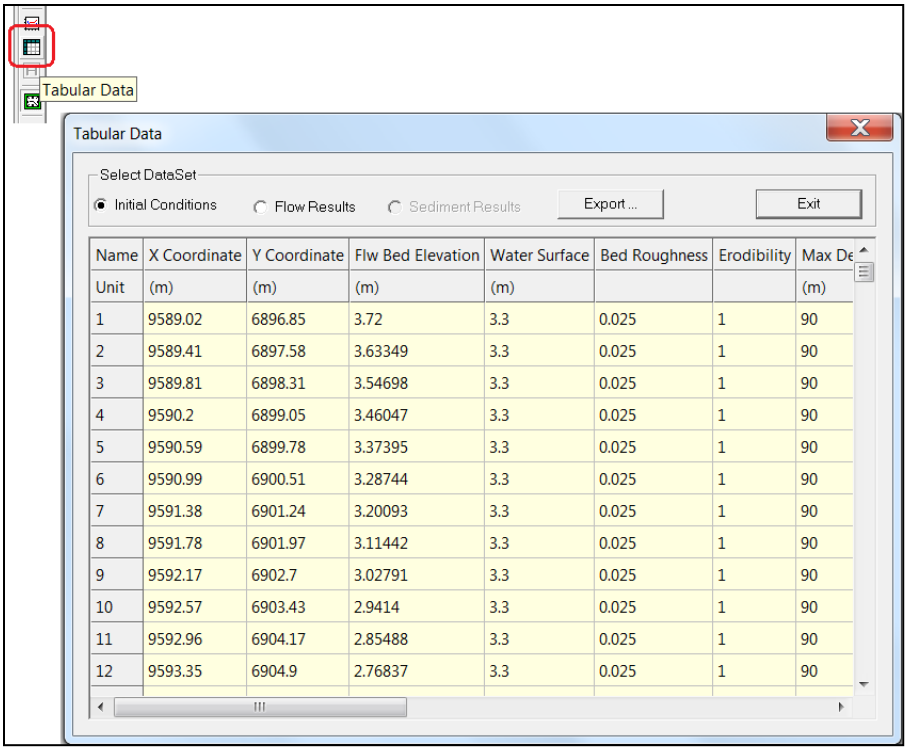


| Name | X Coordinate | Y Coordinate | Flw Bed Elevation | Water Surface | Bed Roughness | Erodibility | Max De |
|---|---|---|---|---|---|---|---|
| Unit | (m) | (m) | (m) | (m) | | | (m) |
| 1 | 9589.02 | 6896.85 | 3.72 | 3.3 | 0.025 | 1 | 90 |
| 2 | 9589.41 | 6897.58 | 3.63349 | 3.3 | 0.025 | 1 | 90 |
| 3 | 9589.81 | 6898.31 | 3.54698 | 3.3 | 0.025 | 1 | 90 |
| 4 | 9590.2 | 6899.05 | 3.46047 | 3.3 | 0.025 | 1 | 90 |
| 5 | 9590.59 | 6899.78 | 3.37395 | 3.3 | 0.025 | 1 | 90 |
| 6 | 9590.99 | 6900.51 | 3.28744 | 3.3 | 0.025 | 1 | 90 |
| 7 | 9591.38 | 6901.24 | 3.20093 | 3.3 | 0.025 | 1 | 90 |
| 8 | 9591.78 | 6901.97 | 3.11442 | 3.3 | 0.025 | 1 | 90 |
| 9 | 9592.17 | 6902.7 | 3.02791 | 3.3 | 0.025 | 1 | 90 |
| 10 | 9592.57 | 6903.43 | 2.9414 | 3.3 | 0.025 | 1 | 90 |
| 11 | 9592.96 | 6904.17 | 2.85488 | 3.3 | 0.025 | 1 | 90 |
| 12 | 9593.35 | 6904.9 | 2.76837 | 3.3 | 0.025 | 1 | 90 |

Figure 32 - Numerical Results in Tabular Format

### 5.9.1 Sag River: 8 barbs, 40 and 300 $m^3/s$

Numerical simulations considered a couple of river discharges: 40 $m^3/s$ and 300 $m^3/s$. The first discharge corresponds to the river discharge measured during the bathymetric survey carried out in August 2009. The second discharge corresponds to a somewhat arbitrary number, which should reproduce a high flow condition. No data is available for that type of flow condition.

Figure 33 and Figure 34 show the bathymetries for Sag River for year 2006 (As built) and 2009, respectively. Figure 35 shows the specific discharge in $m^2/s$ for a river discharge of 40 $m^3/s$ and an initial water height of 1.5 m for 2009. Figures 36 and 37 show the total shear stress in $N/m^2$ combined for years 2006 and 2009, for discharges of 40 and 300 $m^3/s$, respectively. The graphs show that the model properly simulates observed conditions during fieldwork conducted in August 2009 (40 $m^3/s$, water height: 1.5 m). Comparing 2006 and 2009 models, simulation results show that the flow is diverted from the left bank. For the 2009 total shear stress simulation, the thalweg seems to be stable. The reader should refer to Appendix E for the full set of the CCHE2D model results.

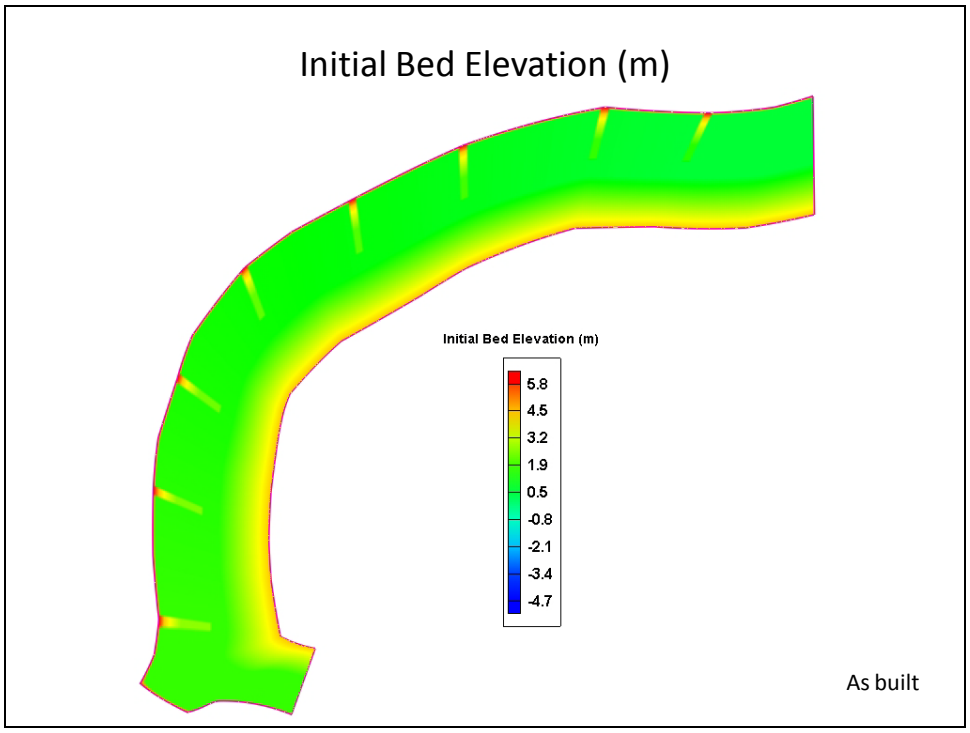


Figure 33 – Initial Bed Elevation (m), As Built, 2006.

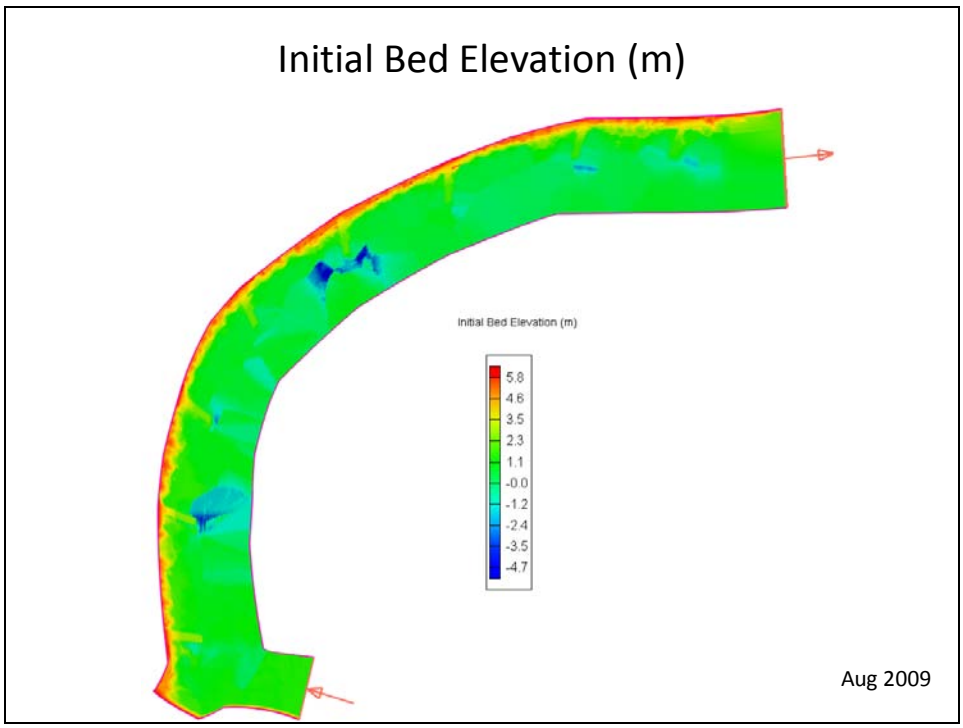


Figure 34 – Initial Bed Elevation (m), 2009.

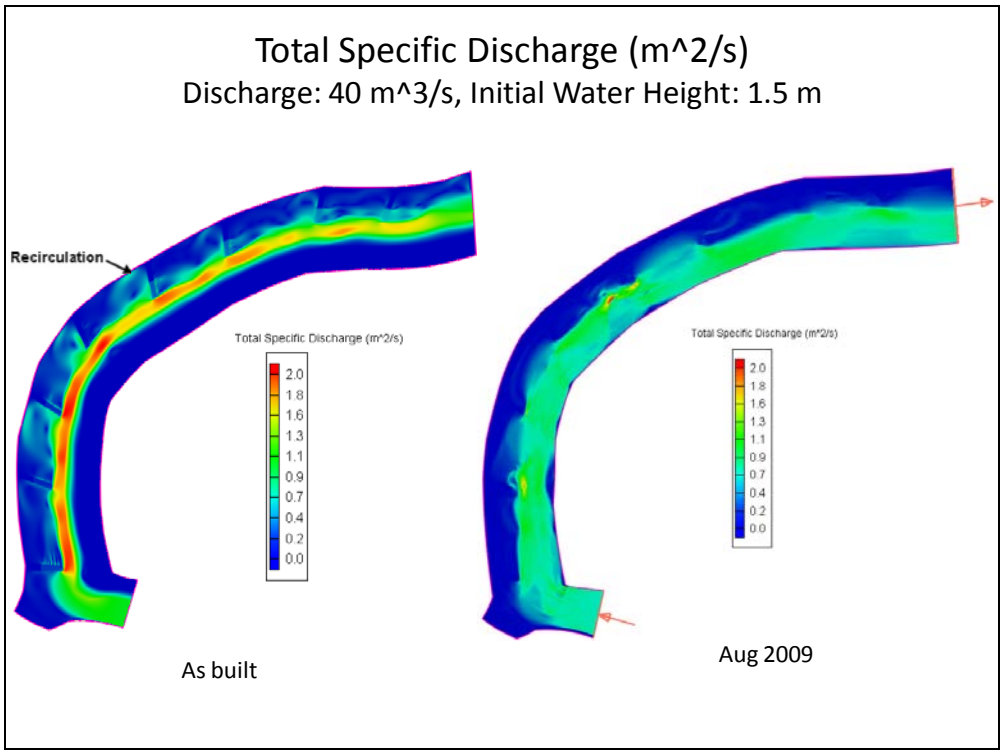


Figure 35 – Total Specific Discharge ($m^2/s$), Q= 40 $m^3/s$, h= 1.5 m, 2006 and 2009.

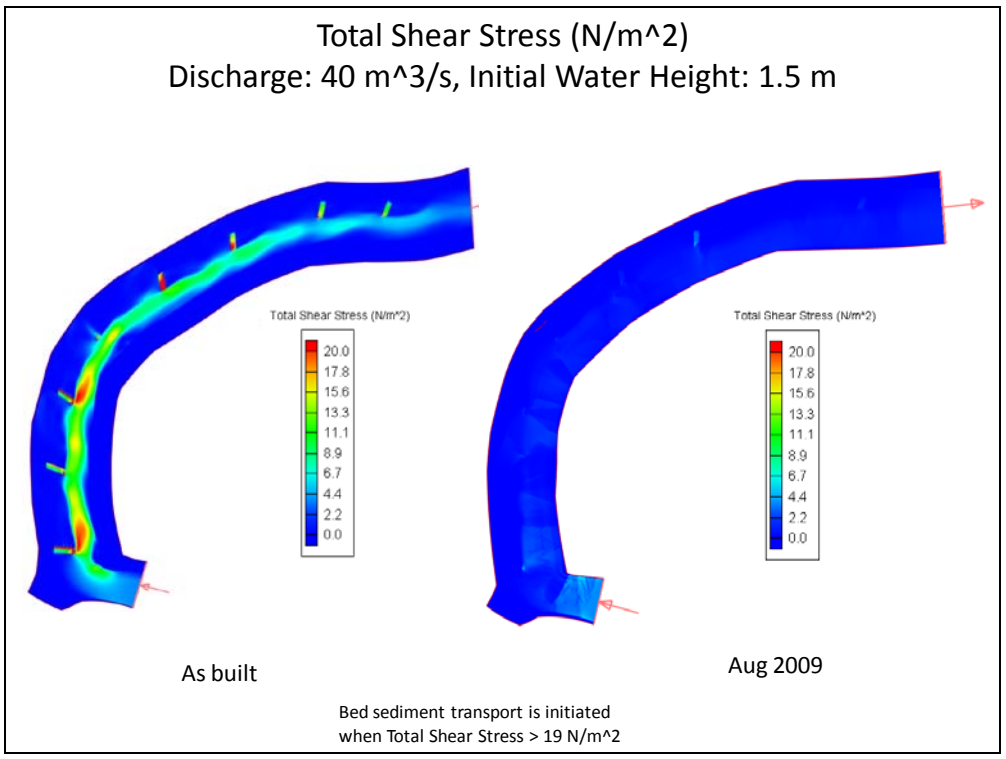


Figure 36 – Total Shear Stress ($N/m^2$), Q= 40 m3/s, h= 1.5 m, 2006 and 2009

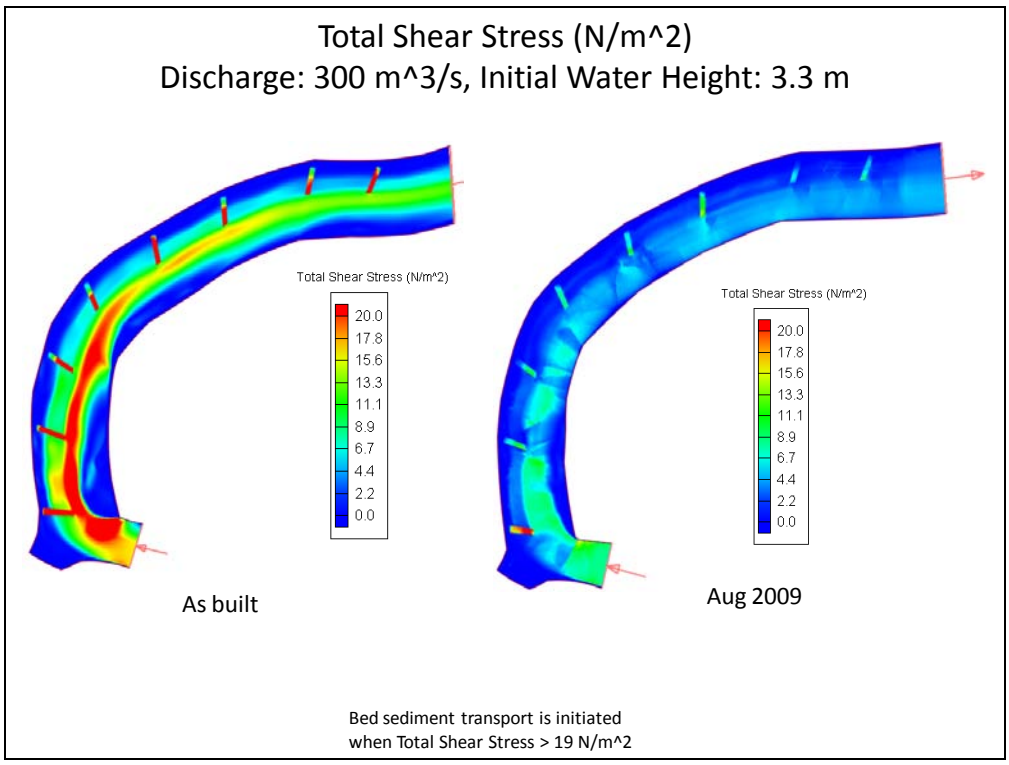


**Figure 37 – Total Shear Stress (N/m$^2$), Q= 300 m$^3$/s, h= 3.3 m, 2006 and 2009.**

### 5.9.2 Sag River: 7, 5, and 4 barbs, 40 m$^3$/s

Figure 38, Figure 39, Figure 40, and Figure 41 show the total shear stress in N/m$^2$ for year 2006 for 8 barbs (left of the graph) and 7, 5, and 4 barbs (right of the graph) with a simulated discharge of 40 m$^3$/s. The simulation results show an increased shear stress for configurations of fewer than 8 barbs. Total shear stress simulations depict the first and second barbs as critical to the performance of the rest of the barbs, the first barb being most critical. Specifically, Figure 38 shows direct flow impacting on the left bank. This situation could generate stability issues on the bank. Figure 41 indicates big areas subject to high shear stress, and consequently, river bed erosion. As the flow is subcritical (Figure 42), the removal of any barb (i.e., a perturbation in the flow) propagates information in both directions: upstream and downstream. The reader should refer to Appendix E for the full set of the CCHE2D model results.

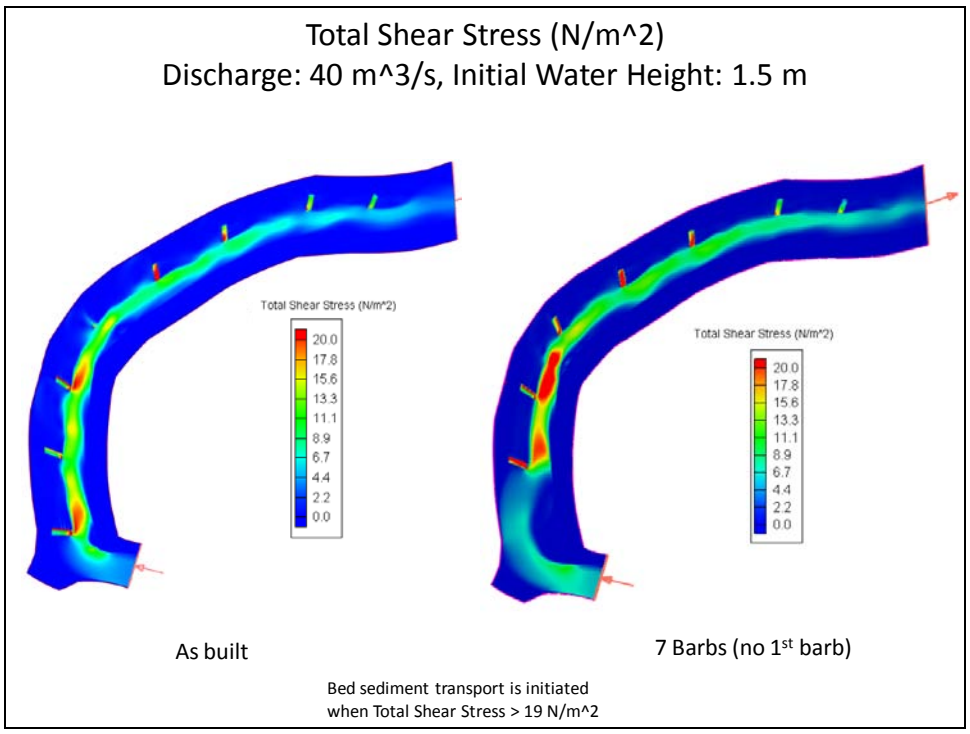


**Figure 38 – Total Shear Stress (N/m$^2$), Q= 40 m$^3$/s, h= 1.5 m, As built and theoretic 7 barbs configuration (no 1$^{st}$ barb)**

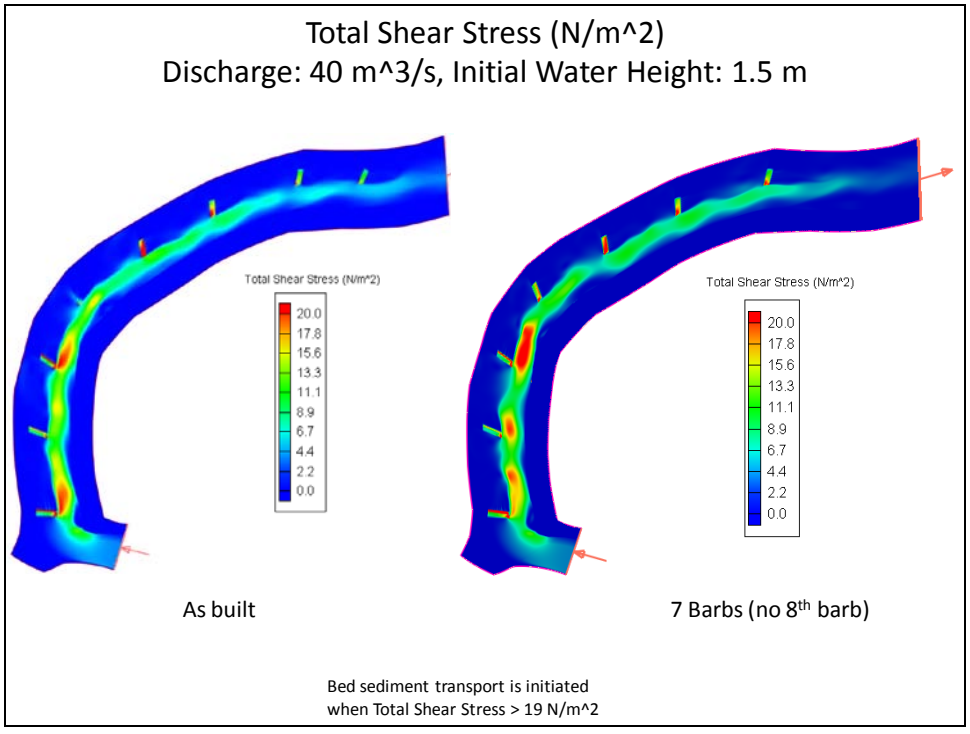


**Figure 39 – Total Shear Stress (N/m$^2$), Q= 40 m$^3$/s, h= 1.5 m, As built and theoretic 7 barbs configuration (no 8$^{th}$ barb)**

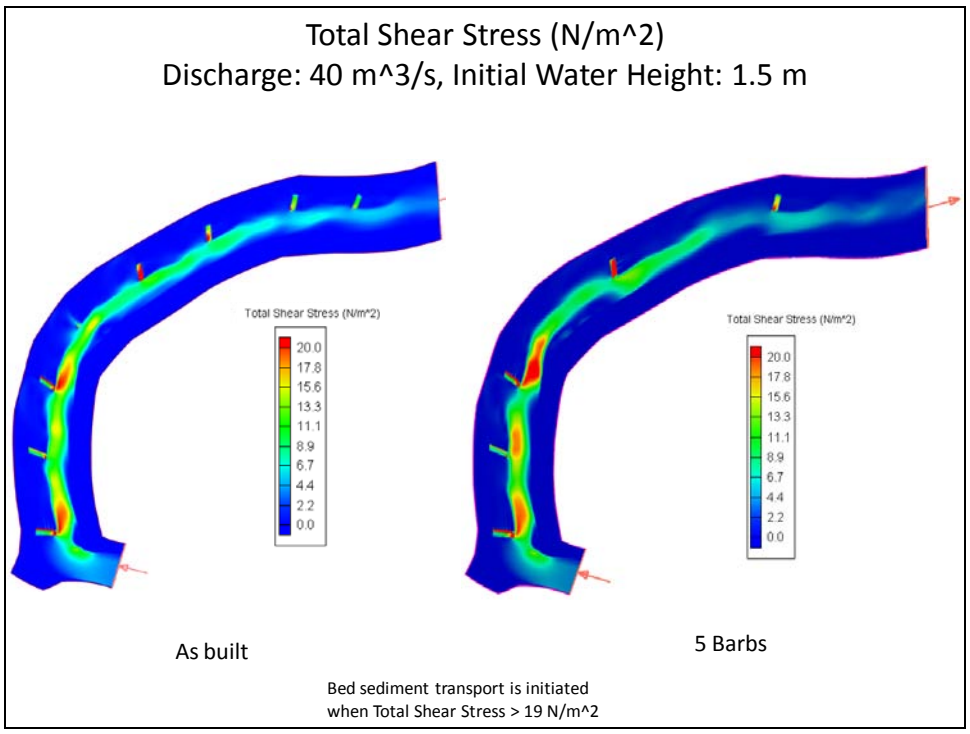


**Figure 40– Total Shear Stress (N/m$^2$), Q= 40 m$^3$/s, h= 1.5 m, As built and theoretic 5 barbs configuration (no 4$^{th}$, 6$^{th}$, and 8$^{th}$ barbs)**

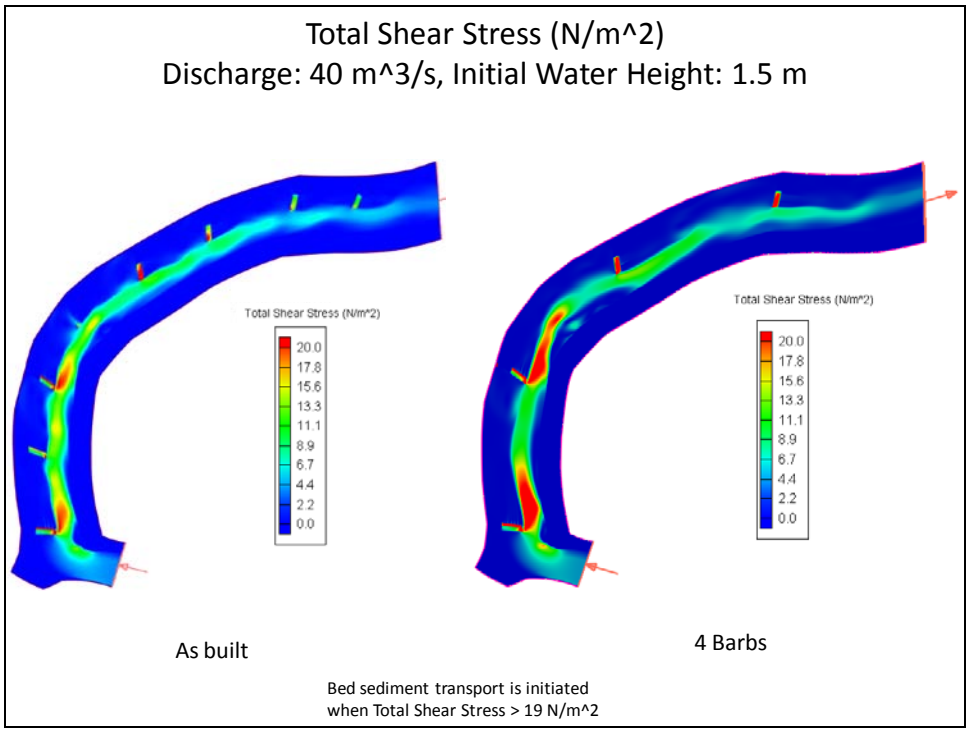


**Figure 41– Total Shear Stress (N/m$^2$), Q= 40 m$^3$/s, h= 1.5 m, As built and theoretic 4 barbs configuration (no 2$^{nd}$, 4$^{th}$, 6$^{th}$, and 8$^{th}$ barbs)**

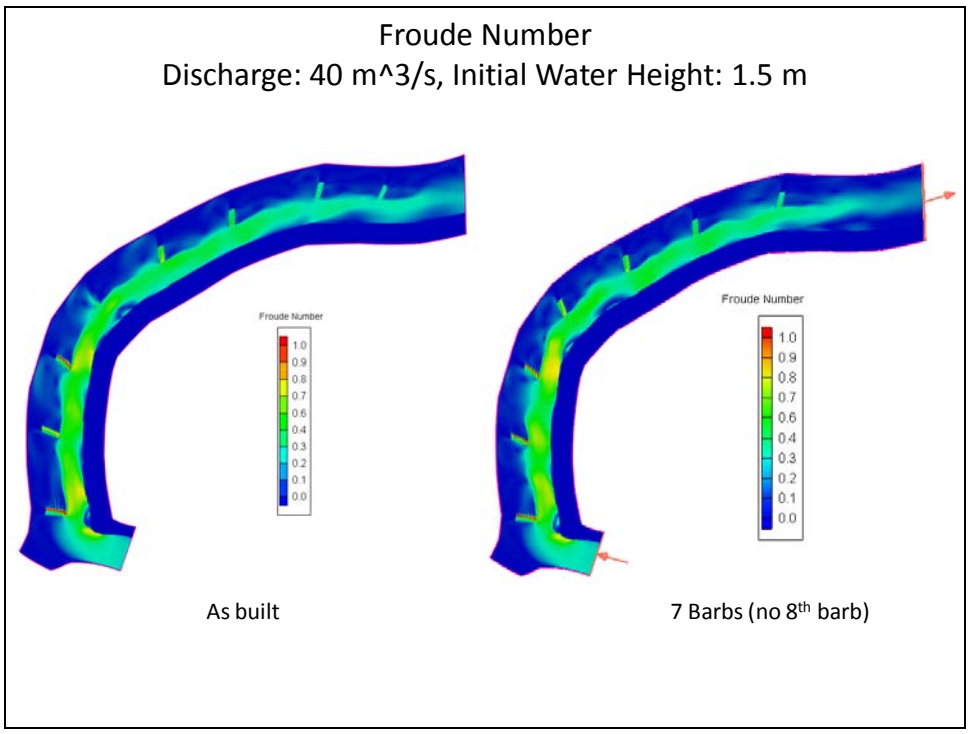


**Figure 42 – Froude Number, Q= 40 $m^3/s$, h= 1.5 m, As built and theoretic 7 barbs configuration (no 8th barb)**

### 5.9.3 Sag River: 7, 5, and 4 barbs, 300 $m^3/s$

Figure 43, Figure 44, Figure 45, and Figure 46 show the total shear stress in $N/m^2$ for year 2006 for 8 barbs (left of the graph) and 7, 5, and 4 barbs (right of the graph) with a simulated discharge of 300 $m^3/s$. The simulation results show increased shear stress for configurations of fewer than 8 barbs. Total shear stress simulations depict the first and second barbs as critical to the performance of the rest of the barbs, the first barb being most critical. Specifically, Figure 43 shows direct flow impacting on the left bank. In addition, flow configuration generates favorable conditions for generalized river bed erosion along the river reach. Thus, stability issues could appear on the left bank and potentially on other barbs. Figure 46 indicates zones near the bank with high shear stress downstream of barb 1, and consequently, river bed erosion. As the flow is subcritical (Figure 47), the removal of any barb propagates information in both directions (i.e., upstream and downstream). The reader should refer to Appendix E for the full set of the CCHE2D model results.

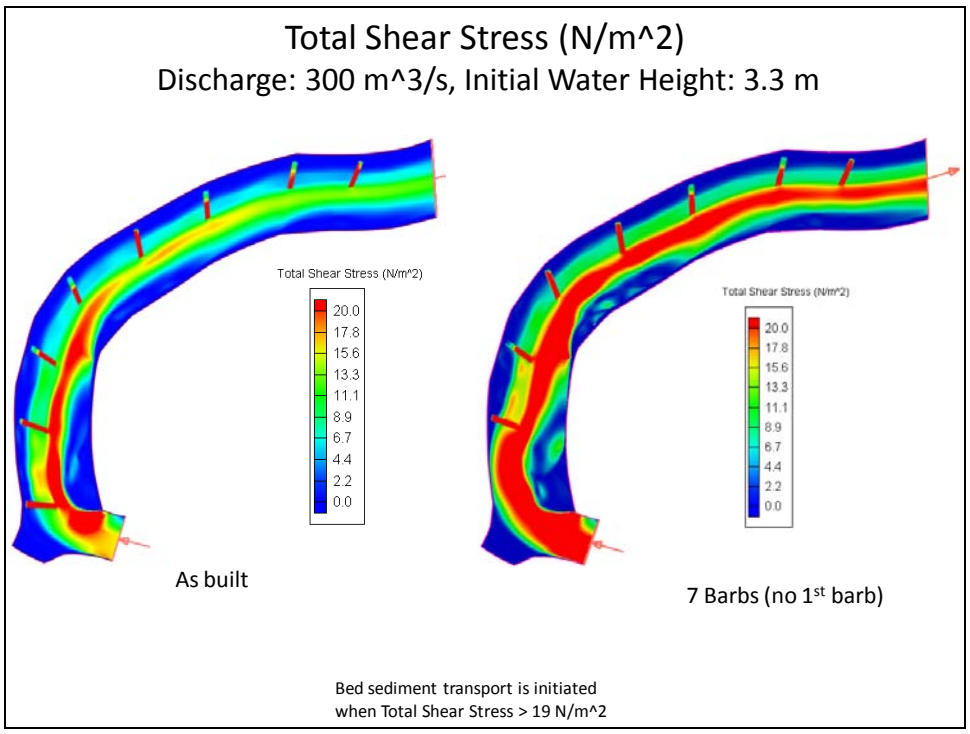


**Figure 43 – Total Shear Stress (N/m$^2$), Q= 300 m$^3$/s, h= 3.3 m, As built and theoretic 7 barbs configuration (no 1$^{st}$ barb)**

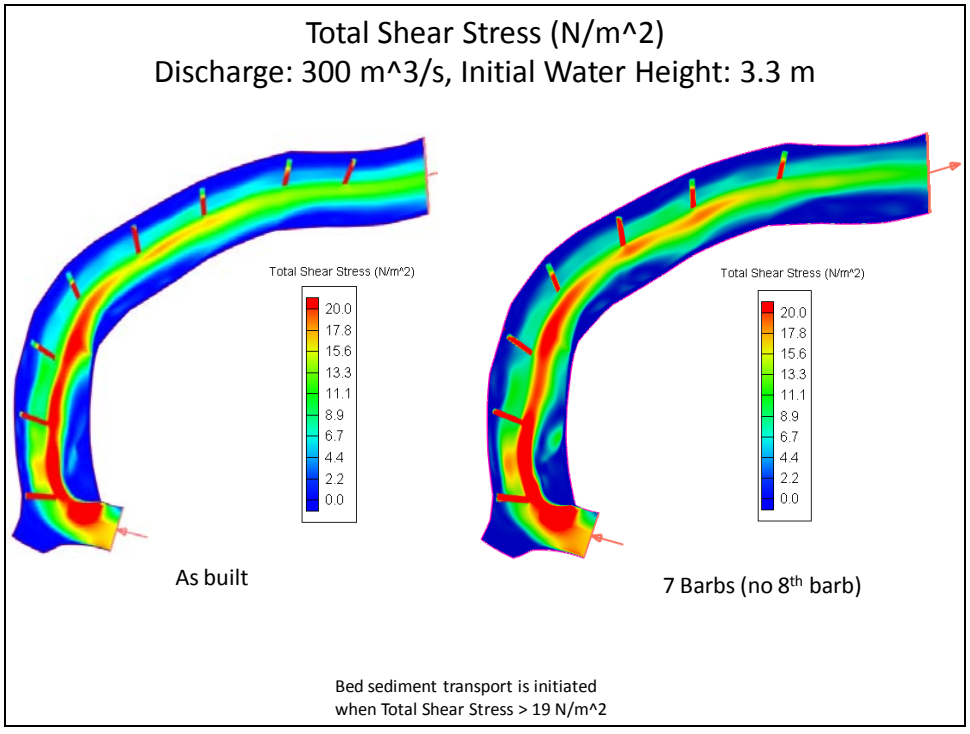


**Figure 44 – Total Shear Stress (N/m$^2$), Q= 300 m$^3$/s, h= 3.3 m, As built and theoretic 7 barbs configuration (no 8$^{th}$ barb)**

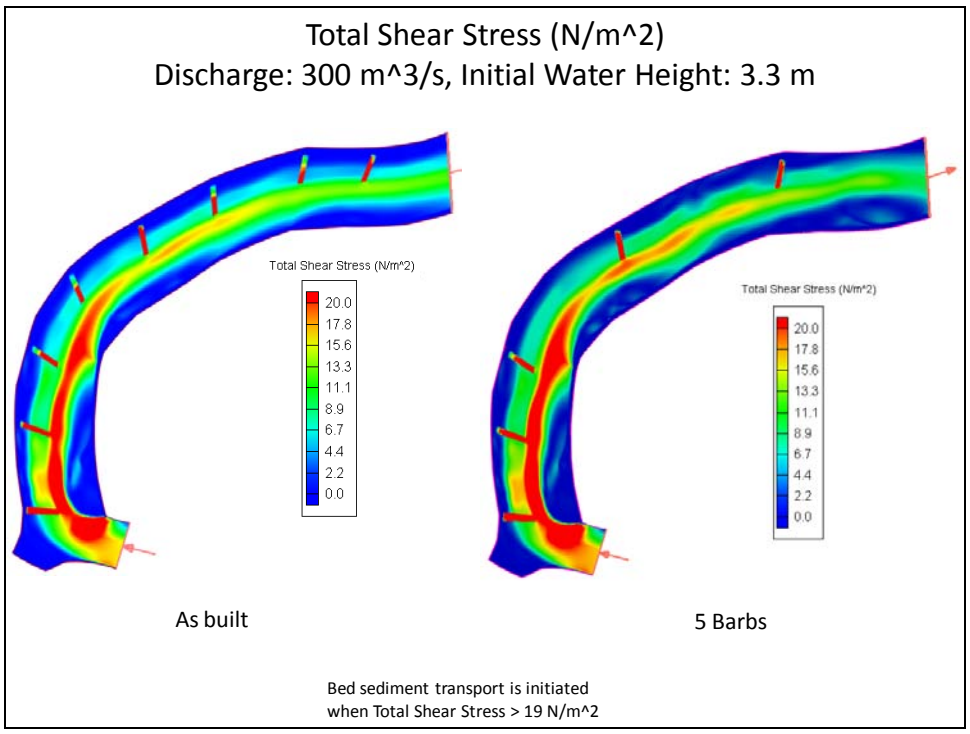


**Figure 45– Total Shear Stress (N/m$^2$), Q= 300 m$^3$/s, h= 3.3 m, As built and theoretic 5 barbs configuration (no 4$^{th}$, 6$^{th}$, and 8$^{th}$ barbs)**

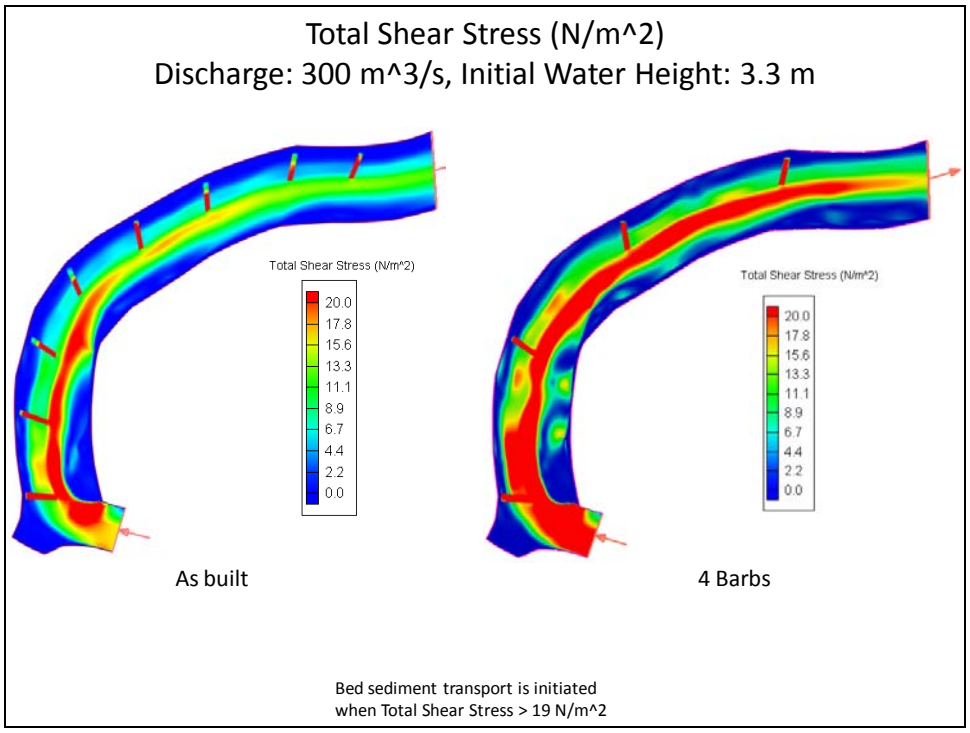


**Figure 46 – Total Shear Stress (N/m$^2$), Q= 300 m$^3$/s, h= 3.3 m, As built and theoretic 4 barbs configuration (no 2$^{nd}$, 4$^{th}$, 6$^{th}$, and 8$^{th}$ barbs)**

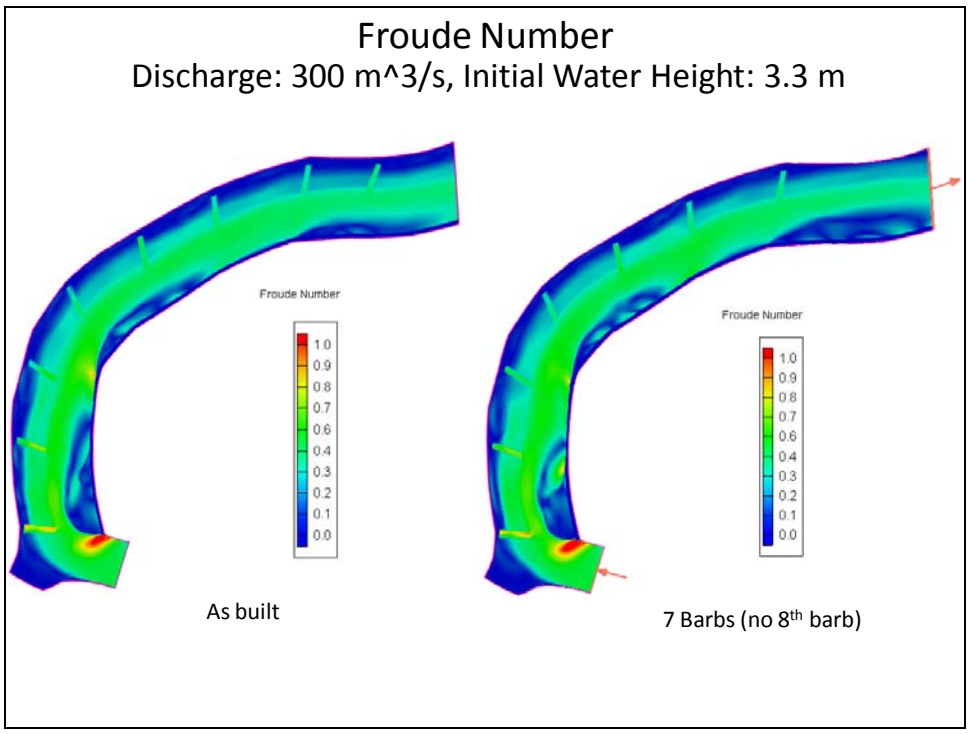


**Figure 47 – Froude Number, Q= 300 $m^3/s$, h= 3.3 m, As built and theoretic 7 barbs configuration (no 8th barb)**

### 5.9.4 Hess Creek: 95.57 $m^3/s$

Bankfull discharge for the Hess Creek in the study area is 95.57 $m^3/s$ (Lai, personal communication). Thus, model simulations were performed using that discharge.

Figure 48 shows the bathymetries for Hess Creek for years 2004 and 2009. The simulation results show that from 2004 to 2009 the thalweg was diverted from the right bank (Figure 49). At simulated bankfull conditions (discharge = 95.57 $m^3/s$, initial water height = 142.9 m over sea level), the model indicates that erosion should be expected at the thalweg due to high shear stress values (Figure 50). As helicoidal flow cannot be simulated by CCHE2D, simulations could not reproduce original flow conditions at the right bank. The reader should refer to Appendix E for the full set of the CCHE2D model results.

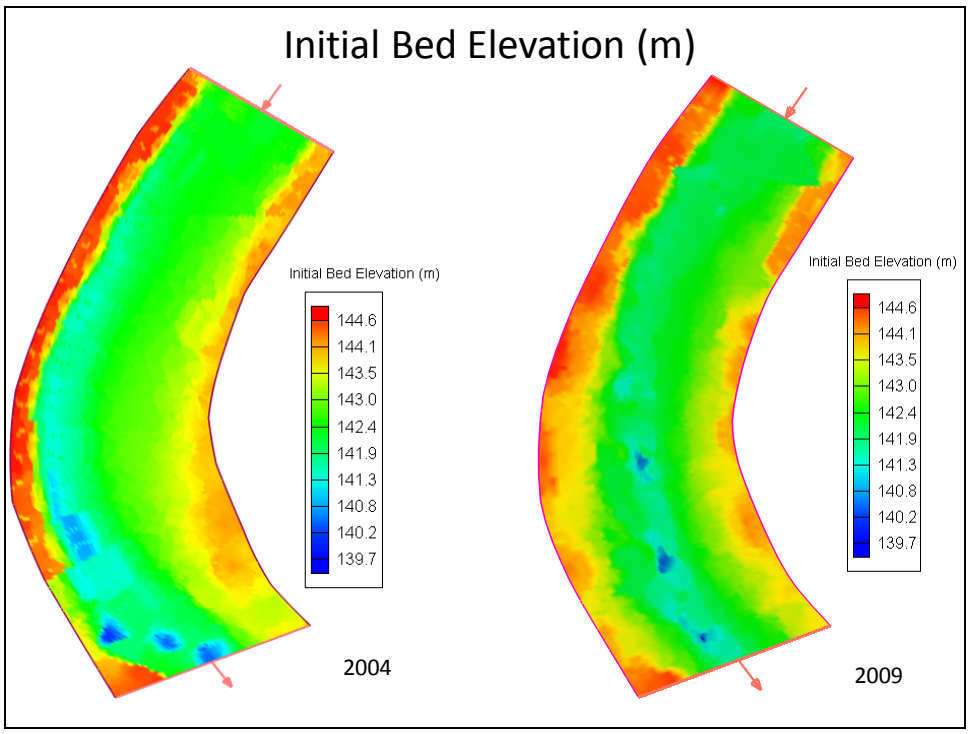


**Figure 48 – Initial Bed Elevation (m), Q= 95.57 $m^3/s$, h= 142.9 m. 2004 and 2009**

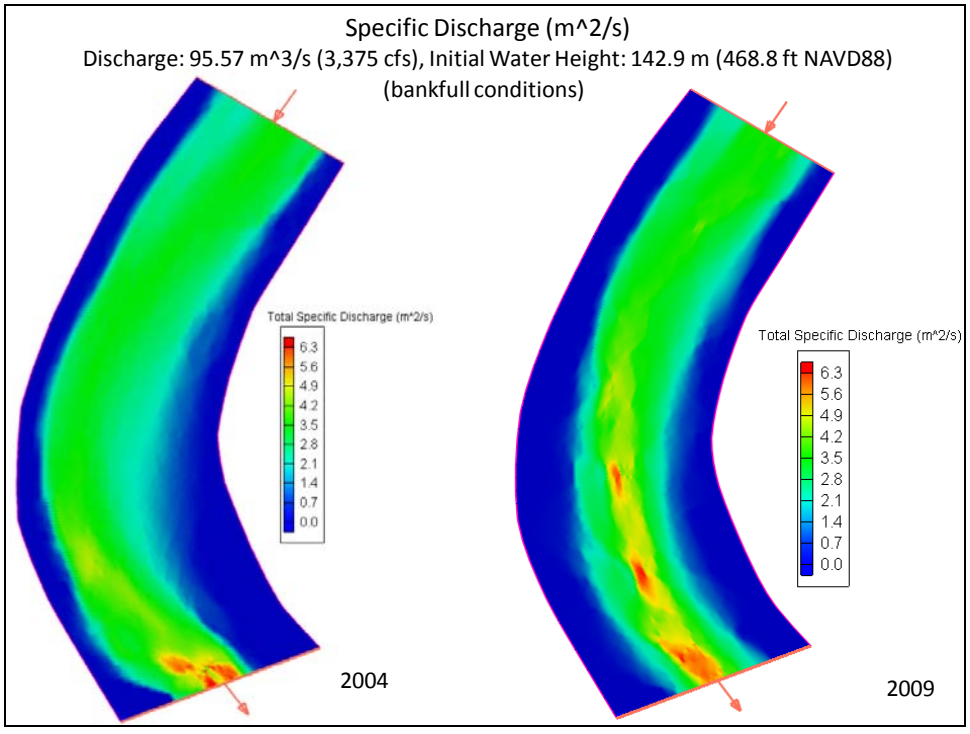


**Figure 49 – Specific Discharge ($m^2/s$), Q= 95.57 $m^3/s$, h= 142.9 m. 2004 and 2009**

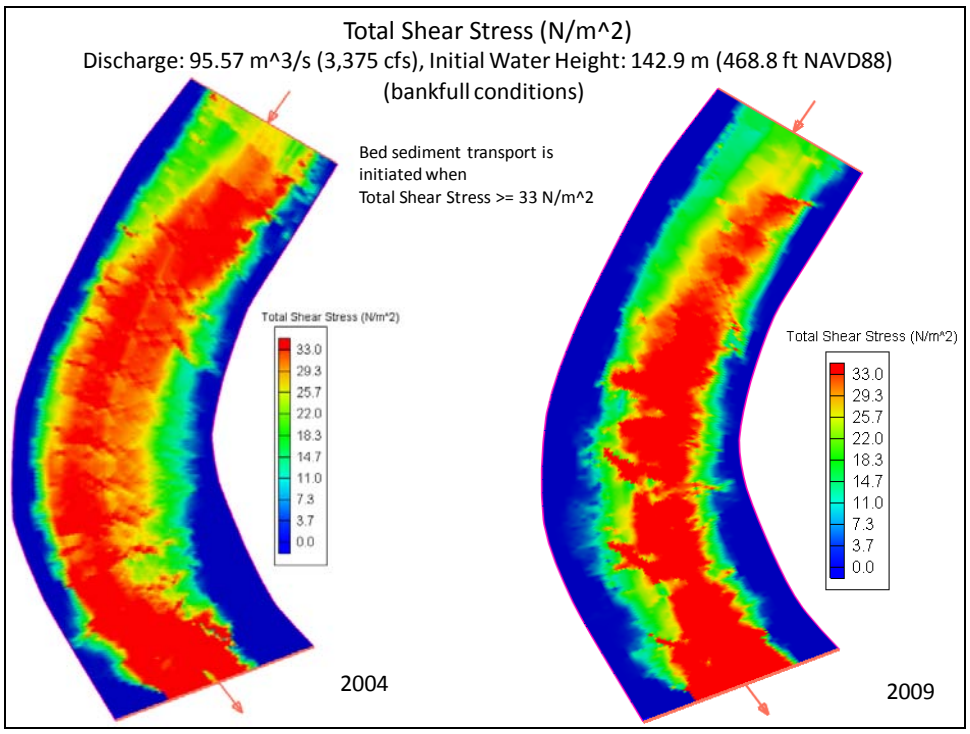


**Figure 50 – Total Shear Stress (N/m$^2$), Q= 95.57 m$^3$/s, h= 142.9 m. 2004 and 2009**

## 5.10 Model Validation

One could argue that model results were partially validated with field observation. However, additional model validations on different settings could be beneficial. To this end, several model applications done by other researchers are presented in the following section. In addition, the project team tested the model for a specific barb configuration. Details are provided in the section, Model Barb Experiment.

### 5.10.1 Simulated Settings

Several researchers performed extensive verification and validation tests to ensure that the numerical model and software implementation are capable of reproducing realistic flows in streams. The model was used to simulate flow conditions for the Lauffen Reservoir on the River Neckar, Germany, and in a meandering reach of the East Fork River in Wyoming, U.S.

Flow associated with in-stream hydraulic structures was simulated at multiple locations (Hotophia Creek, Victoria Bendway, Red River) in the Mississippi River, Louisiana, U.S., and downstream of Wanan Reservoir, Wanan River, China, for modeling flow in a channel reach with multiple dikes (Jia and Wang, 2001b).

### 5.10.2 Model Barb Experiment

Experiments on a physical barb model at laboratory scale were performed by Kjos (2003). These experiments were used as validation of CCHE2D simulation of open-channel flows and sediment-transport models in a channel with a stream barb as a bank-protection structure.

A 10.4 m long, 1.2 m wide, and 1.2 m deep recirculating flume was built, with a mobile bed installed for a scour experiment. The fully developed flow was determined to occur 6.7 m downstream from the inflow side of the box. The model setup was scaled with Froude similarity and roughness from a prototype stream located at the North Fork of the Toutle River in the state of Washington. This river has a multiple barb configuration along its course (Kjos, 2003).

Table 9 and 10 list barb and stream characteristics, respectively, for the experimental setup. Figure 51 shows the experimental model barb, and Figure 52 shows the flow around the barb looking downstream. Figure 53 shows the CCHE2D model barb initial elevation in m, and Figure 54 the simulated velocity magnitude around the barb, applying the same settings used for the physical barb model experiment.

**Table 9 – Barb Characteristics for Experimental Model Setup (Kjos, 2003)**

| Barb Characteristics | Value |
|---|---|
| Barb Tip | |
| Height (m) | 0.06 |
| Crest Width (m) | 0.34 |
| Slope | 2:1 |
| Main Body Section | |
| Height (m) | 0.12 |
| Crest Width (m) | 0.34 |
| Length (m) | 0.49 |
| Slope | 10:1 |
| Transition Section to Bank | |
| Height (m) | N/A |
| Crest Width (m) | 0.34 |
| Length (m) | 0.30 |
| Slope (m) | 4:1 to 5:1 |

Table 10 – Stream Characteristics for Experimental Model Setup (Kjos, 2003)

| Stream Characteristics | Value |
|---|---|
| Channel Geometry | |
| Channel Slope | 0.00450 |
| Bank Slope | N/A |
| Channel Width (m) | 1.22 |
| Channel Depth (m) | 0.1524 |
| Roughness Coefficient (n) | 0.0191 |
| Flow | |
| Discharge ($m^3/s$) | 0.034 |
| Velocity (m/s) | 0.183 |
| Sediment | |
| Median Particle Size (mm) | 7.1 |
| Specific Gravity | 2.65 |

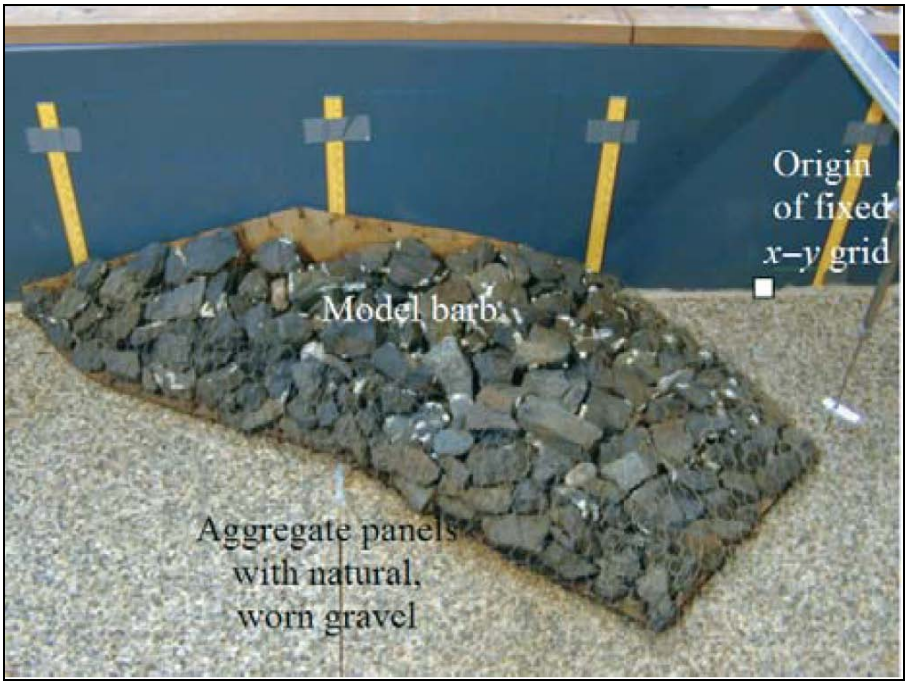


Figure 51 – Physical Model Barb View (Kjos, 2003)

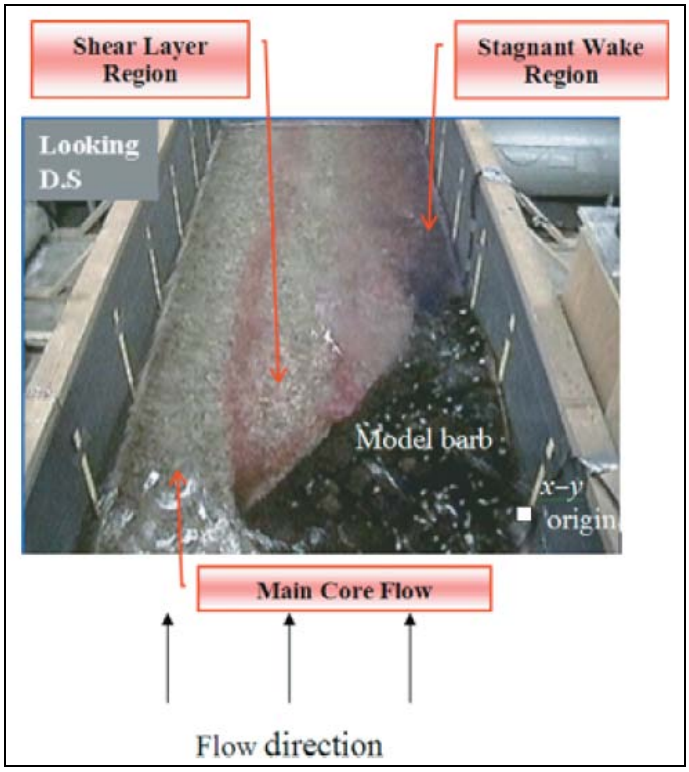


Figure 52 – Flow around the Partially Submerged Barb Looking Downstream (Kjos, 2003)

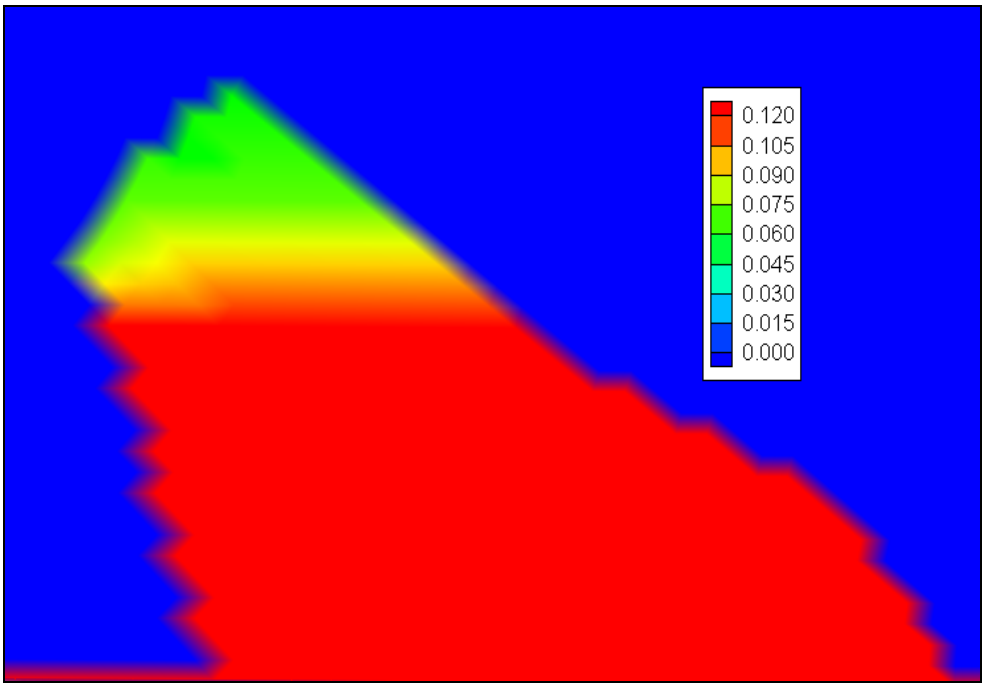


Figure 53 – CCHE2D Model Barb Initial Elevation (m)

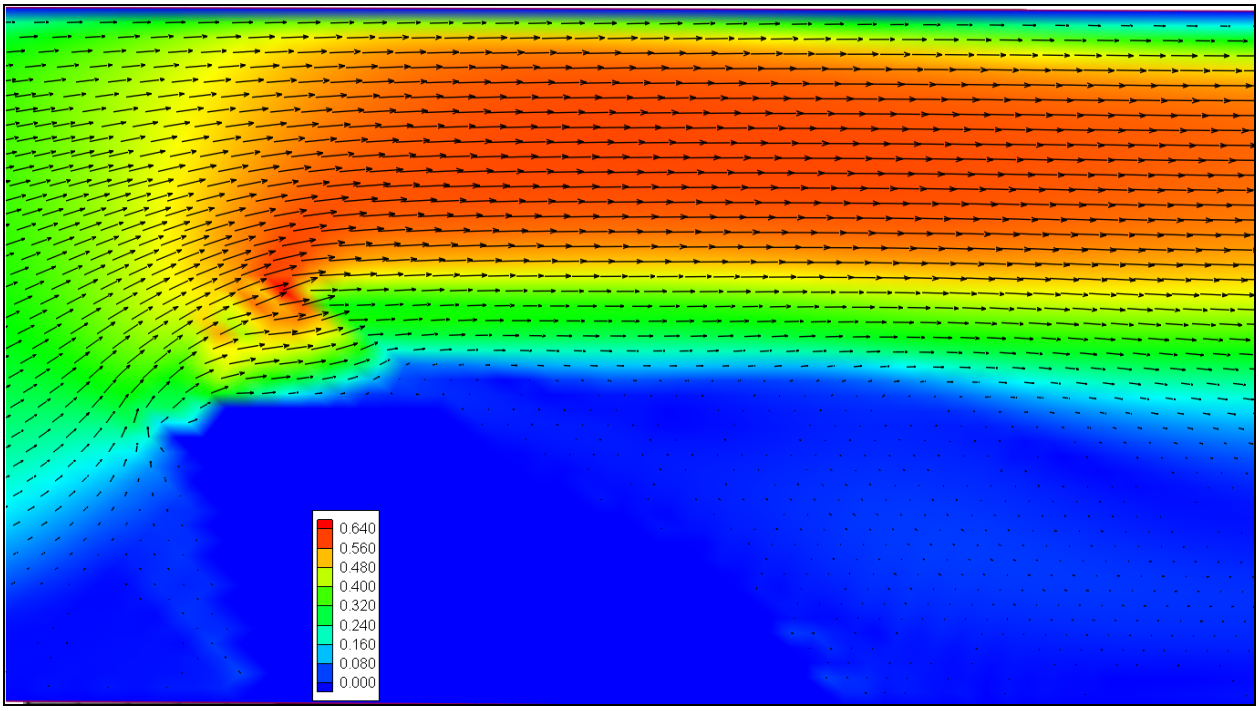


**Figure 54 – CCHE2D Model Barb Velocity Magnitude (m/s)**

The following parameters were used for both the experimental setup and the CCHE2D simulation (Figures 55a and 55b): Q=0.034 m3/s, water height= 0.1524 m, time= 870 min, d50= 7.1 mm.

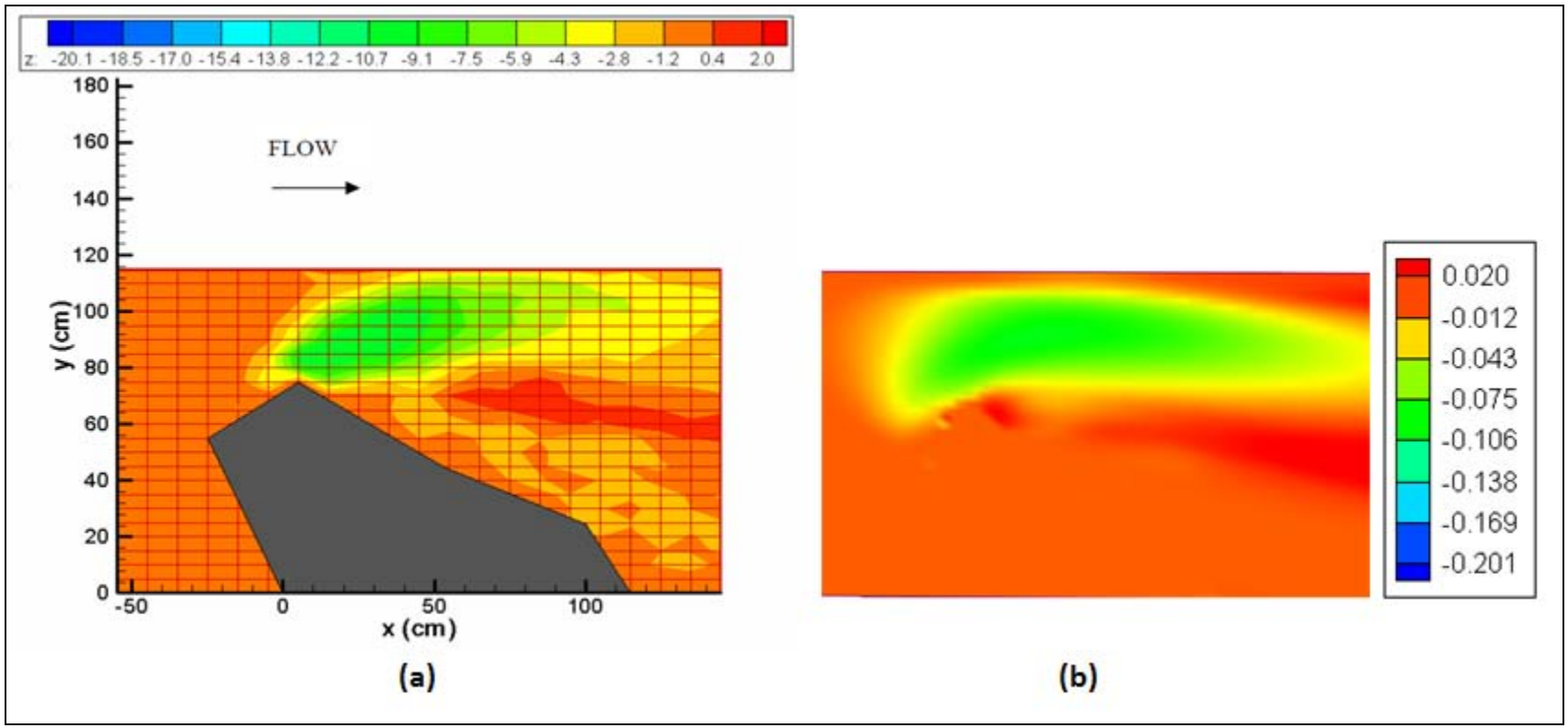


**Figure 55 – Total Scour and Deposition (Q=0.034 m3/s, water height= 0.1524 m, time= 870 min, d50= 7.1 mm): a) Physical Model Barb (cm). (Kjos, 2003); b) CCHE2D Model Simulation (m)**

## 5.11 Model Limitations

### 5.11.1 Secondary Flows

Being a two-dimensional model, CCHE2D cannot properly represent helicoidal flows, which develop on the outer slopes of river bends and could be an essential component in the formation of meanders (Tanner, 1960). In meandering channels, these secondary flows affect the distribution of primary velocity and bed-shear stress in a significant manner, and their velocities may constitute 10 to 20% of primary flow velocity (Pizzuto et al., 2008). To overcome this limitation, some researchers have incorporated special techniques into two-dimensional depth-averaged models to approximate secondary flows in bends (Spasojevic et al., 2008).

### 5.11.2 Runs Ended before Completion

Table 11 lists the simulation runs that terminated before completion. On these runs, the model could not converge to a solution for the given boundary conditions.

**Table 11 – Failed Runs for Sag River Simulation**

| Inlet (Discharge, $m^3/s$) | Outlet (Water Level Height, m) |
|---|---|
| 100 | 2.5 |
| 200 | 2.4 |
| 200 | 2.5 |
| 200 | 2.8 |
| 200 | 3.0 |
| 200 | 3.3 |
| 300 | 2.4 |
| 300 | 2.5 |
| 300 | 3.0 |
| 300 | 3.1 |
| 300 | 3.2 |

# 6. Conclusions and Recommendations

A combination of fieldwork, numerical modeling, and analysis were carried out in this research. Fieldwork consisted of bathymetric surveys and high-frequency velocity measurements in Fall, and breakup monitoring in the Sag River in Spring. Numerical modeling, a component that was not initially included in the project, proved to be the most important tool for the research team. Turbulence analysis provided insight on flow characteristics.

Velocity measurements indicate strong vertical currents in both directions near the scour holes located at the tip of the barbs (Sag River). Dimensional velocity graphs show flow similarity along the reach where vanes were installed (Hess Creek), indicating that the reach was in equilibrium at the time of measurements.

Comparison of the four time-lapse movies recorded during the Spring 2010 breakup shows that flow is diverted downstream from the left bank in the Sag River; for example, the first barb cannot be seen while the eighth barb is clearly visible. The breakup event was recorded on videos during the morning of May 25. The maximum river ice thickness was estimated to be from 10.5 to 13.1 in. (26.7 to 33.3 cm). Water level height ranged from 1.40 m (pre-breakup) to 3.30–3.50 m (breakup).

An existing two-dimensional model, the CCHE2D, was used in both streams to simulate several scenarios. The model was successfully validated with barb geometry built at laboratory scale at another university.

Simulation results for the Sag River show that the model properly simulates observed conditions during fieldwork conducted in August 2009 (40 $m^3$/s, water height: 1.5 m). A comparison between 2006 and 2009 model results shows that the flow is diverted from the left bank. The thalweg seems to be stable for the 2009 simulation.

Results of simulations of configurations with fewer than 8 barbs show an increased shear stress along the reach. Total shear stress simulations depict the first and second barbs as critical to the performance of the rest of the barbs, the first barb being the most critical. As the flow is subcritical, the removal of any barb propagates information upstream and downstream.

Simulations did not take into account a new channel-formation scenario and its possible effect on river flow conditions along the study area.

Simulation results for Hess Creek show that from 2004 to 2009, the thalweg was diverted from the right bank. At simulated bankfull conditions (discharge = 95.57 $m^3$/s, initial water height = 142.9 m), the model indicates that erosion should be expected at the thalweg due to high shear stress values. As helicoidal flow cannot be simulated, CCHE2D could not reproduce original flow conditions at the right bank.

Based on field measurements (Figures 24 and 25) and numerical simulations (Figures 35 and 49), one could conclude that both structures are accomplishing their design objective (i.e., moving the thalweg away from the bank). While the upstream barbs produce dramatic changes in flow direction, the design seems to promote fish habitat in winter (scour holes). However, the scour at the tip of the barb could impose stability concerns. Change in flow direction is gradual in the vanes, which in turns diminishes the scour holes.

Although no definitive conclusion can be made on the selection of a given approach (i.e., upstream barbs vs. vanes), the available information seems to indicate that upstream barbs would be preferred when designers need to consider overwinter fish conditions in the design. Also, engineers should pay special attention to the first and second barbs in future designs.

It is recommended that numerical modeling be applied in future bank-protection designs. It is envisioned that the model would allow testing several design alternatives, which in turn could improve the economics of the entire project. Additional bathymetric surveys (i.e., one survey every 2–4 years) are recommended to check river conditions.

## 7. Notation

The following symbols are used in this report:

$A_{xy}$ = adjustable coefficient of eddy viscosity;

$C_m$ = coefficient for the Mixing Length turbulence model;

$C_\mu$ = empirical constant for the $k$ – ε turbulence model;

$f_c$ = friction factor;

$f_{cor}$ = Coriolis parameter;

$g$ = gravitational acceleration;

$h$ = local water depth;

$K$ = von Karman constant;

$k$ = turbulent kinetic energy;

$k_s$ = bed surface roughness height;

$\bar{l}$ = mixing length;

$n$ = Manning coefficient;

$t$ = time;

$U$ = magnitude of the depth-integrated velocity components $u$ and $v$;

$U^*$ = shear velocity;

$u,v$ = depth-integrated velocity components in the $x$ and $y$ directions respectively;

$x,y,z$ = Cartesian coordinates directions;

$z_0$ = zero-velocity level;

$Z$ = water surface elevation;

$\varepsilon$ = rate of dissipation of turbulent energy;

$\nu$ = fluid kinematic viscosity;

$\nu_t$ = eddy viscosity;

$\frac{\partial \bar{U}}{\partial z}$ = depth integrated velocity gradient along the vertical coordinate;

$\rho$ = water density;

$\tilde{\phi}$ = depth-integrated variable of a three-dimensional variable $\phi$

$\tau_{bx}$, $\tau_{by}$ = shear stresses on the bed surface;

$\tau_{xx}$, $\tau_{xy}$, $\tau_{yx}$, $\tau_{yy}$ = depth integrated Reynolds stresses.

## 8. References

**Jia, Y., and Wang, S.** (1999). "Numerical Model for Channel Flow and Morphological Change Studies." *Journal of Hydraulic Engineering*, 125(9), 924–933.

**Jia, Y., and Wang, S.** (2001a). "CCHE2D: Two-dimensional Hydrodynamic and Sediment Transport Model for Unsteady Open Channel Flows Over Loose Bed." National Center for Computational Hydroscience and Engineering, Technical Report No. NCCHE-TR-2001-1, February.

**Jia, Y., and Wang, S.** (2001b). "CCHE2D Verification and Validation Tests Documentation." National Center for Computational Hydroscience and Engineering, Technical Report No. NCCHE-TR-2001-2, August.

**Jia, Y., Wang, S., and Yichun, X.** (2002). "Validation and Application of a 2D Model to Channels with Complex Geometry." *International Journal of Computational Engineering Science*, 3, 57–71.

**Kjos, L.J.** (2003). "Local Scour Around Barbs." M.S. diss., Washington State University.

**Lai, A., and Gaboury, M.** (2008). "Channel Realignment Using Natural Channel Design Principles." Ninth International Conference on Permafrost, 1015–1018.

**Langendoen, E.J.** (2001). "Evaluation of the effectiveness of selected computer models of depth-averaged free surface flow and sediment transport to predict the effects of hydraulic structures on river morphology." Project Report, USDA-ARS National Sedimentation Laboratory, Oxford M.S., October.

**Muste, M, Yu, K., Pratt, T., and Abraham, D.** (2004). Practical aspects of ADCP data use for quantification of mean river flow characteristics; Part II: Fixed-vessel measurements. *Flow Measurement and Instrumentation*, 15, 17–24.

**Odgaard, A.** (2009). "River Training and Sediment Management with Submerged Vanes." ASCE Press, 171 pp.

**Pizzuto, J.E., and ASCE Task Committee on Hydraulics, Bank Mechanics, and Modeling of River Width Adjustment.** (2008). "Streambank Erosion and River Width Adjustment." Ed. García, M.H. Sedimentation engineering: processes, measurements, modeling, and practice, ASCE Publications, 387–438.

**Spasojevic, M., and Holly, F.** (2008). "Two- and Three-Dimensional Numerical Simulation of Mobile-Bed Hydrodynamics and Sedimentation." Ed. García, M.H. Sedimentation engineering: processes, measurements, modeling, and practice, ASCE Publications, 683–761.

**Tanner, W.F.** (1960). "Helicoidal Flow, a Possible Cause of Meandering." *Journal of Geophysical Research*, 65(3), 993–995.

**Tennekes, U., and Lumley, J.** (1972). *A First Course in Turbulence*. MIT Press, Cambridge, MA.

**Thomas, W., and Chang, H.** (2008). "Computational Modeling of Sedimentation Processes." Ed. García, M.H.. Sedimentation engineering: processes, measurements, modeling, and practice, ASCE Publications, 649–681.

**Toniolo, H., Duvoy, P., Vanlesberg, S., and Johnson, J.** Article in press. "Modeling and Field Measurements in Support of the Hydrokinetic Resource Assessment for the Tanana River at Nenana, Alaska." *Journal of Power and Energy*.

**Tuthill, A.M.** (2008) “Ice Considerations in the Design of River Restoration Structures.” ERDC/CRREL TN-O8-2, U.S. Army Engineer Research and Development Center, Cold Regions Research and Engineering Laboratory, Hanover, New Hampshire, February.

**Water and Rivers Commission.** (2001). “Stream Stabilization.” Water and Rivers Commission, Government of Western Australia. River Restoration Report No. RR 10.

**White, K.D.** (2004) Method to estimate river ice thickness based on meteorological data. U.S. Army Engineer Research and Development Center, Hanover, New Hampshire, ERDC/CRREL Technical Note TN-04-3.

**Wu, W.** (2007). *Computational River Dynamics*. Taylor & Francis, November.

**Zhang, Y.** (2006). “CCHE-GUI – Graphical Users Interface for NCCHE Model User’s Manual – Version 3.0.” National Center for Computational Hydroscience and Engineering, Technical Report No. NCCHE-TR-2006-2, October.

**Zhang, Y., and Jia, J.** (2009). “CCHE-MESH: 2D Structured Mesh Generator User’s Manual – Version 3.x.” National Center for Computational Hydroscience and Engineering, Technical Report No. NCCHE-TR-2009-1, February.

# Appendix A – Turbulence Analysis Graphs

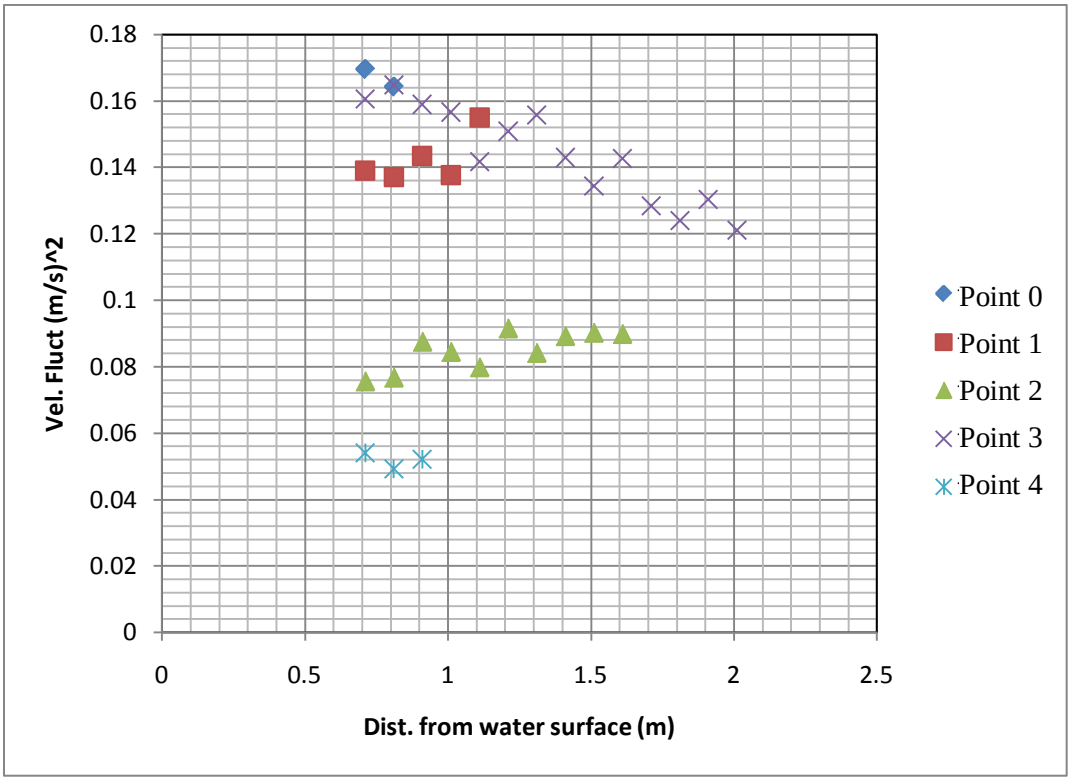


Figure 56 – East-East Velocity Fluctuations at Different Points of Sag River

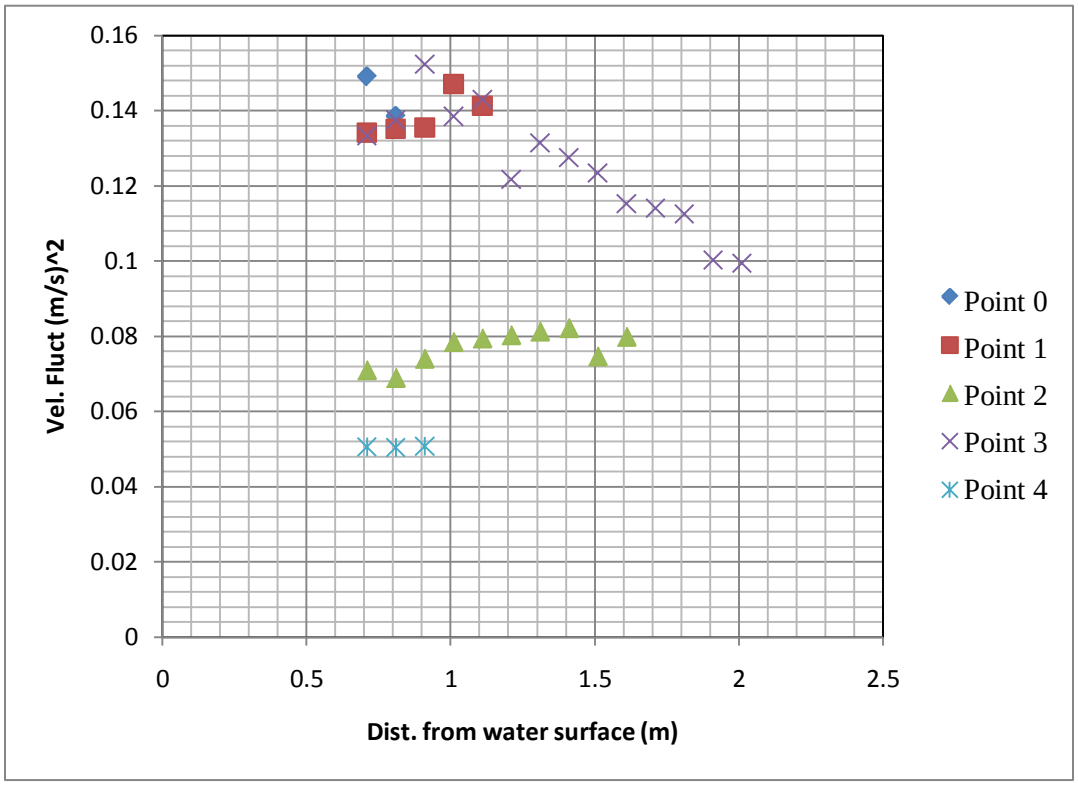


Figure 57 – North-North Velocity Fluctuations at Different Points of Sag River

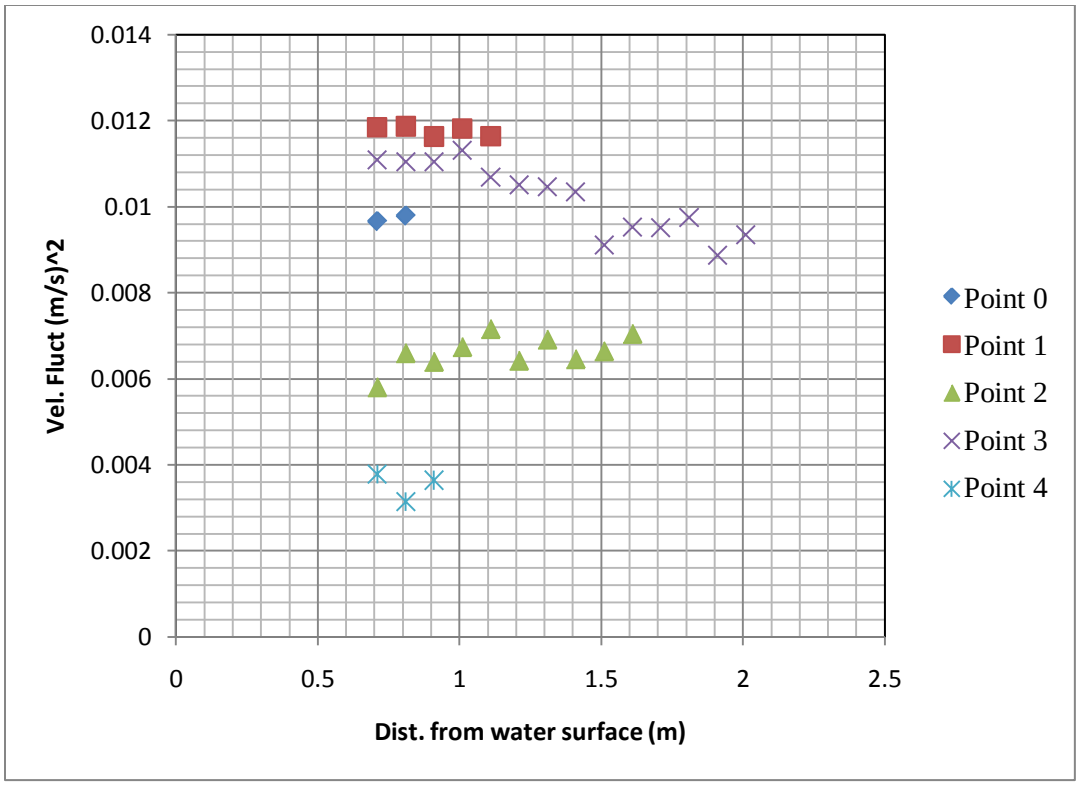


Figure 58 – Vertical-Vertical Velocity Fluctuations at Different Points of Sag River

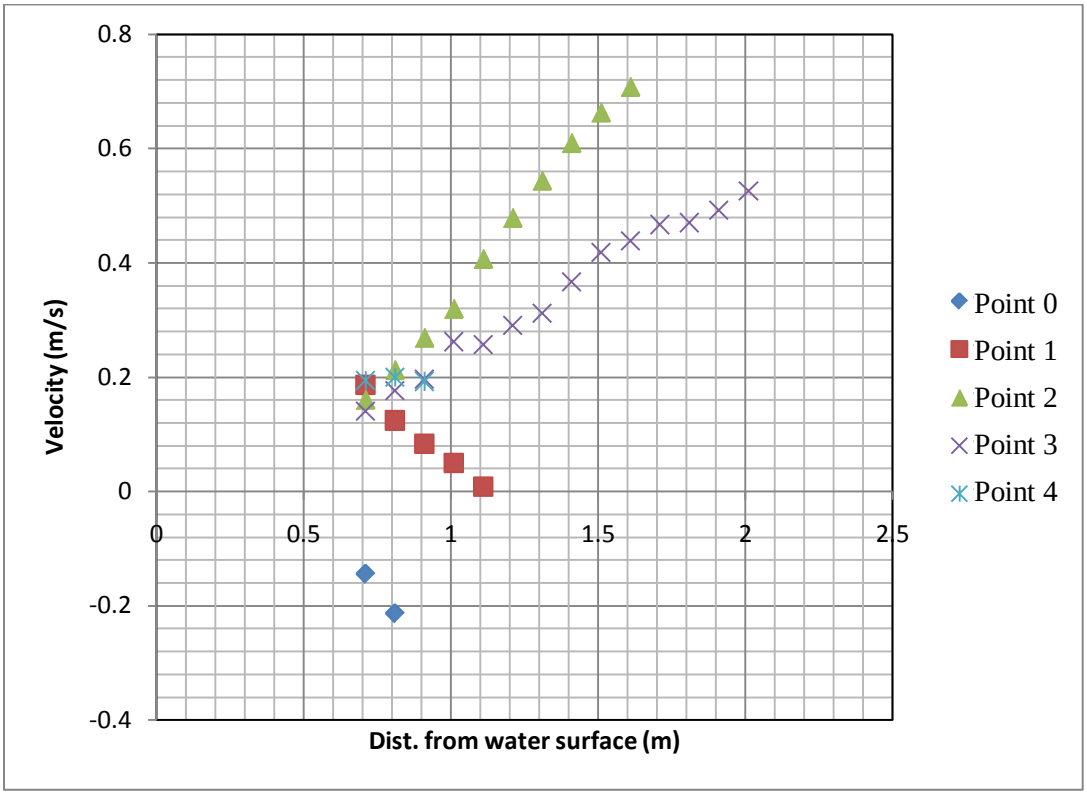


Figure 59 – East Velocity Fluctuations at Different Points of Sag River

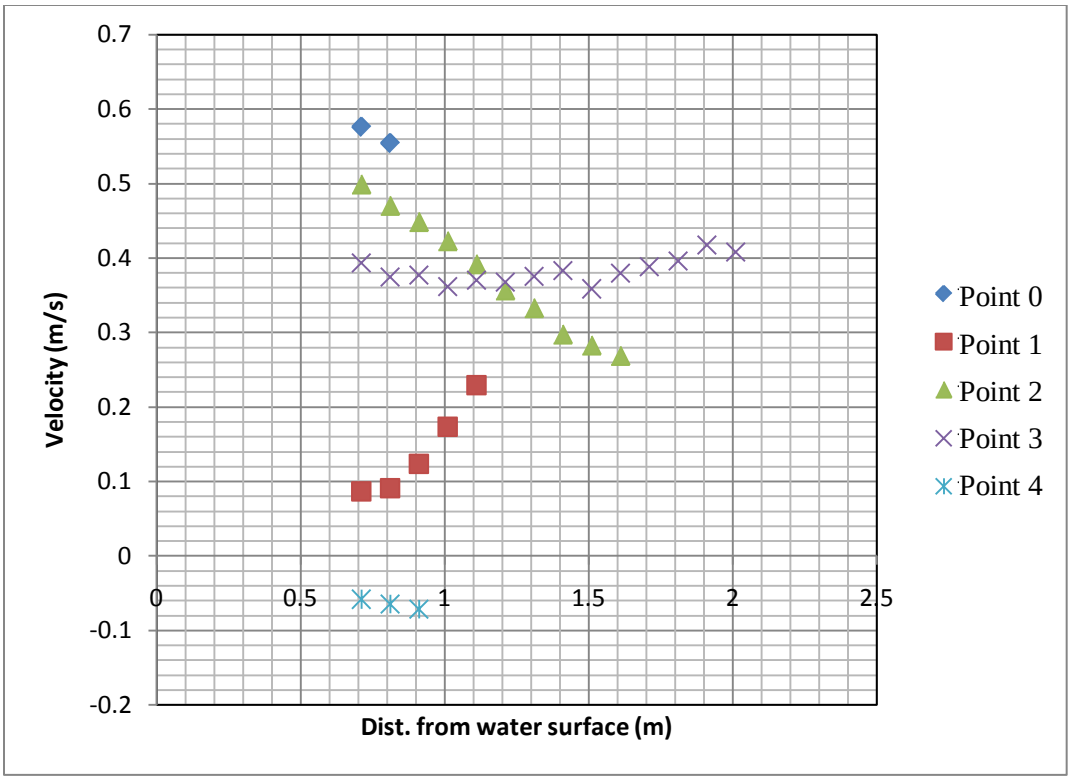


Figure 60 – North Velocity Fluctuations at Different Points of Sag River

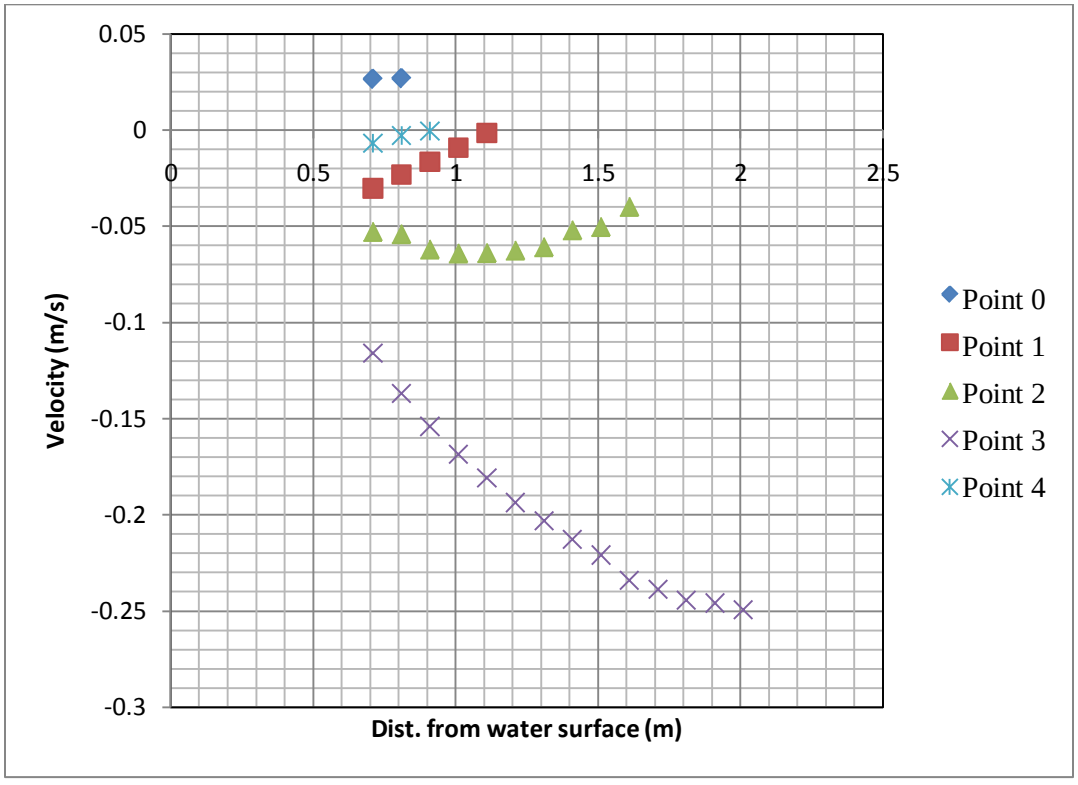


Figure 61 - Vertical Velocity Fluctuations at Different Points of Sag River

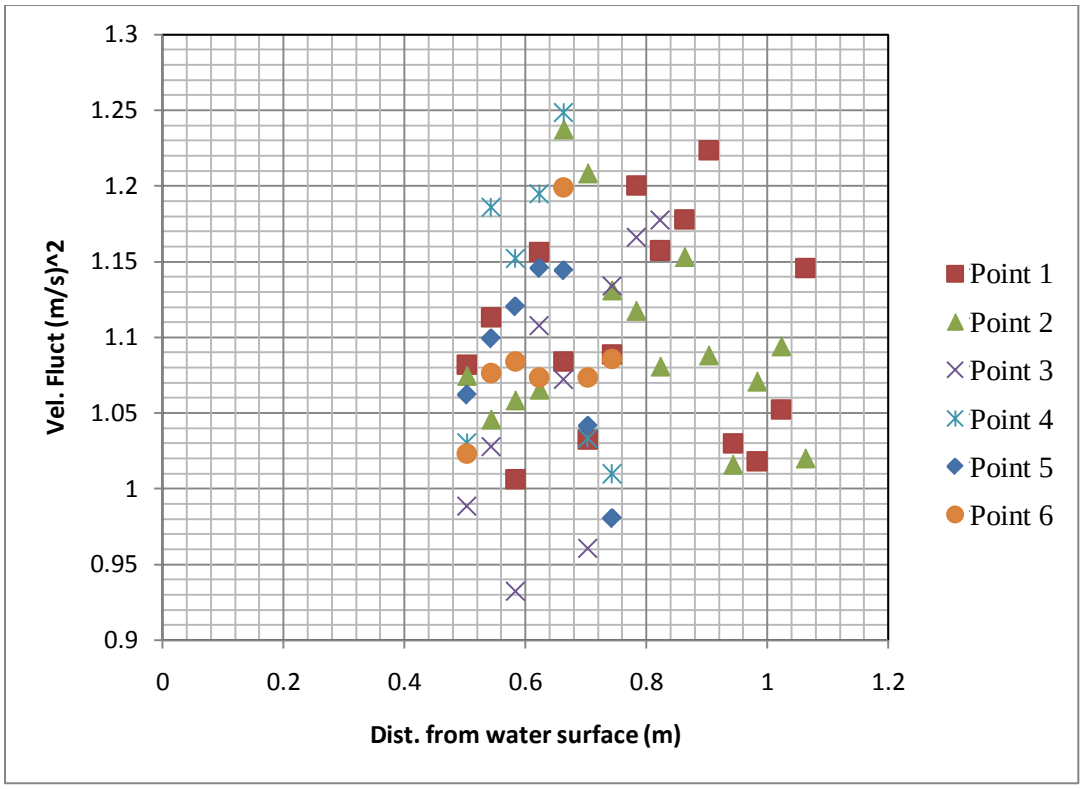


Figure 62 – East-East Velocity Fluctuations at Different Points of Hess Creek

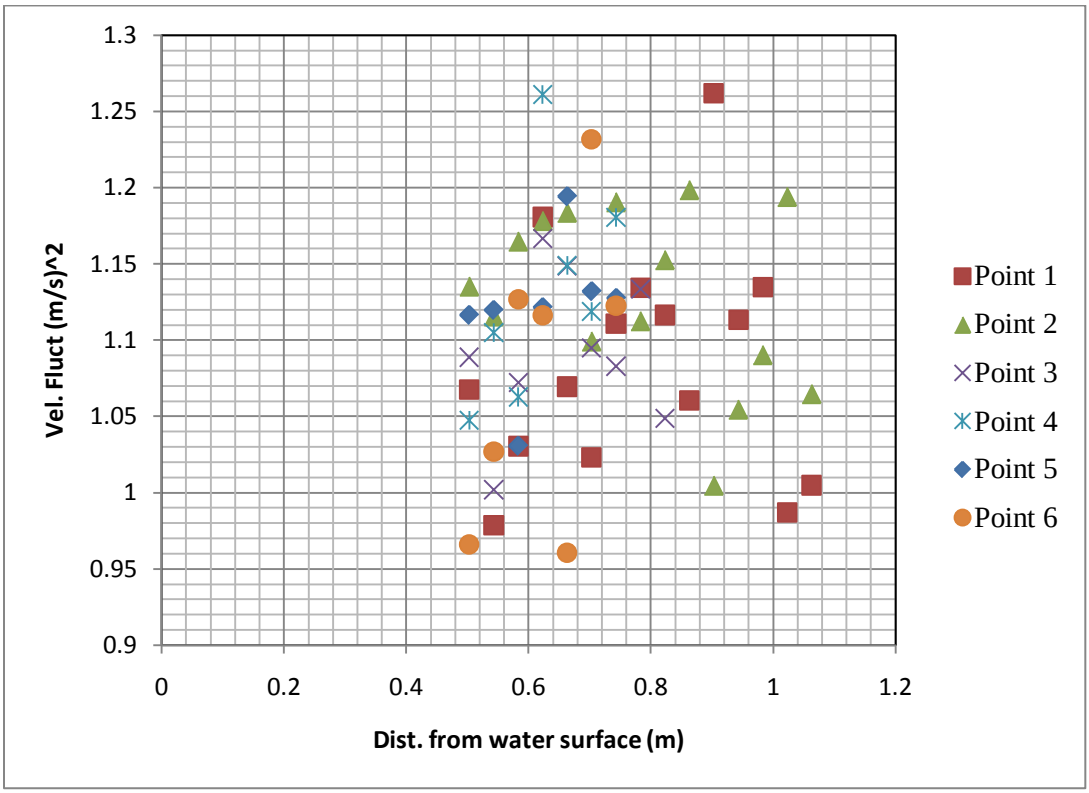


Figure 63 – North-North Velocity Fluctuations at Different Points of Hess Creek

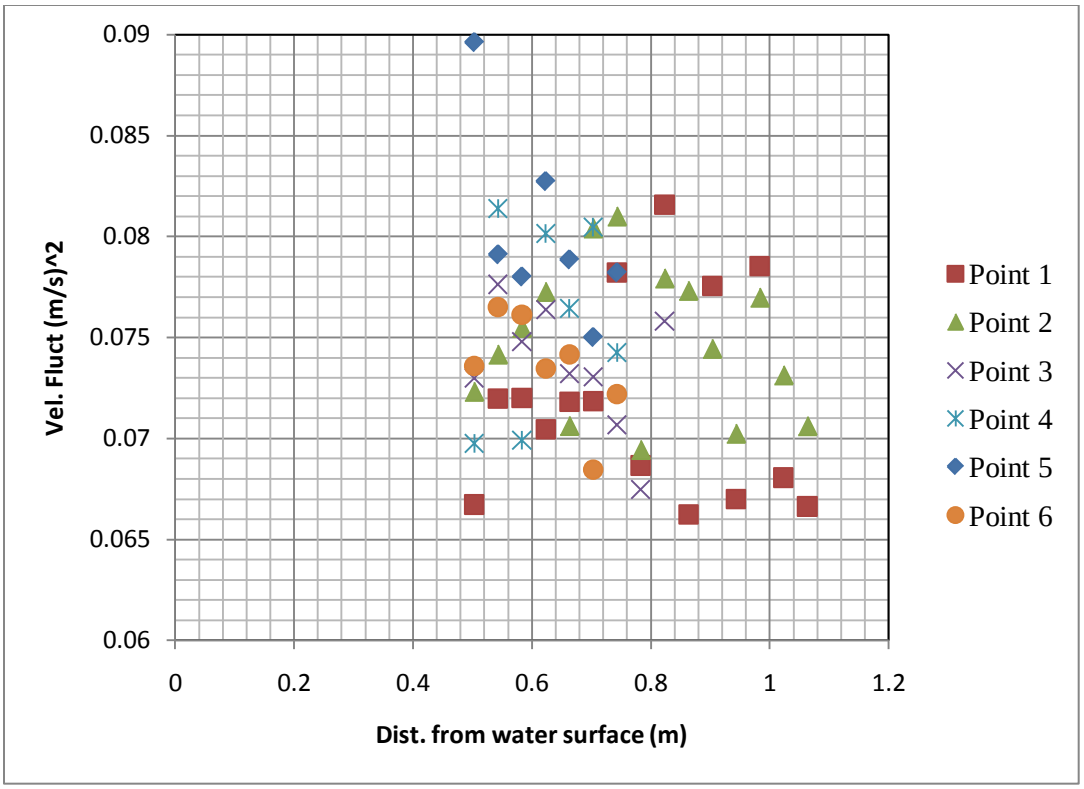


Figure 64 – Vertical-Vertical Velocity Fluctuations at Different Points of Hess Creek

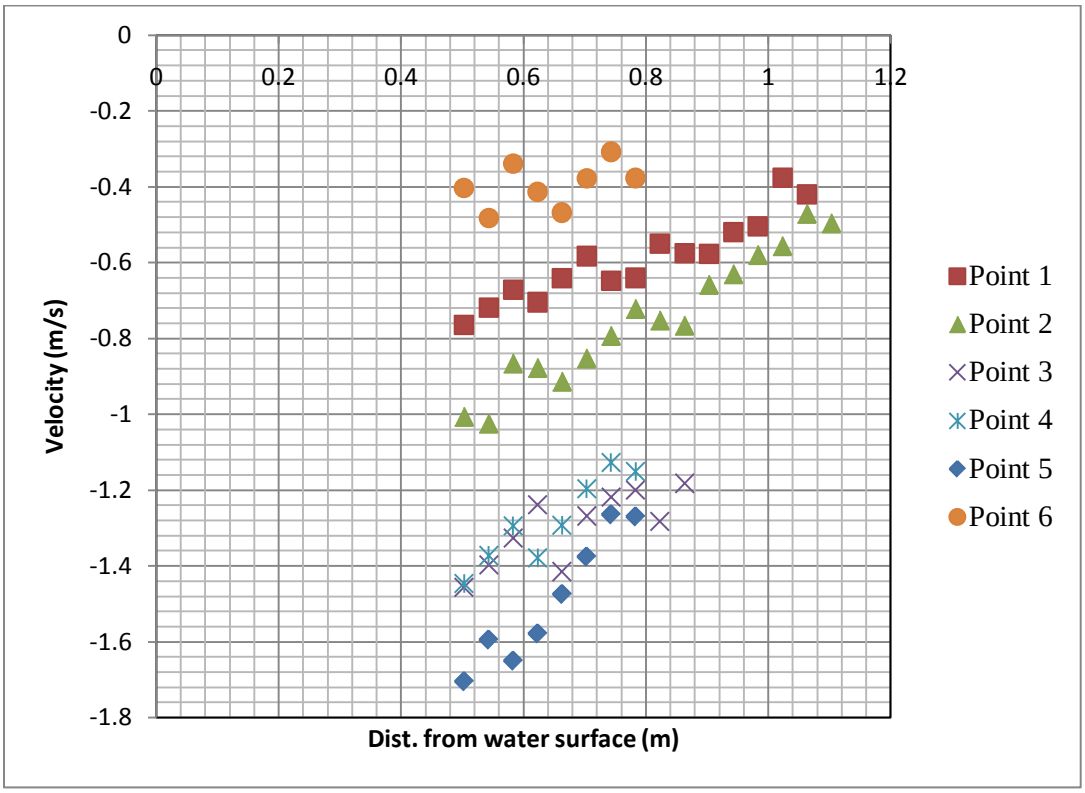


Figure 65 – East Velocity Fluctuations at Different Points of Hess Creek

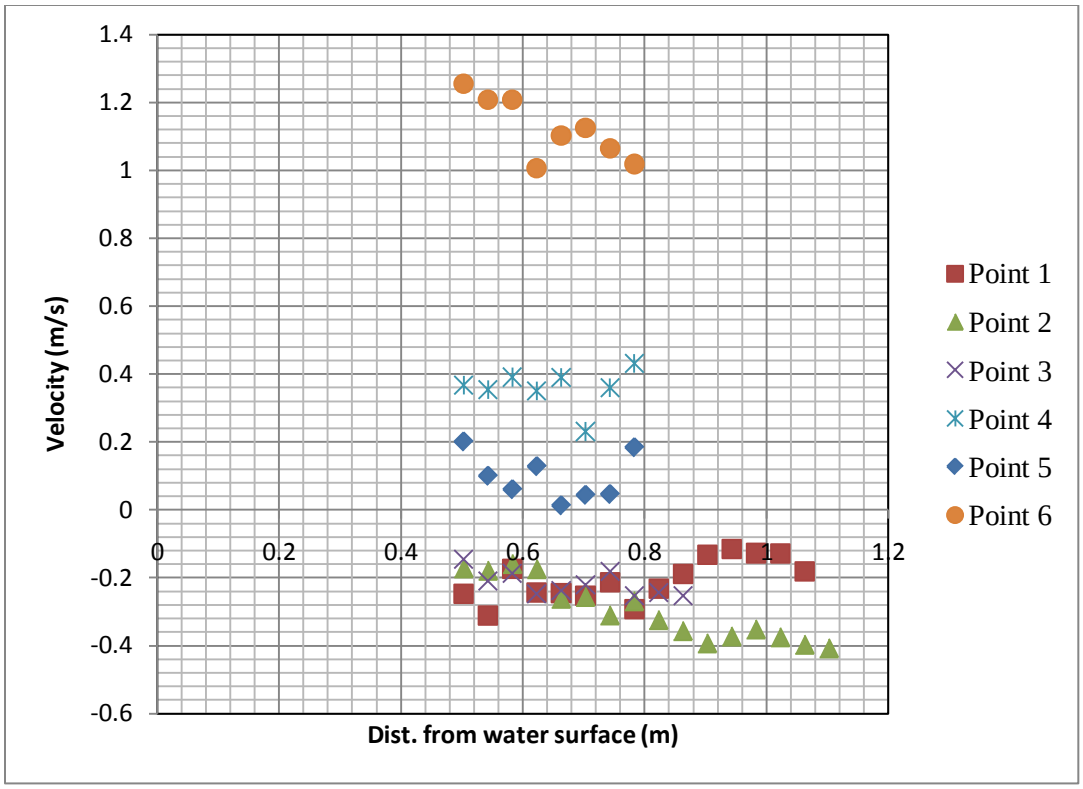


Figure 66 – North Velocity Fluctuations at Different Points of Hess Creek

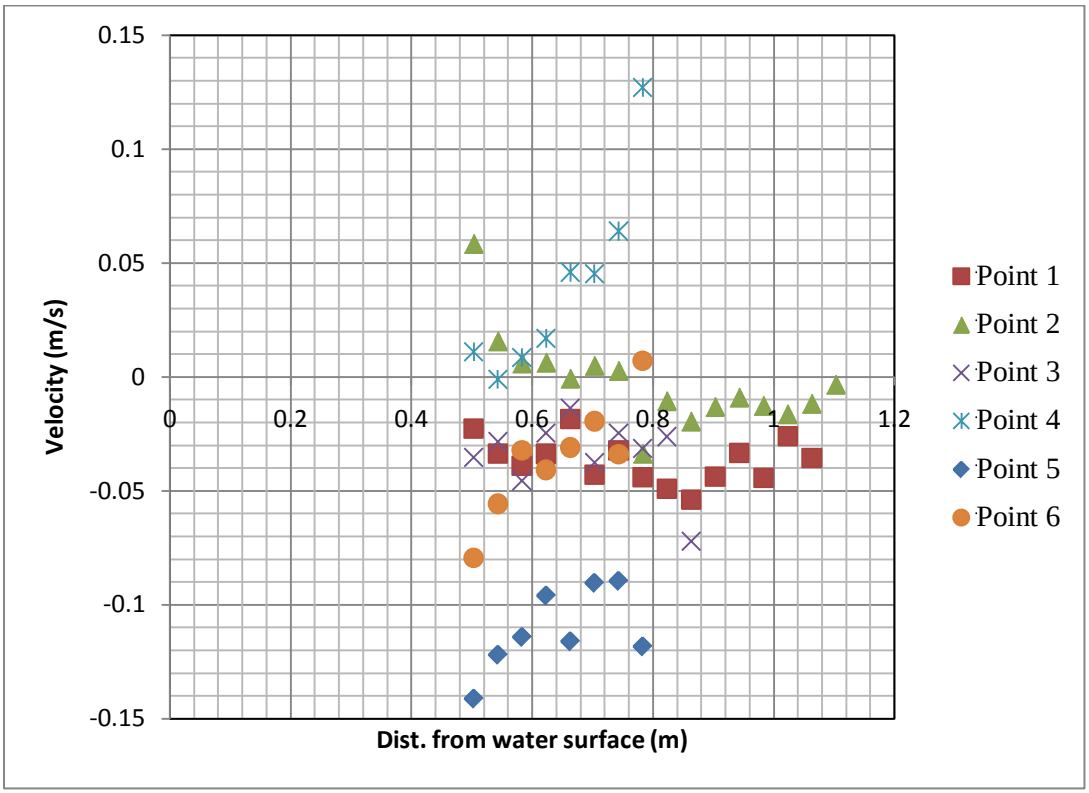


Figure 67 – Vertical Velocity Fluctuations at Different Points of Hess Creek

# Appendix B – Model Parameters

The following settings are configured through the CCHE-GUI menu (Figure 68): simulation, bed roughness, and advanced parameters. Figure 69, Figure 70, and Figure 71 show the screenshots with the default configuration for each setting, respectively.

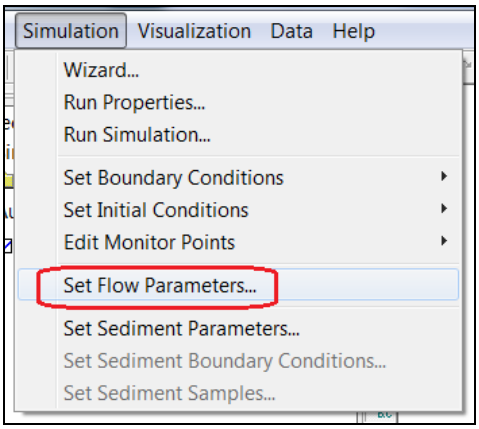


Figure 68 – Model Parameters Option

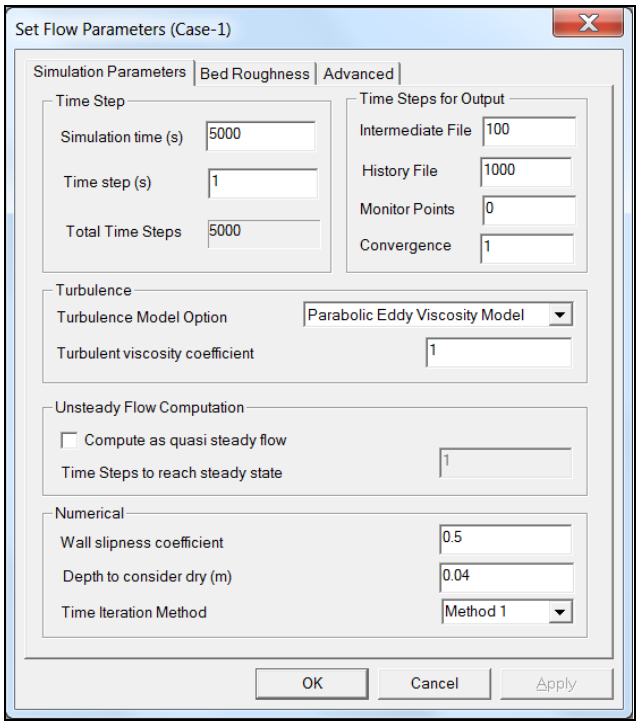


Figure 69 – Simulation Parameters

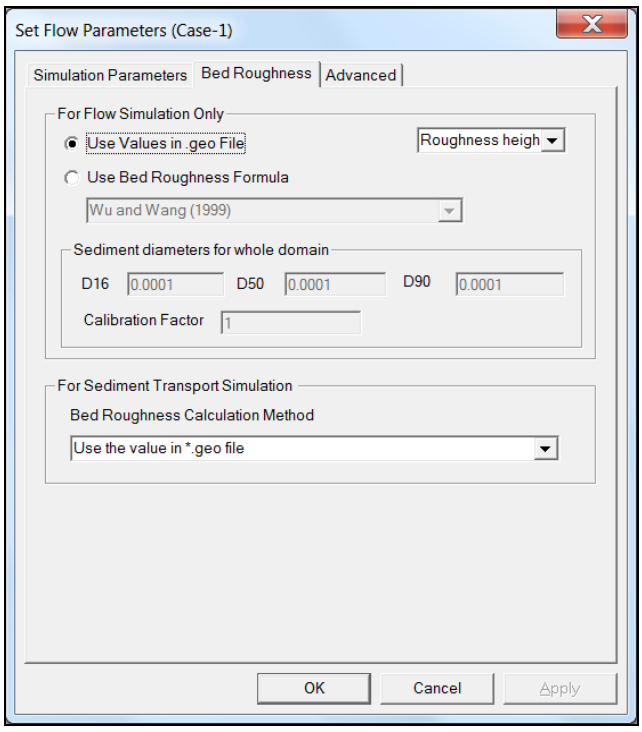


**Figure 70 – Roughness Parameters**

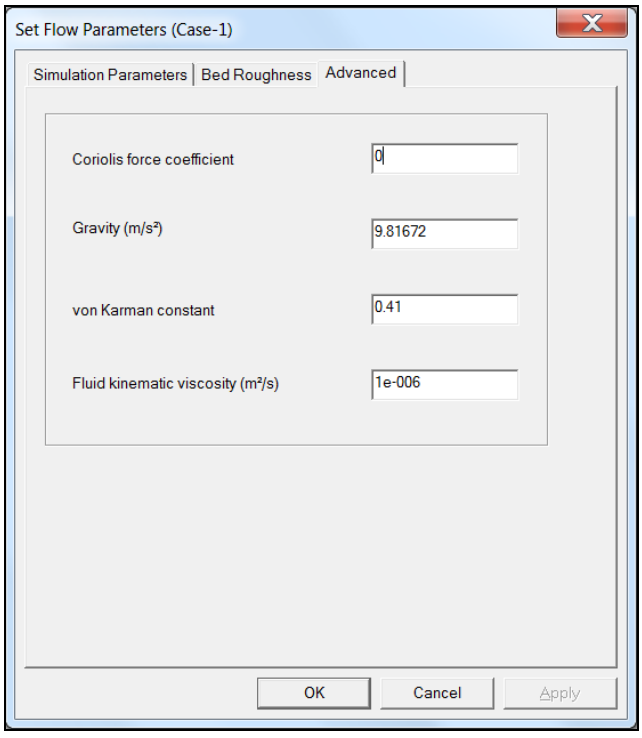


**Figure 71 – Advanced Parameters**

## Appendix C – Mesh and Bathymetry Generation Steps

Using CCHE-MESH, a two-boundary process is used to generate the algebraic mesh by placing an equal number of boundary control points along the domain to be discretized (Figure 72). A bitmap picture or map can be imported to assist with the control points positioning process. Each pair of boundary points gives shape to a control line (Figure 73) (Zhang and Jia, 2009).

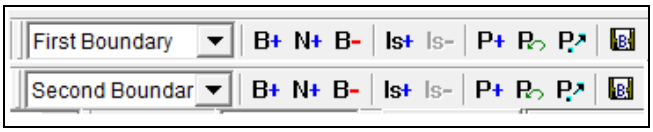


Figure 72 – CCHE-MESH tool to select boundary points

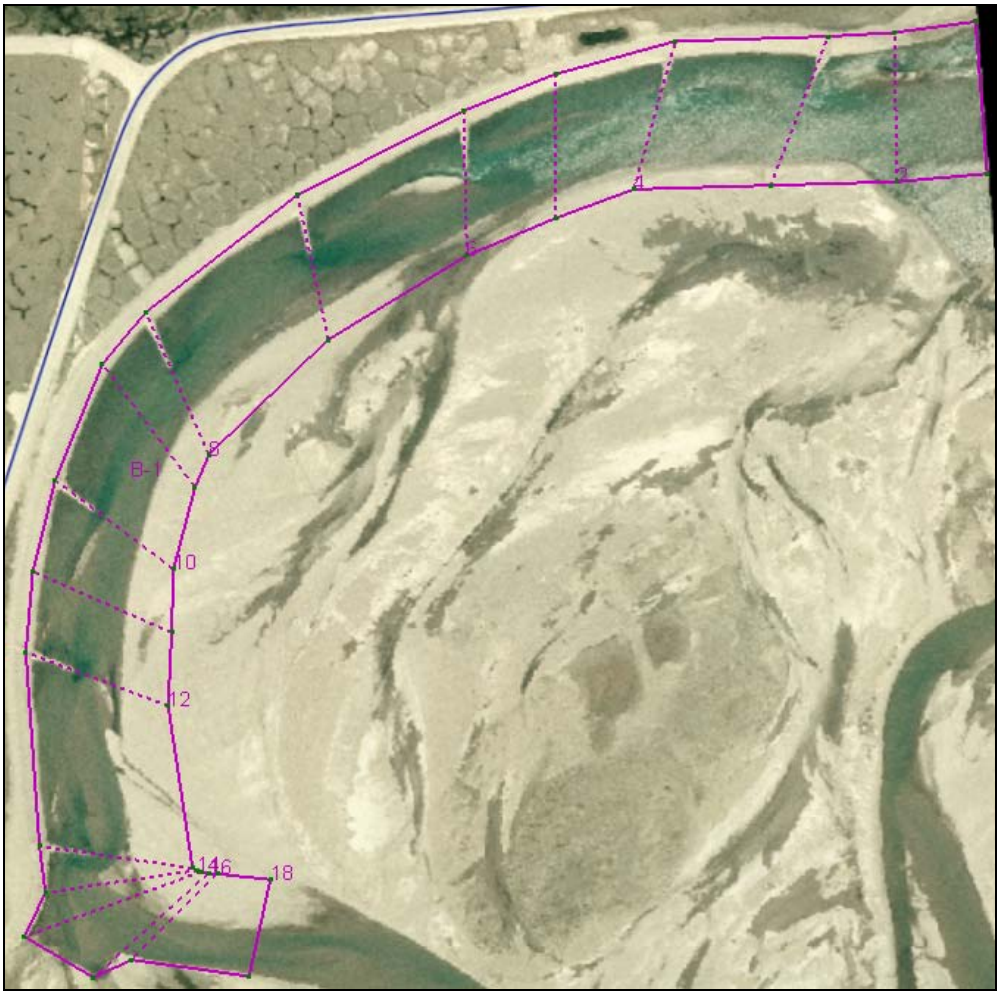


Figure 73 – Control Lines along Boundary Points

Once the boundaries are defined, the algebraic mesh can be generated specifying the number of horizontal and vertical lines along the control lines where the mesh nodes will be distributed (Figure 74 and Figure 75).


**Figure 74 – Number of Horizontal and Vertical Lines along Control Lines**

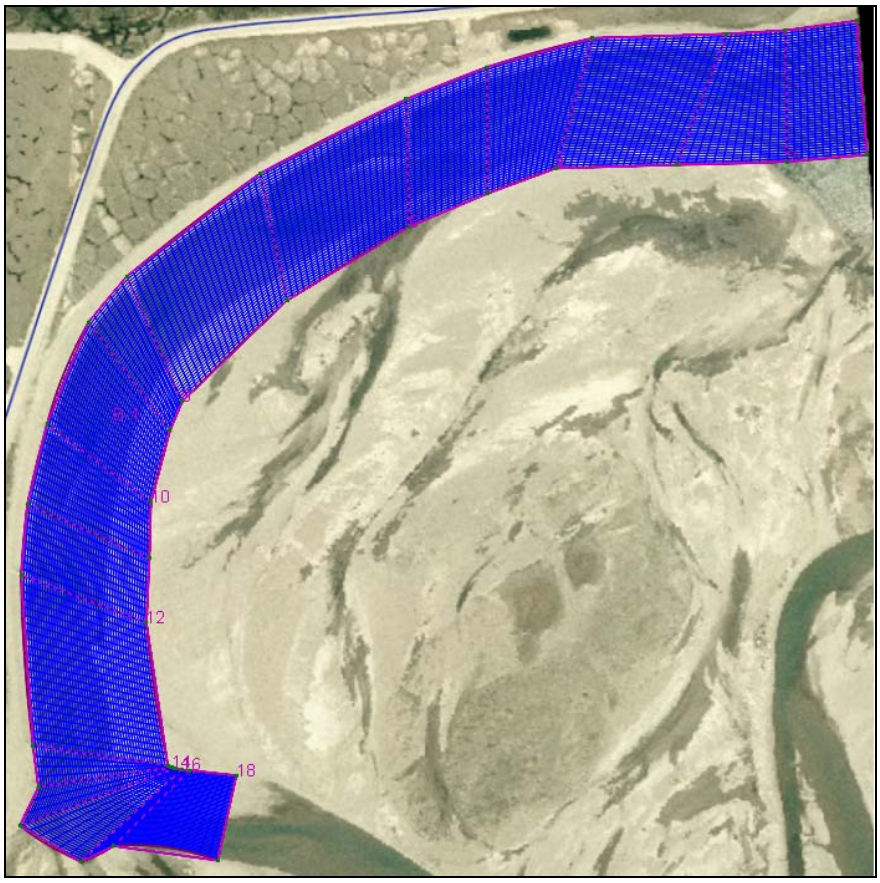


**Figure 75 – Generated Mesh over the Domain**

The bathymetry is then imported over the mesh using the CCHE-MESH menu (Figure 76).

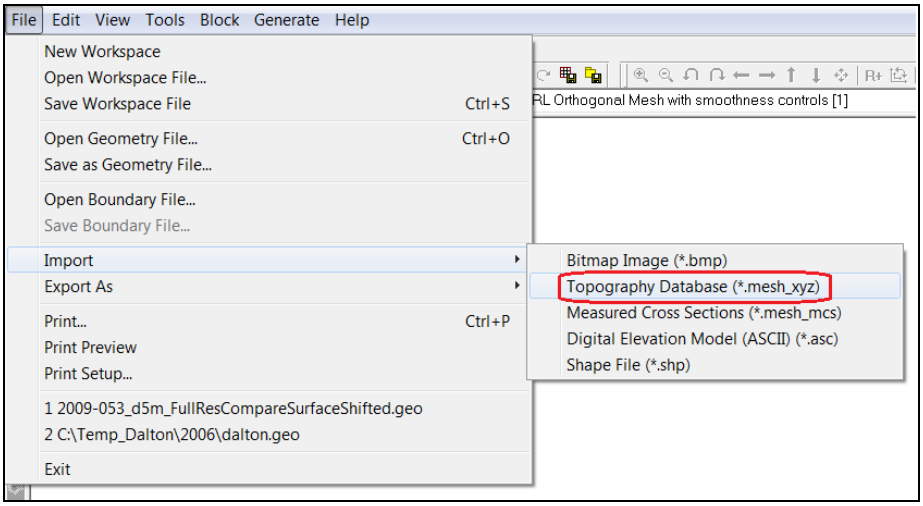


**Figure 76 - Selection of a Bathymetry File**

The bathymetric file shown in Figure 77 is an ASCII text file with the extension .mesh_xyz that contains bathymetry data with the following format (Zhang and Jia, 2009):

- Number of Points
- *X*-coordinate, *Y*-coordinate, Elevation (one line for each point)

1-378A1104_NAD83-NAVD88_PRE-CONST_TOPO.mesh_xyz

```
1   682
2   -4267566.75 1780707.87  472.78
3   -4267352.09 1780824.19  474.91
4   -4267614.76 1780812.15  470.77
5   -4267332.77 1781520.54  468.3
6   -4267475.91 1781139.16  470.73
7   -4267492.15 1780673.94  470.77
8   -4267479.5  1780679.71  472.38
9   -4267471.46 1780683.35  472.49
10  -4267469.44 1780685.02  470.14
```

**Figure 77 – Example of Bathymetry File**

Once the bathymetry is imported, it is applied over the previously configured mesh (Figure 78). Then bed elevation can be interpolated from the bathymetry onto the mesh nodes using the interpolation tools depicted in Figure 79 (Zhang and Jia, 2009). The resulting interpolated bed elevation is shown in Figure 80.

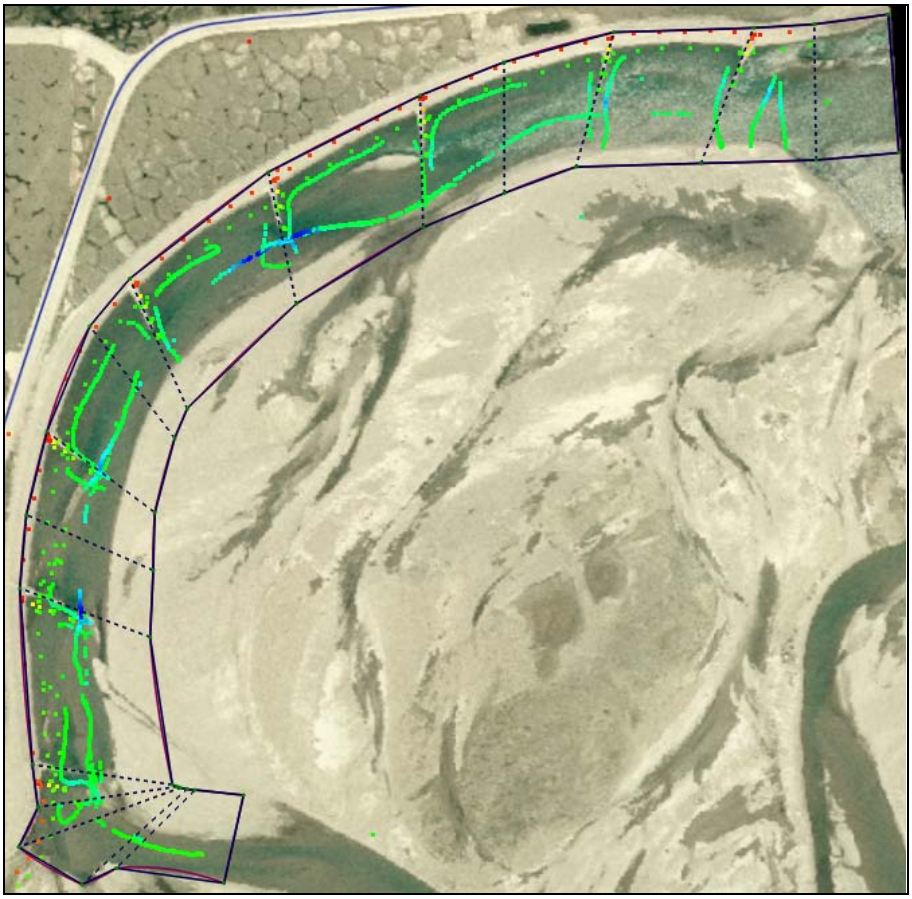

Figure 78 - Importation of Original Bathymetry

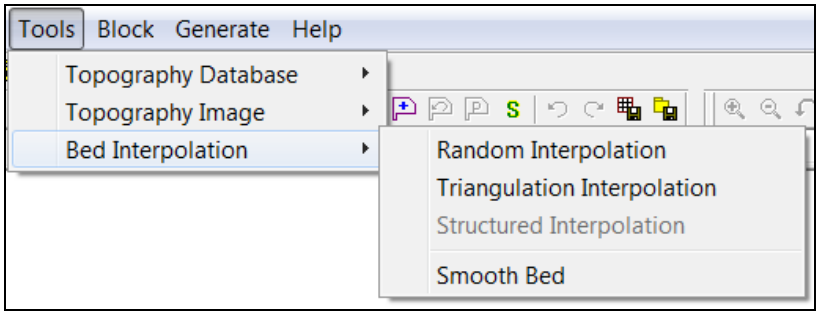


Figure 79 - Bed Interpolation Tools

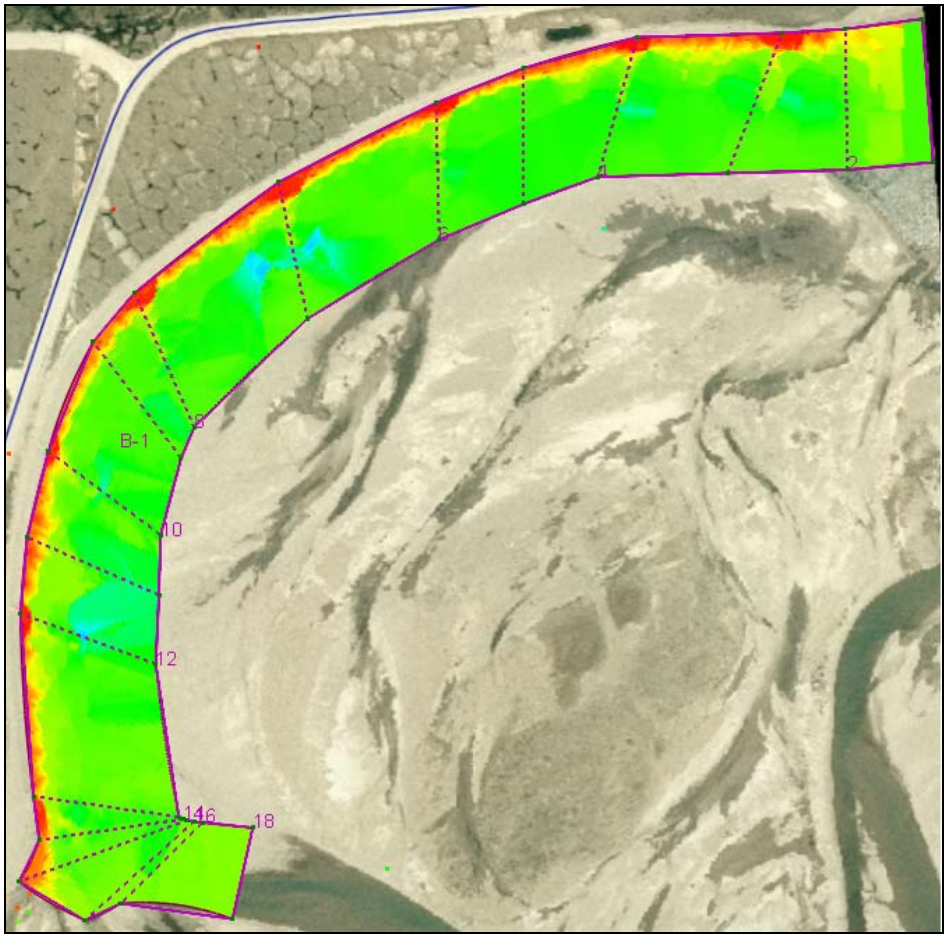


**Figure 80 – Interpolated Bathymetry**

In cases where no bathymetry existed (As-built case for Sag River) or where different settings need to be tested (7 and 5 barbs configuration for Sag River), the .mesh_xyz file was created and altered manually using MS Excel. For the previously mentioned cases, the bathymetry was built based on the barb schematics shown in Figure 81 and Table 12.

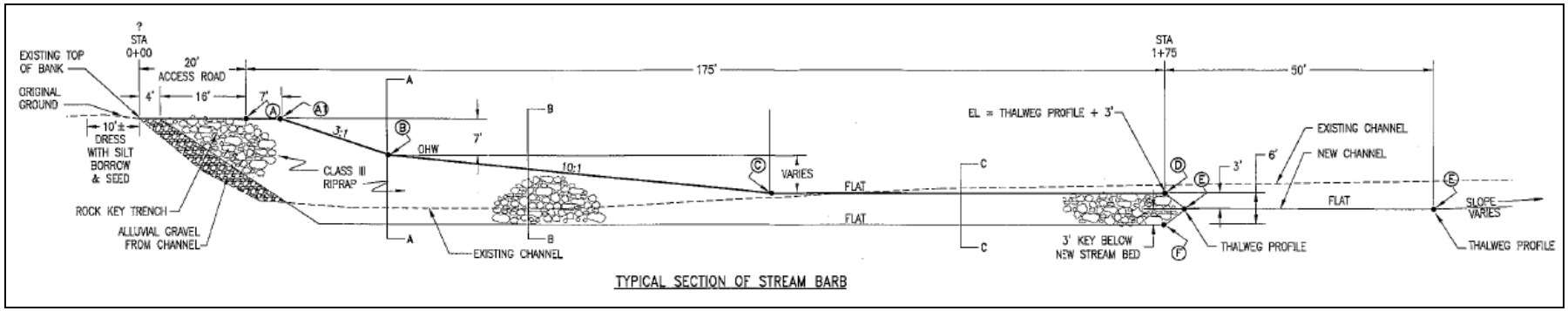


**Figure 81 – Barb Schematic**

**Table 12 – a) Height of Every Barb Point (m)*; b) Distance between Points (m)***

| [m] | A1 | B | C | D | E |
|---|---|---|---|---|---|
| Barb 1 | 5.86 | 3.72 | 2.00 | 2.00 | 1.09 |
| Barb 2 | 5.86 | 3.72 | 1.84 | 1.84 | 0.93 |
| Barb 3 | 5.86 | 3.72 | 1.69 | 1.69 | 0.78 |
| Barb 4 | 5.86 | 3.72 | 1.53 | 1.53 | 0.62 |
| Barb 5 | 5.86 | 3.72 | 1.37 | 1.37 | 0.46 |
| Barb 6 | 5.86 | 3.72 | 1.22 | 1.22 | 0.31 |
| Barb 7 | 5.86 | 3.72 | 1.06 | 1.06 | 0.14 |
| Barb 8 | 5.86 | 3.72 | 0.91 | 0.91 | 0.00 |

| [m] | A1-B | B-C | C-D | D-E | TOTAL |
|---|---|---|---|---|---|
| Barb 1 | 6.40 | 17.22 | 27.59 | Negligible | 51.21 |
| Barb 2 | 6.40 | 18.84 | 25.97 | Negligible | 51.21 |
| Barb 3 | 6.40 | 20.33 | 24.48 | Negligible | 51.21 |
| Barb 4 | 6.40 | 21.95 | 22.86 | Negligible | 51.21 |
| Barb 5 | 6.40 | 23.53 | 21.28 | Negligible | 51.21 |
| Barb 6 | 6.40 | 25.02 | 19.79 | Negligible | 51.21 |
| Barb 7 | 6.40 | 26.67 | 18.14 | Negligible | 51.21 |
| Barb 8 | 6.40 | 28.10 | 16.71 | Negligible | 51.21 |

* 0 m. is an arbitrary datum and corresponds to the lowest point of the thalweg in 2006.

Figure 82 and Figure 83 show the 2006 and 2009 three-dimensional views of the interpolated bathymetries generated for the Sag River; Figure 84 and Figure 85 show them for the 2004 and 2009 interpolated bathymetries generated for Hess Creek.

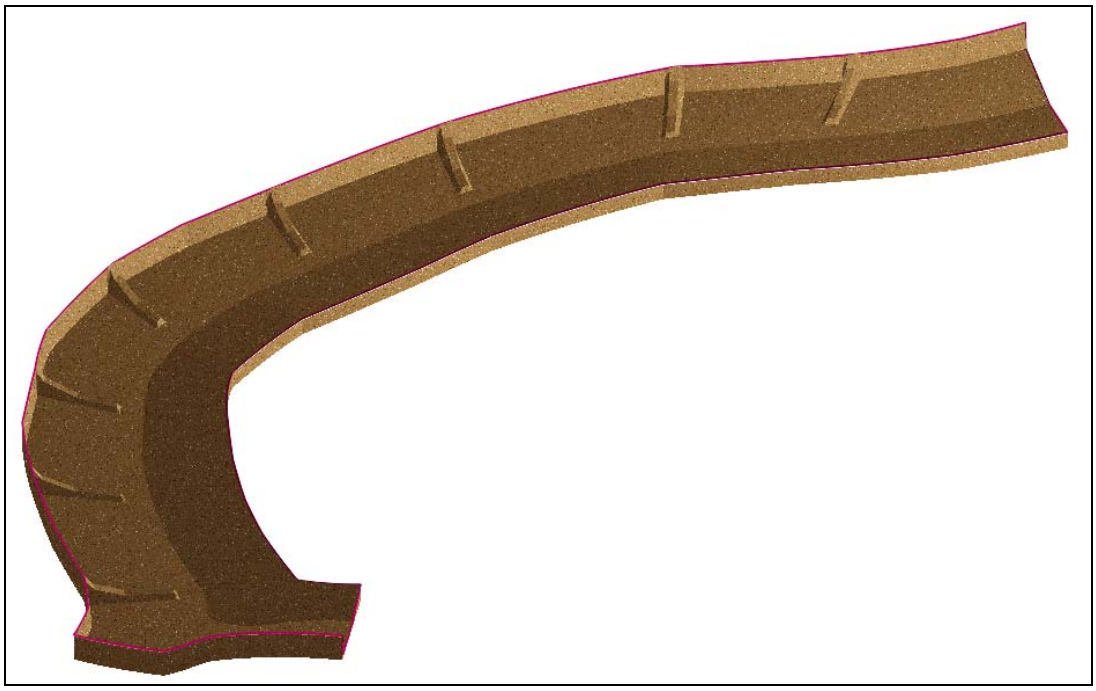

**Figure 82 – 3D Model View of Sag River (As Built)**

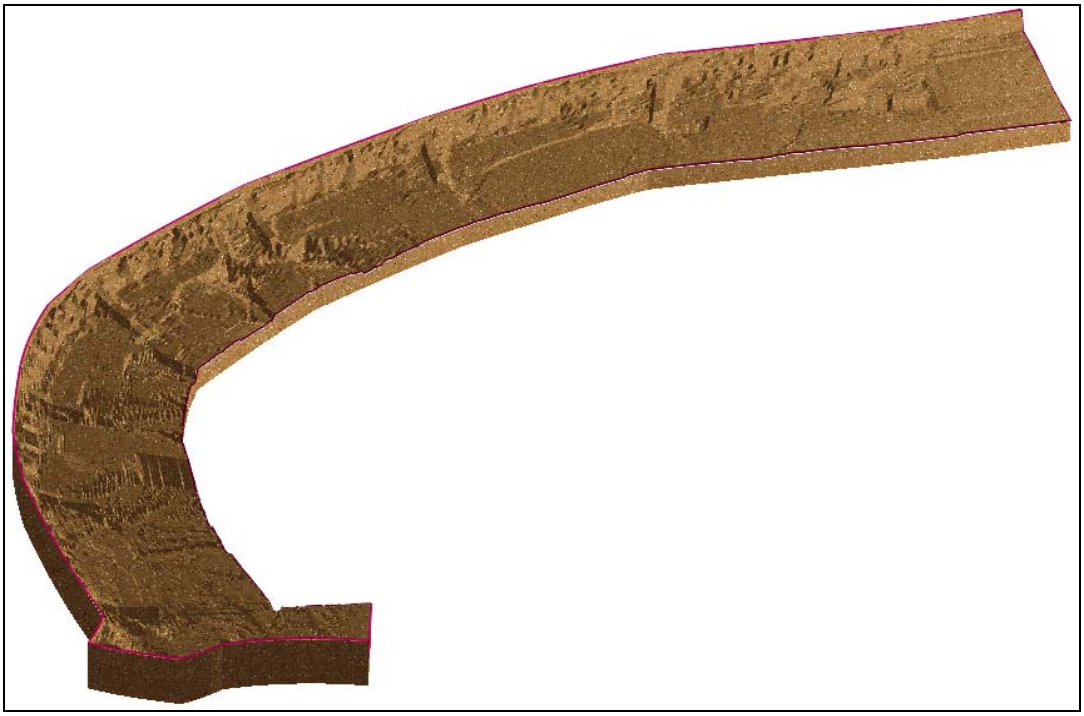

**Figure 83- 3D Model View of Sag River (2009)**

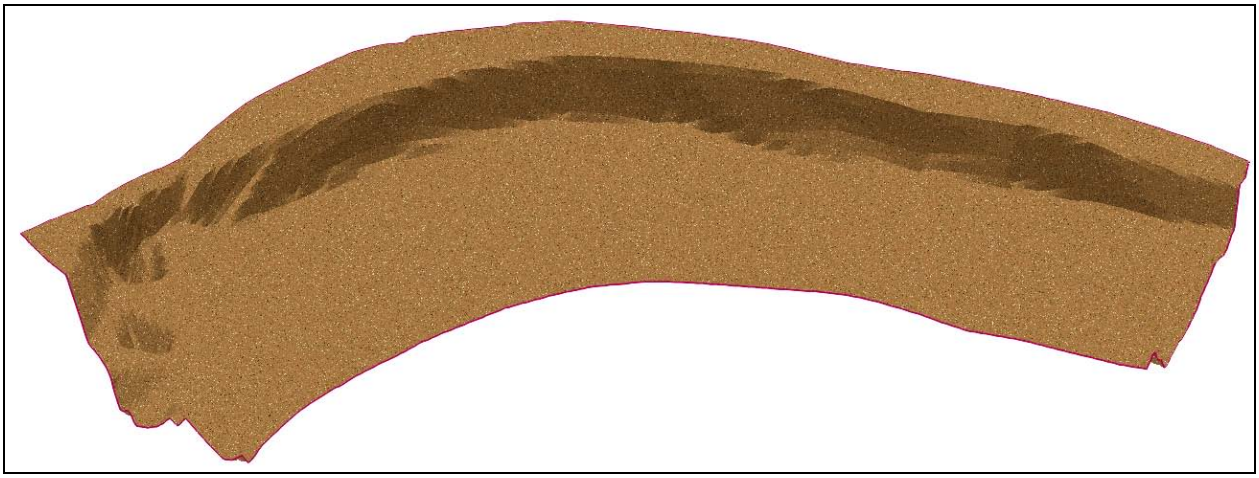

Figure 84 - 3D Model View of Hess Creek (2004)

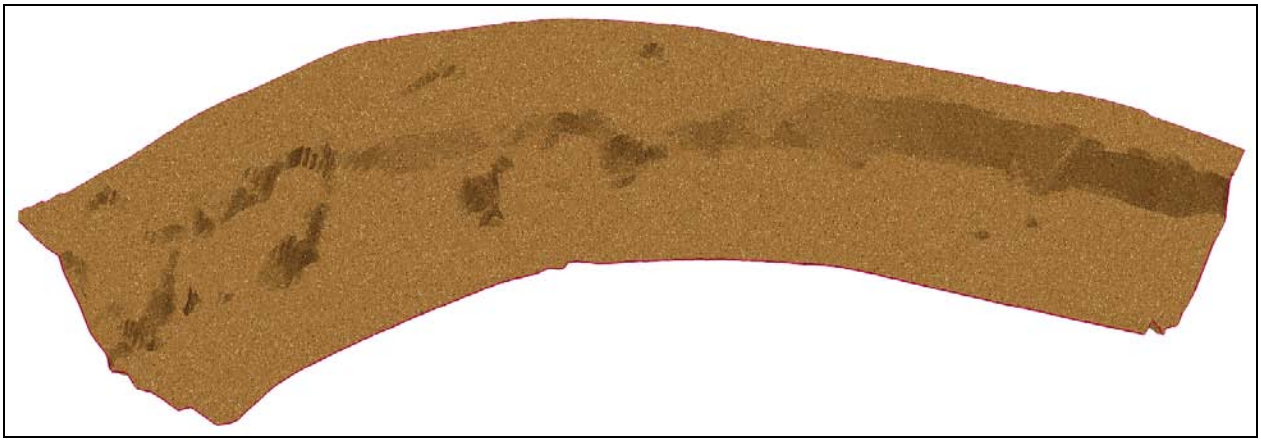

Figure 85 - 3D Model View of Hess Creek (2009)

# Appendix D – Boundary Conditions

Boundary conditions are configured through the CCHE-GUI menu (Figure 86). Figure 87 and Figure 88 show the screenshots of these settings for the model domain.

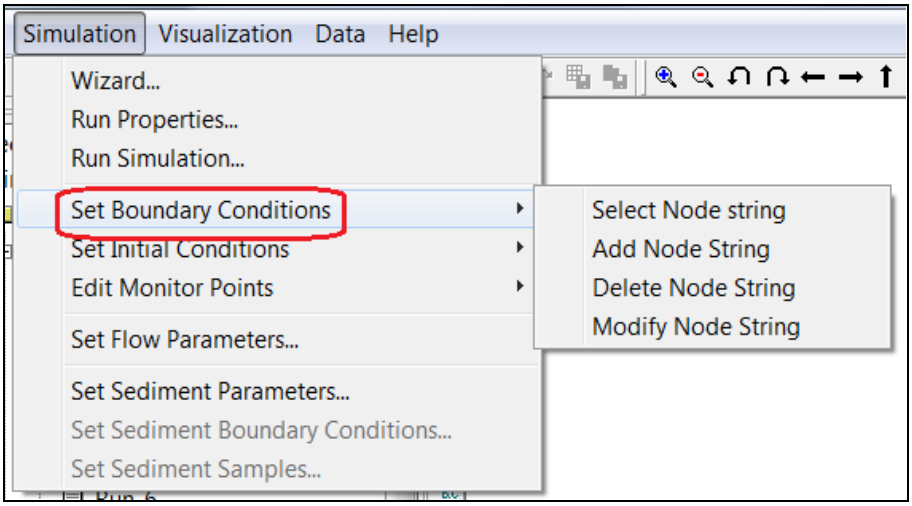


Figure 86 - Boundary Conditions Specification

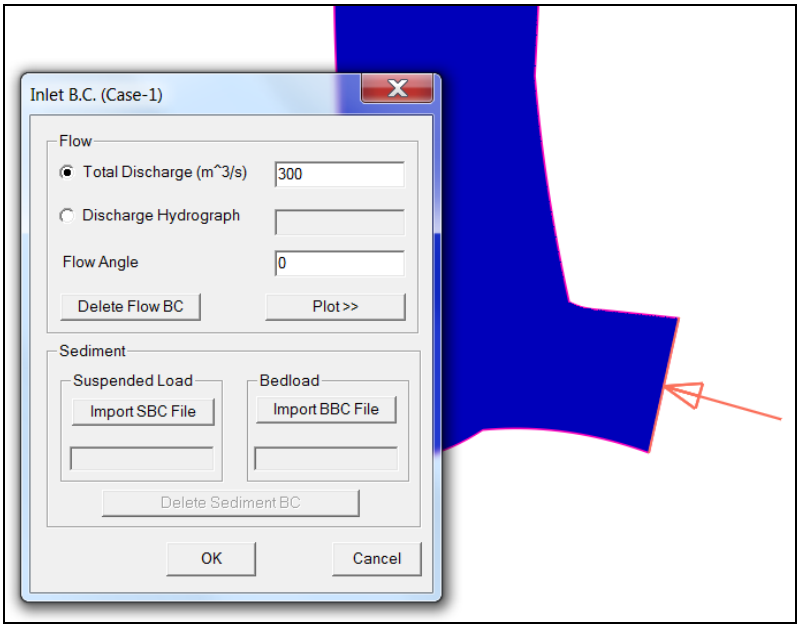


Figure 87 - Inlet Boundary Condition

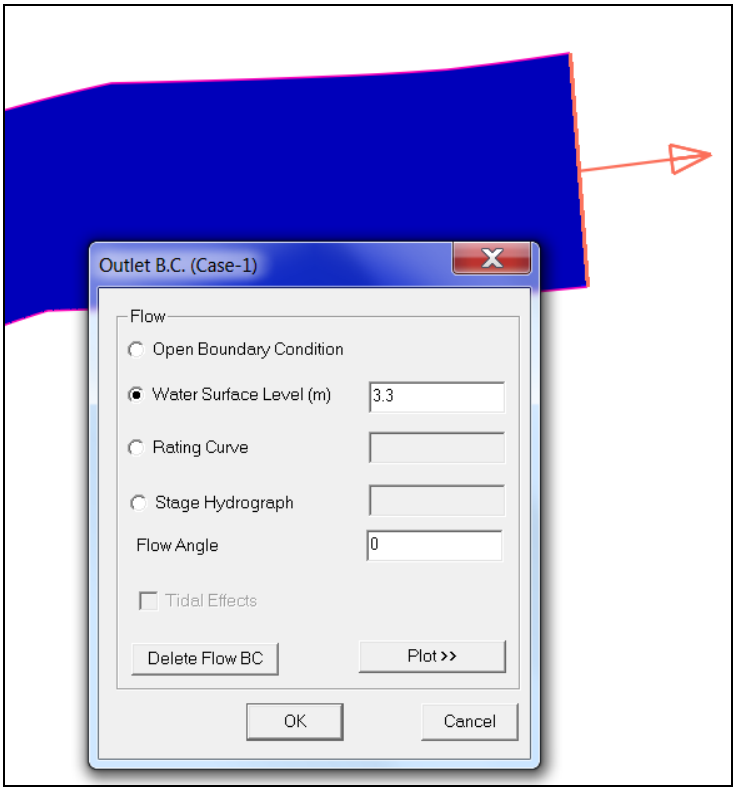


Figure 88 - Outlet Boundary Condition

# Appendix E – Full Results Visualization

Table 13 lists all output files generated by Hess Creek and Sag River CCHE2D models in PowerPoint format:

Table 13 – List of Result Files for Hess Creek and Sag River

| Description | Location |
|---|---|
| Hess Creek, 2004 and 2009 simulations | Hess (2004 & 2009).pptx |
| Sag River, 2006 and 2009 simulations | Sag (2006 & 2009).pptx |
| Sag River, 7, 5, and 4 barbs simulations, Q = 40 $m^3/s$ | Sag 7 and 5 Barbs (40 cms).pptx |
| Sag River, 7, 5, and 4 barbs simulations, Q = 300 $m^3/s$ | Sag 7 and 5 Barbs (300 cms).pptx |

# Study to Compare the Performance of Two Designs to Prevent River Bend Erosion in Arctic Environments

Sag River
2006 and 2009 simulations

# Initial Bed Elevation (m)

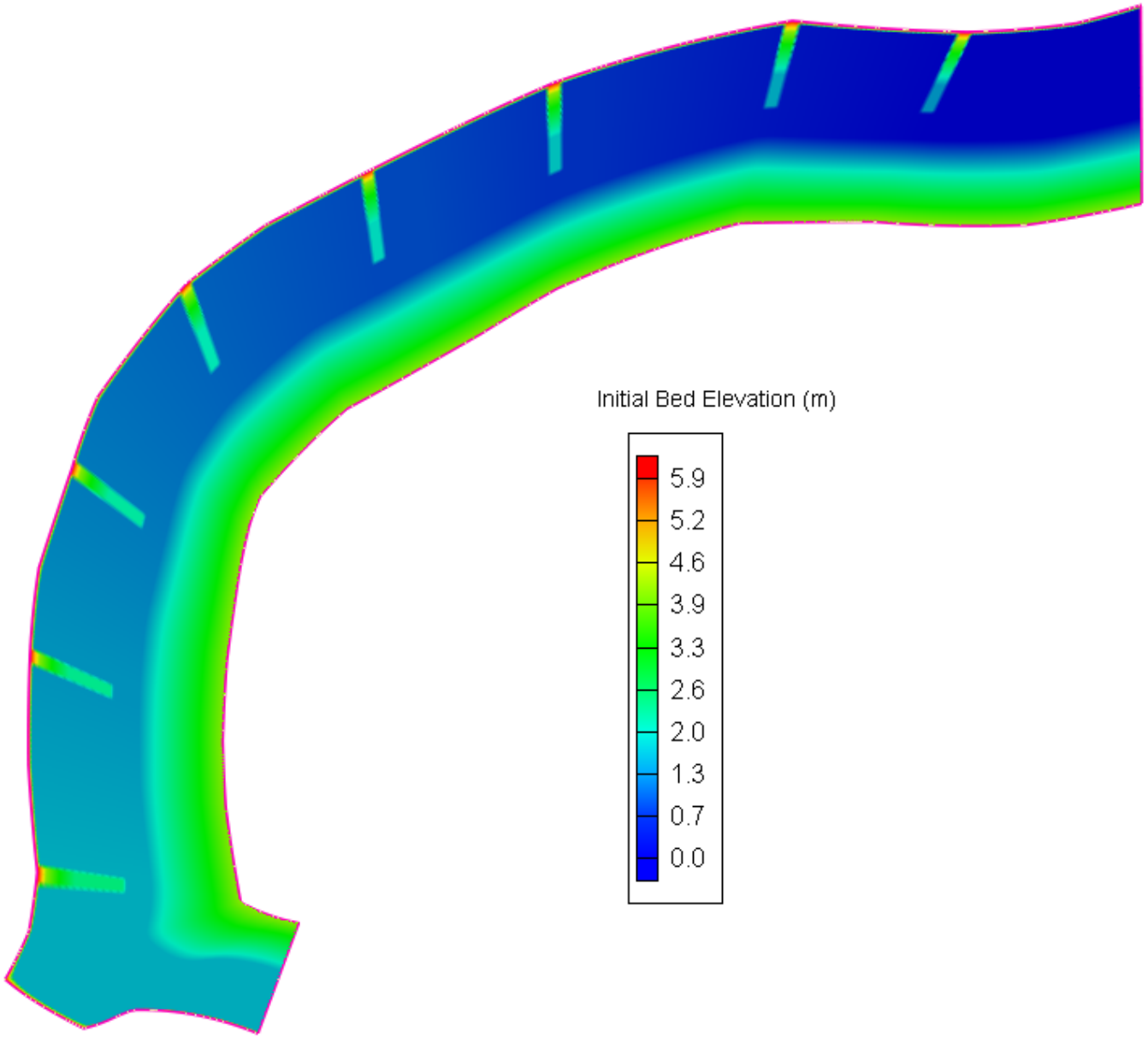


As built

# Velocity Magnitude (m/s) near Stream Barb #3

## Discharge: 40 m^3/s, Initial Water Height: 1.5 m

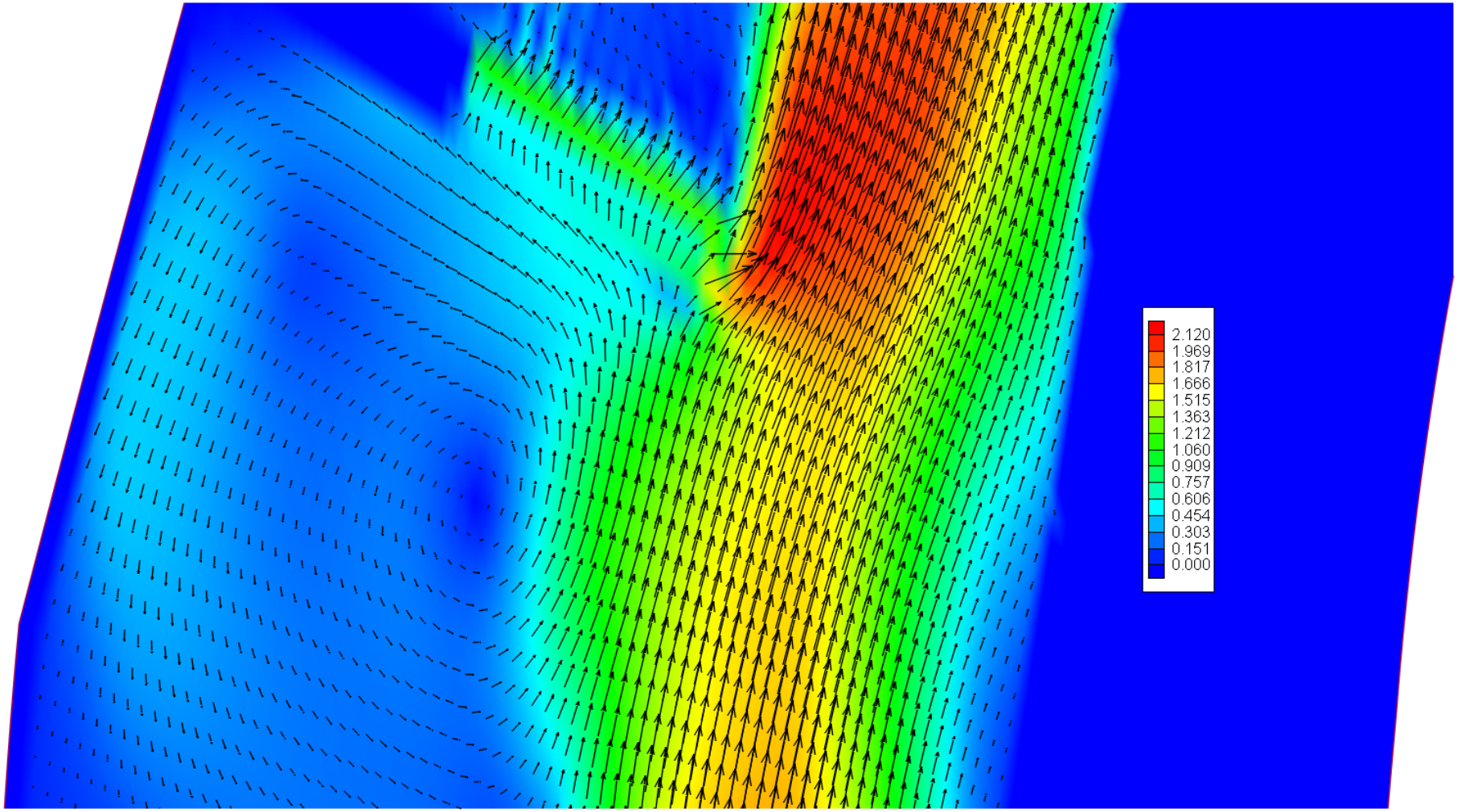


As built

# Initial Bed Elevation (m)

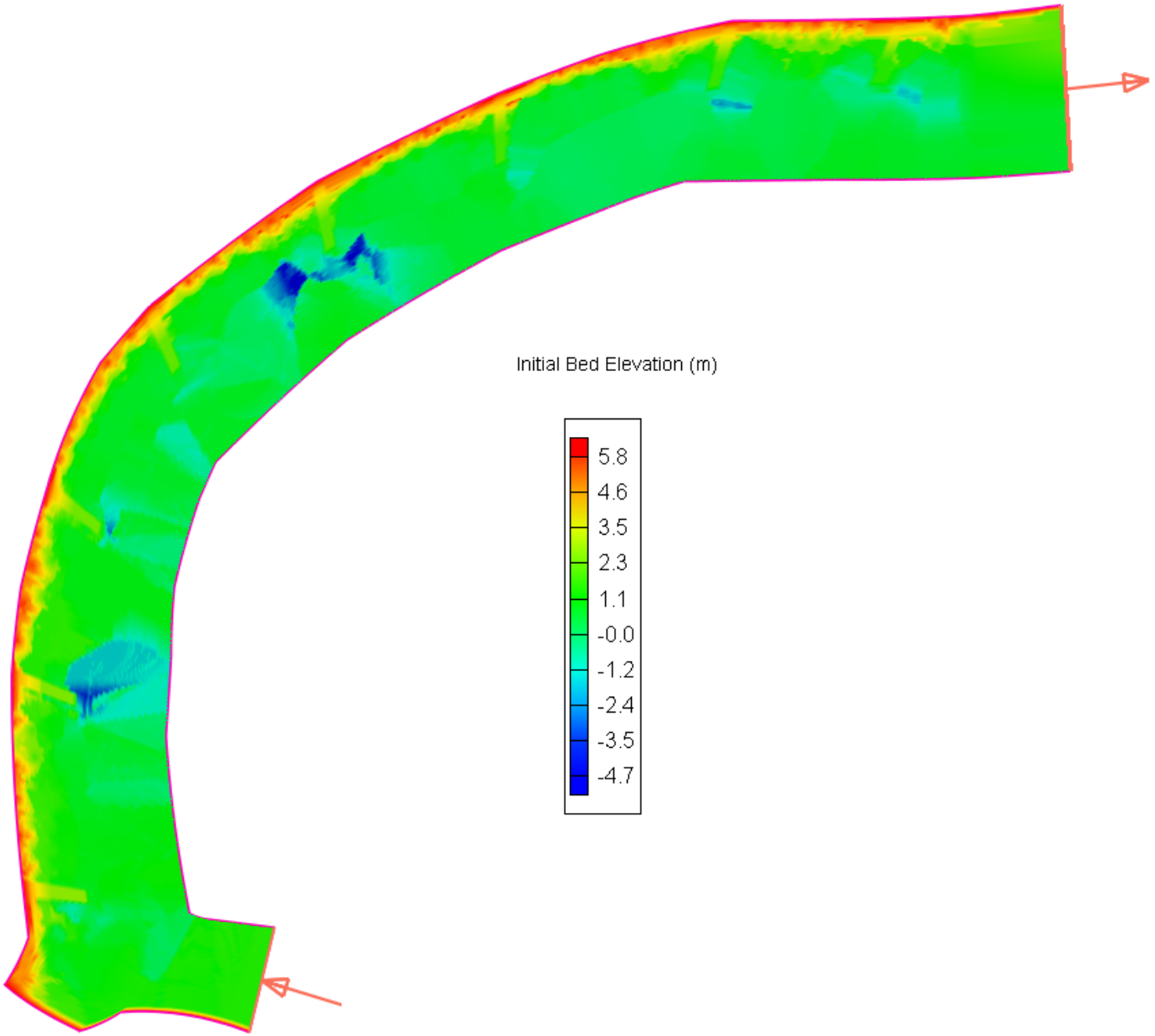


Aug 2009

# Velocity Magnitude (m/s)

## Discharge: 40 m^3/s, Initial Water Height: 1.5 m

## (observed conditions during fieldwork conducted on August 2009)

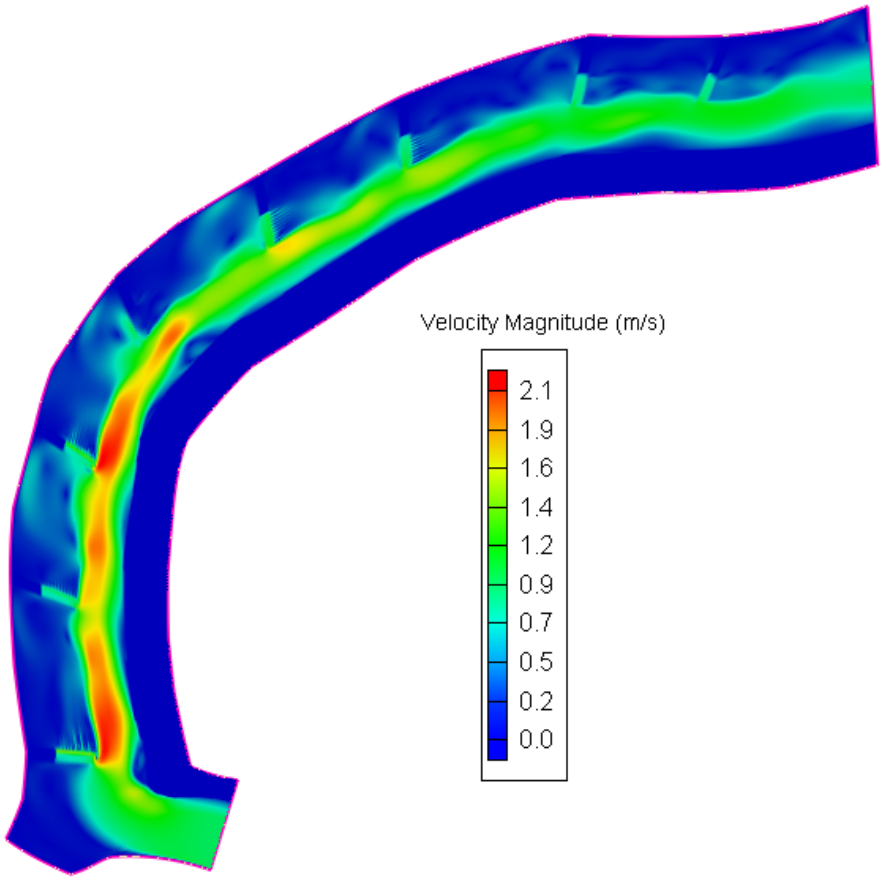


As built

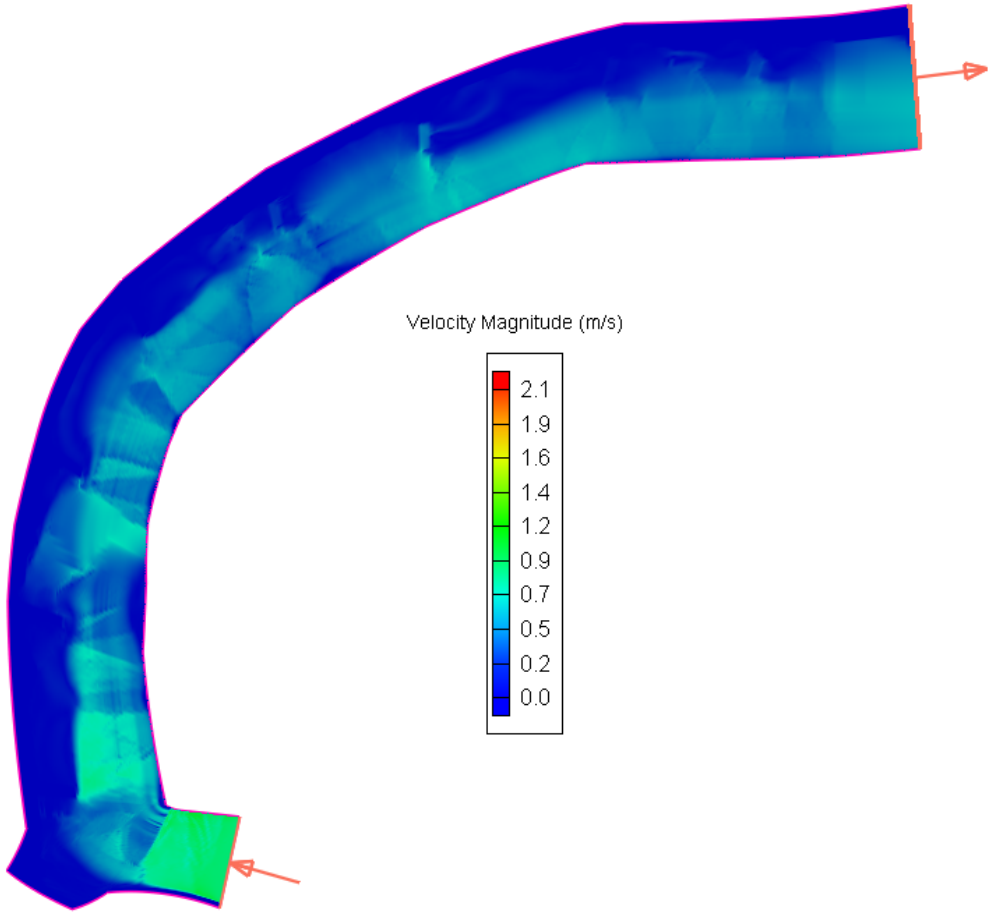


Aug 2009

# Total Specific Discharge (m^2/s)

## Discharge: 40 m^3/s, Initial Water Height: 1.5 m

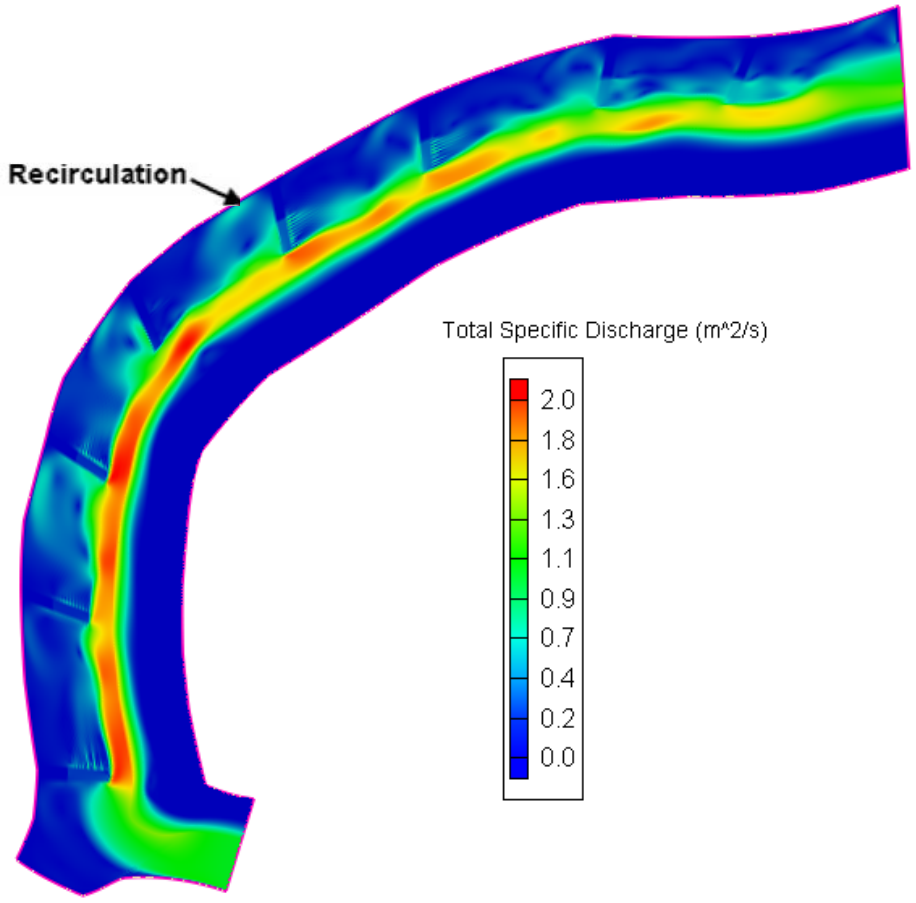


As built

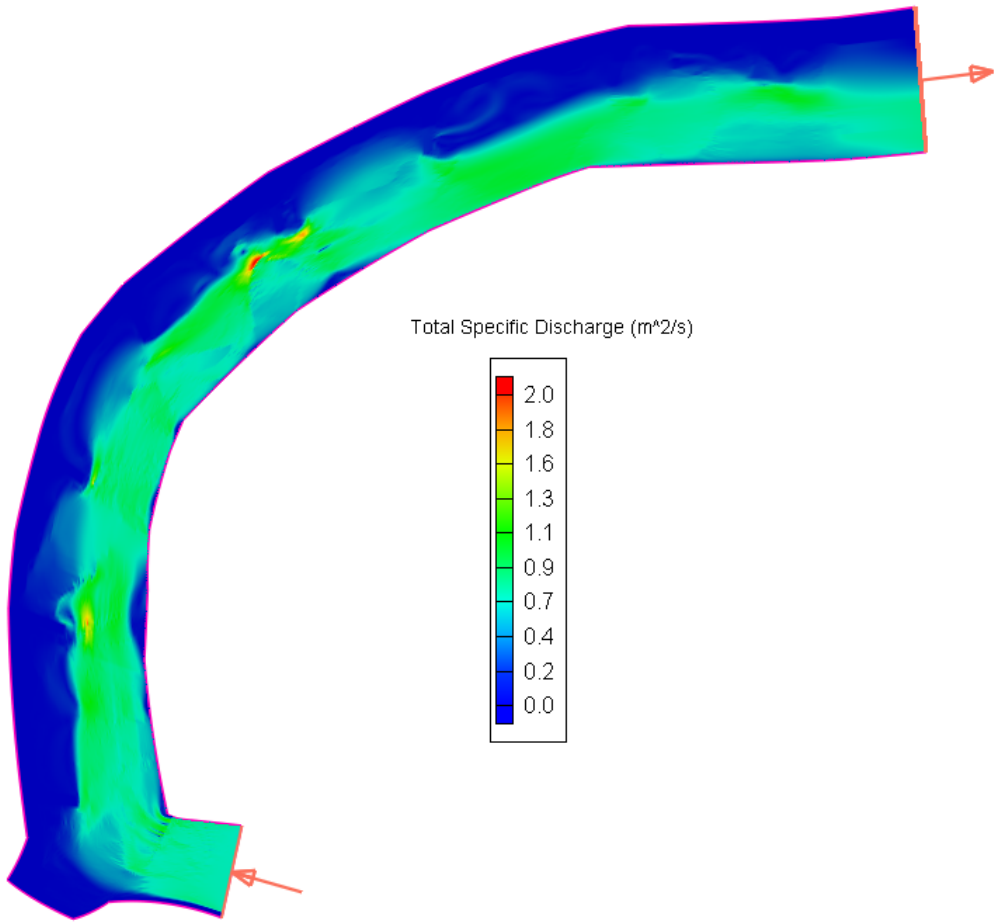


Aug 2009

# Total Shear Stress (N/m^2)
# Discharge: 40 m^3/s, Initial Water Height: 1.5 m

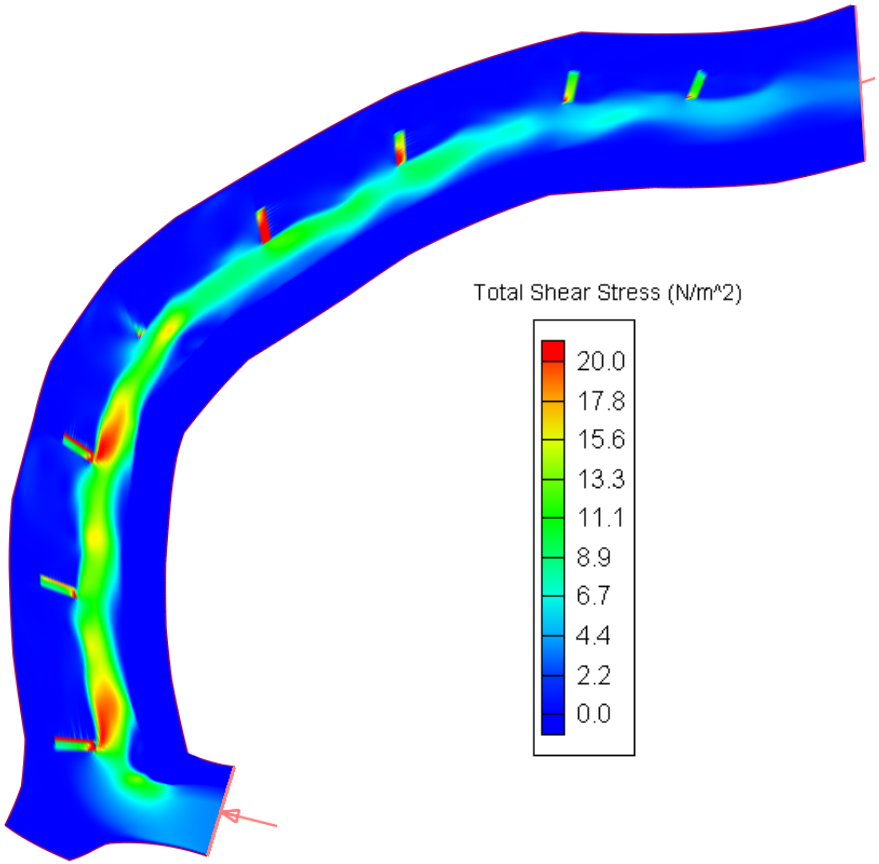


As built

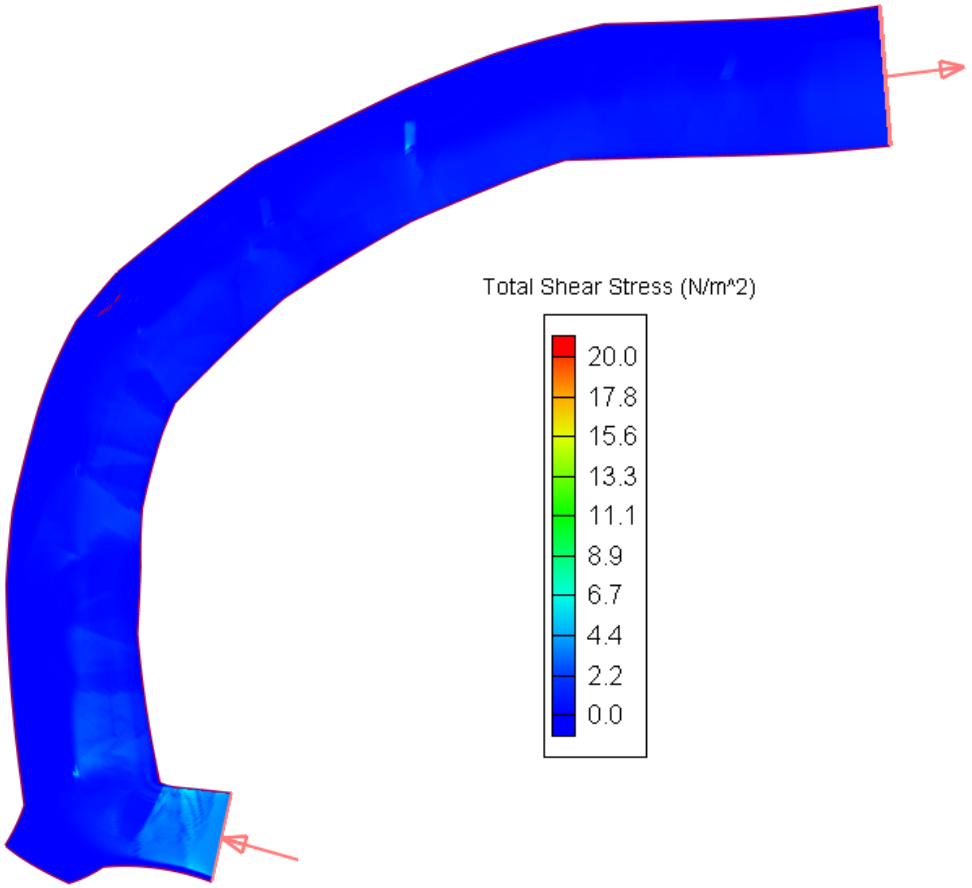


Aug 2009

Bed sediment transport is initiated
when Total Shear Stress > 19 N/m^2

# Total Shear Stress (N/m^2)
# Discharge: 300 m^3/s, Initial Water Height: 3.3 m

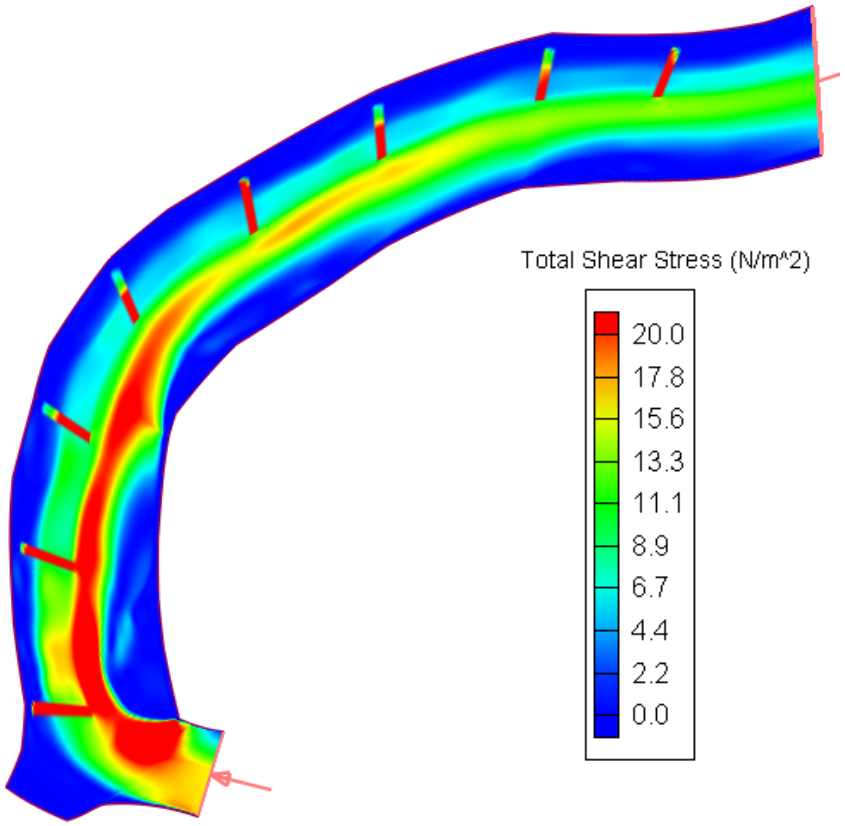


As built

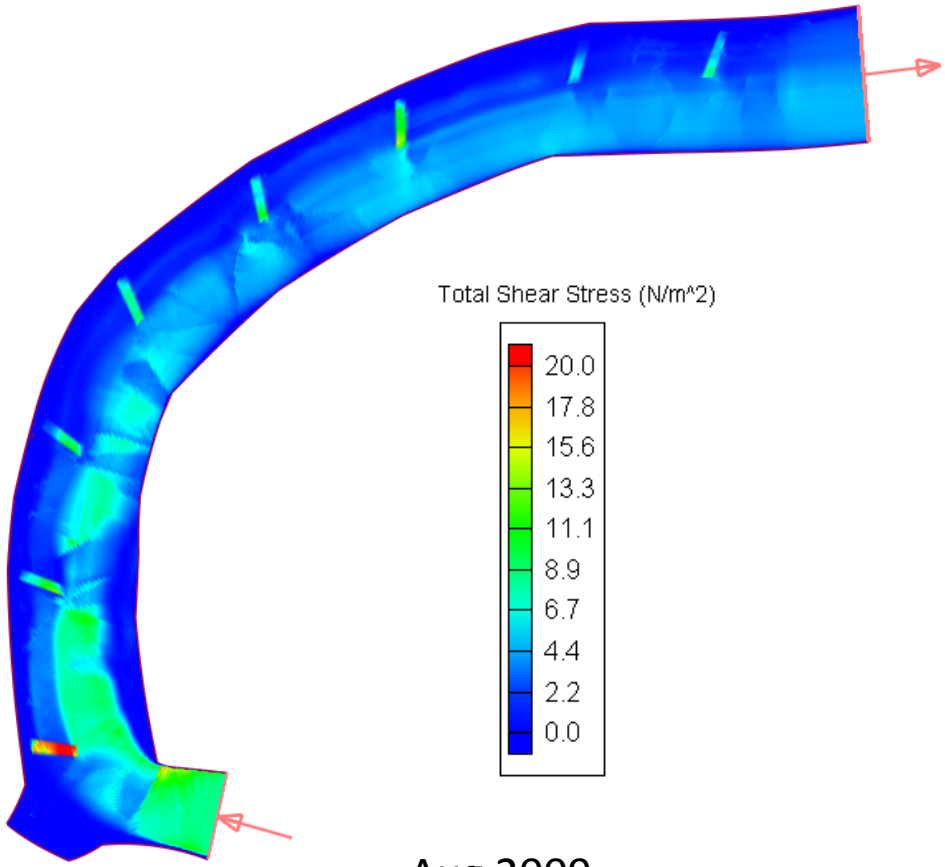


Aug 2009

Bed sediment transport is initiated
when Total Shear Stress > 19 N/m^2

# Study to Compare the Performance of Two Designs to Prevent River Bend Erosion in Arctic Environments

Sag River

7, 5, and 4 barbs simulations

$Q = 40\ m^3/s$

# 7 Barbs - No 1st Barb

Discharge: 40 m^3/s, Initial Water Height: 1.5 m

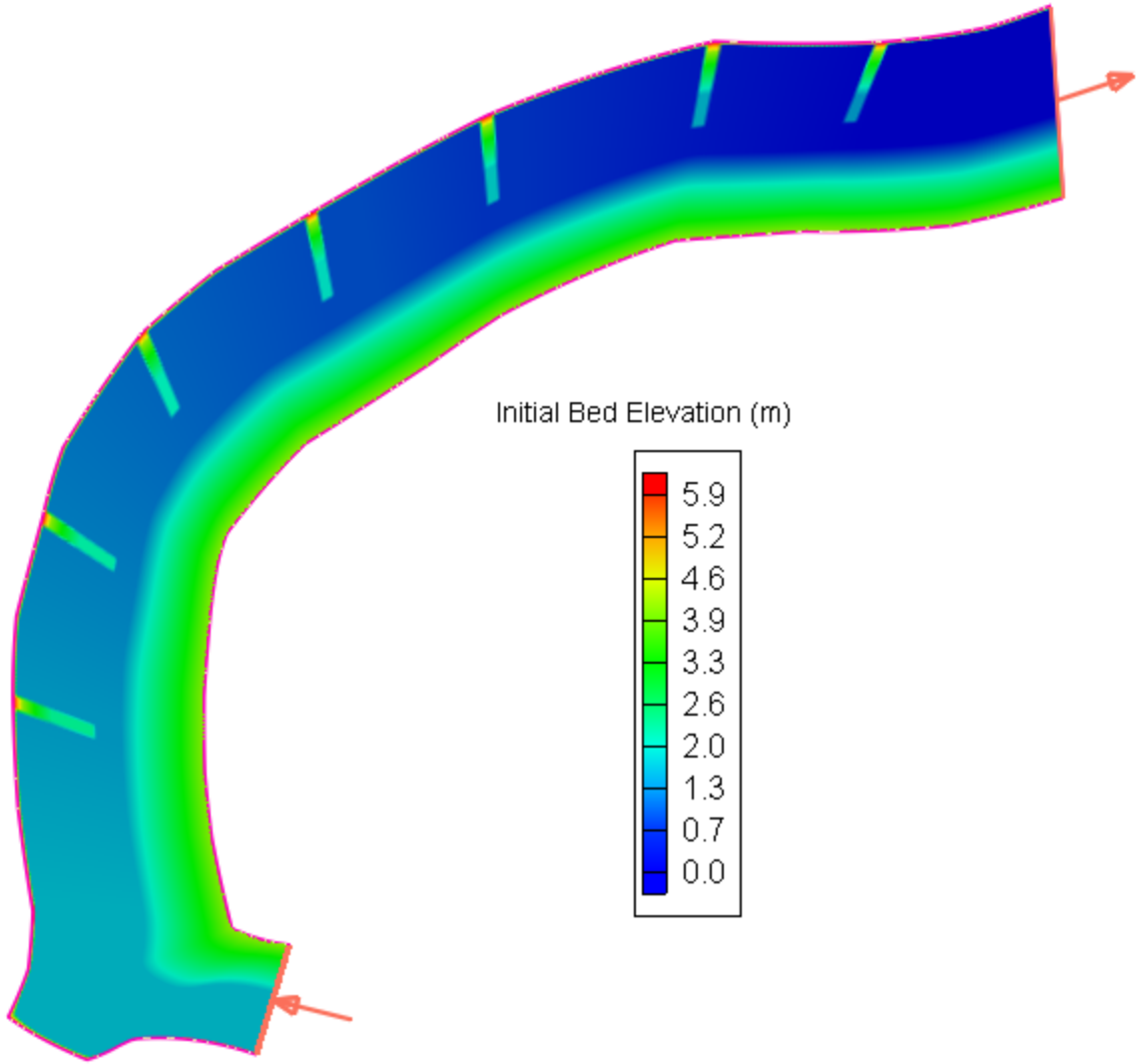

# Velocity Magnitude (m/s)

## Discharge: 40 m^3/s, Initial Water Height: 1.5 m

## (observed conditions during fieldwork conducted on August 2009)

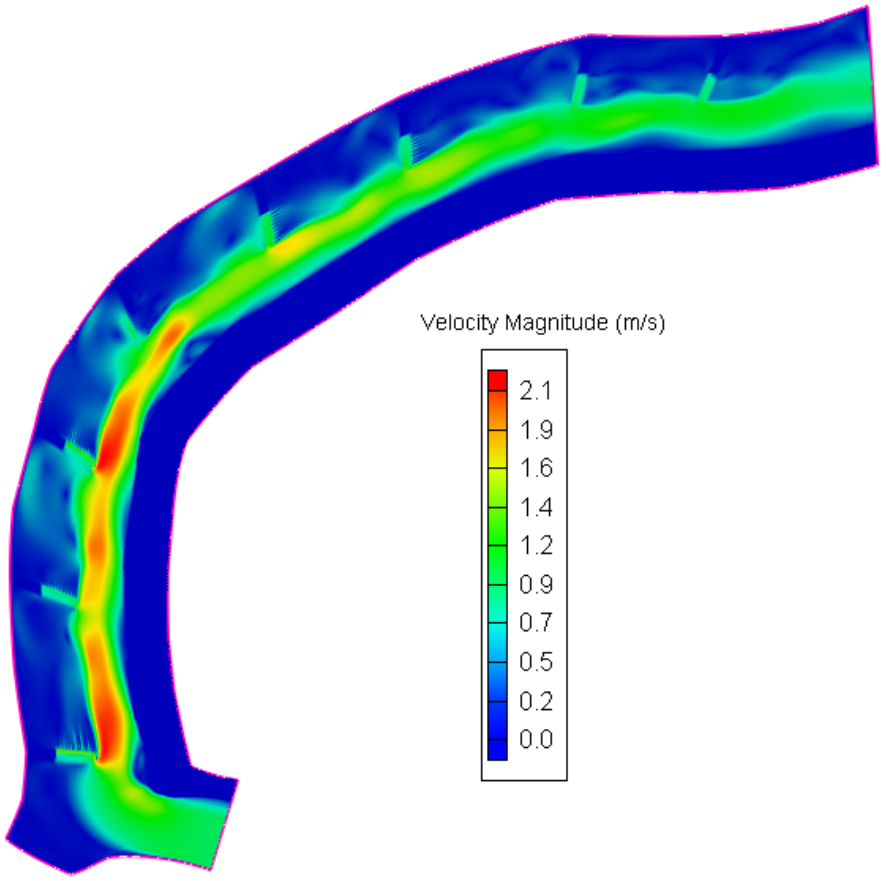


As built

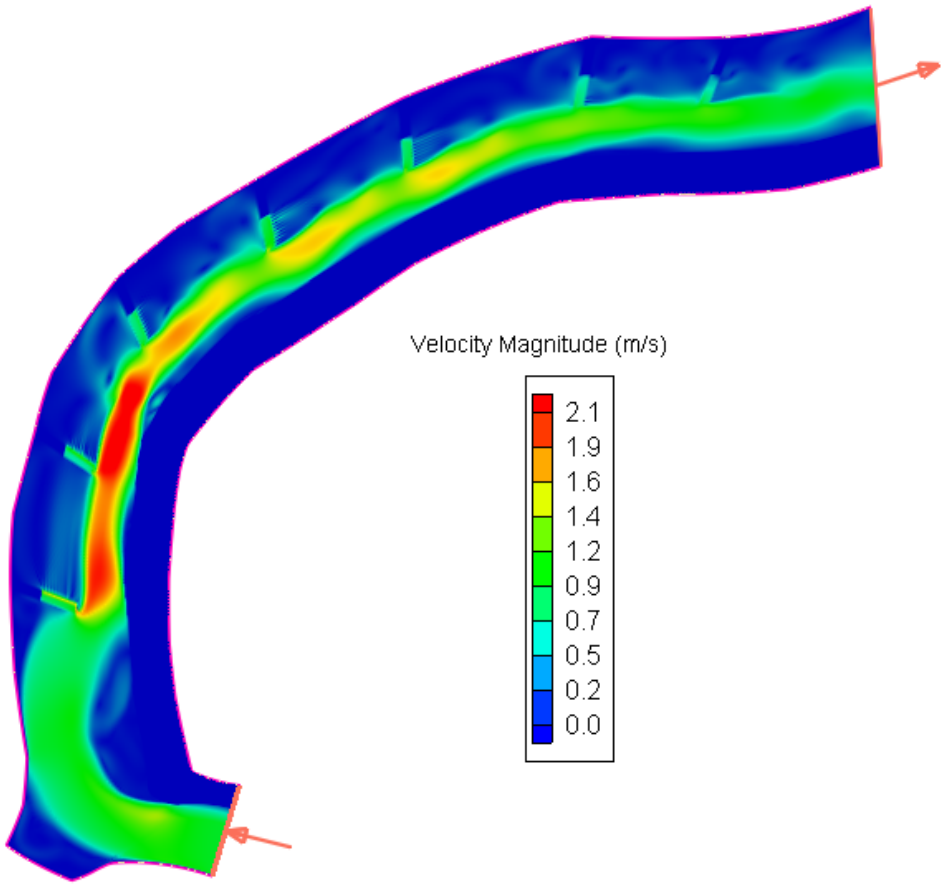


7 Barbs (no 1st barb)

# Total Specific Discharge (m^2/s)

## Discharge: 40 m^3/s, Initial Water Height: 1.5 m

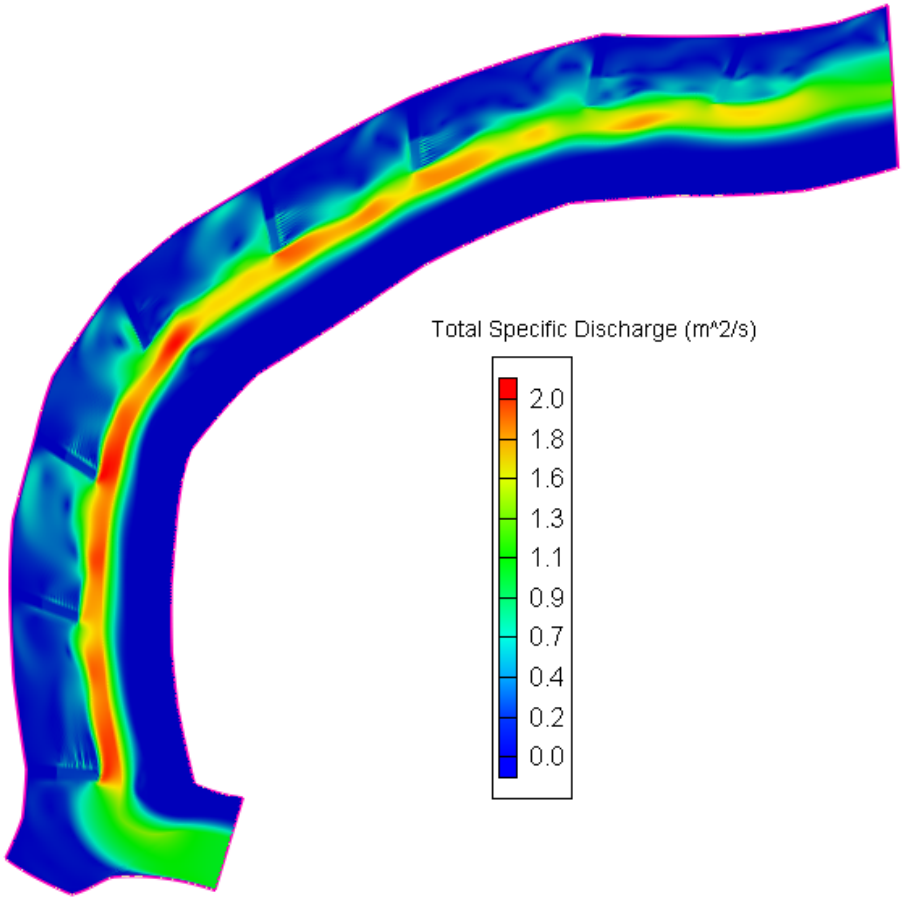


As built

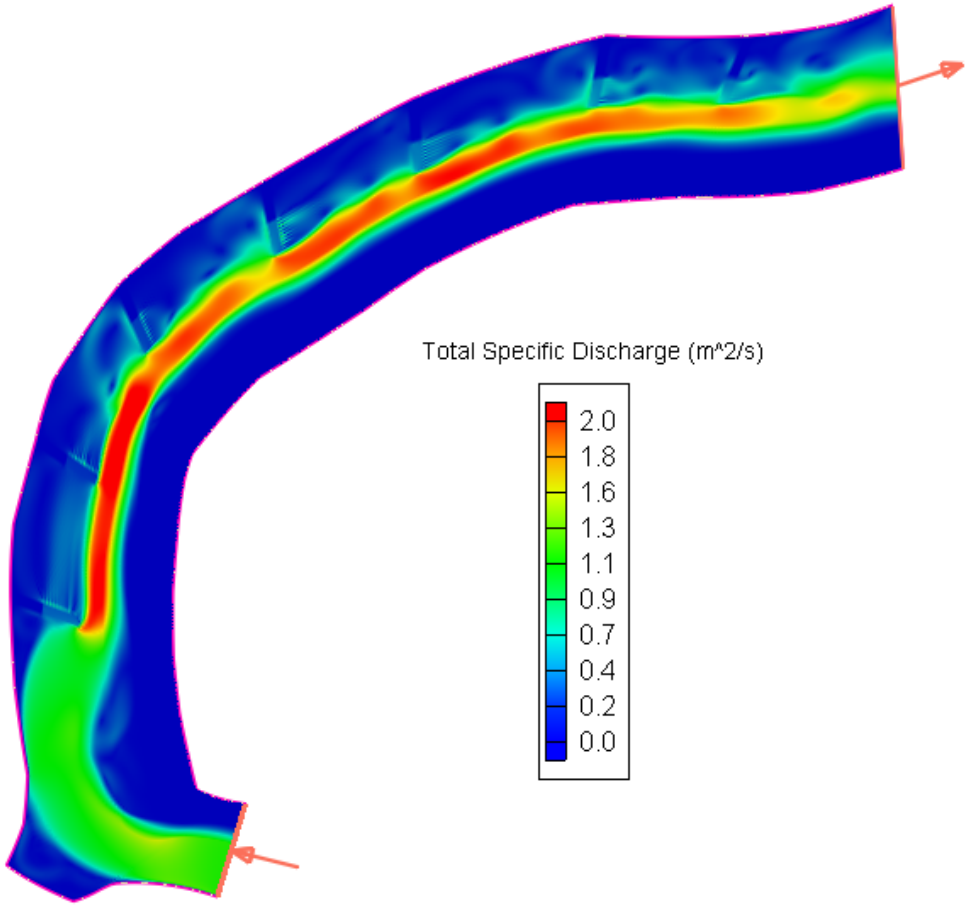


7 Barbs (no 1st barb)

# Froude Number
# Discharge: 40 m^3/s, Initial Water Height: 1.5 m

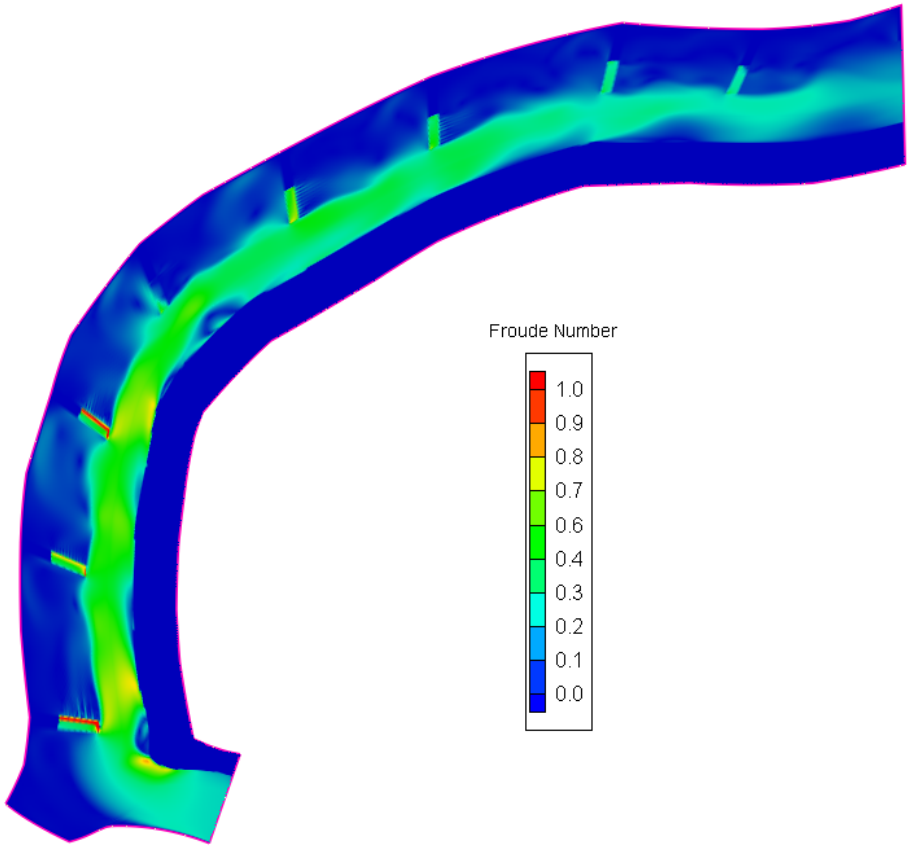


As built

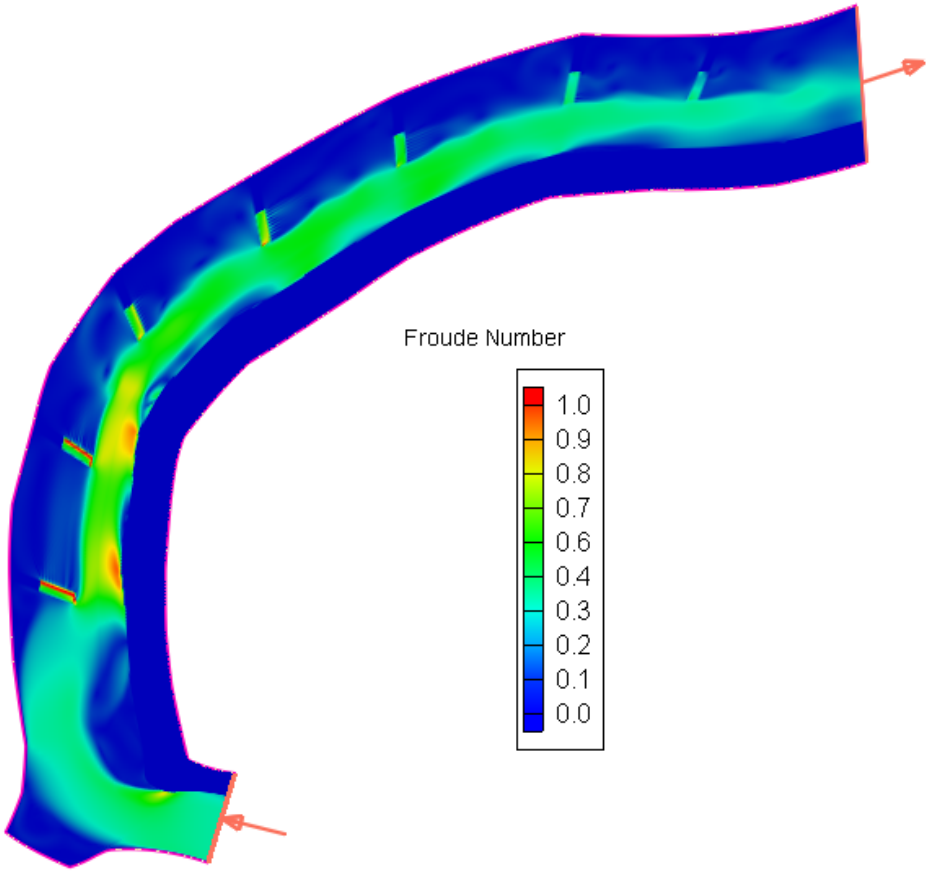


7 Barbs (no 1st barb)

# Total Shear Stress (N/m^2)
# Discharge: 40 m^3/s, Initial Water Height: 1.5 m

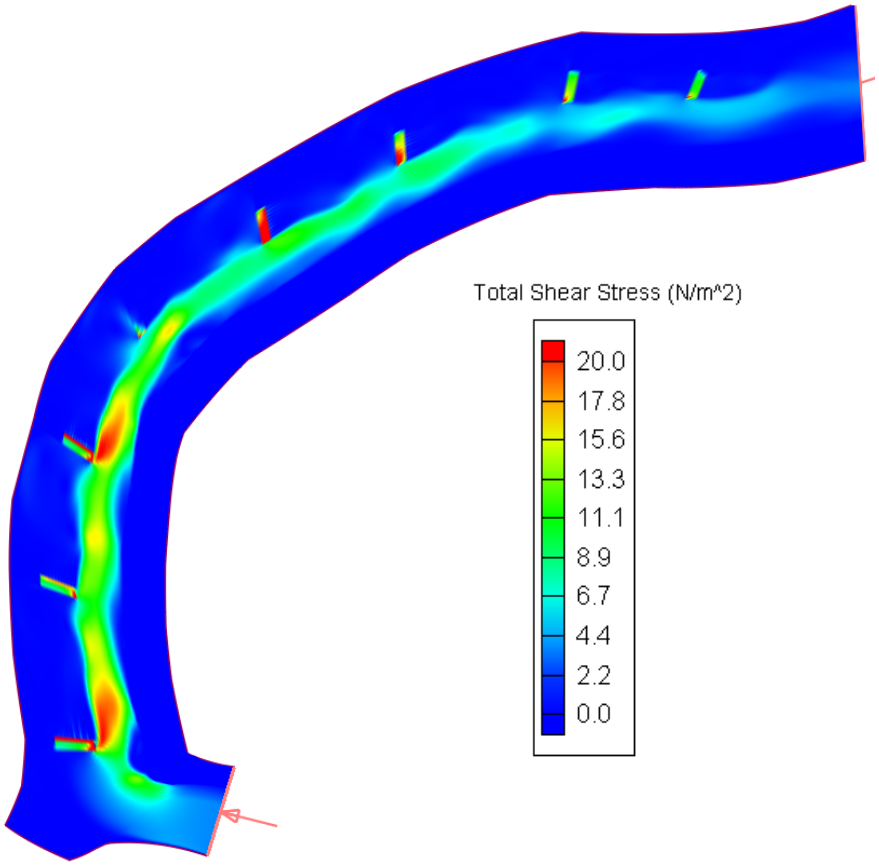


As built

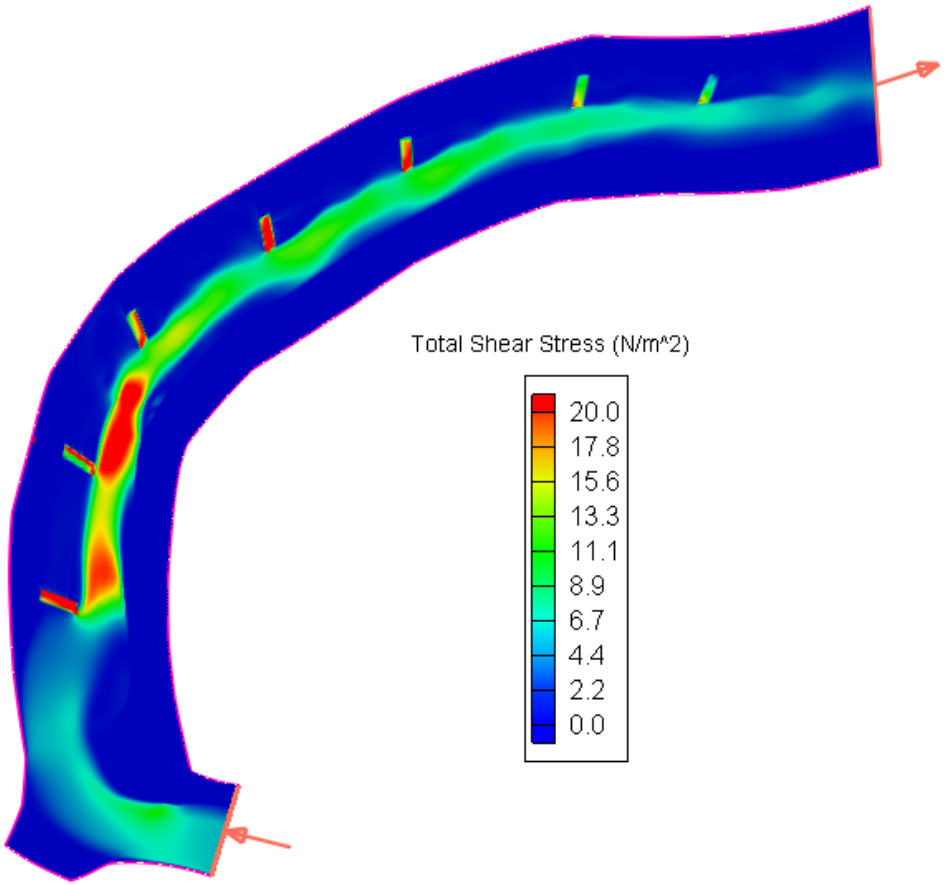


7 Barbs (no 1st barb)

Bed sediment transport is initiated
when Total Shear Stress > 19 N/m^2

# 7 Barbs - No 2nd Barb

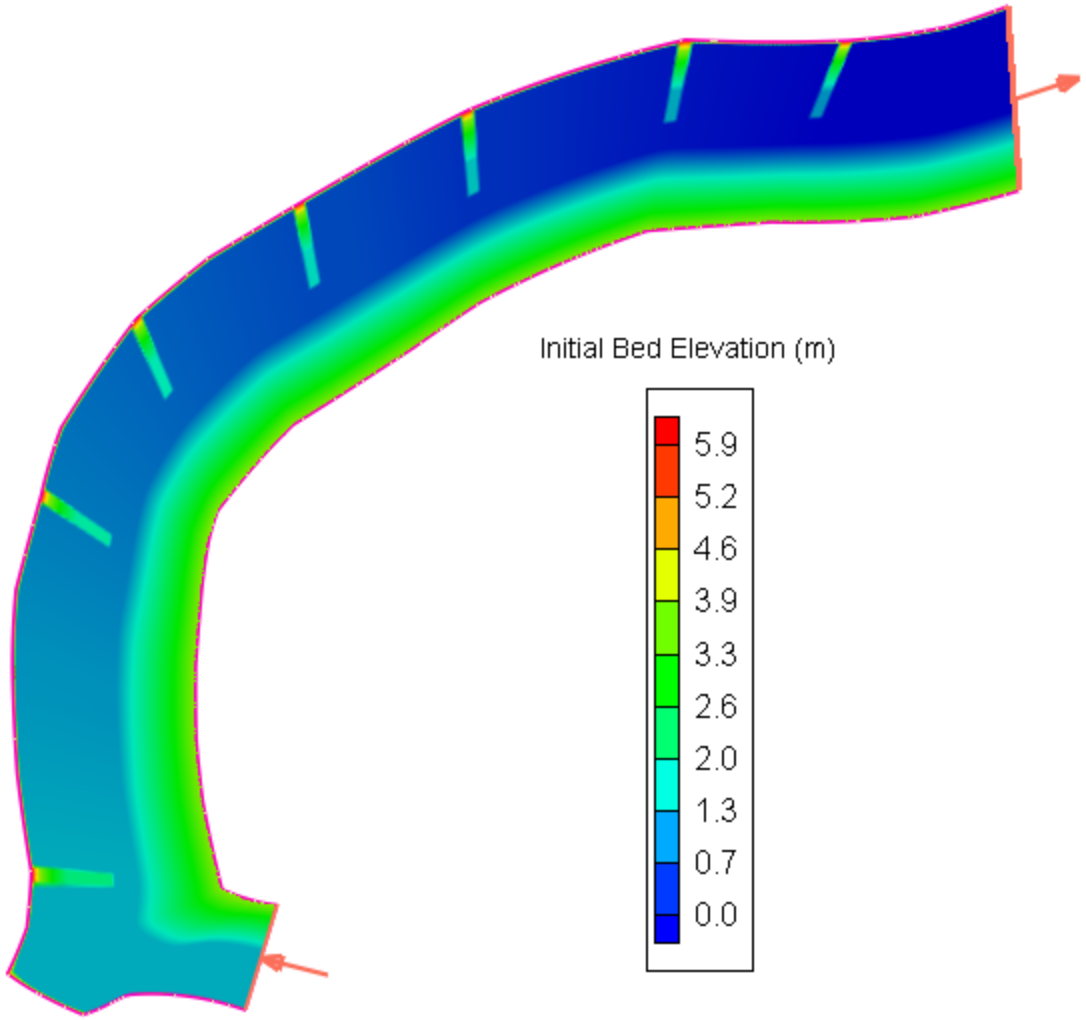

# Velocity Magnitude (m/s)

## Discharge: 40 m^3/s, Initial Water Height: 1.5 m

## (observed conditions during fieldwork conducted on August 2009)

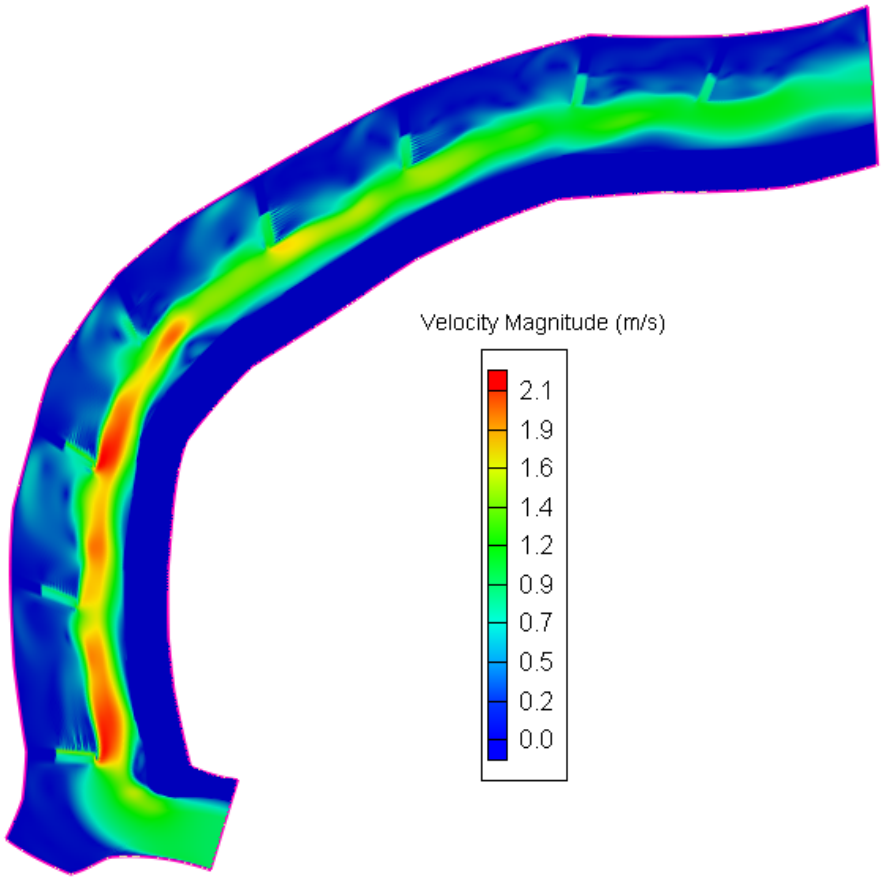


As built

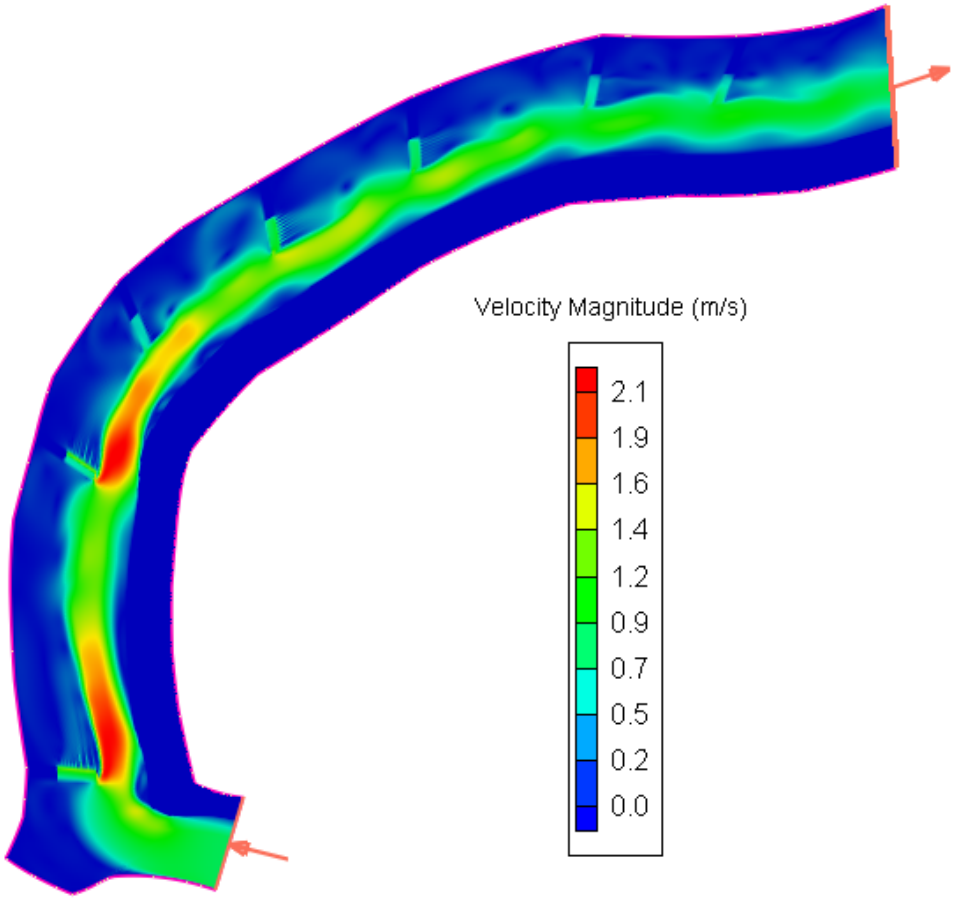


7 Barbs (no 2nd barb)

# Total Specific Discharge (m^2/s)

## Discharge: 40 m^3/s, Initial Water Height: 1.5 m

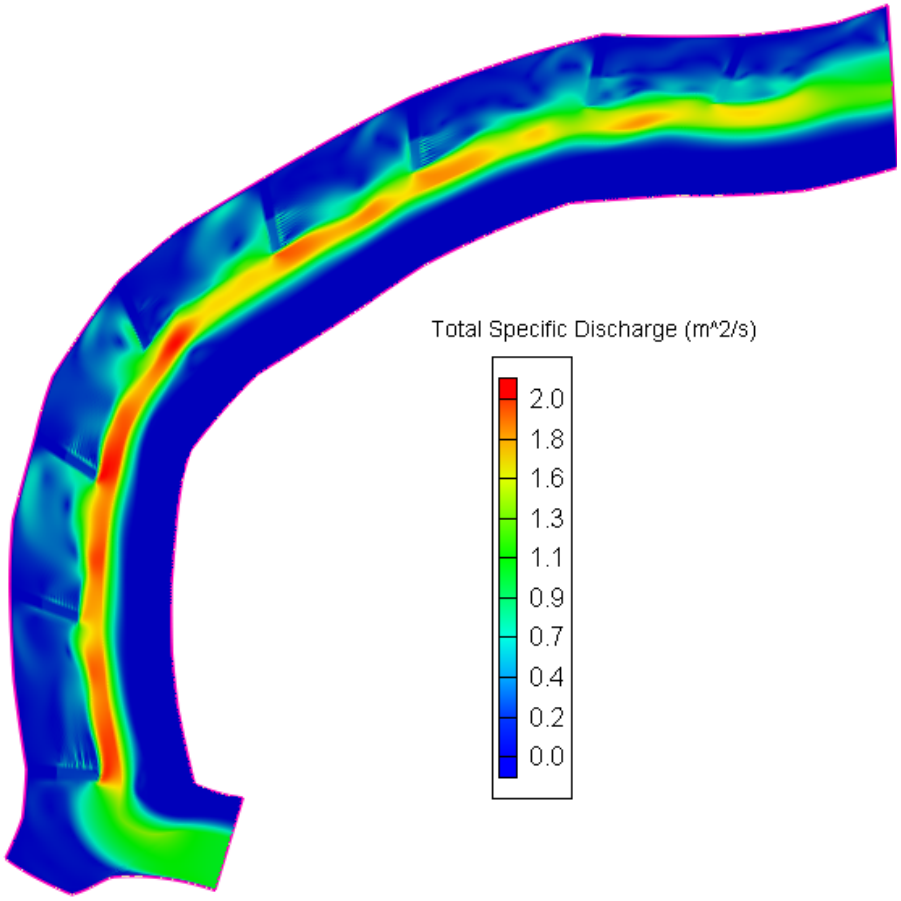


As built

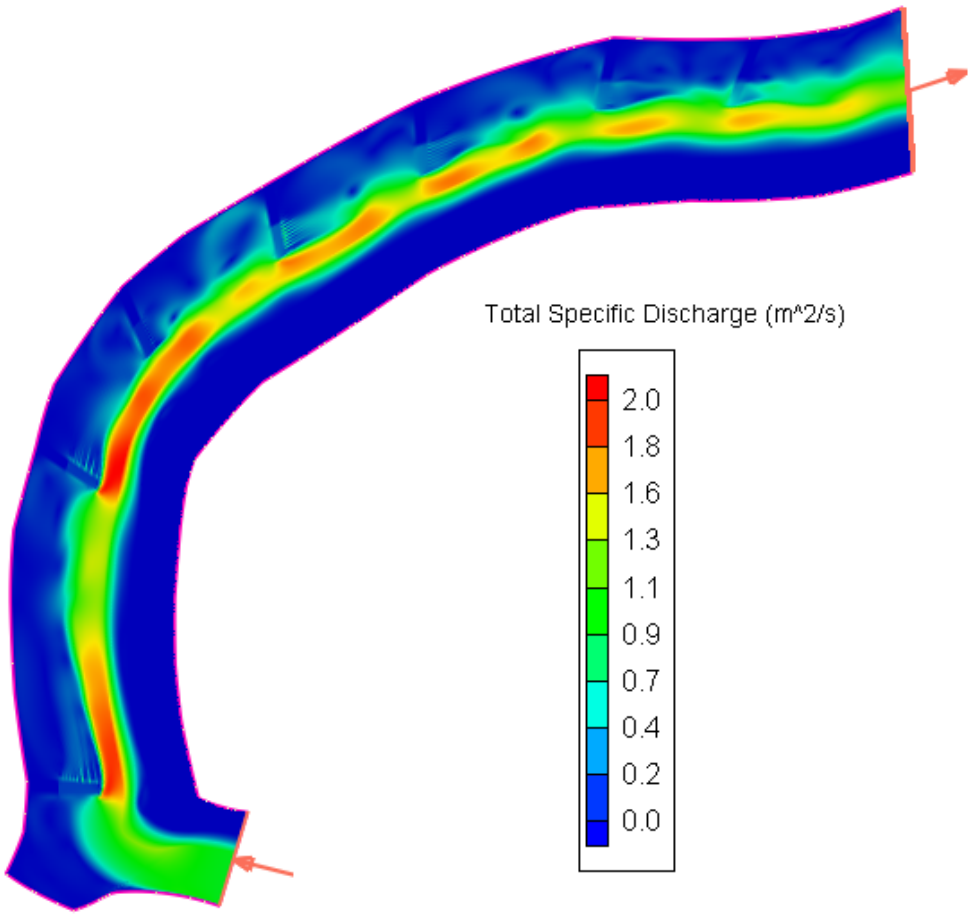


7 Barbs (no 2nd barb)

# Froude Number
# Discharge: 40 m^3/s, Initial Water Height: 1.5 m

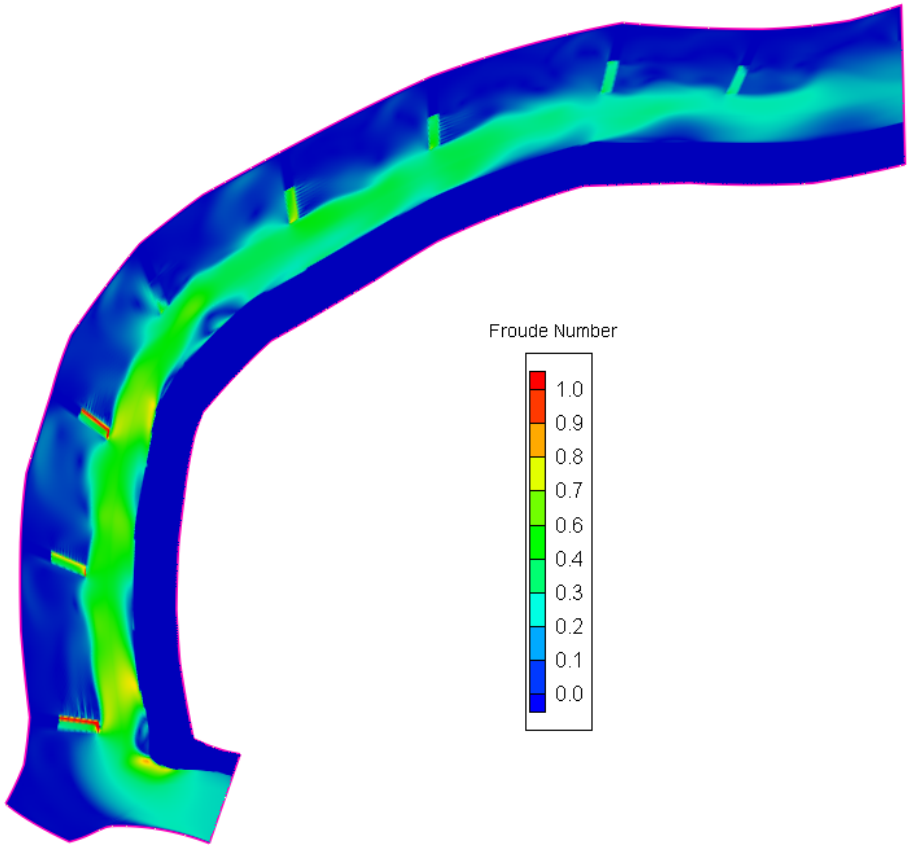


As built

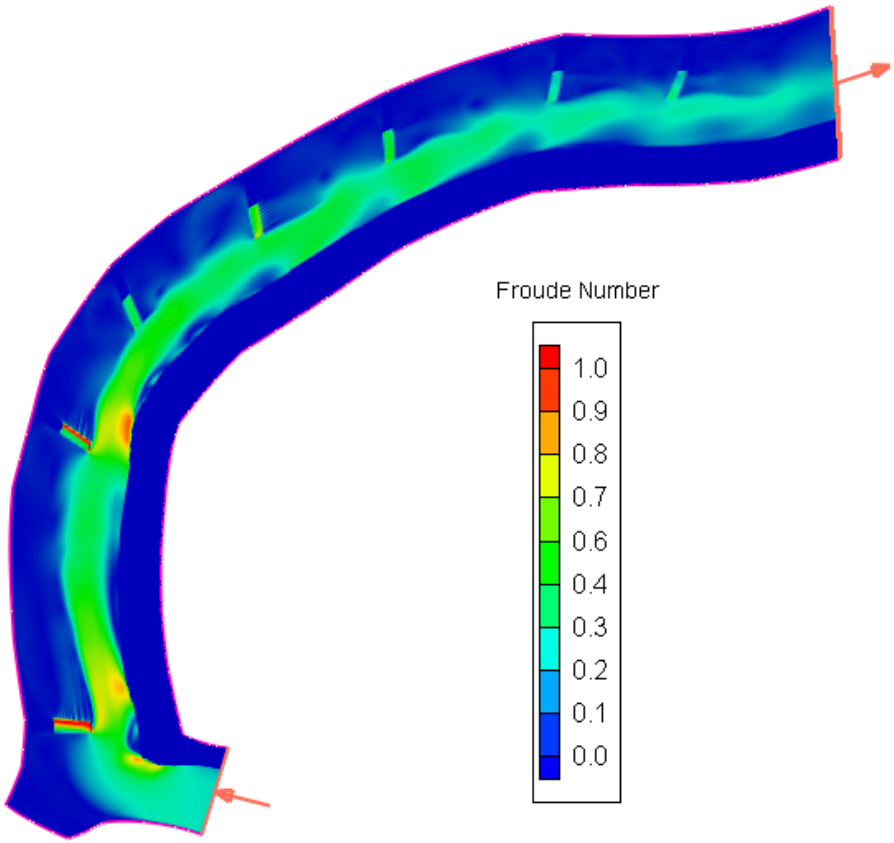


7 Barbs (no 2nd barb)

# Total Shear Stress (N/m^2)
# Discharge: 40 m^3/s, Initial Water Height: 1.5 m

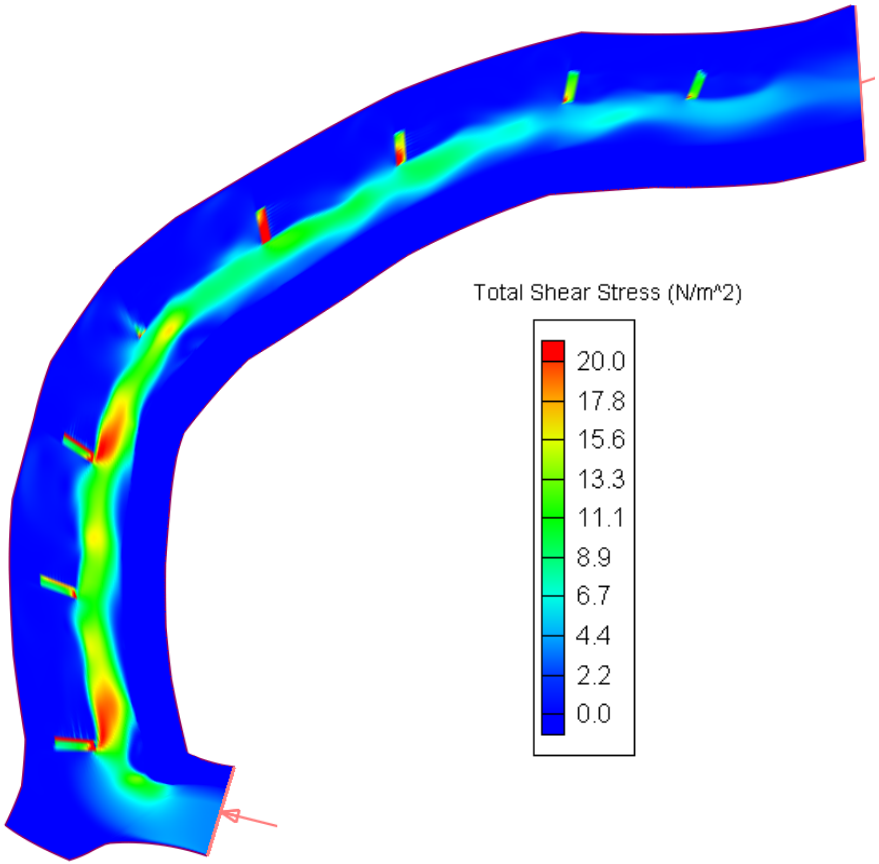


As built

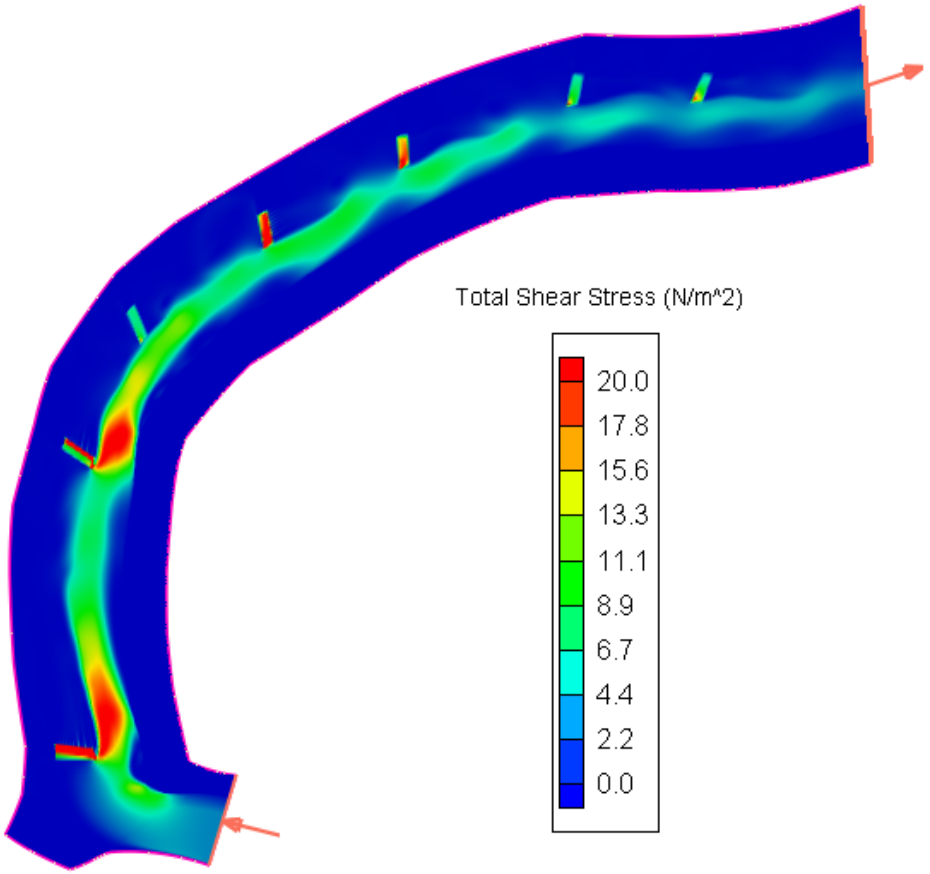


7 Barbs (no 2nd barb)

Bed sediment transport is initiated
when Total Shear Stress > 19 N/m^2

# 7 Barbs - No 3rd Barb

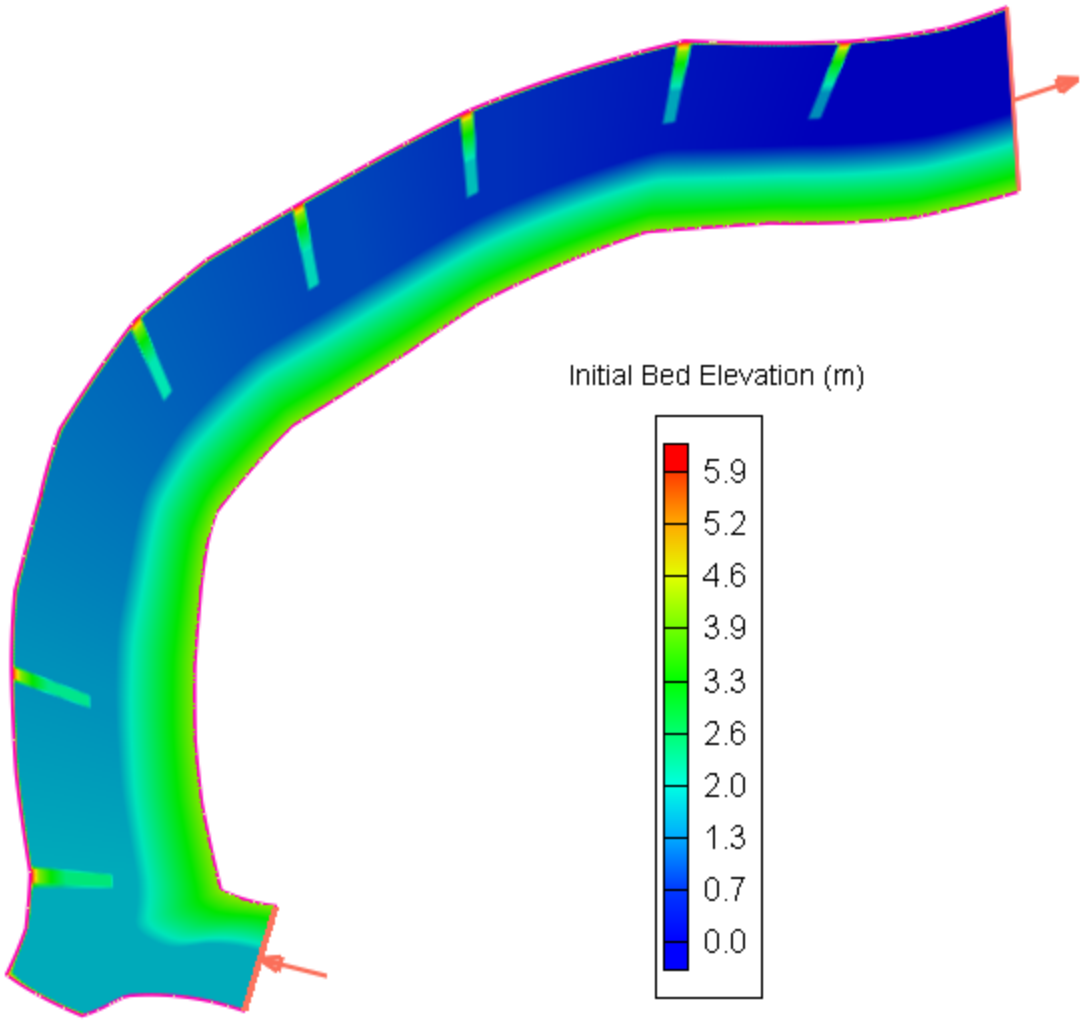

# Velocity Magnitude (m/s)

## Discharge: 40 m^3/s, Initial Water Height: 1.5 m

## (observed conditions during fieldwork conducted on August 2009)

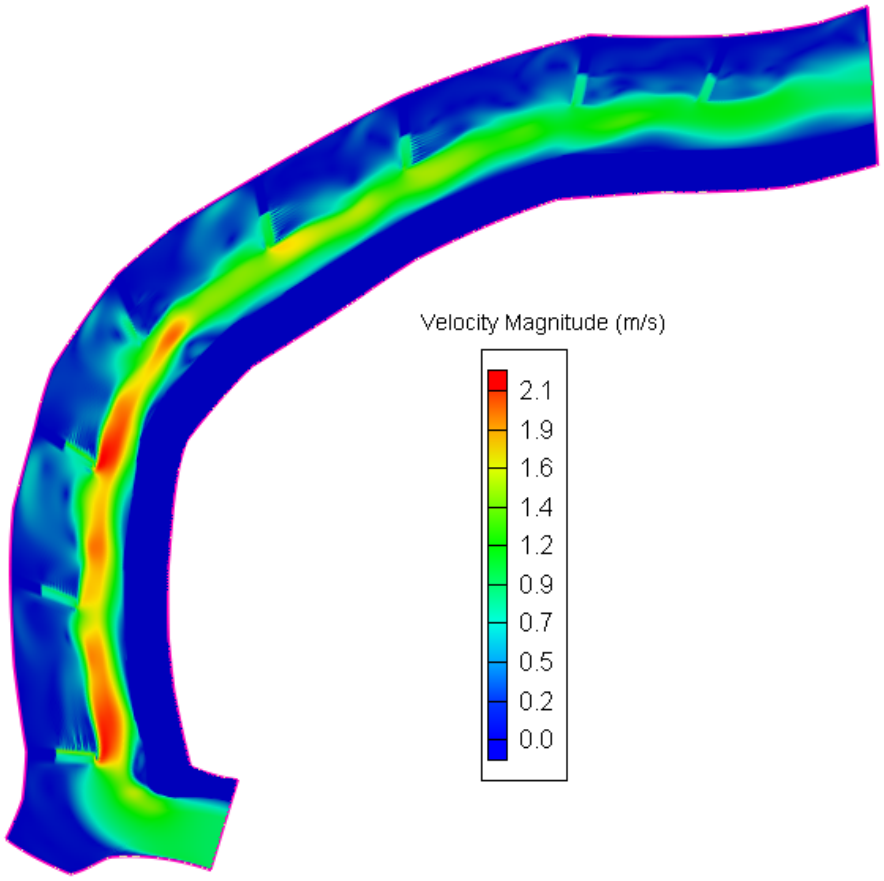


As built

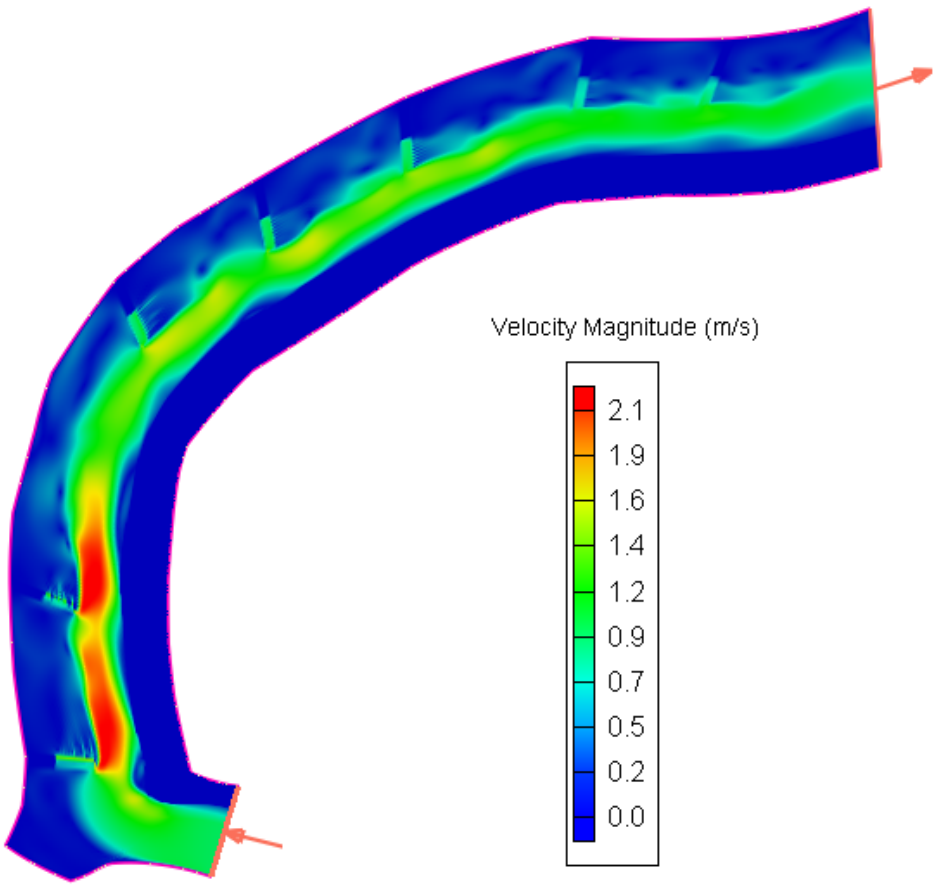


7 Barbs (no 3rd barb)

# Total Specific Discharge (m^2/s)

## Discharge: 40 m^3/s, Initial Water Height: 1.5 m

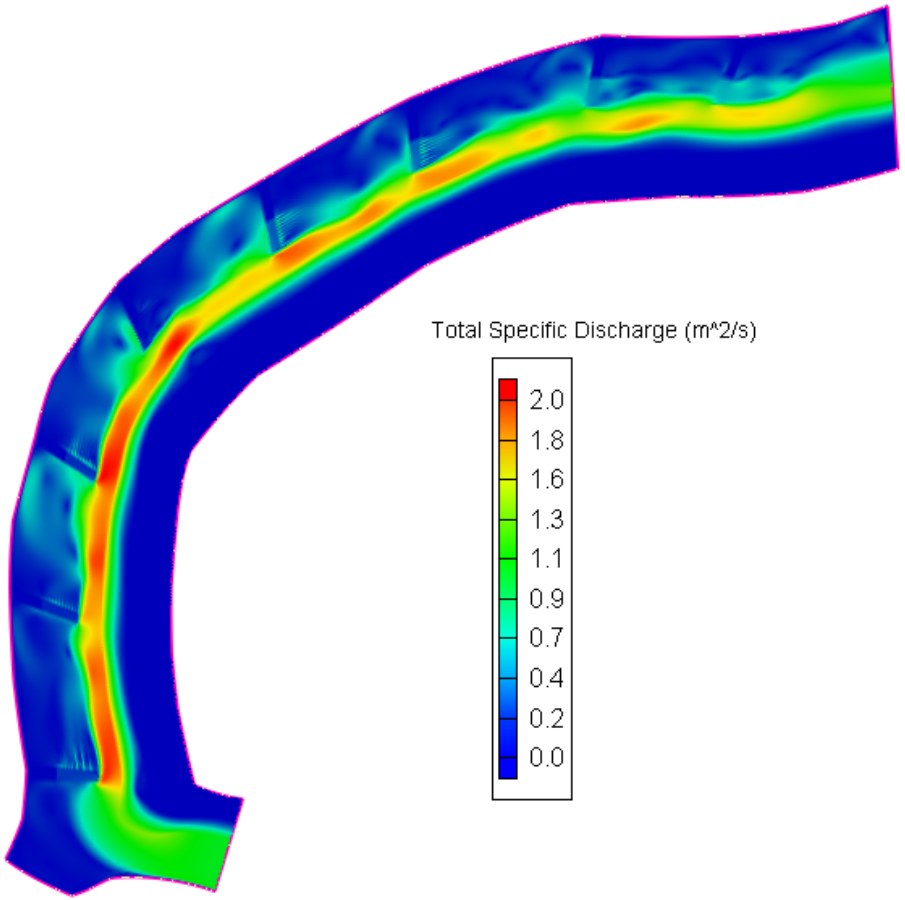


As built

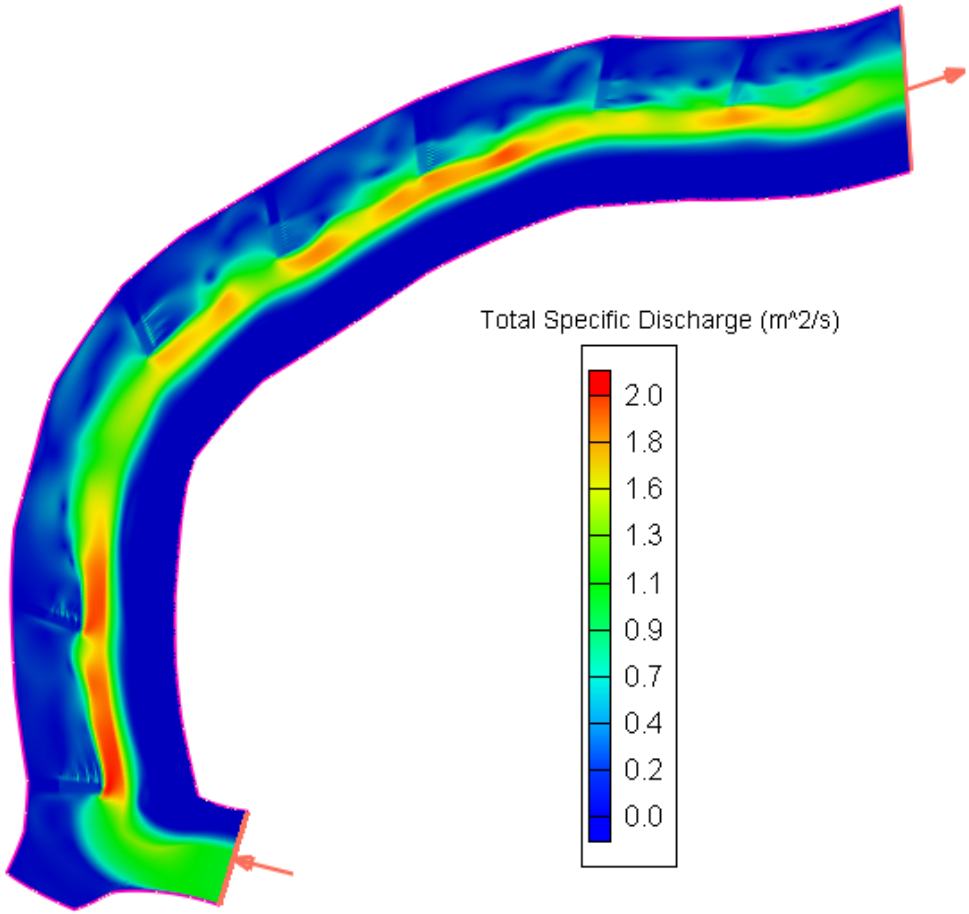


7 Barbs (no 3rd barb)

# Froude Number
# Discharge: 40 m^3/s, Initial Water Height: 1.5 m

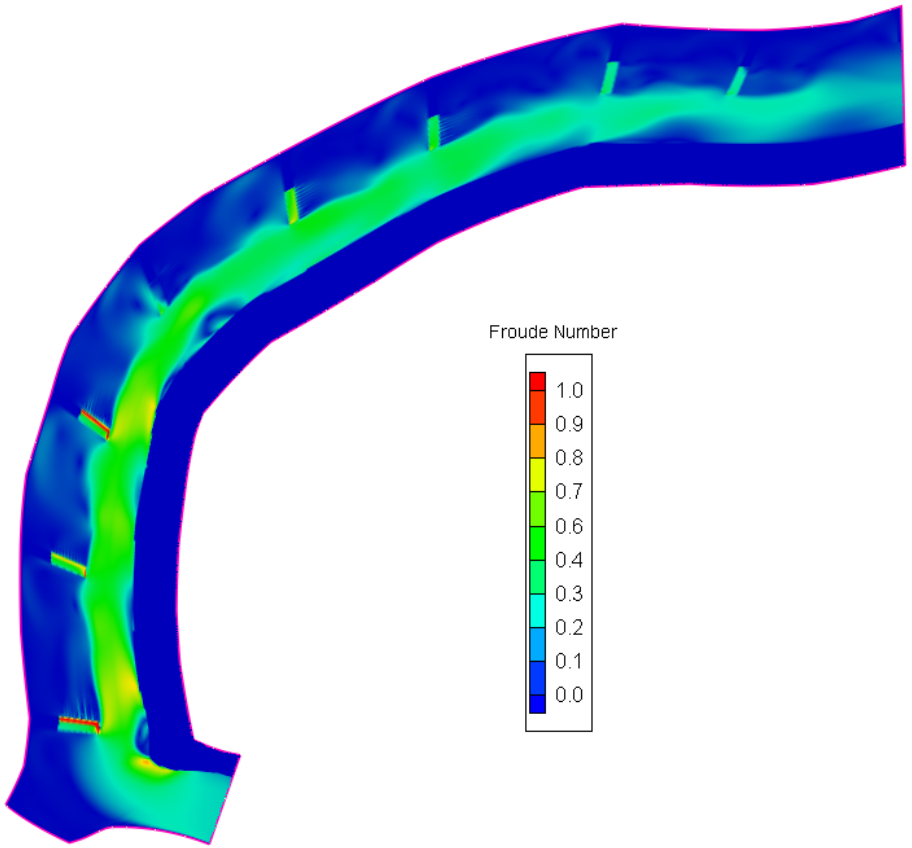


As built

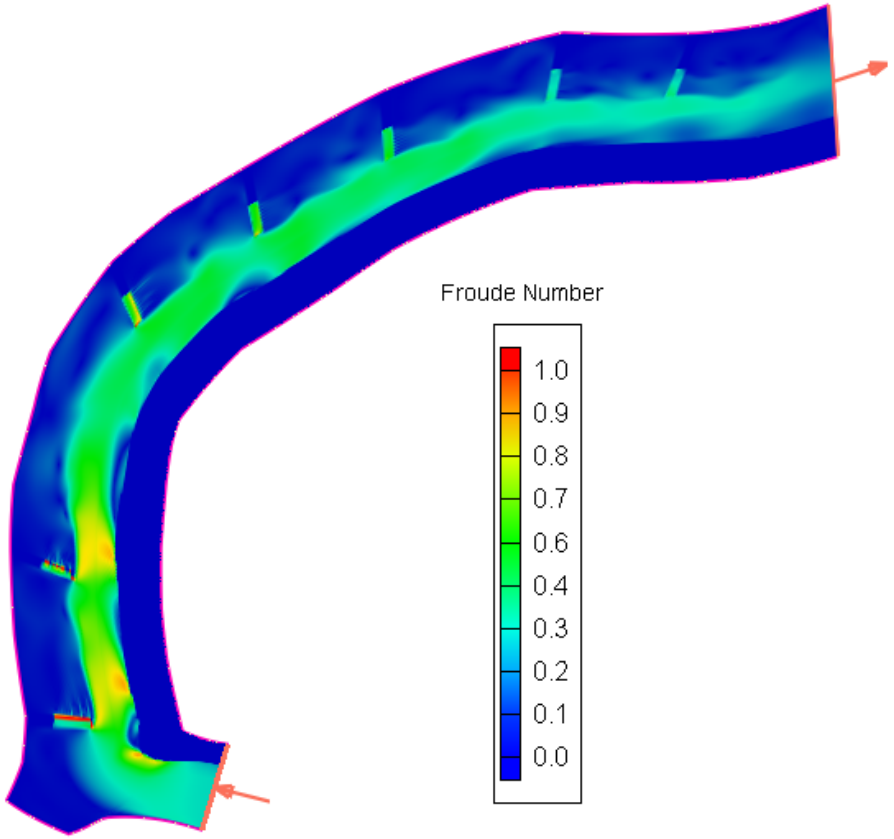


7 Barbs (no 3rd barb)

# Total Shear Stress (N/m^2)
# Discharge: 40 m^3/s, Initial Water Height: 1.5 m

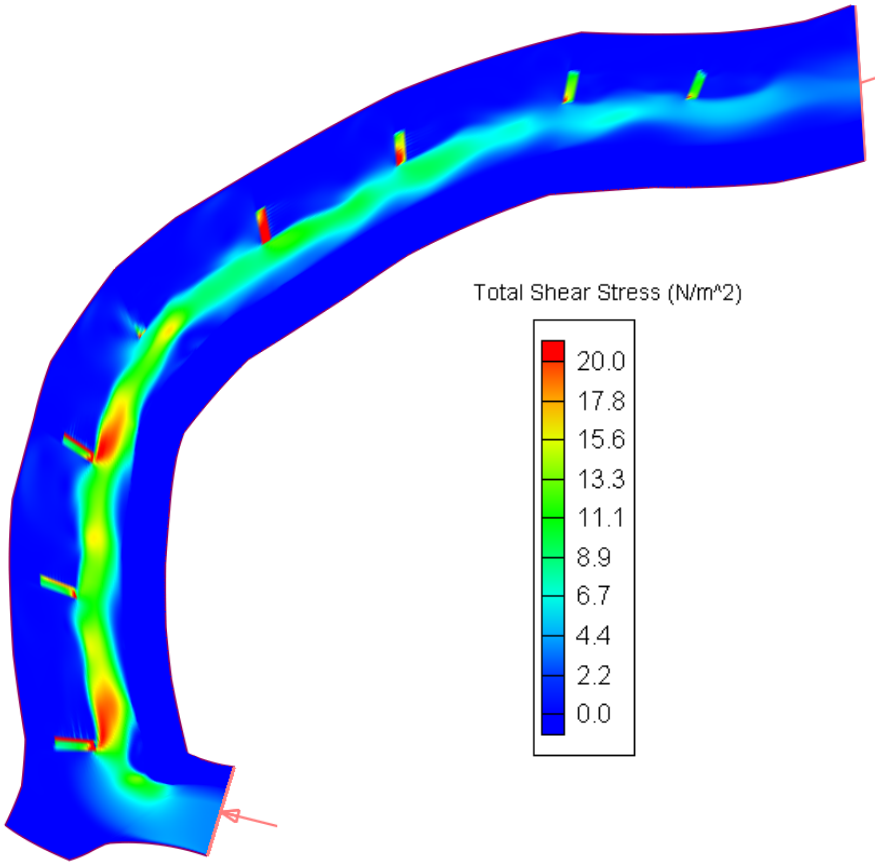


As built

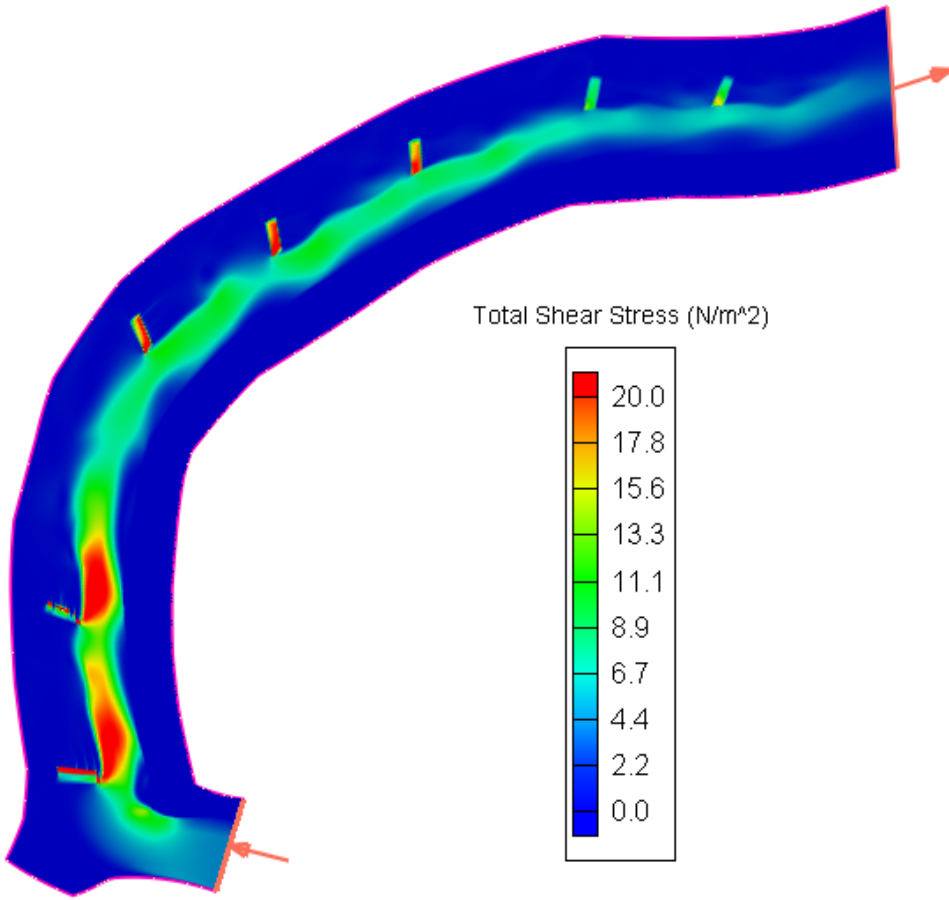


7 Barbs (no 3rd barb)

Bed sediment transport is initiated
when Total Shear Stress > 19 N/m^2

# 7 Barbs - No 4th Barb

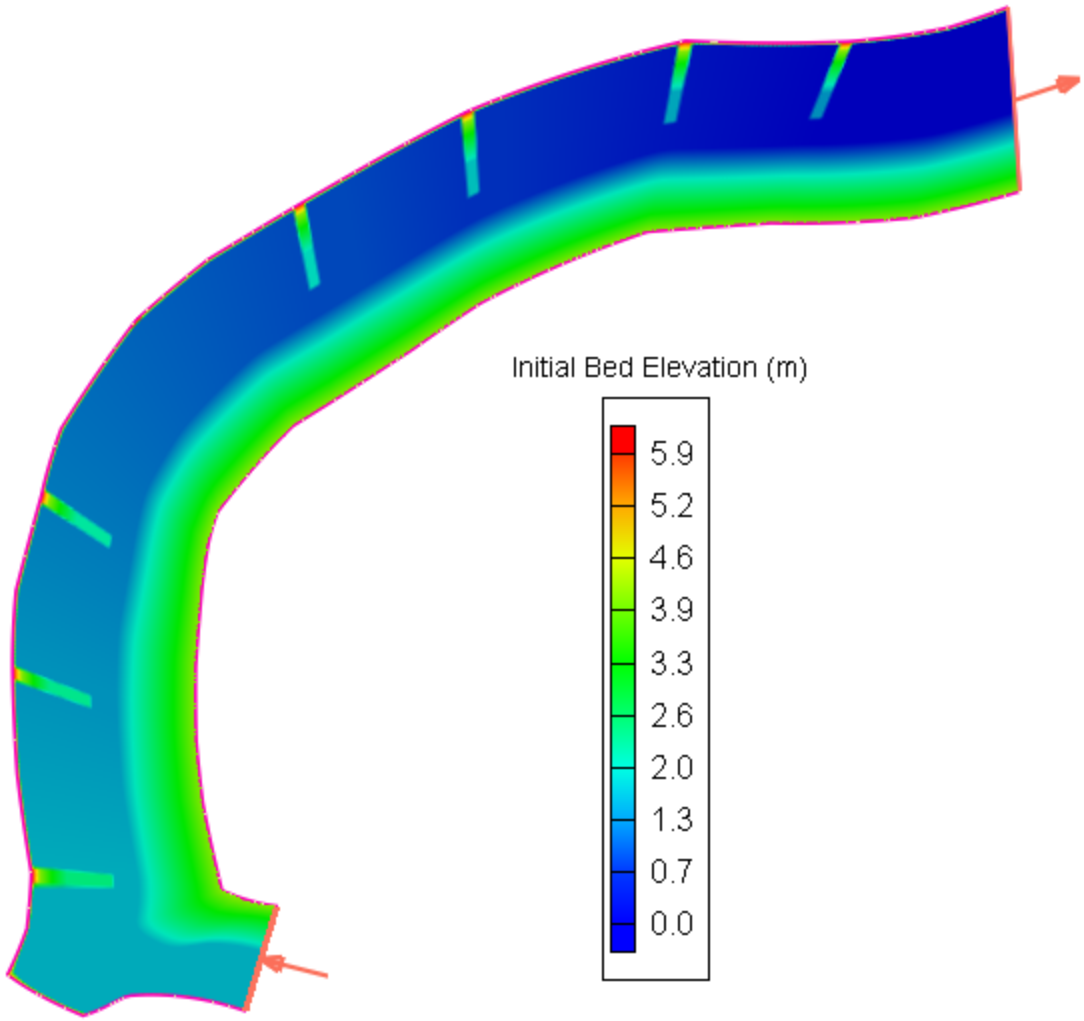

# Velocity Magnitude (m/s)

## Discharge: 40 m^3/s, Initial Water Height: 1.5 m

## (observed conditions during fieldwork conducted on August 2009)

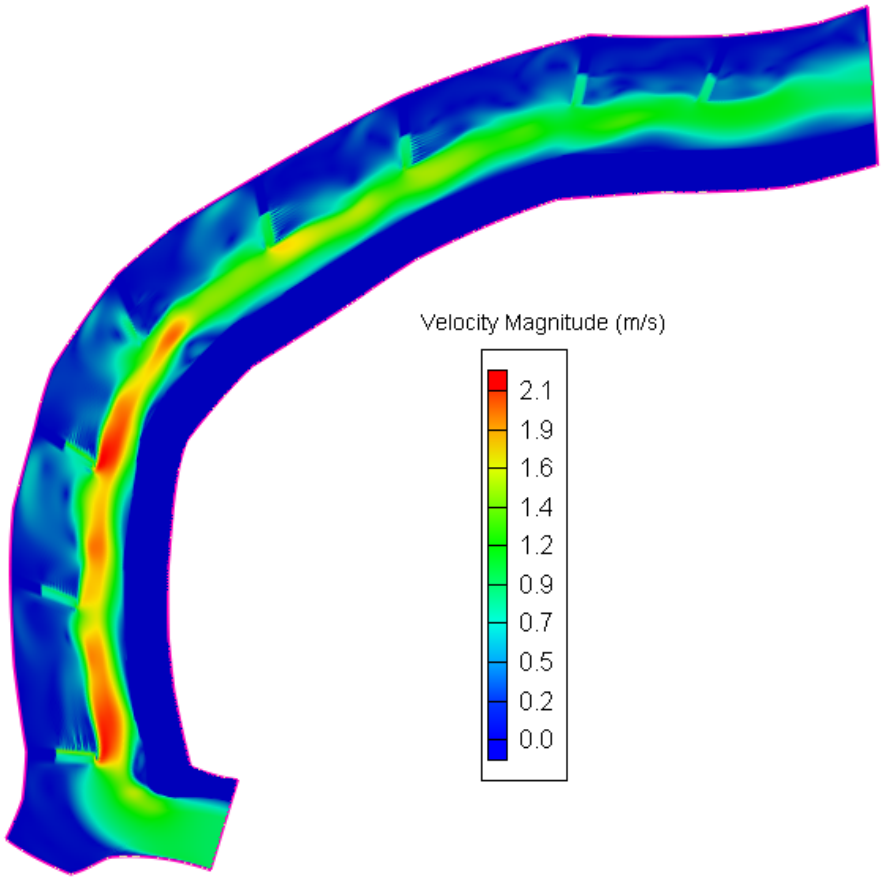


As built

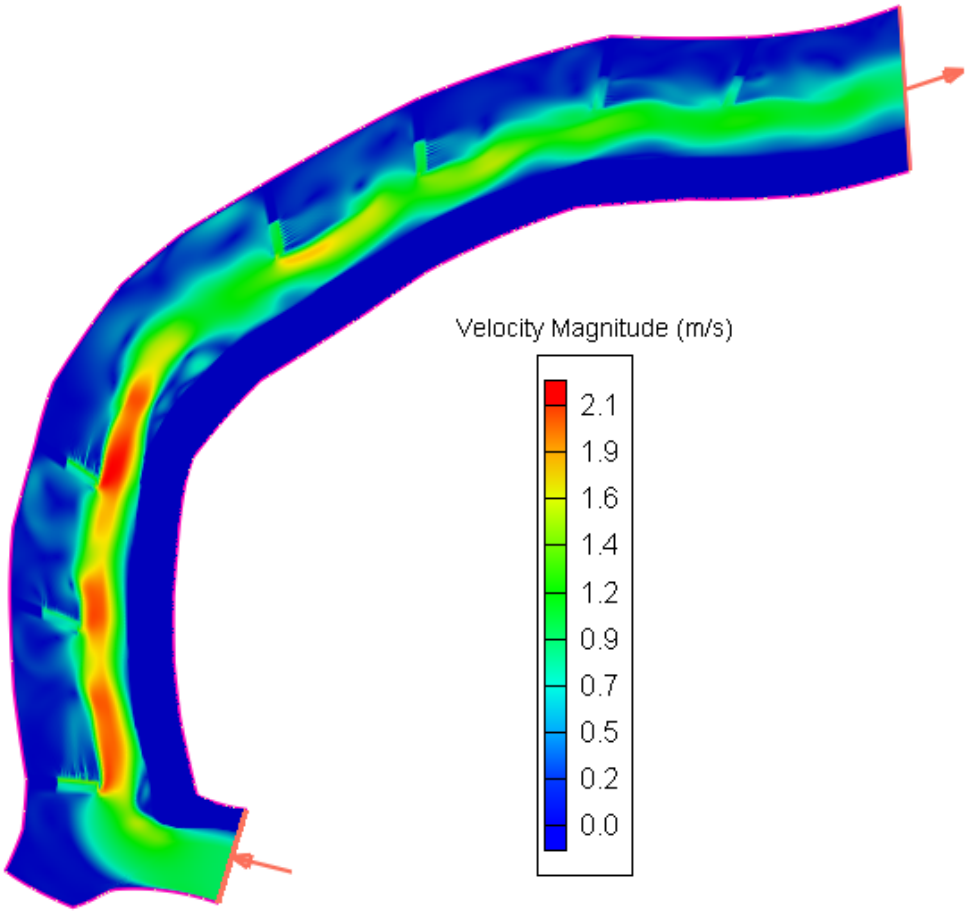


7 Barbs (no 4th barb)

# Total Specific Discharge (m^2/s)

## Discharge: 40 m^3/s, Initial Water Height: 1.5 m

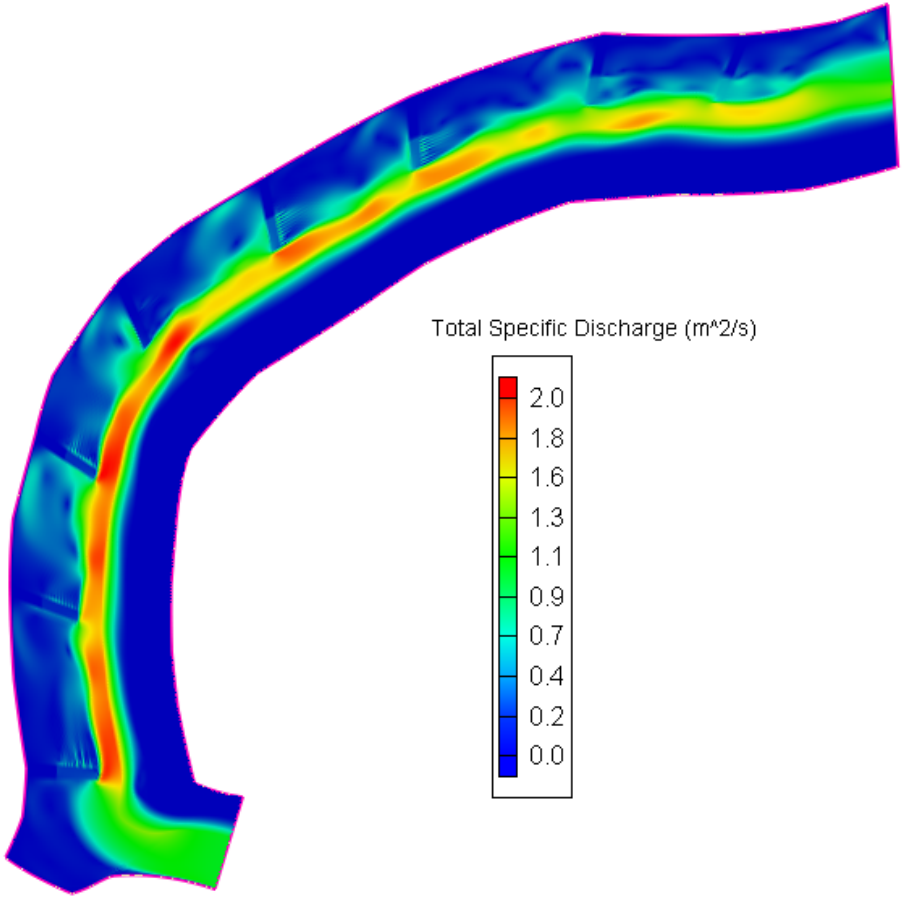


As built

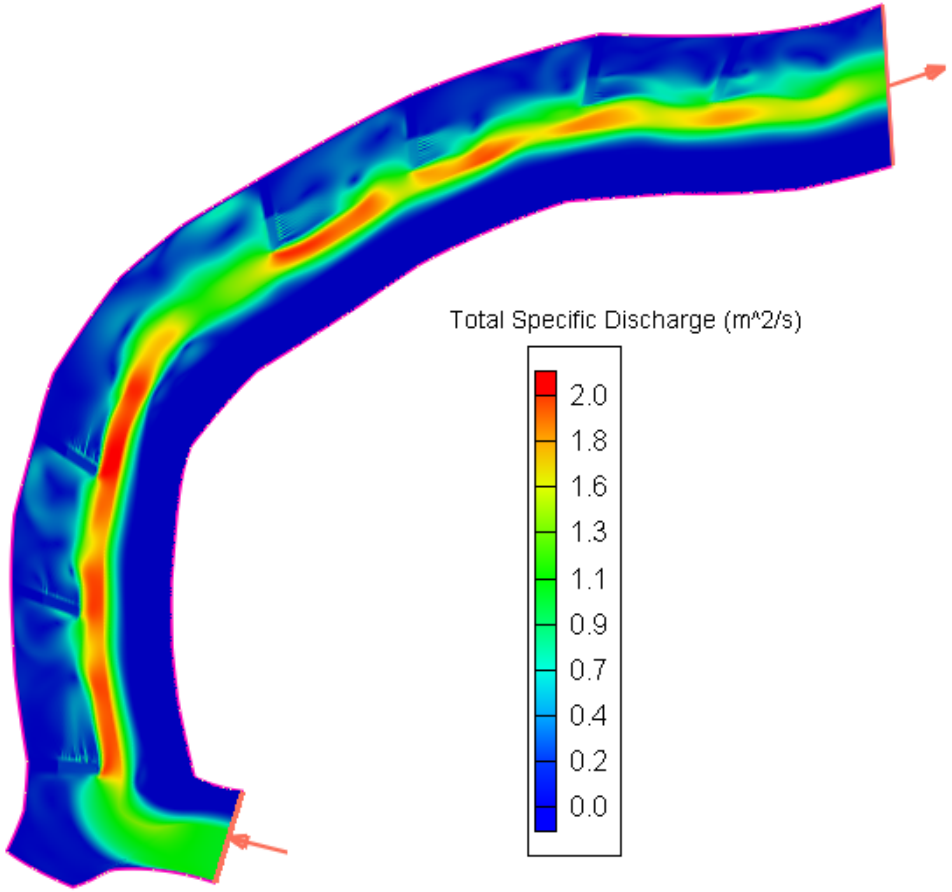


7 Barbs (no 4th barb)

# Froude Number
# Discharge: 40 m^3/s, Initial Water Height: 1.5 m

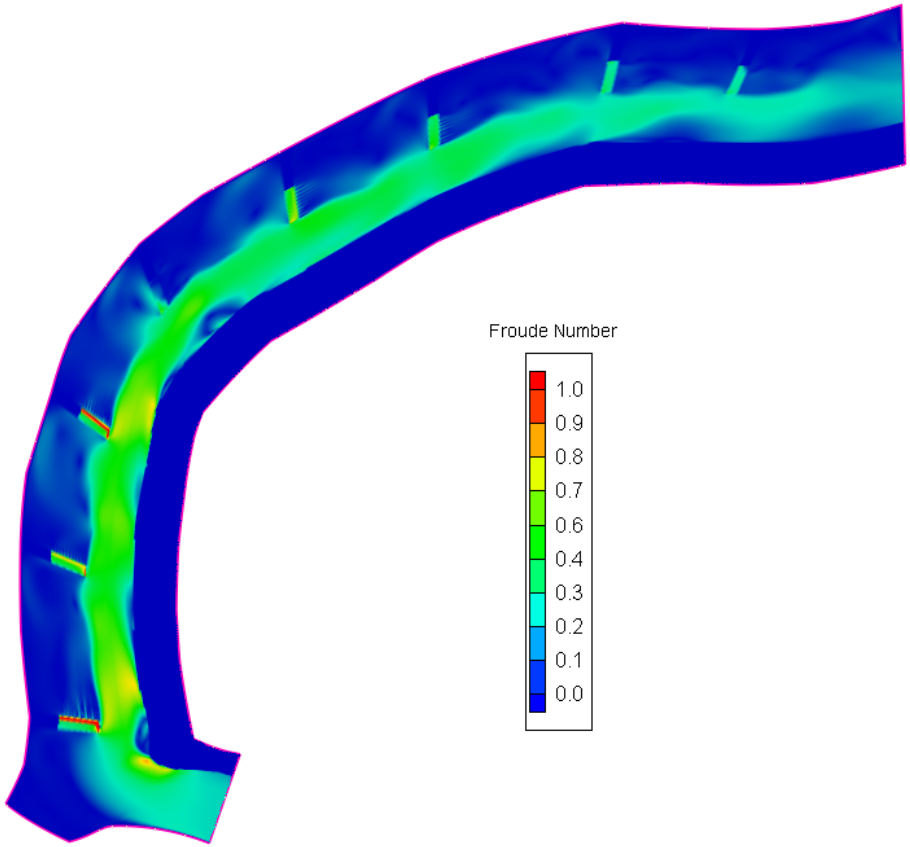


As built

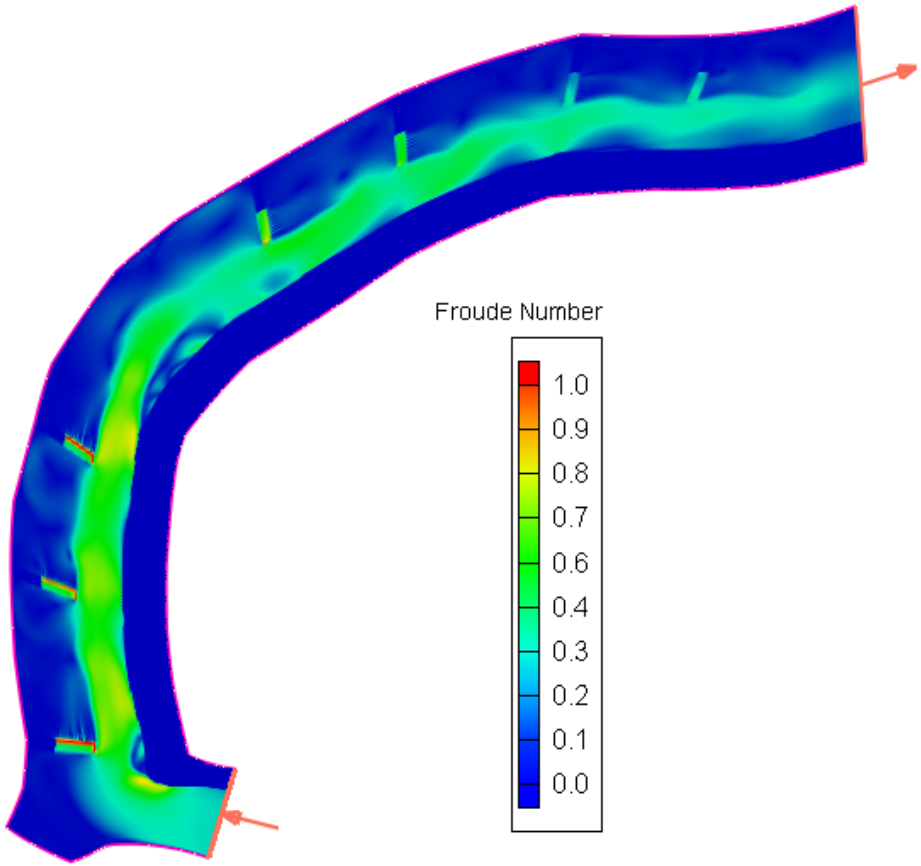


7 Barbs (no 4th barb)

# Total Shear Stress (N/m^2)
# Discharge: 40 m^3/s, Initial Water Height: 1.5 m

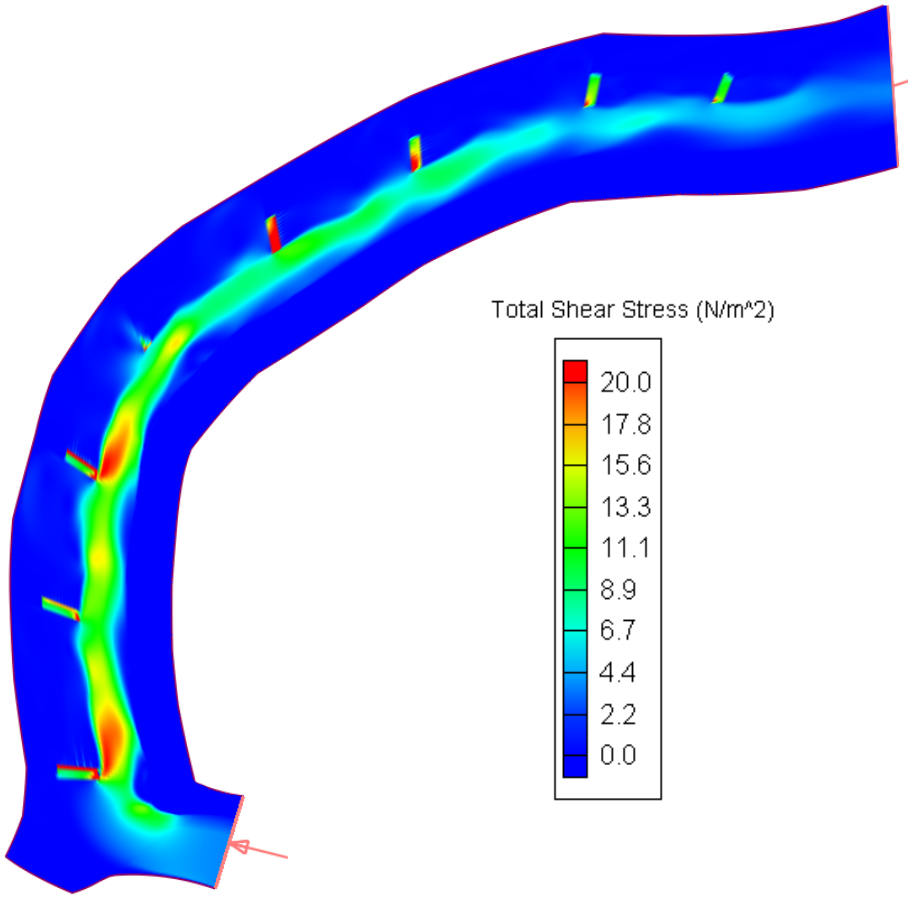


As built

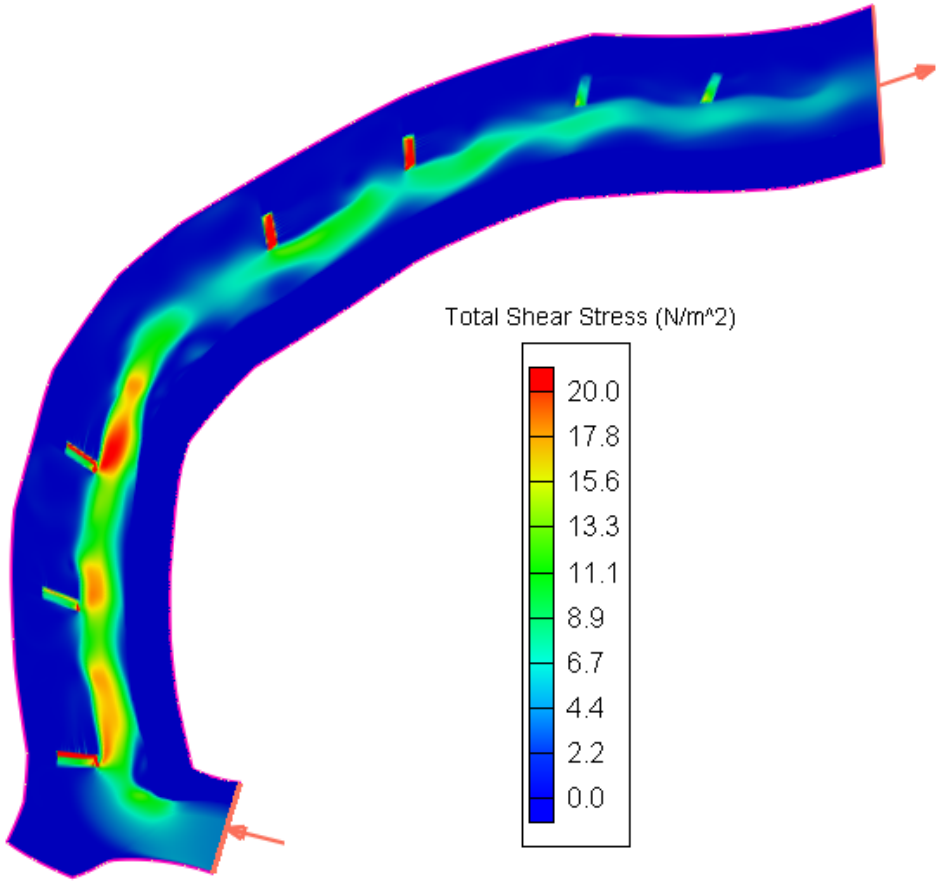


7 Barbs (no 4th barb)

Bed sediment transport is initiated
when Total Shear Stress > 19 N/m^2

# 7 Barbs - No 5th Barb

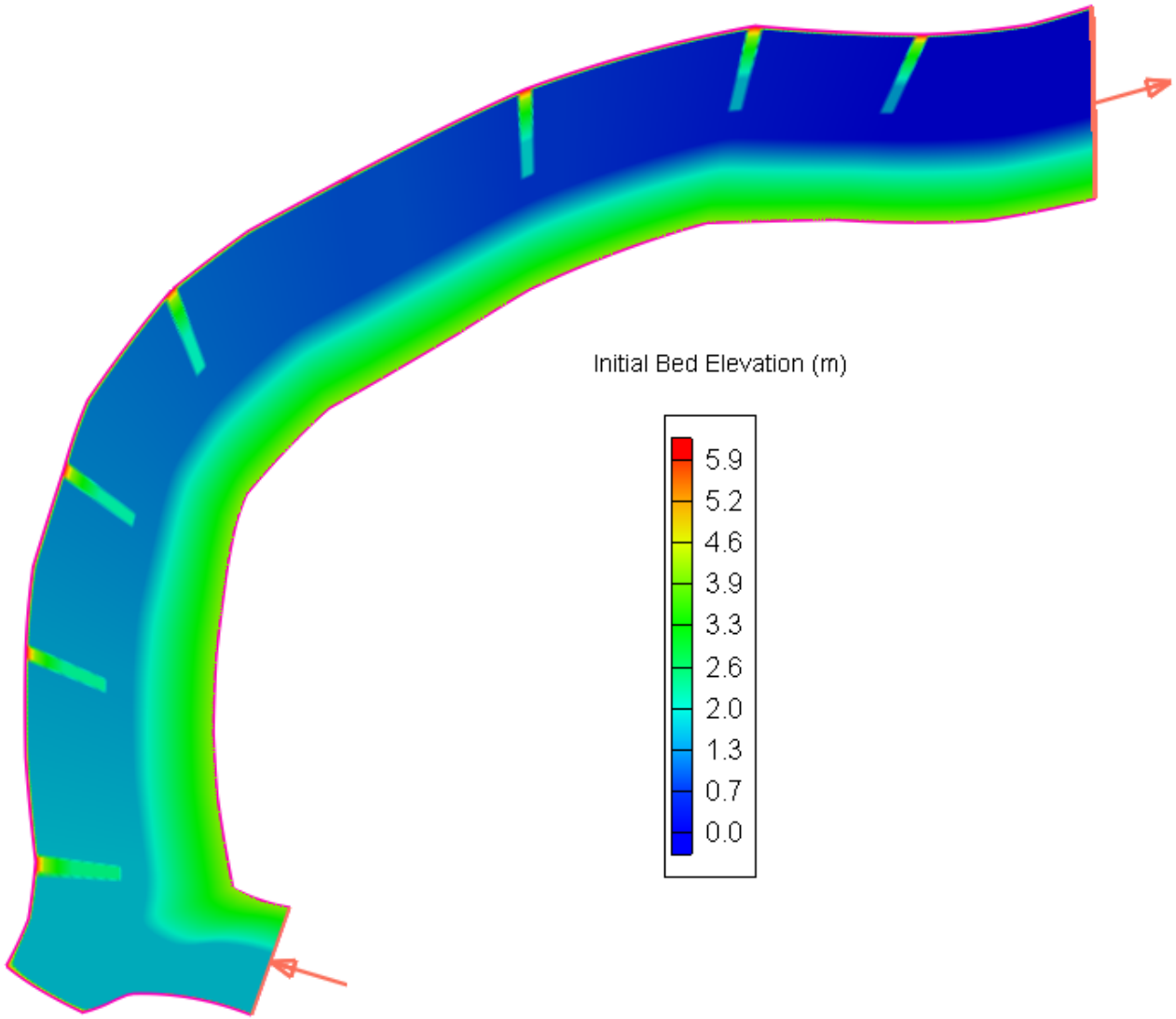

# Velocity Magnitude (m/s)

## Discharge: 40 m^3/s, Initial Water Height: 1.5 m

## (observed conditions during fieldwork conducted on August 2009)

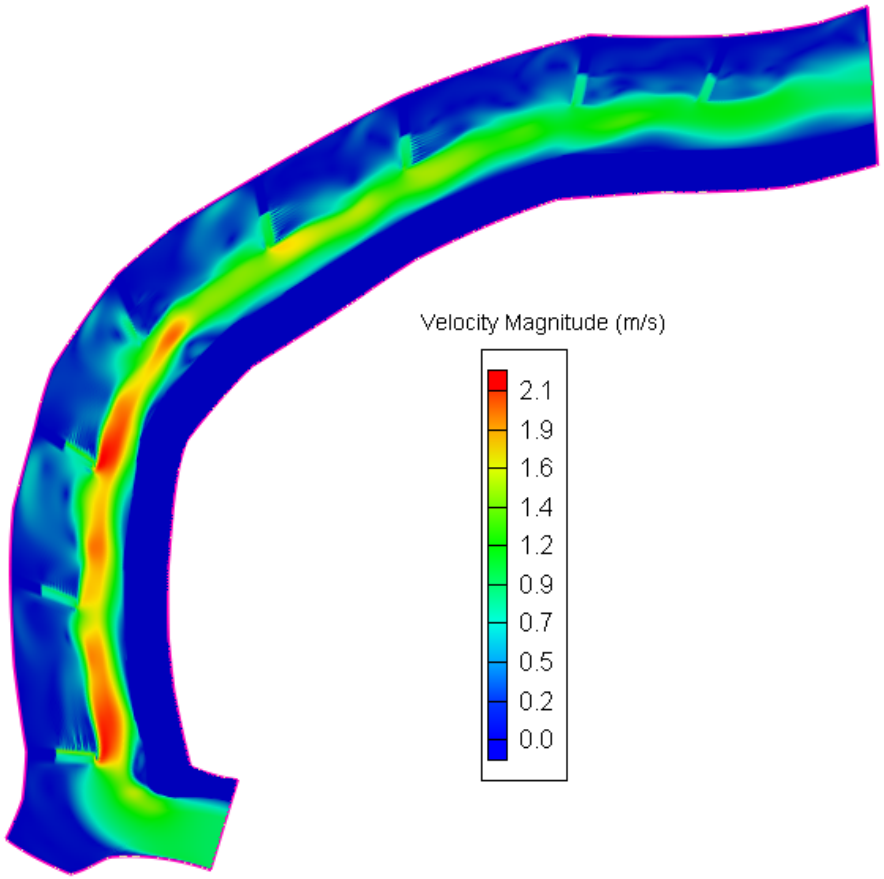


As built

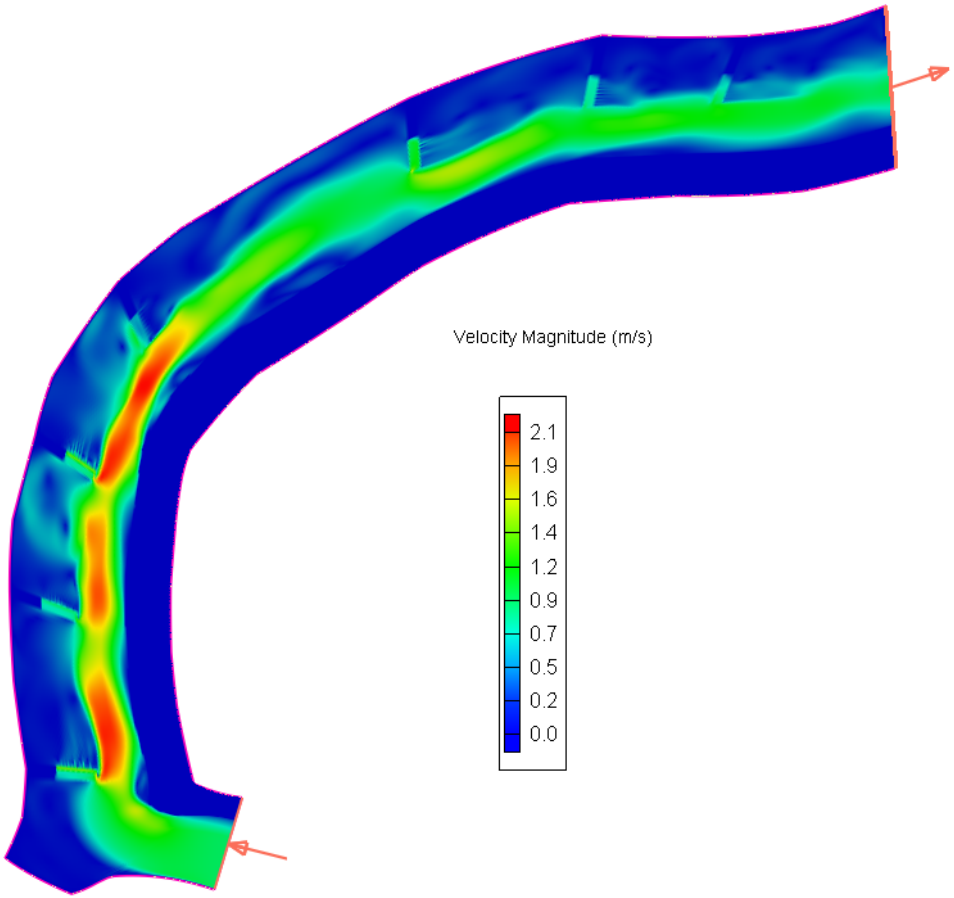


7 Barbs (no 5th barb)

# Total Specific Discharge (m^2/s)

## Discharge: 40 m^3/s, Initial Water Height: 1.5 m

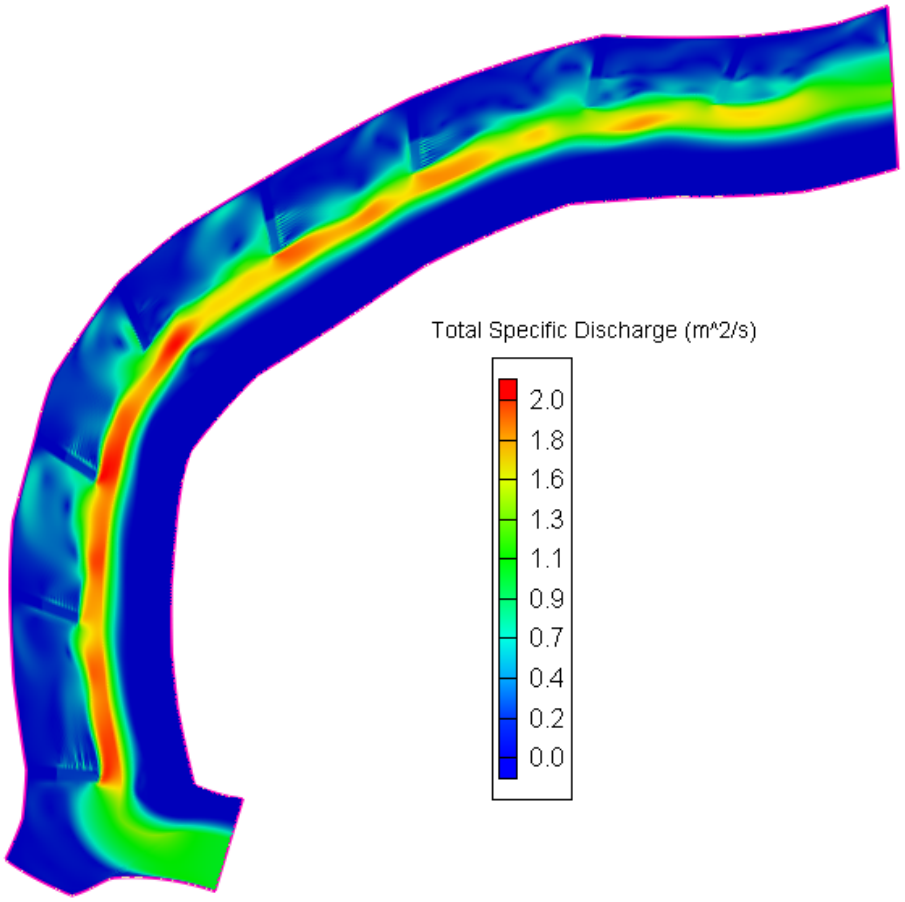


As built

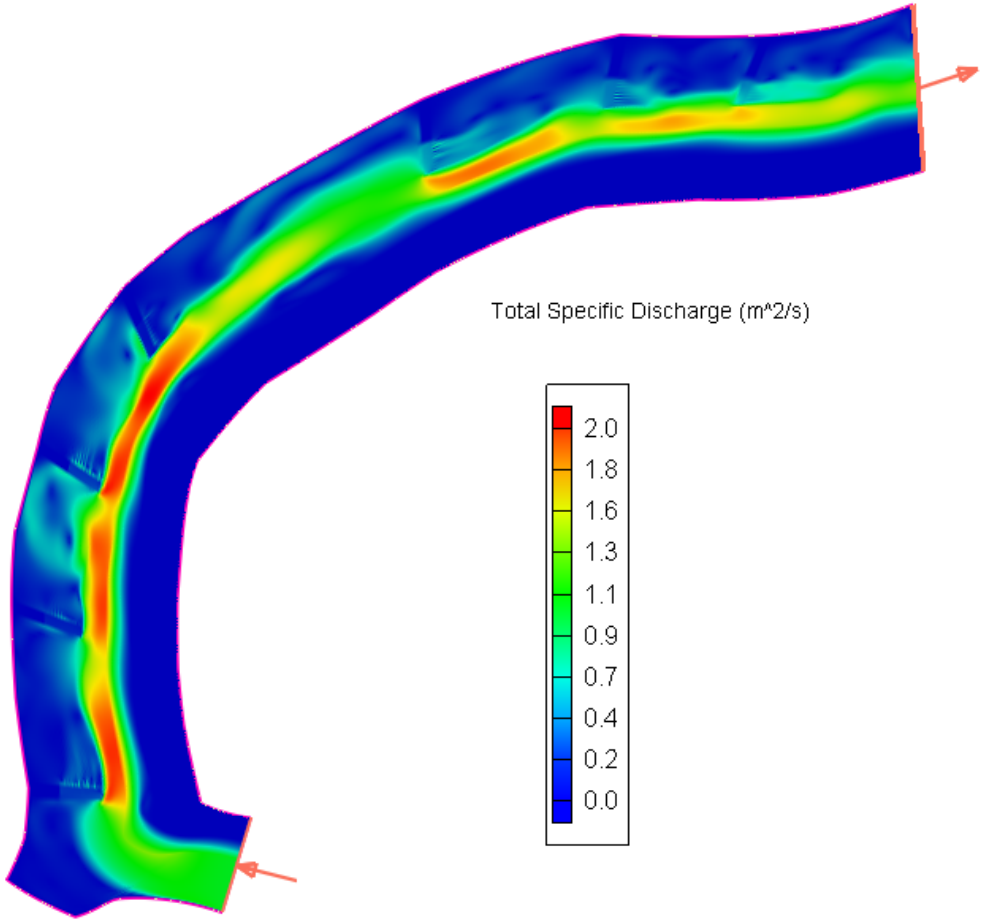


7 Barbs (no 5st barb)

# Froude Number
## Discharge: 40 m^3/s, Initial Water Height: 1.5 m

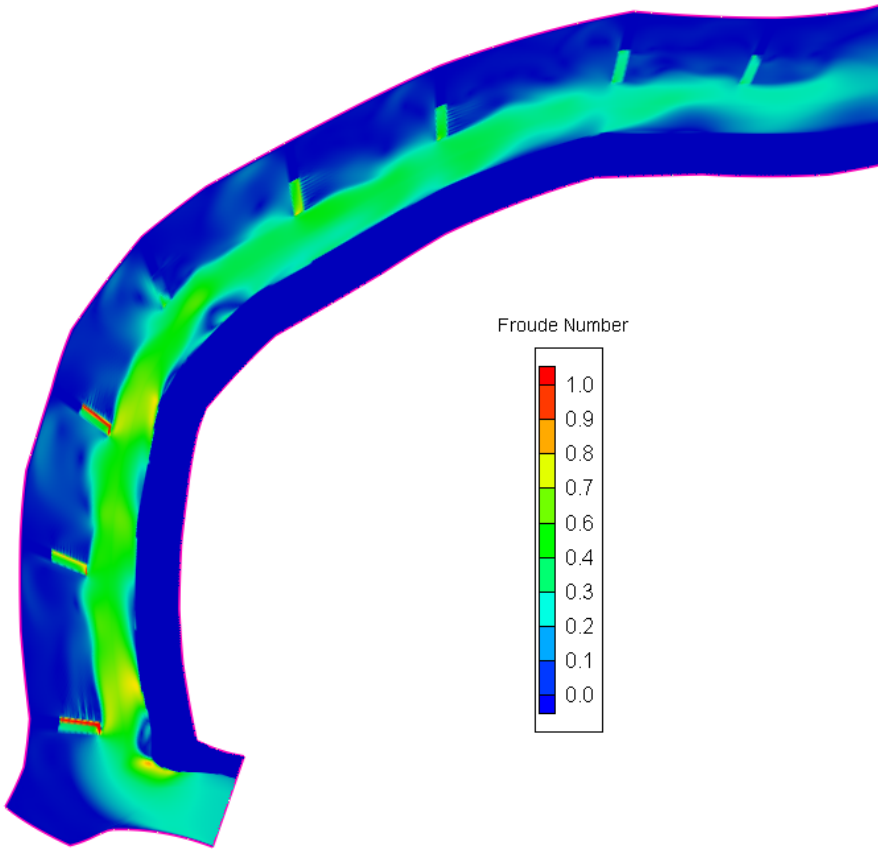


As built

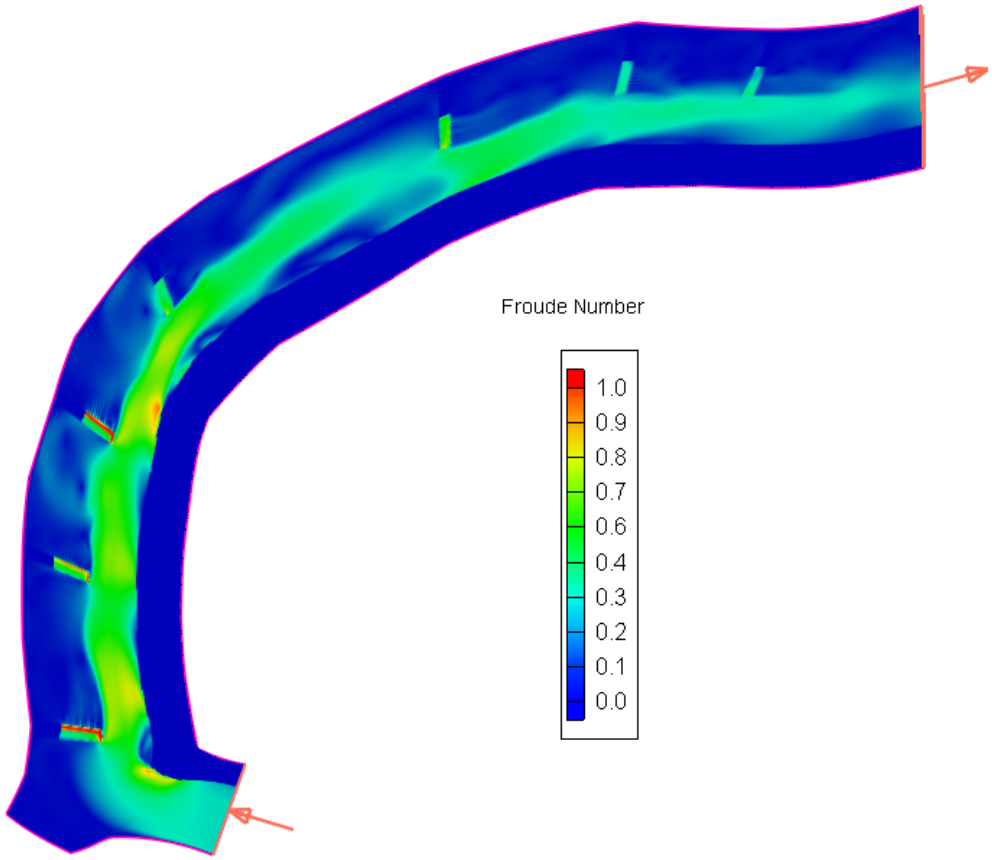


7 Barbs (no 5th barb)

# Total Shear Stress (N/m^2)
# Discharge: 40 m^3/s, Initial Water Height: 1.5 m

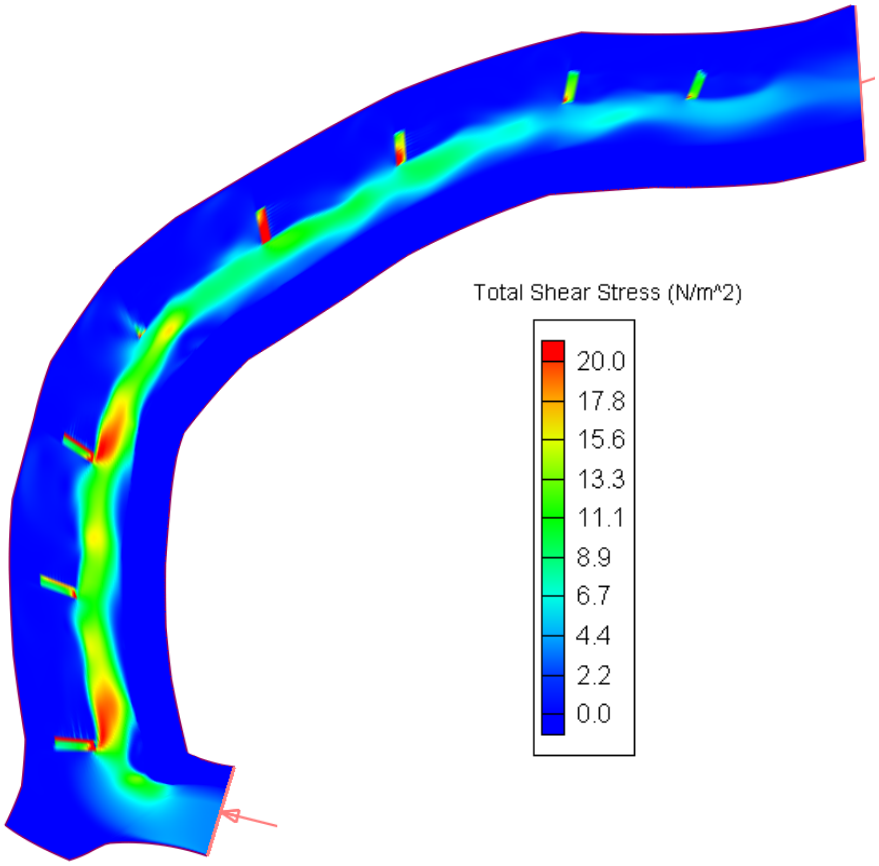


As built

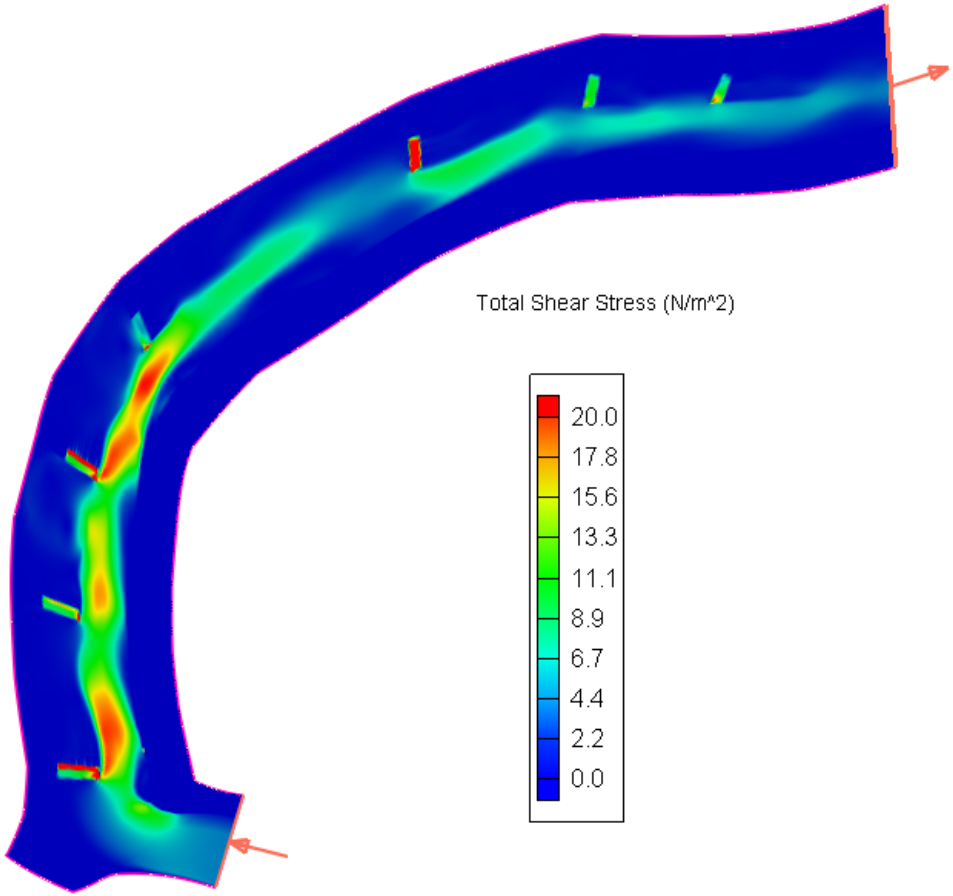


7 Barbs (no 5th barb)

Bed sediment transport is initiated
when Total Shear Stress > 19 N/m^2

# 7 Barbs - No 6th Barb

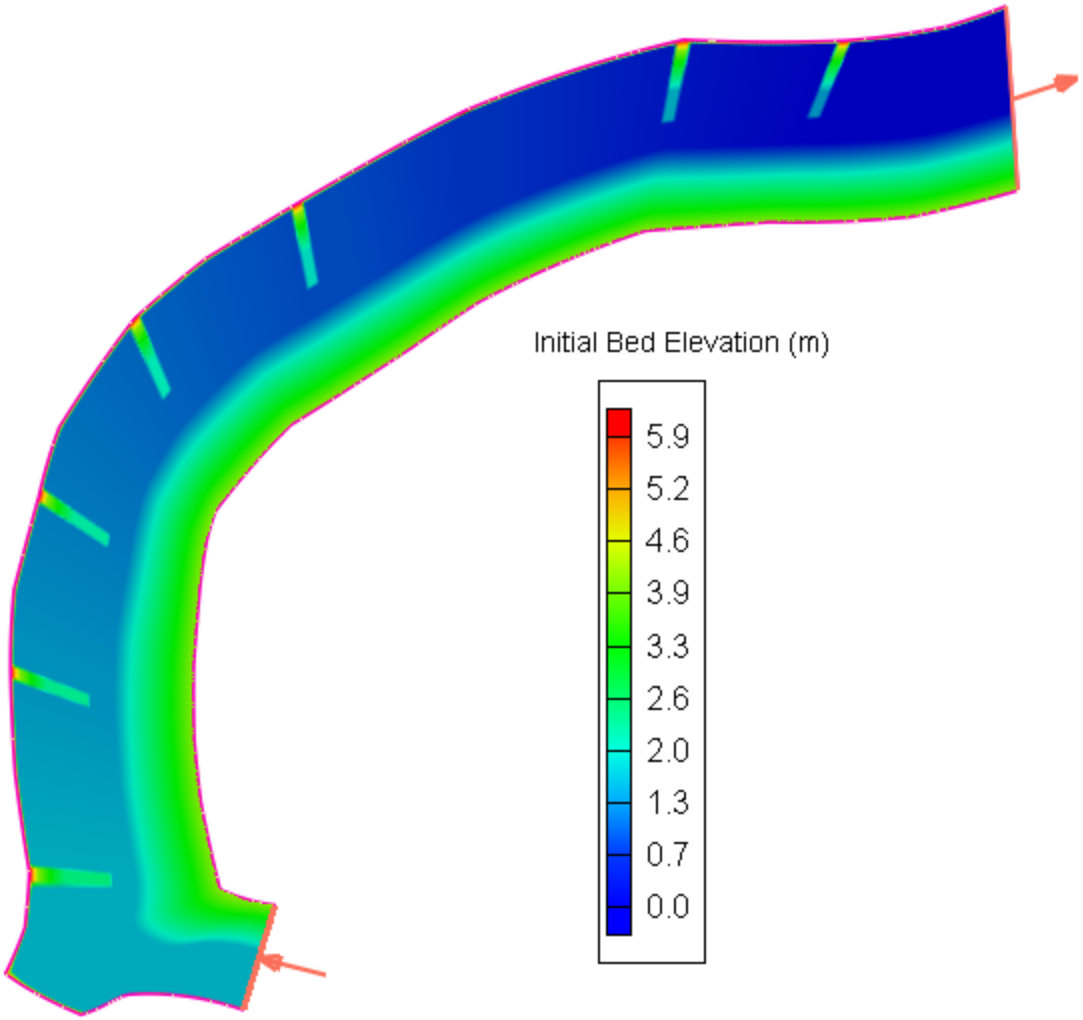

# Velocity Magnitude (m/s)

## Discharge: 40 m^3/s, Initial Water Height: 1.5 m

## (observed conditions during fieldwork conducted on August 2009)

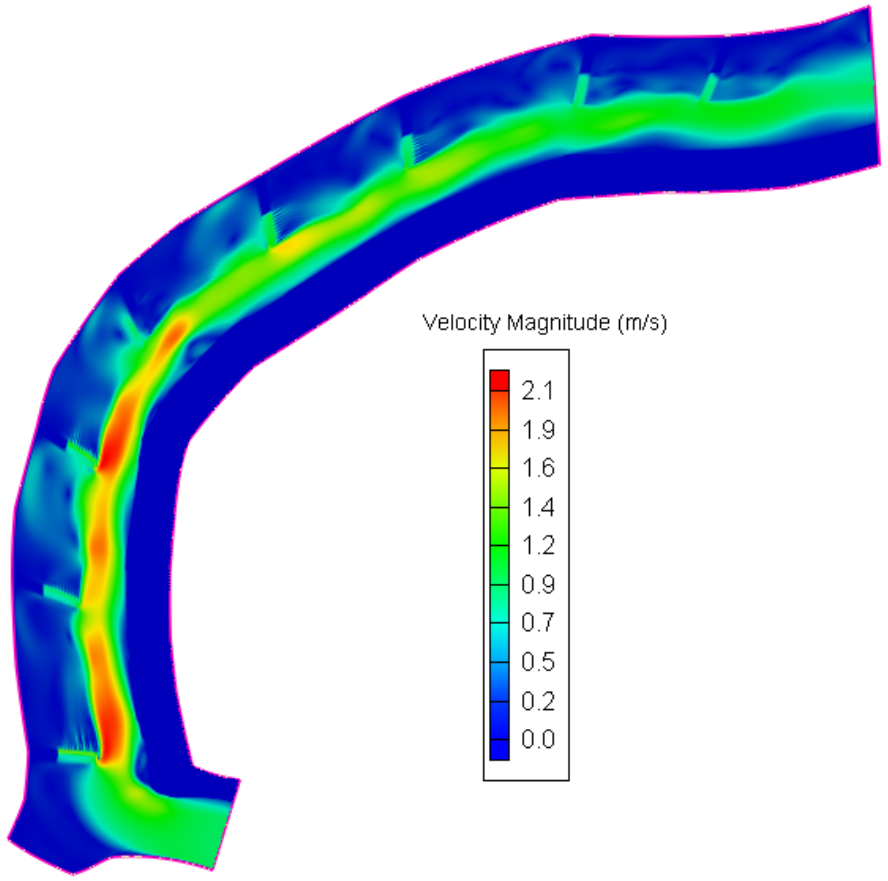


As built

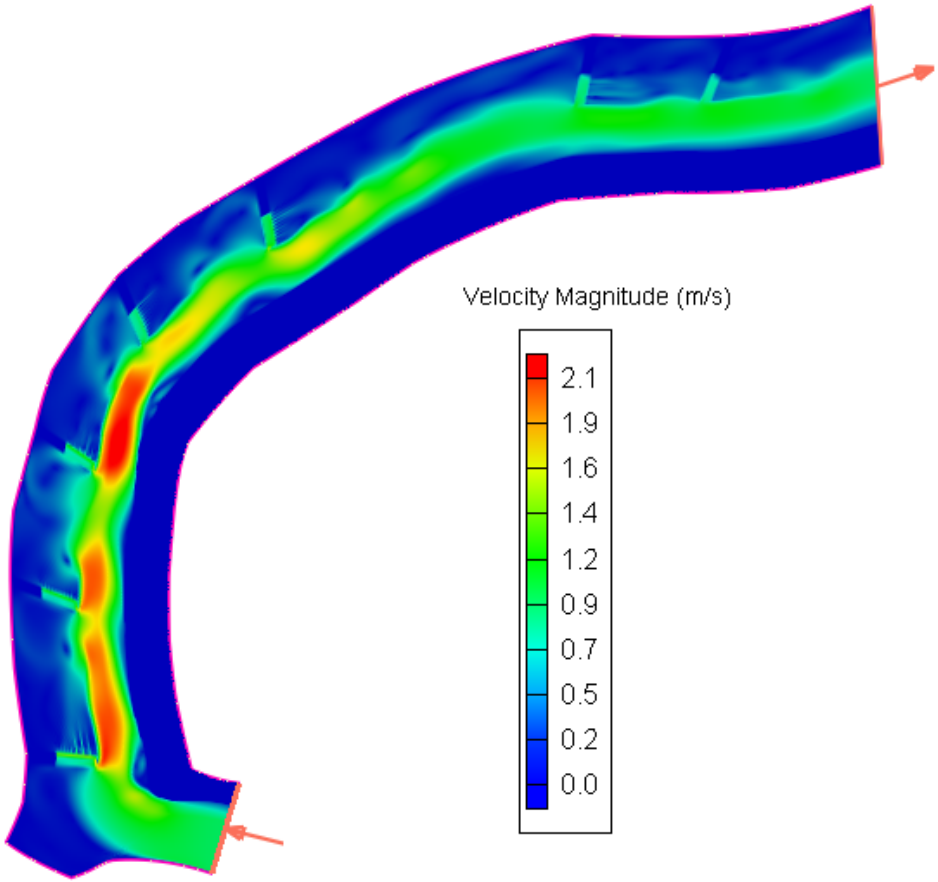


7 Barbs (no 6th barb)

# Total Specific Discharge (m^2/s)

## Discharge: 40 m^3/s, Initial Water Height: 1.5 m

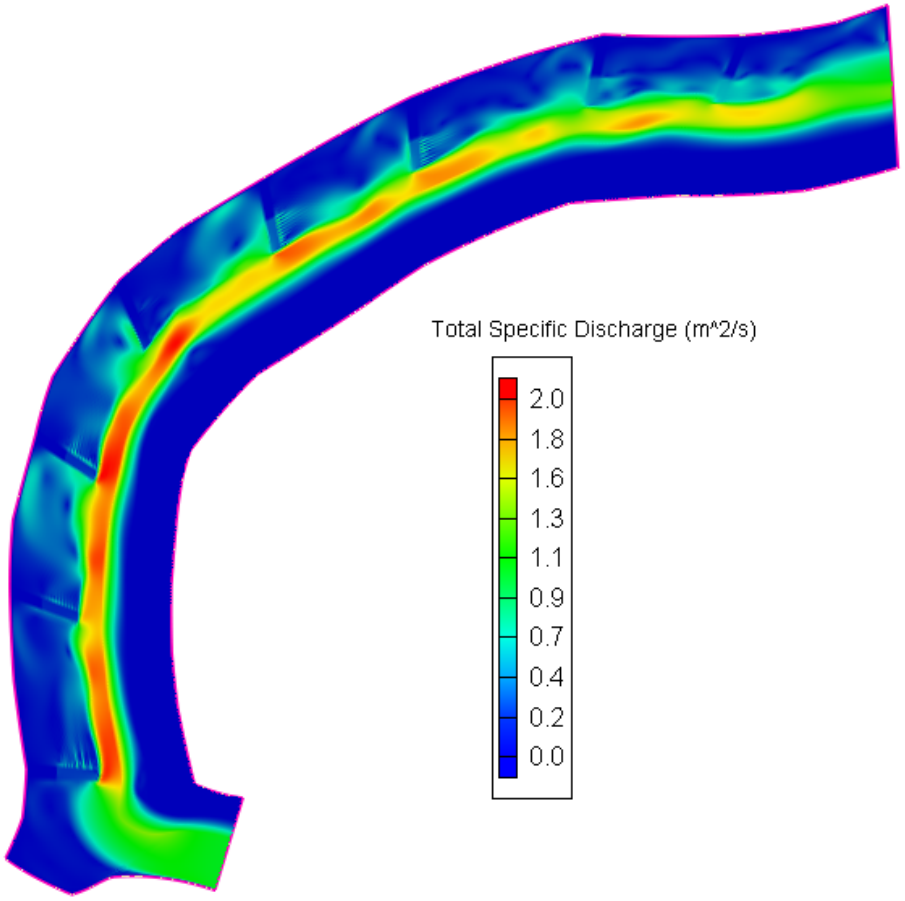


As built

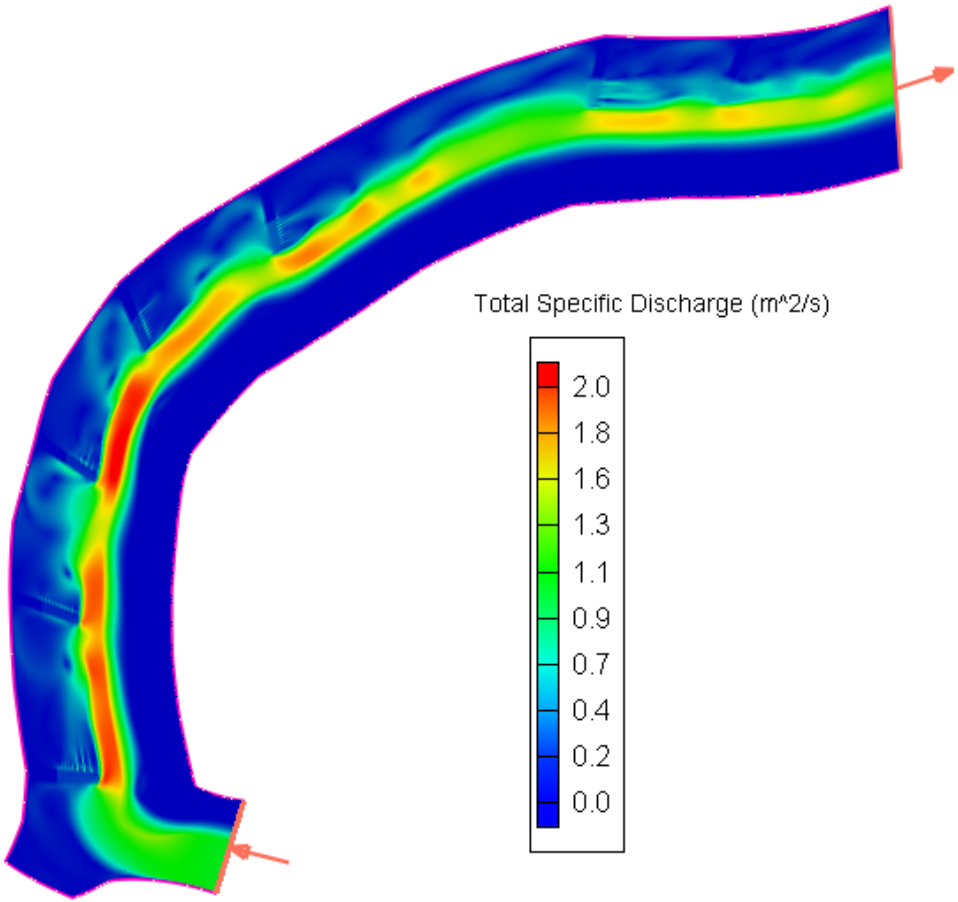


7 Barbs (no 6th barb)

# Froude Number
# Discharge: 40 m^3/s, Initial Water Height: 1.5 m

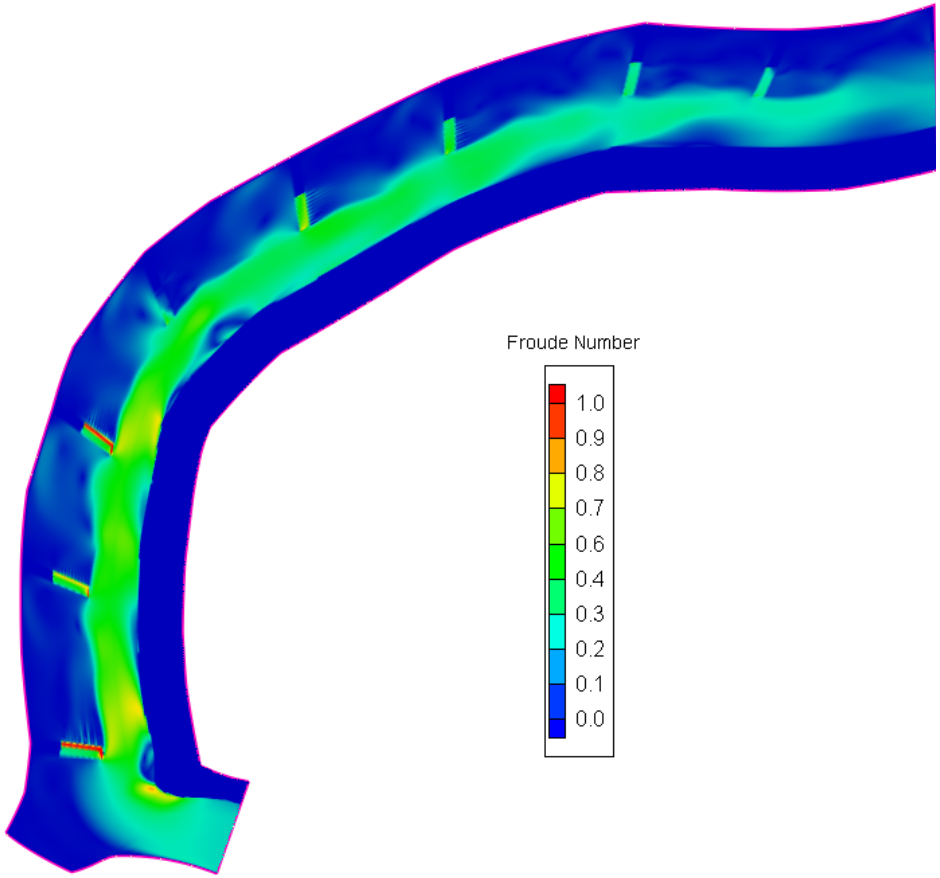


As built

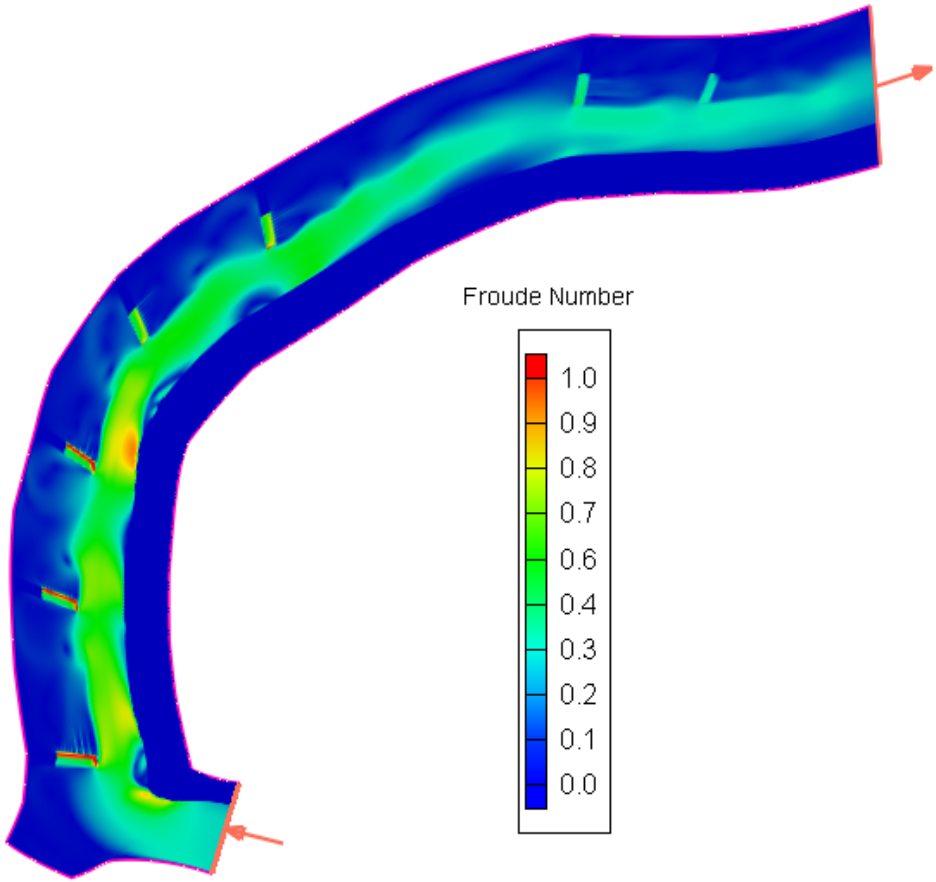


7 Barbs (no 6th barb)

# Total Shear Stress (N/m^2)
# Discharge: 40 m^3/s, Initial Water Height: 1.5 m

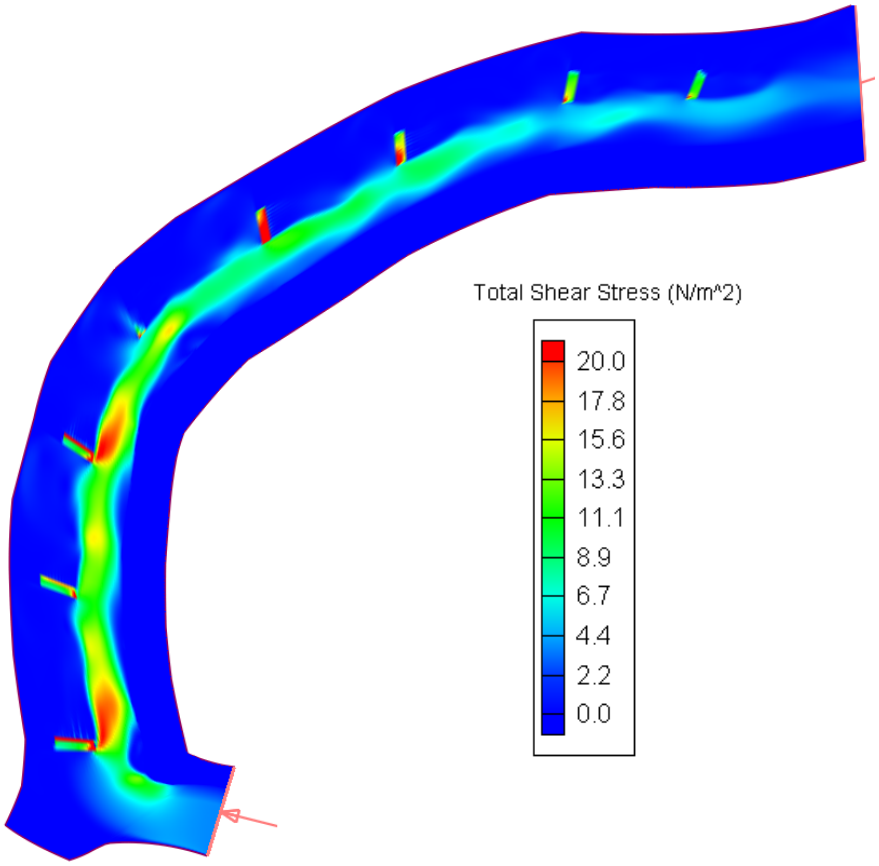


As built

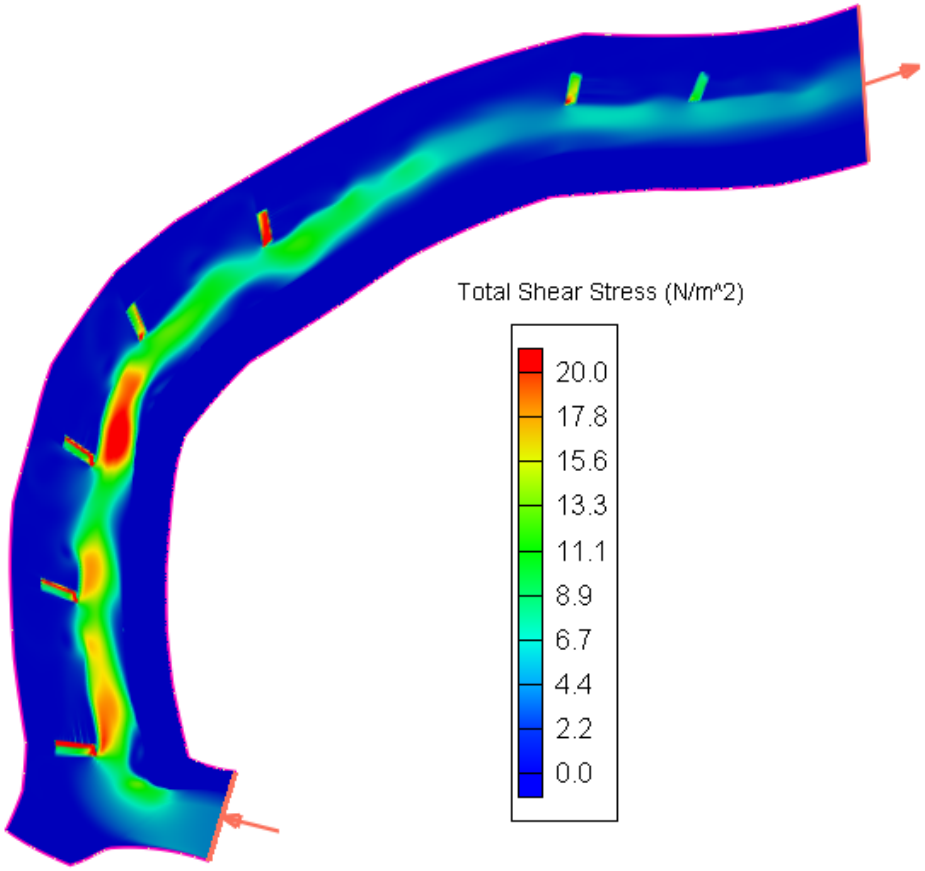


7 Barbs (no 6th barb)

Bed sediment transport is initiated
when Total Shear Stress > 19 N/m^2

# 7 Barbs - No 7th Barb

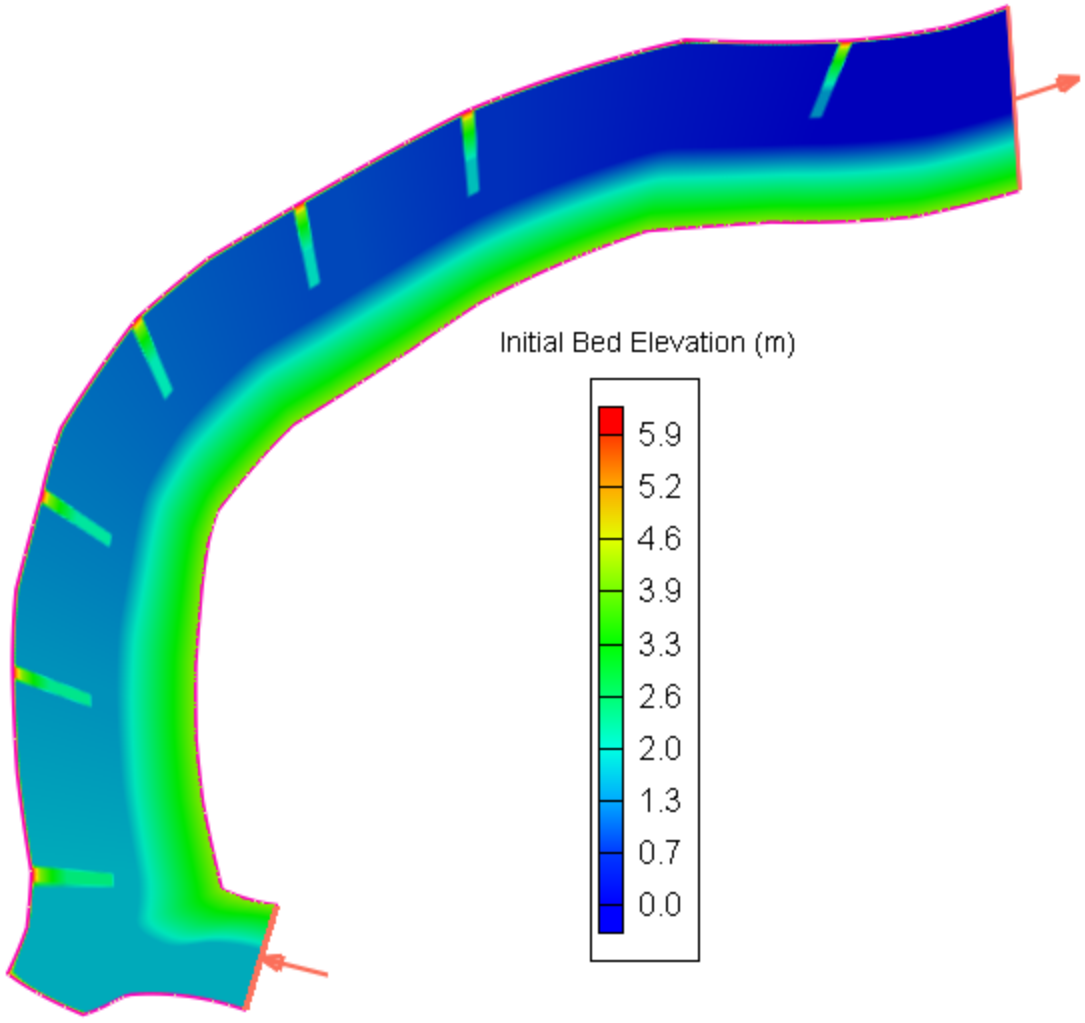

# Velocity Magnitude (m/s)

## Discharge: 40 m^3/s, Initial Water Height: 1.5 m

## (observed conditions during fieldwork conducted on August 2009)

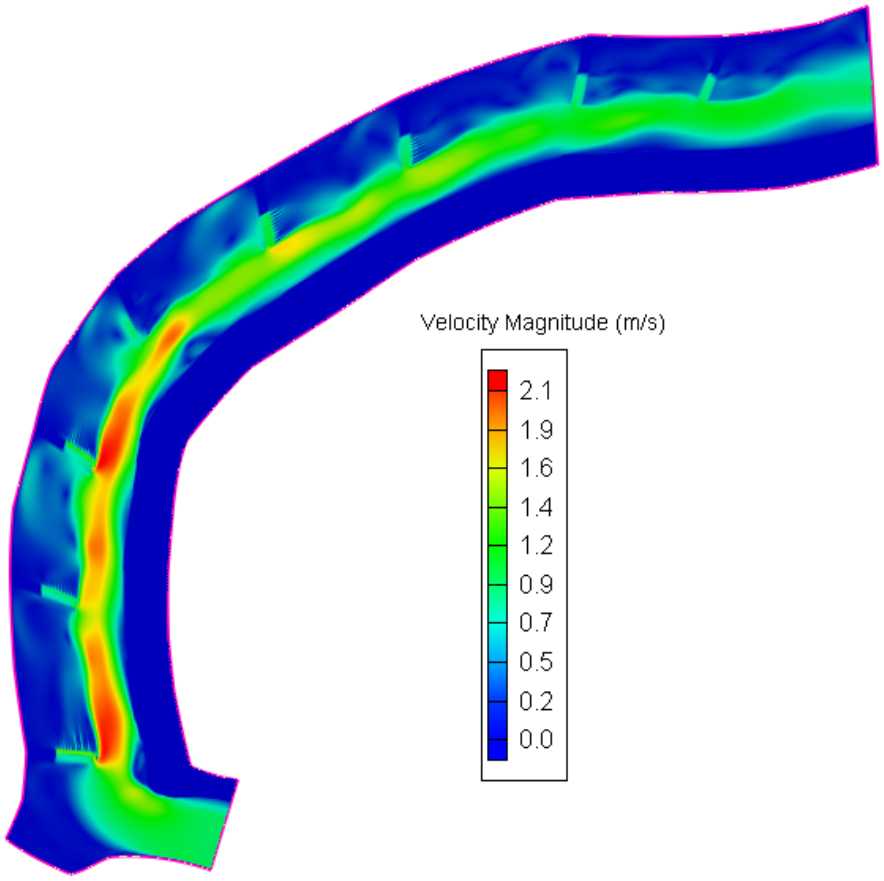


As built

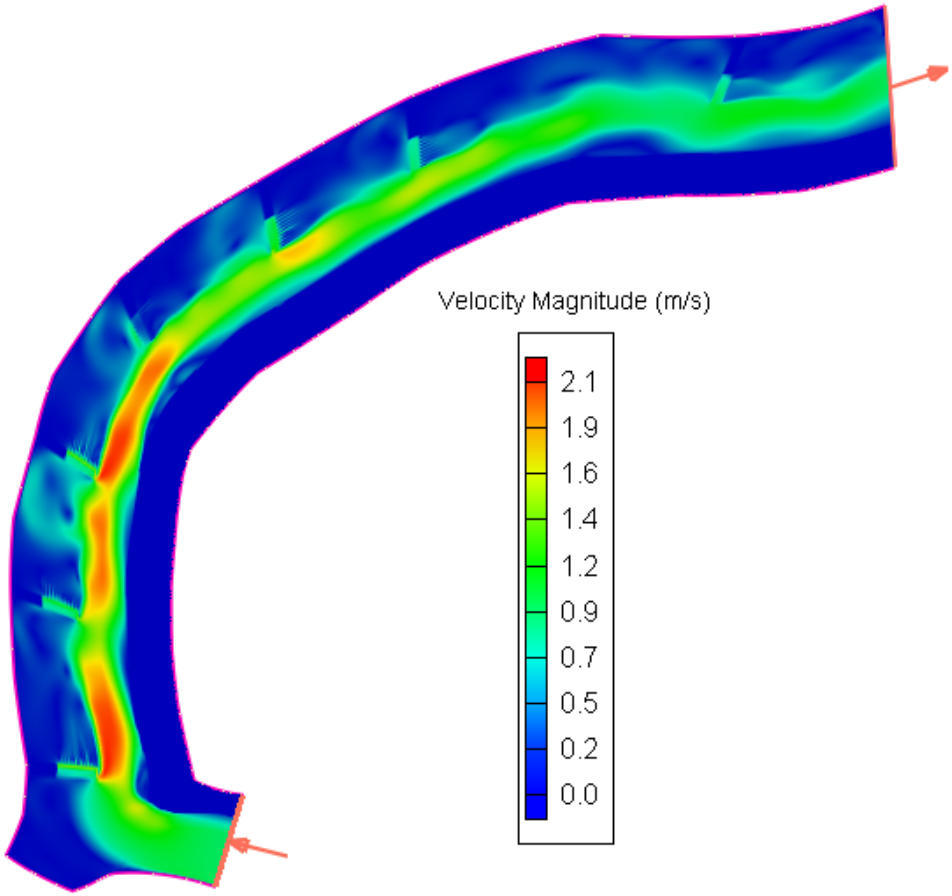


7 Barbs (no 7th barb)

# Total Specific Discharge (m^2/s)

## Discharge: 40 m^3/s, Initial Water Height: 1.5 m

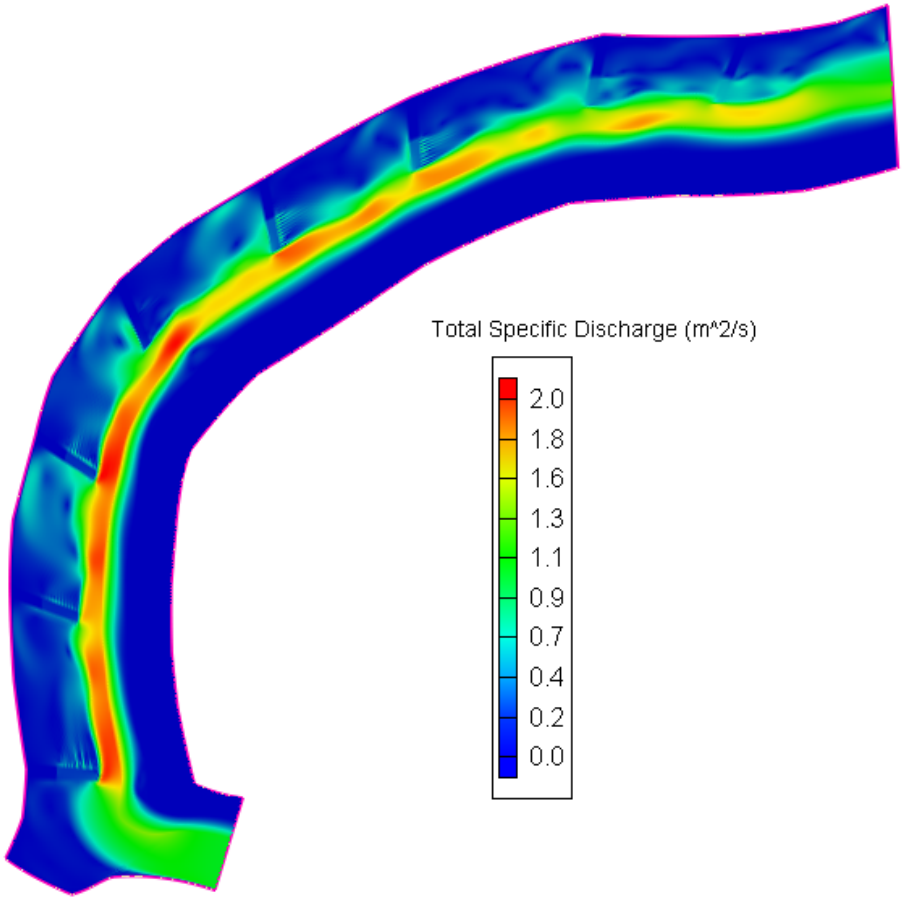


As built

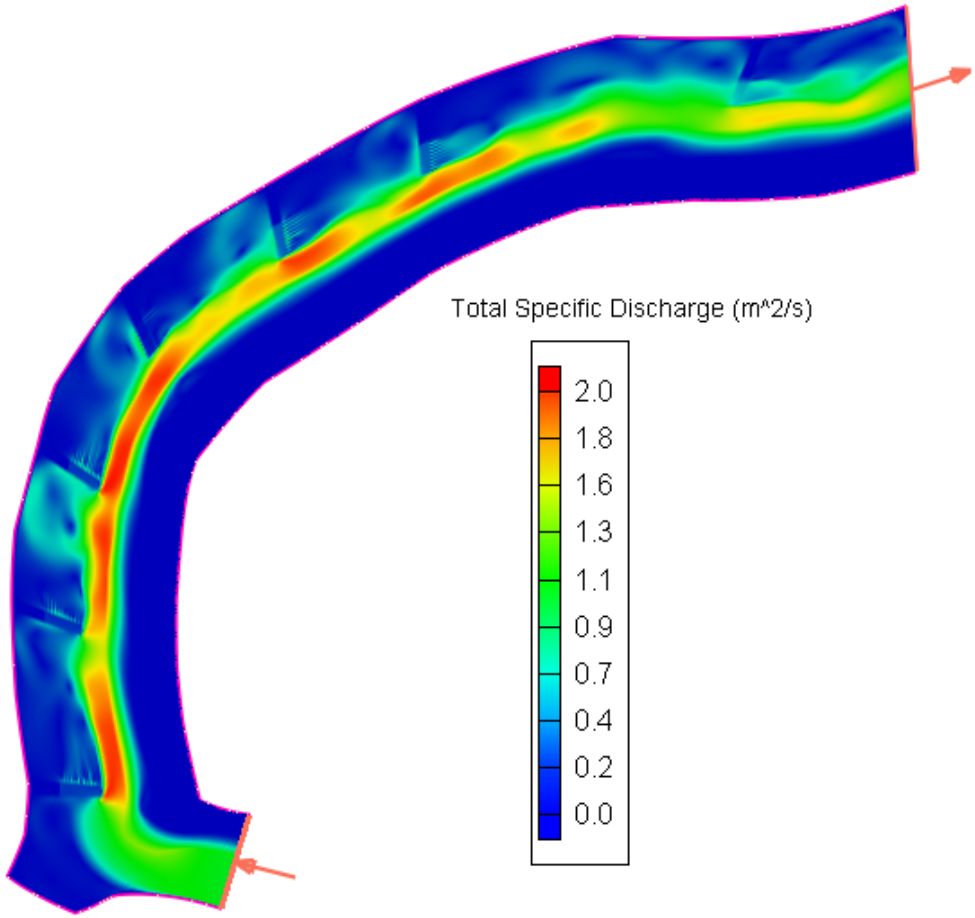


7 Barbs (no 7$^{th}$ barb)

# Froude Number
# Discharge: 40 m^3/s, Initial Water Height: 1.5 m

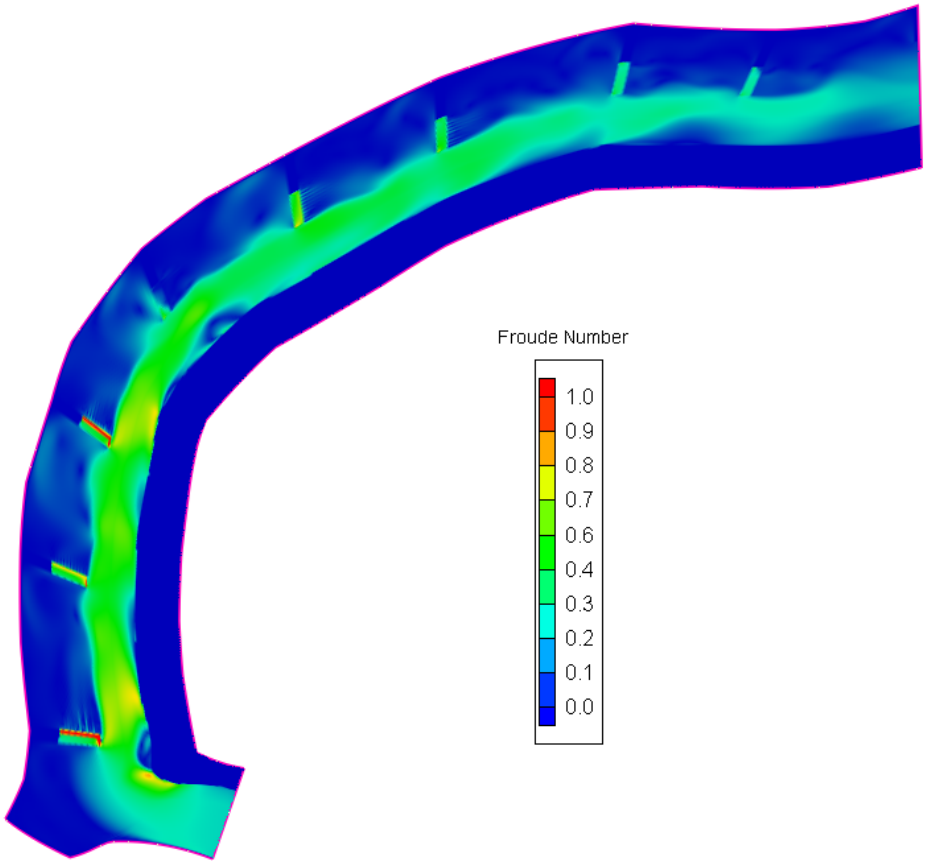


As built

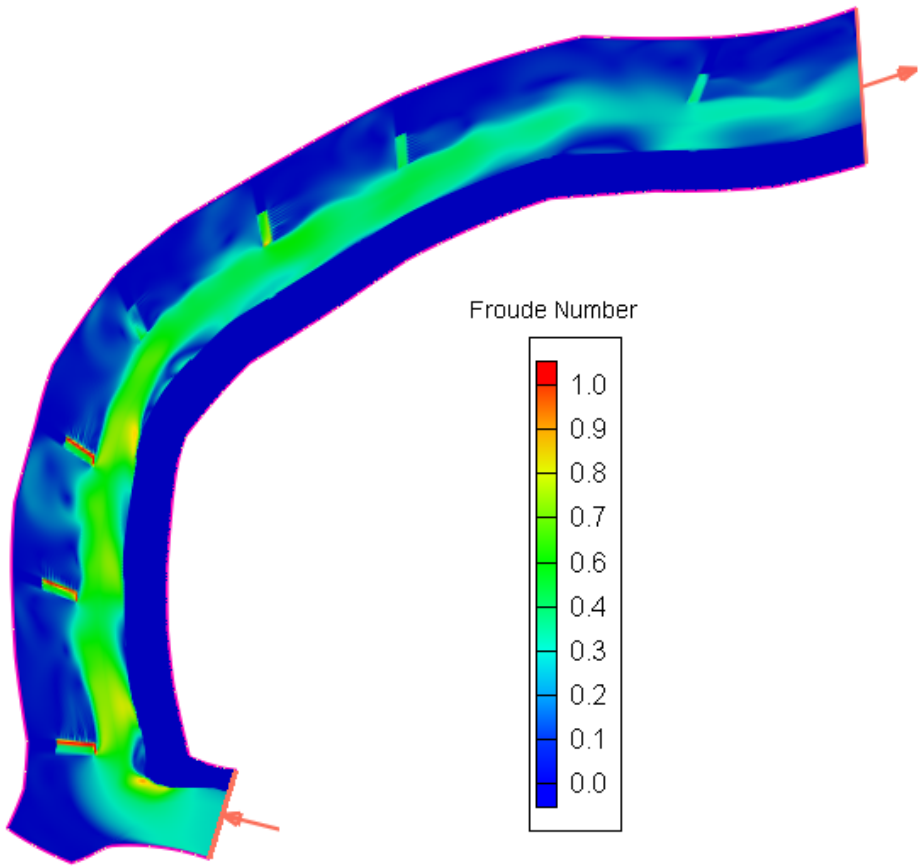


7 Barbs (no 7th barb)

# Total Shear Stress (N/m^2)
# Discharge: 40 m^3/s, Initial Water Height: 1.5 m

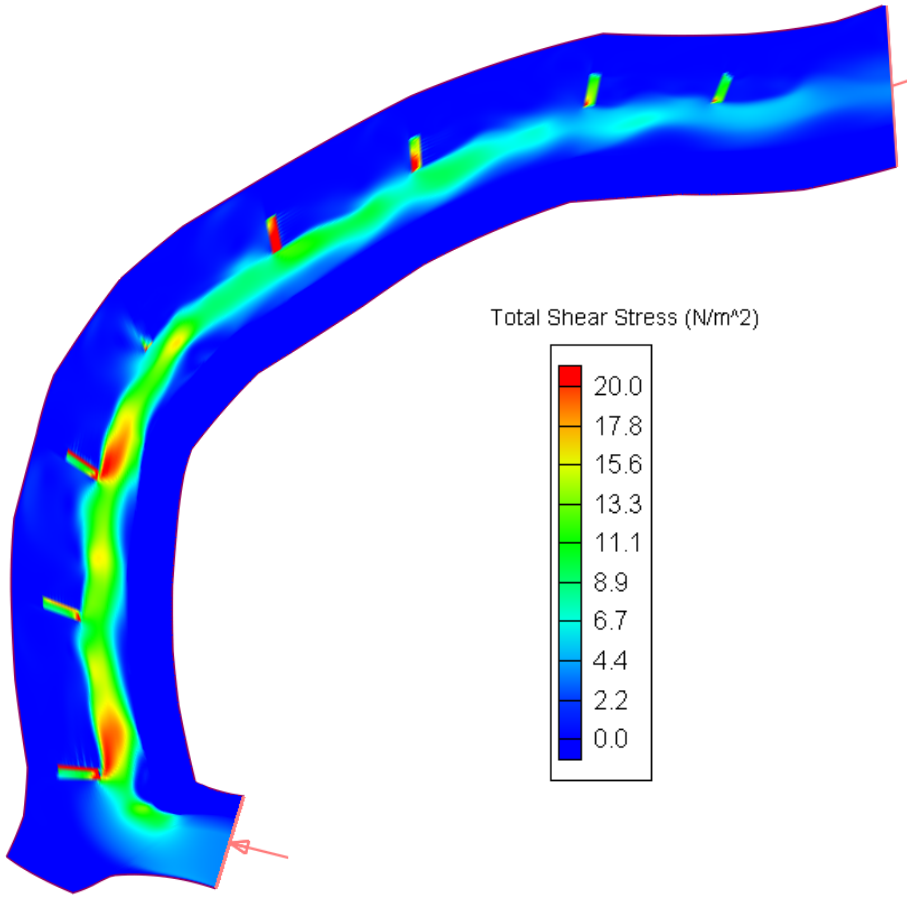


As built

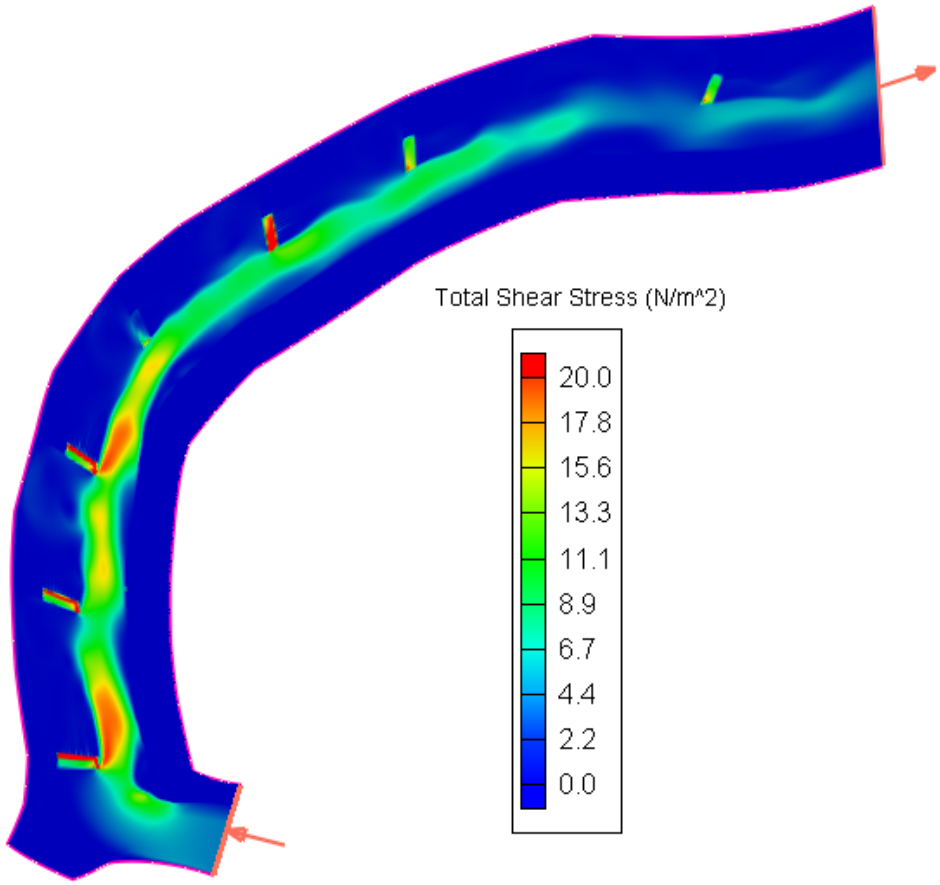


7 Barbs (no 7th barb)

Bed sediment transport is initiated
when Total Shear Stress > 19 N/m^2

# 7 Barbs - No 8th Barb

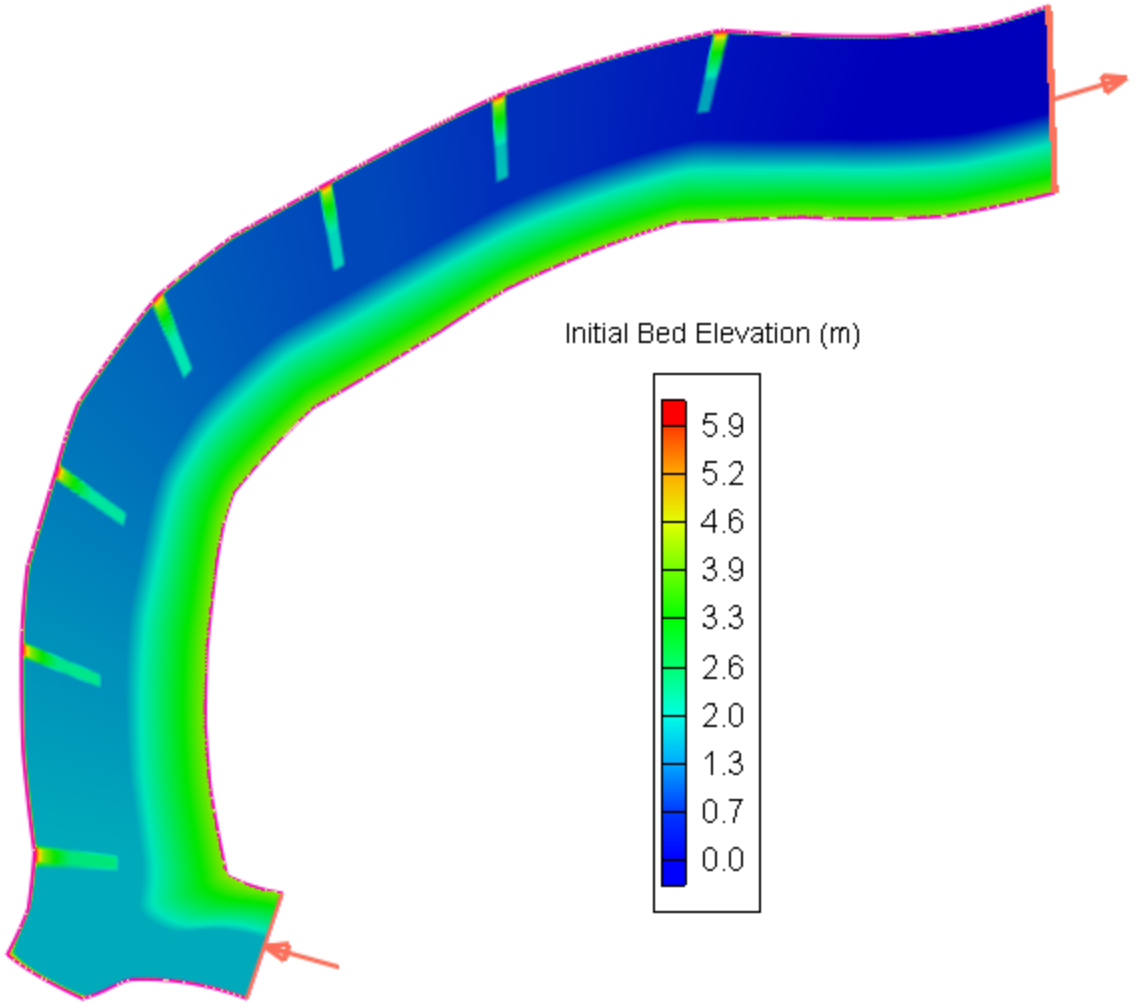

# Velocity Magnitude (m/s)

## Discharge: 40 m^3/s, Initial Water Height: 1.5 m

## (observed conditions during fieldwork conducted on August 2009)

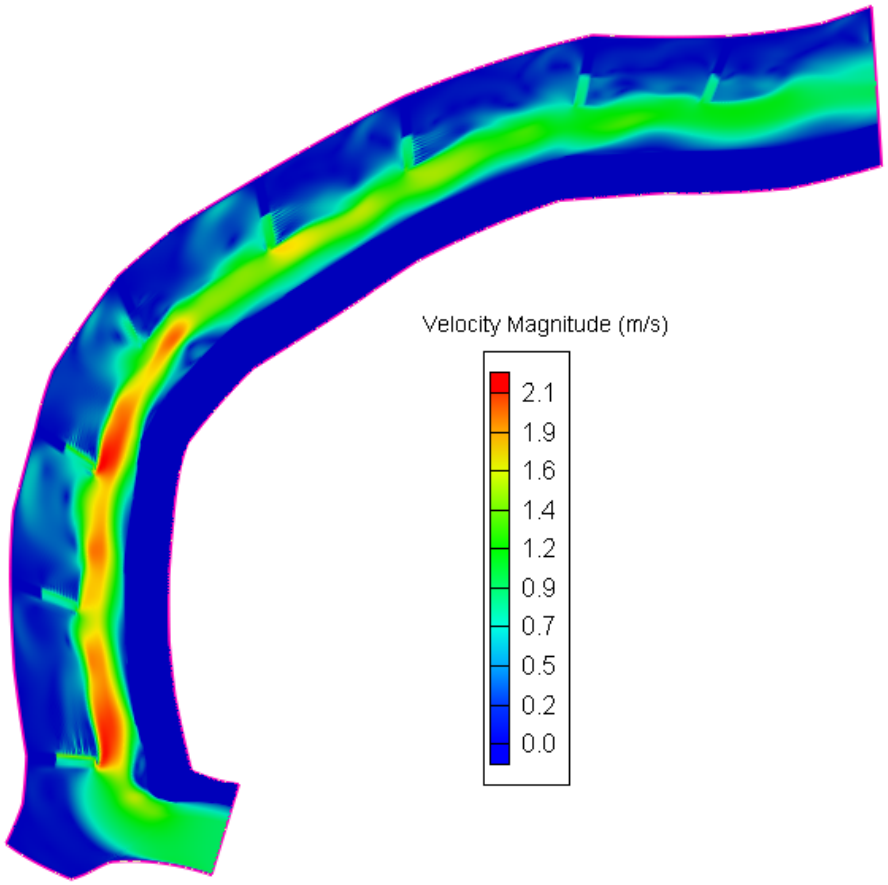


As built

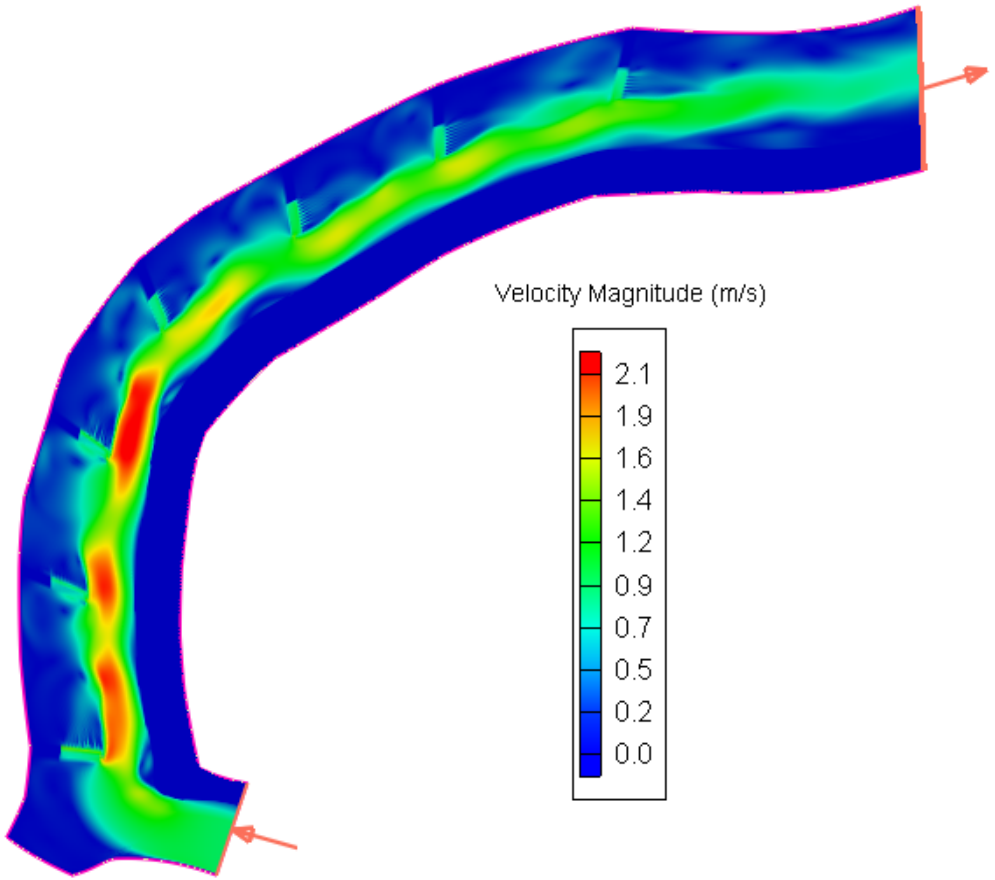


7 Barbs (no 8th barb)

# Total Specific Discharge (m^2/s)

## Discharge: 40 m^3/s, Initial Water Height: 1.5 m

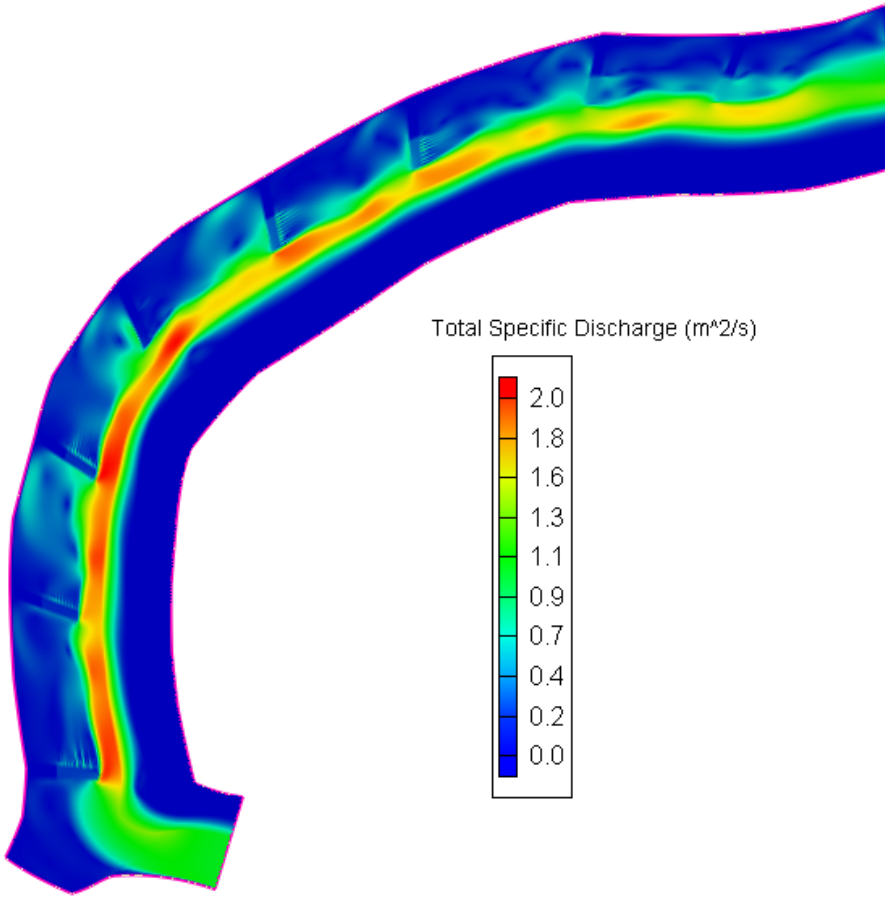


As built

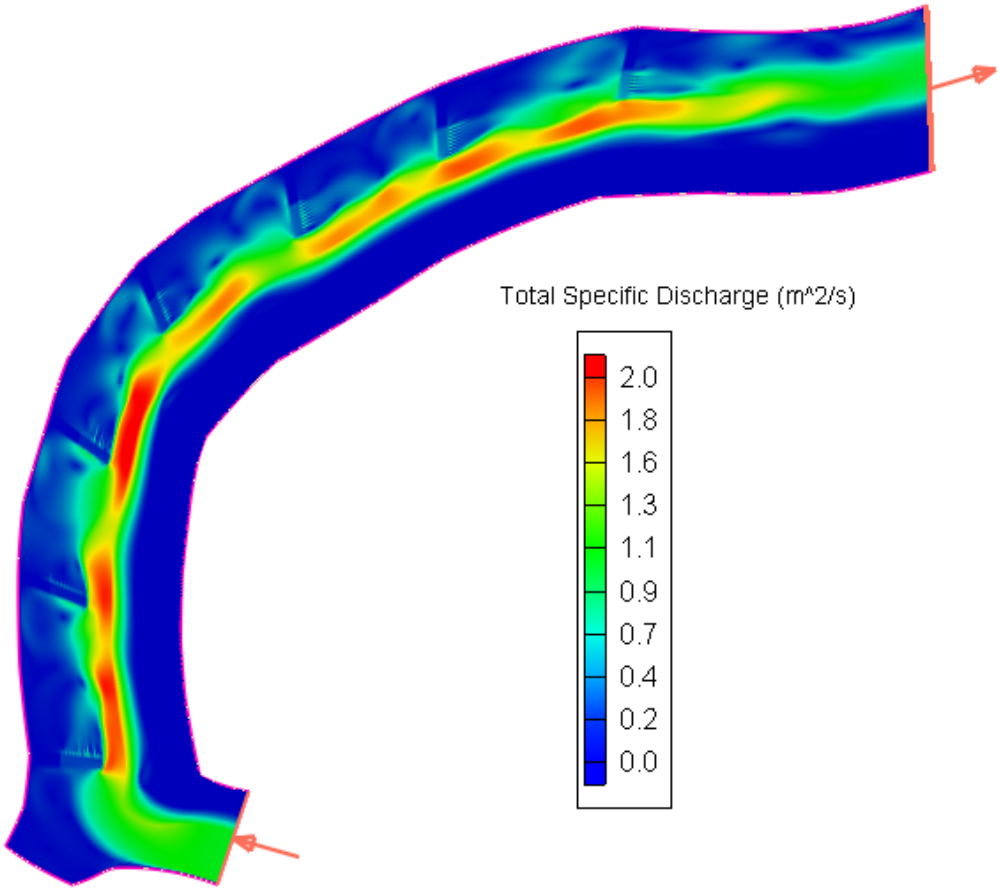


7 Barbs (no 8th barb)

# Froude Number
# Discharge: 40 m^3/s, Initial Water Height: 1.5 m

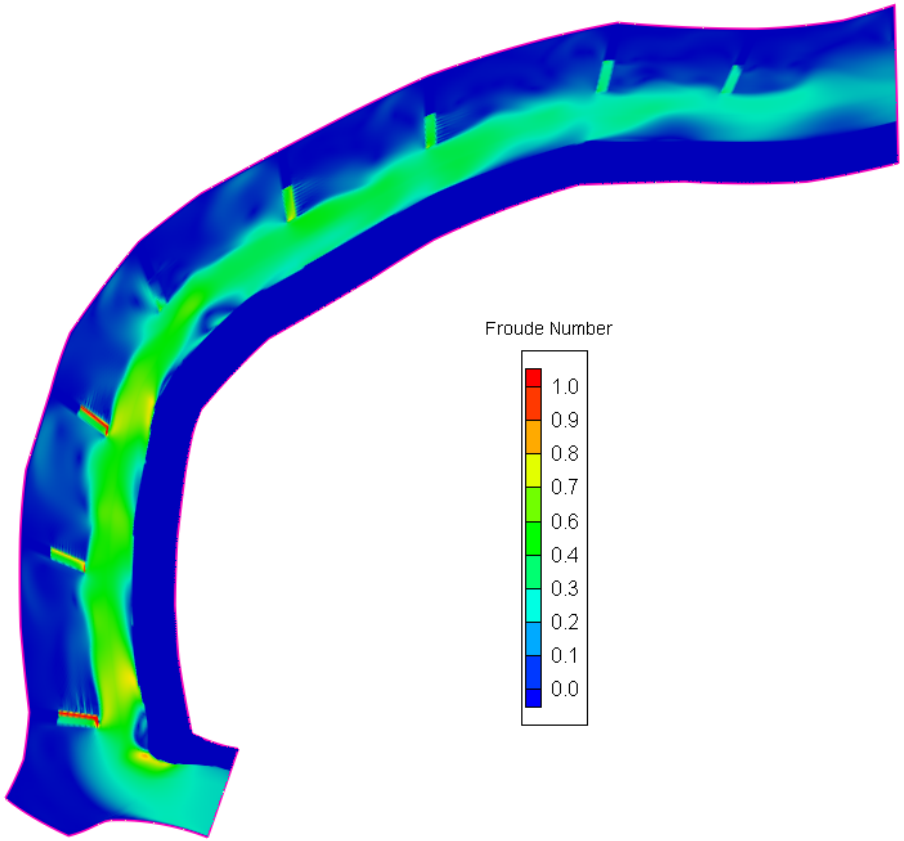


As built

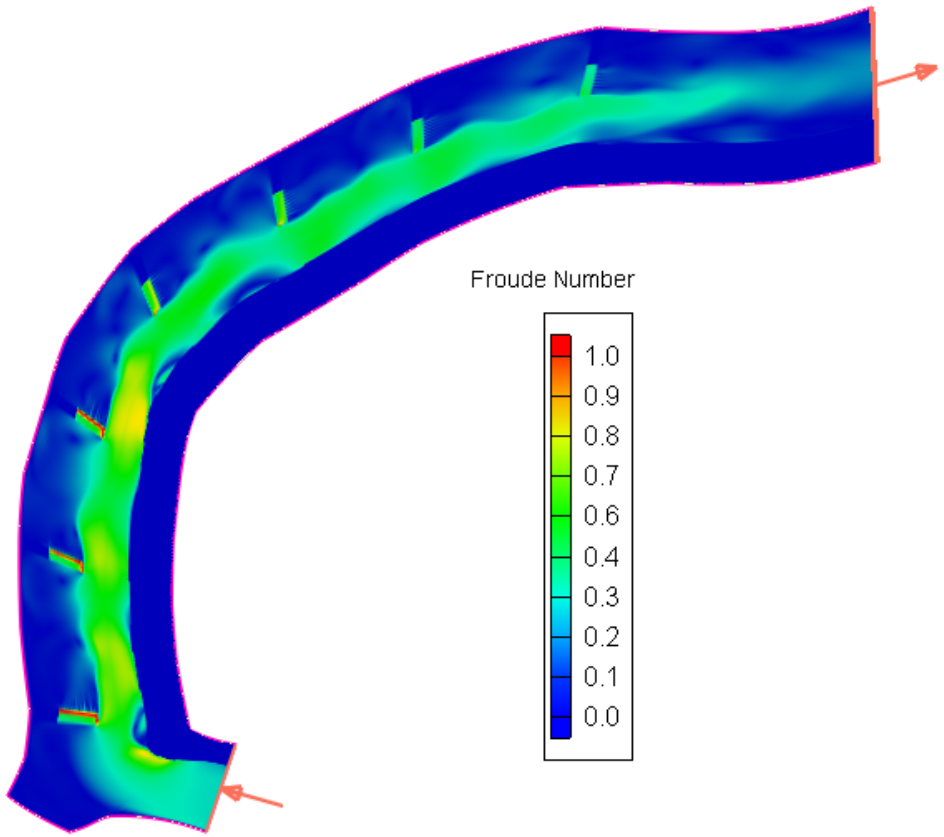


7 Barbs (no 8th barb)

# Total Shear Stress (N/m^2)
# Discharge: 40 m^3/s, Initial Water Height: 1.5 m

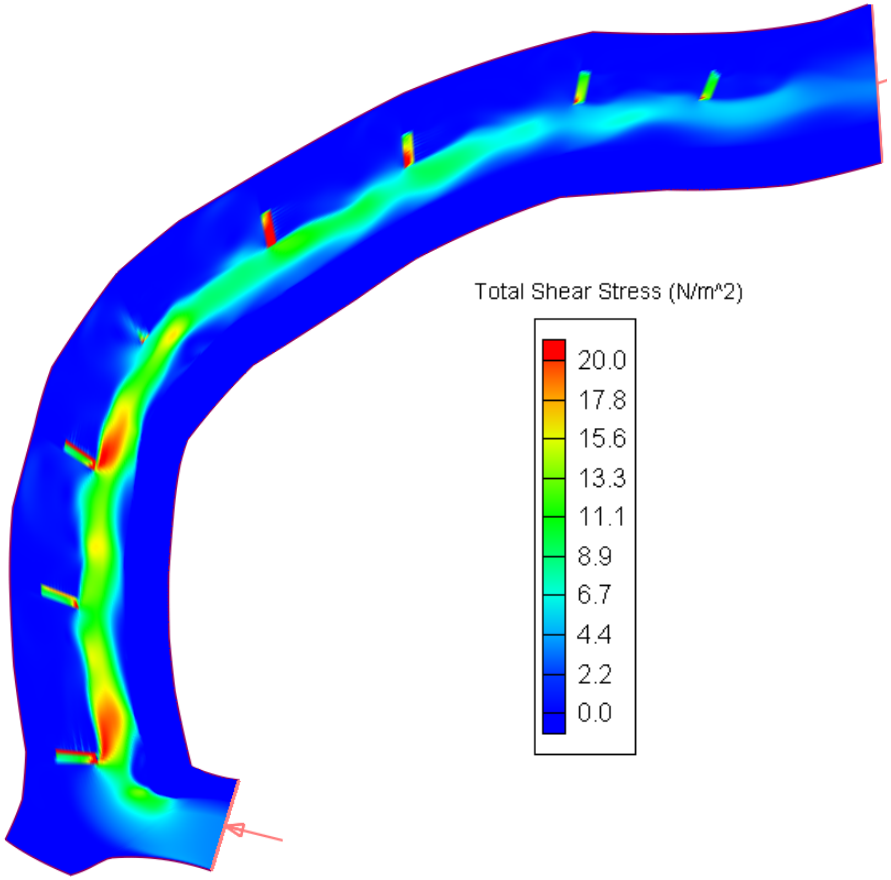


As built

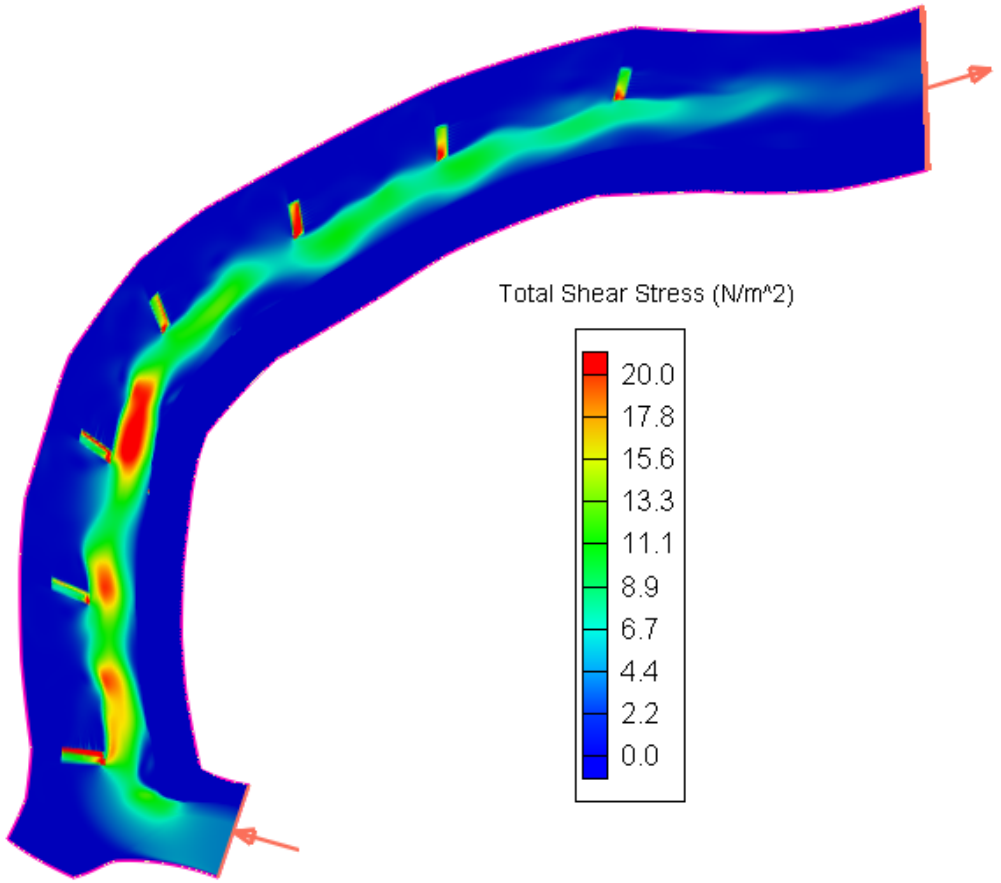


7 Barbs (no 8th barb)

Bed sediment transport is initiated
when Total Shear Stress > 19 N/m^2

# 4 Barbs - No 2nd, 4th, 6th, & 8th Barbs

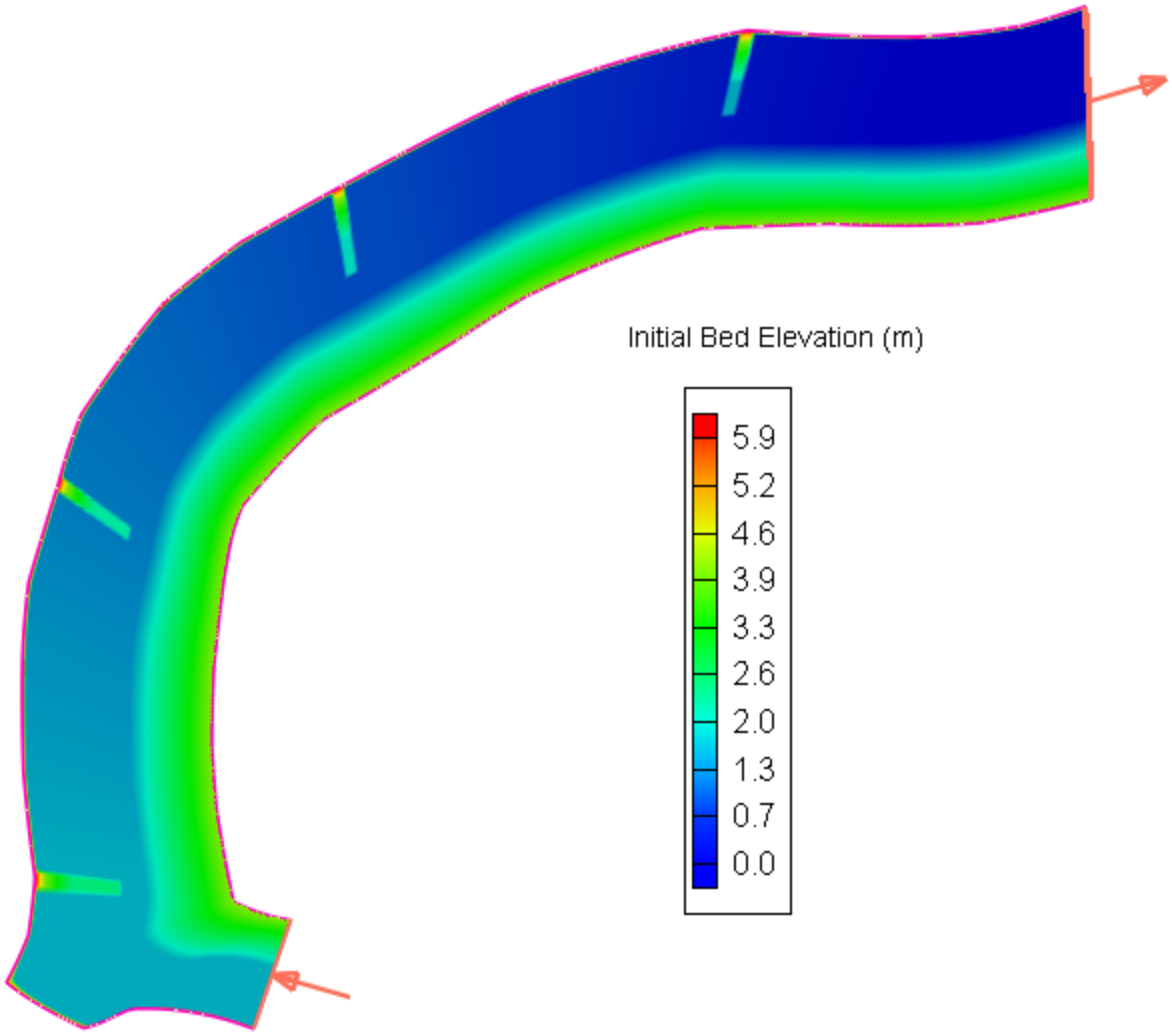

# Velocity Magnitude (m/s)

## Discharge: 40 m^3/s, Initial Water Height: 1.5 m

## (observed conditions during fieldwork conducted on August 2009)

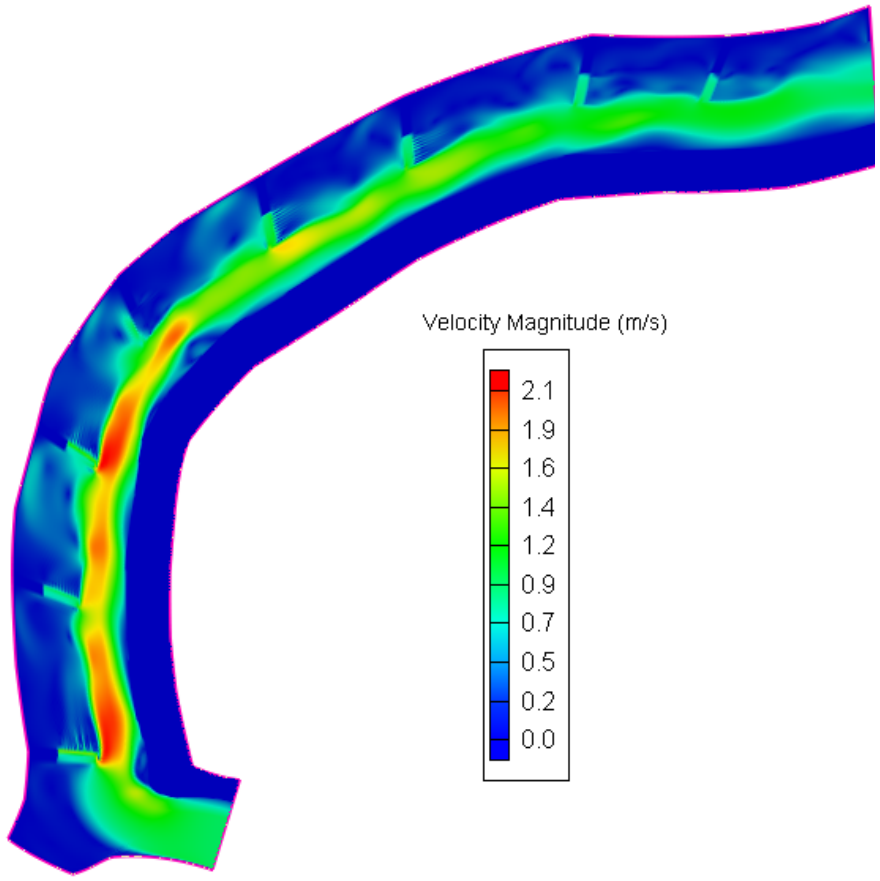


As built

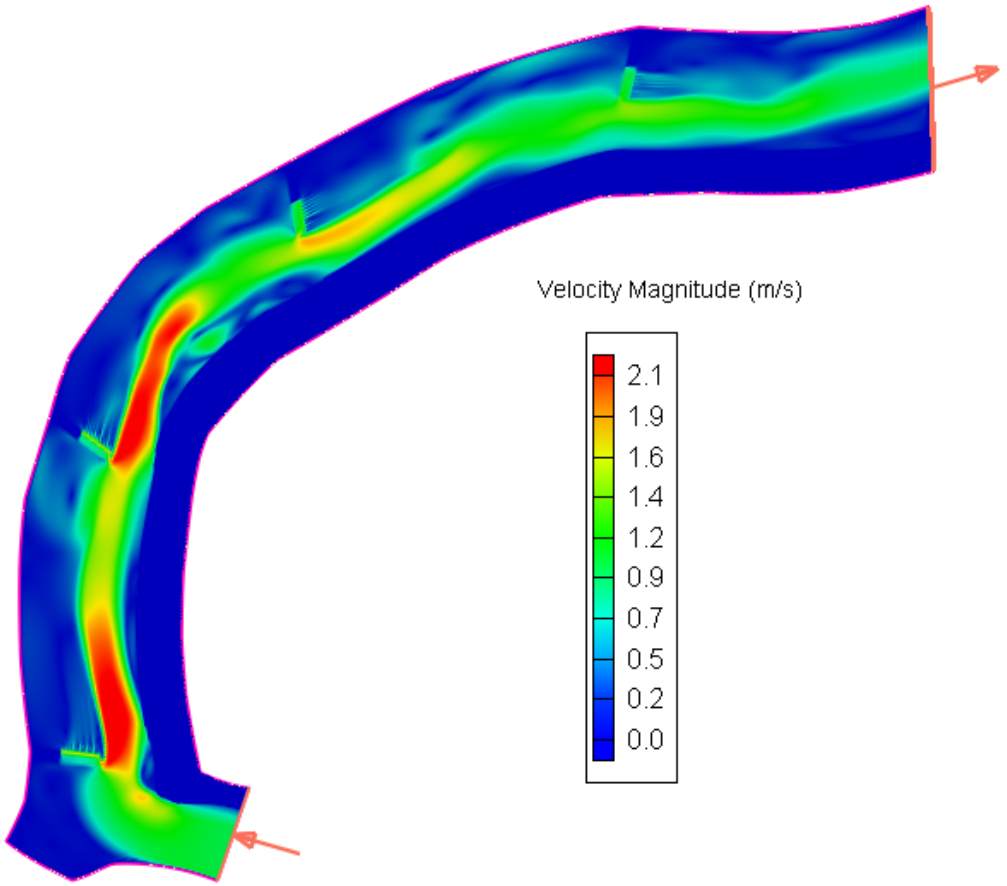


4 Barbs

# Total Specific Discharge (m^2/s)

## Discharge: 40 m^3/s, Initial Water Height: 1.5 m

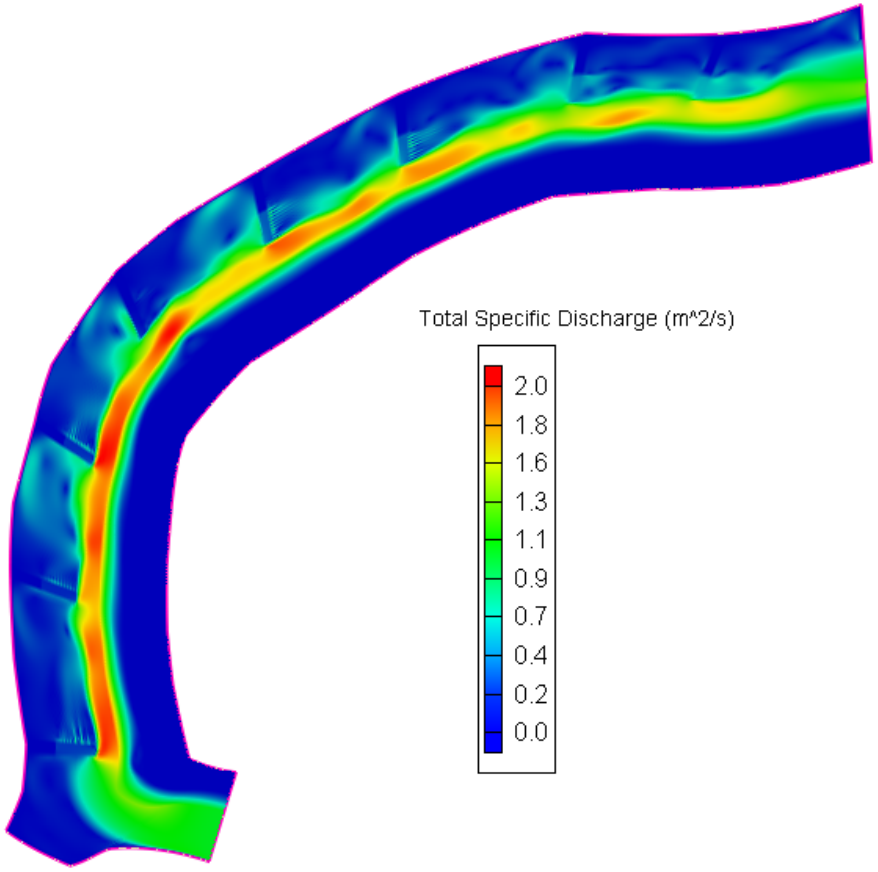


As built

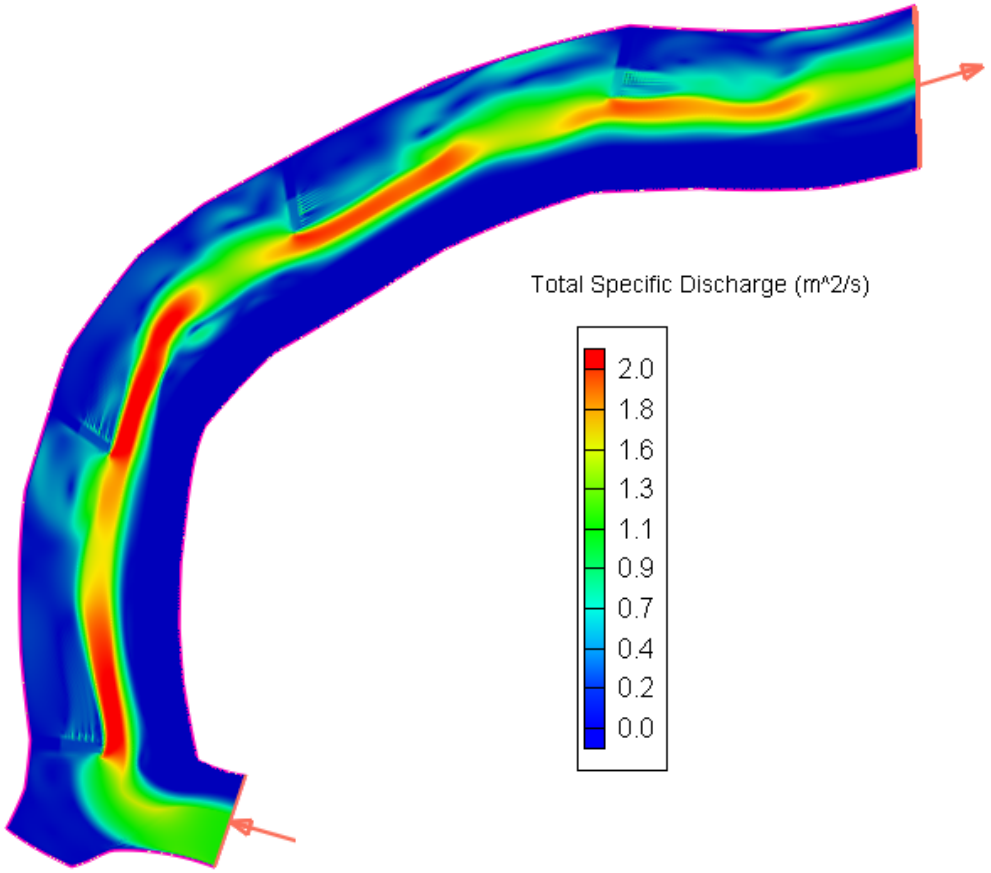


4 Barbs

# Froude Number
# Discharge: 40 m^3/s, Initial Water Height: 1.5 m

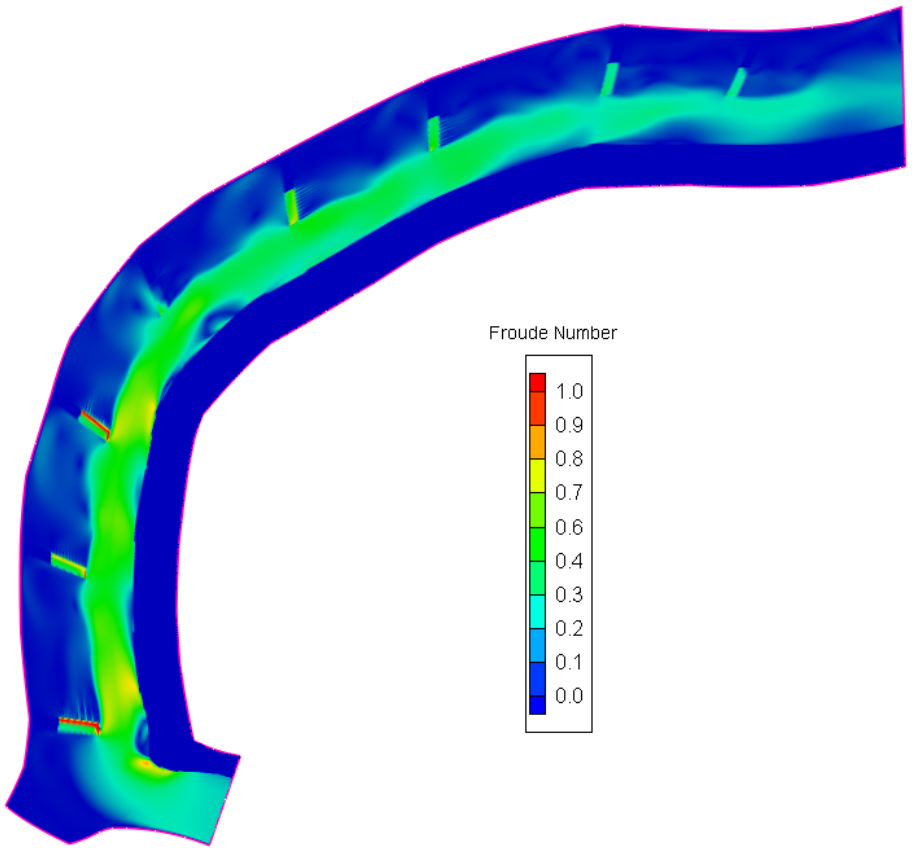


As built

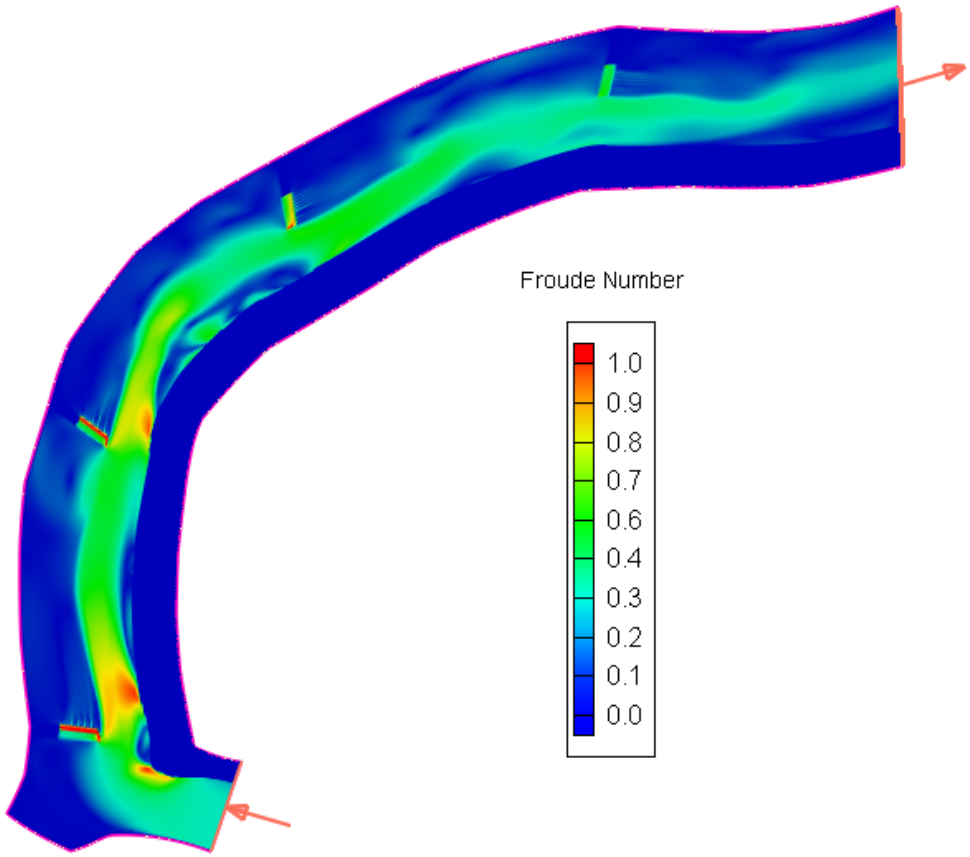


4 Barbs

# Total Shear Stress (N/m^2)
# Discharge: 40 m^3/s, Initial Water Height: 1.5 m

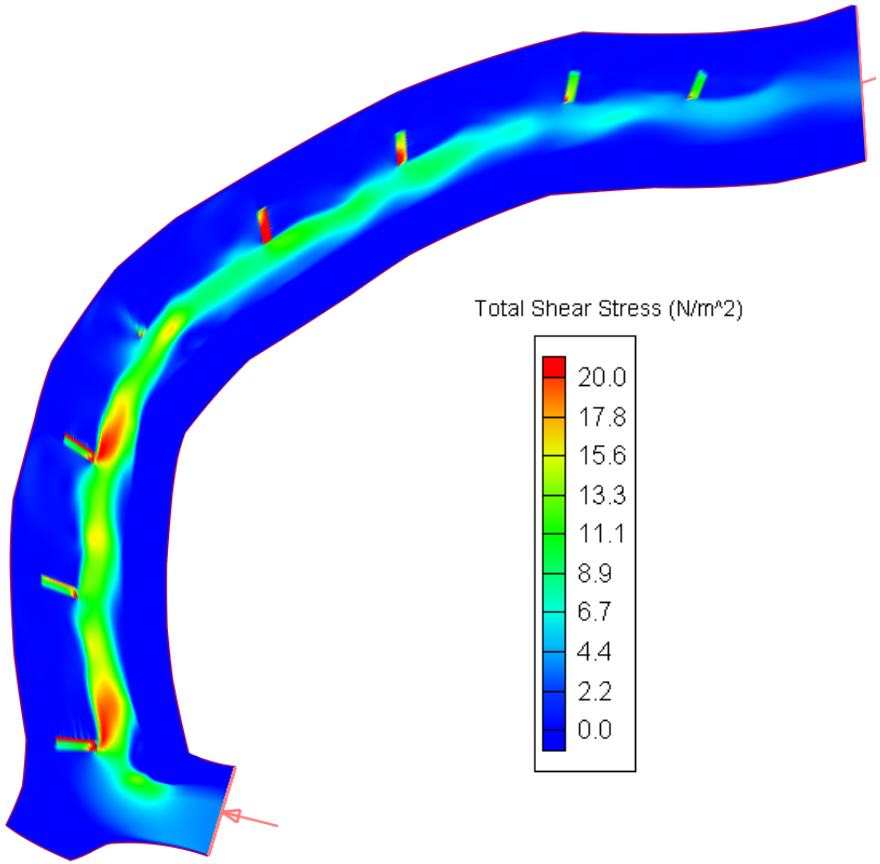


As built

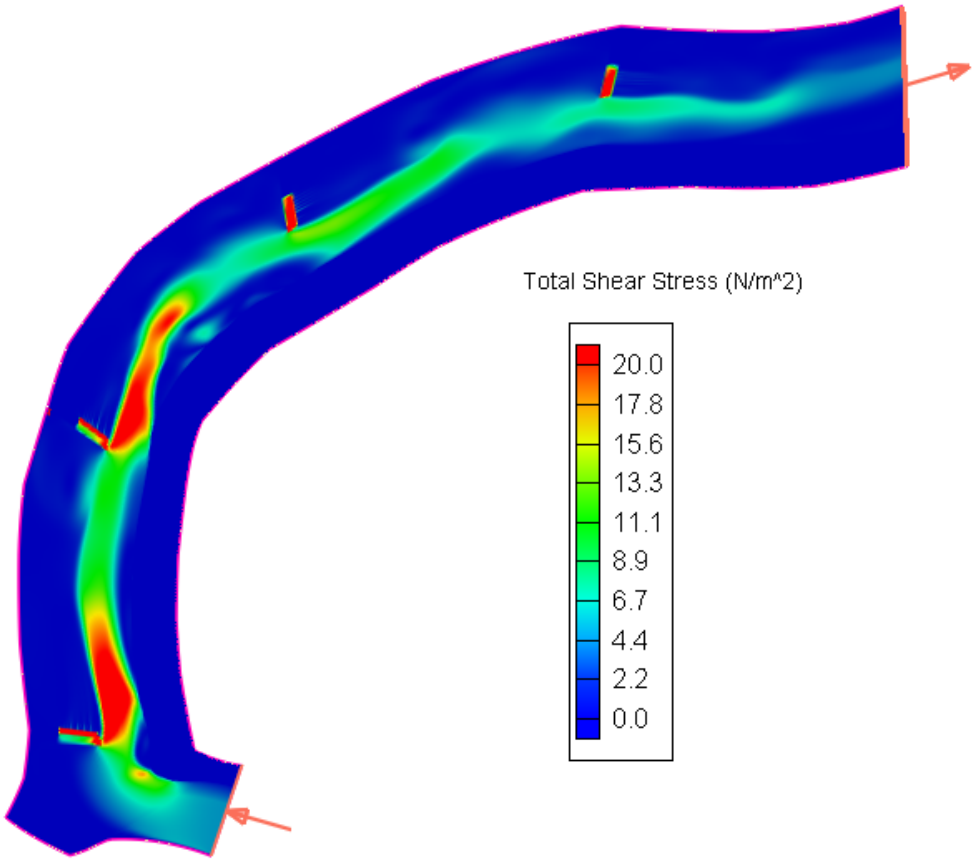


4 Barbs

Bed sediment transport is initiated
when Total Shear Stress > 19 N/m^2

# 5 Barbs - No 4th, 6th, & 8th Barbs

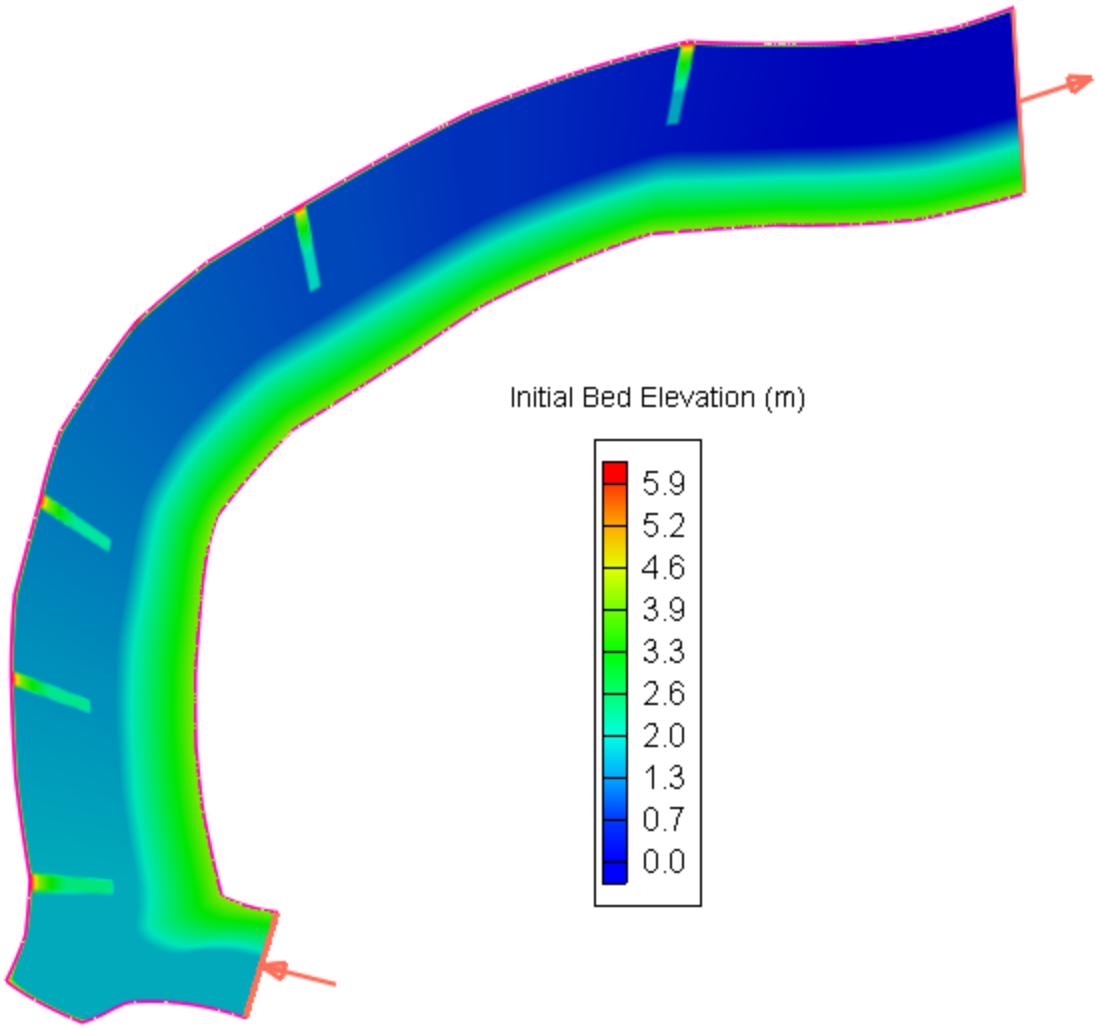

# Velocity Magnitude (m/s)

## Discharge: 40 m^3/s, Initial Water Height: 1.5 m

## (observed conditions during fieldwork conducted on August 2009)

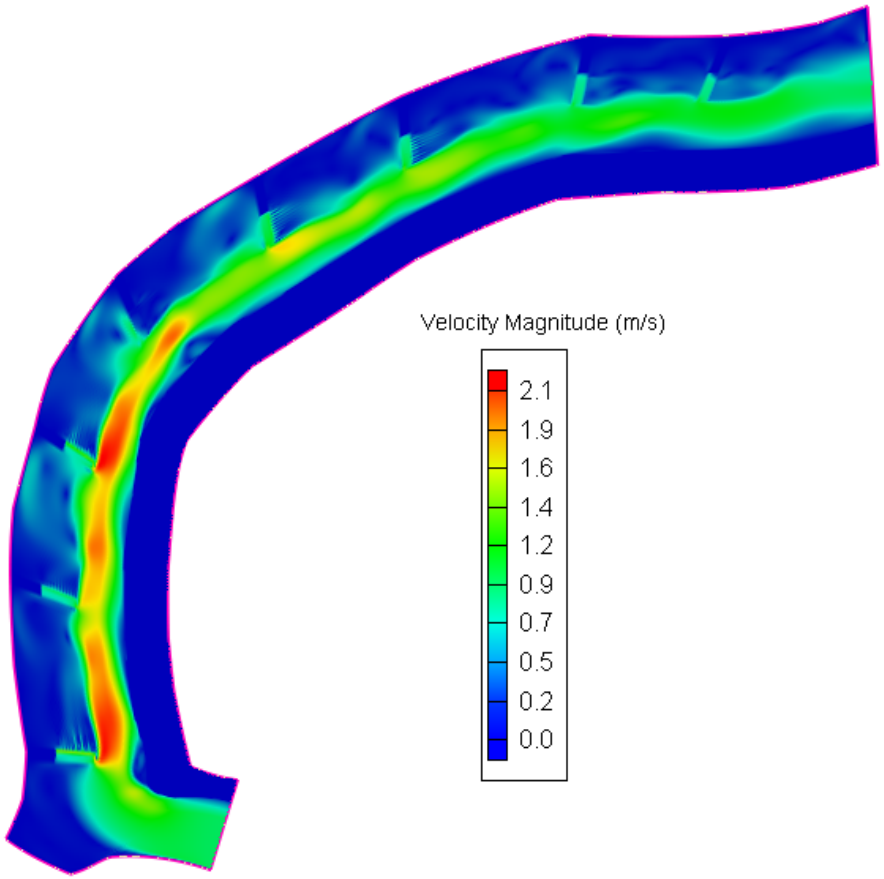


As built

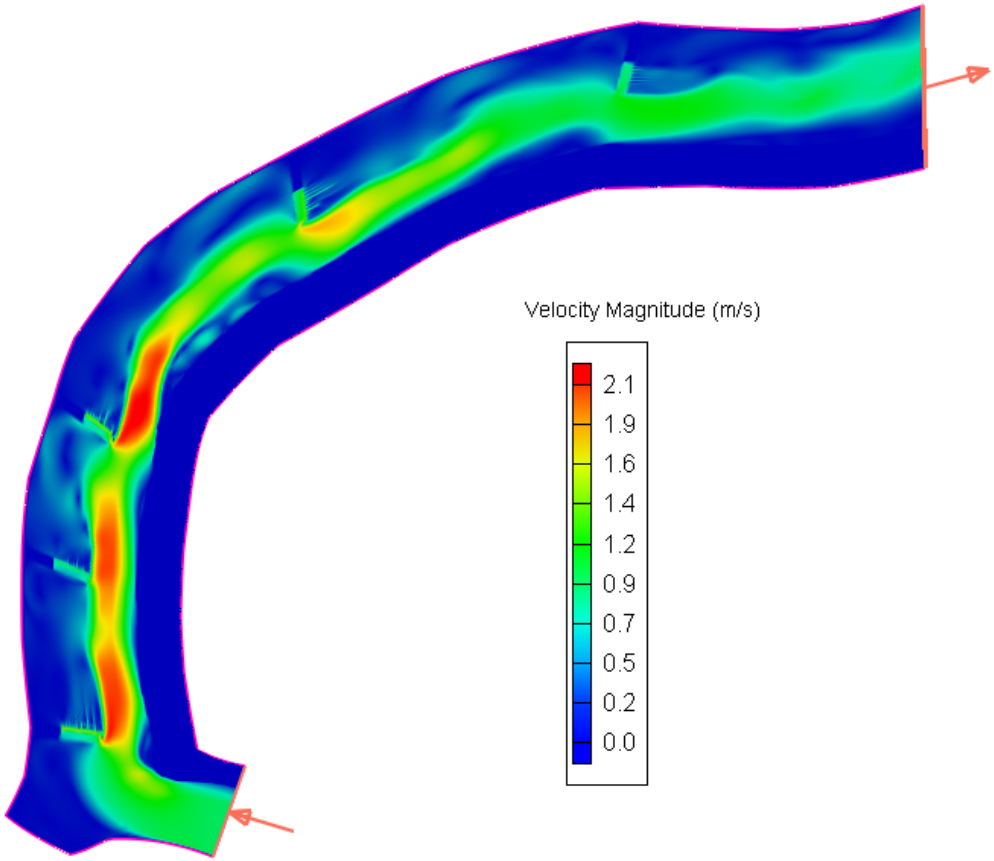


5 Barbs

# Total Specific Discharge (m^2/s)

## Discharge: 40 m^3/s, Initial Water Height: 1.5 m

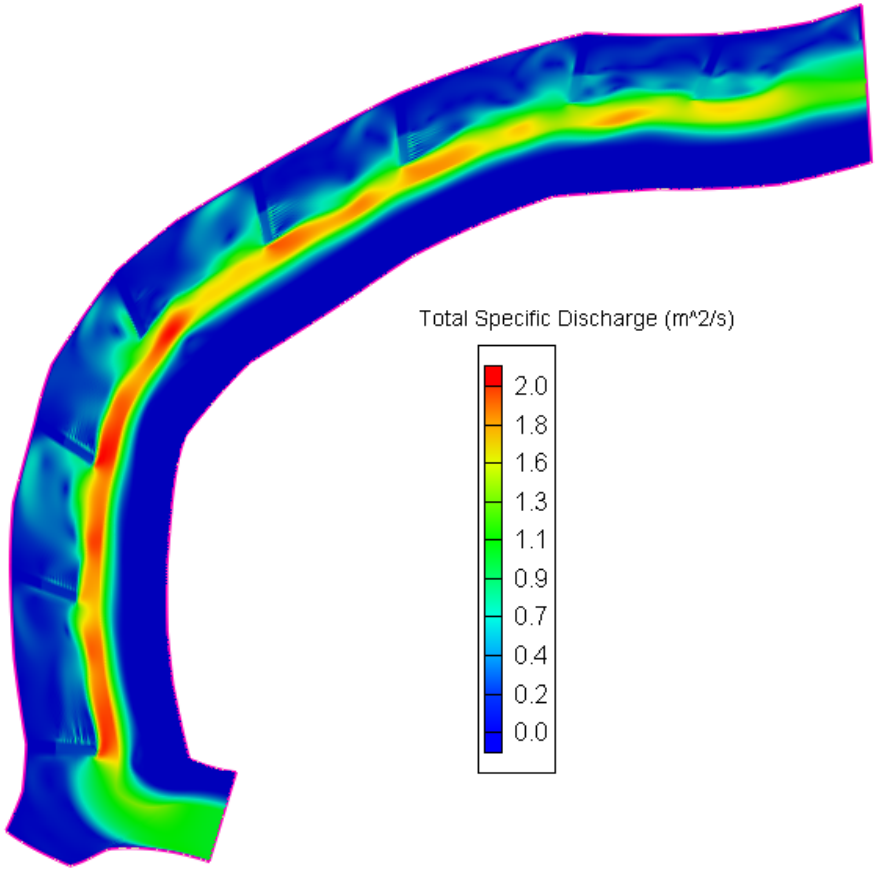


As built

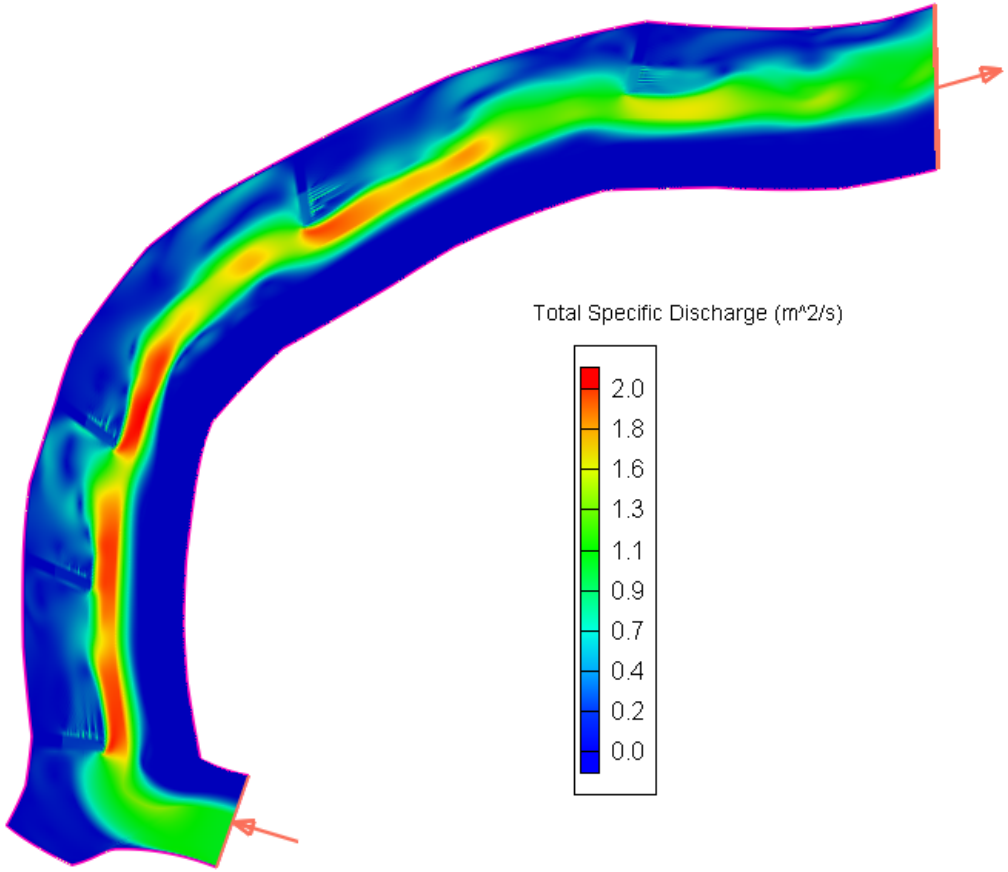


5 Barbs

# Froude Number
## Discharge: 40 m^3/s, Initial Water Height: 1.5 m

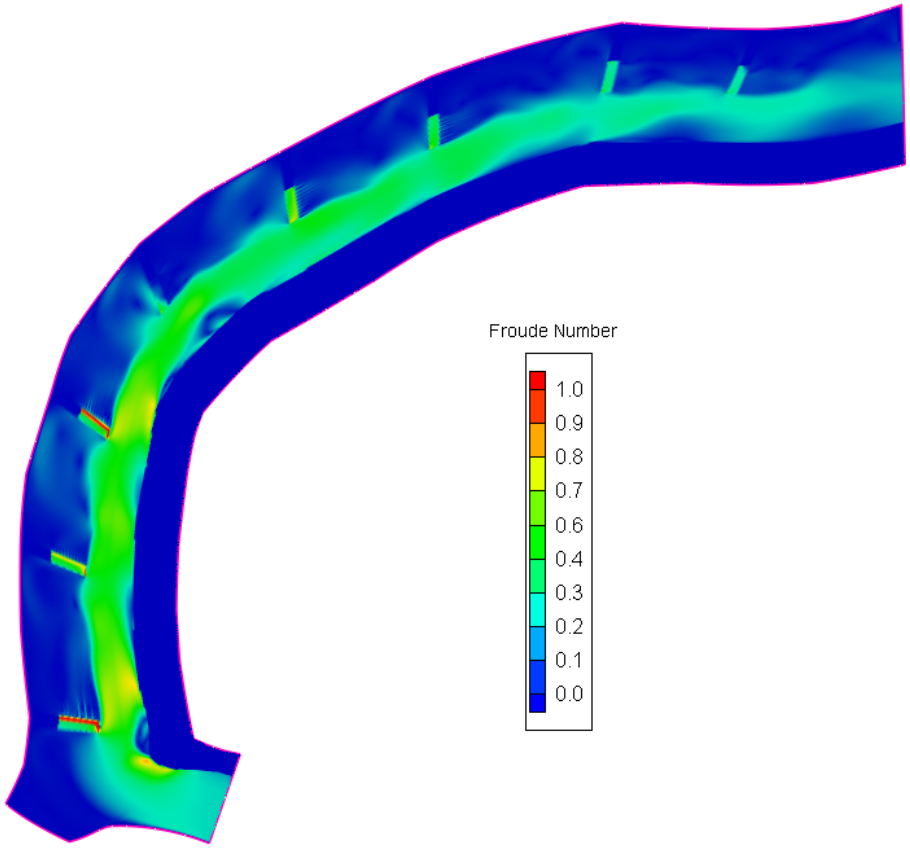


As built

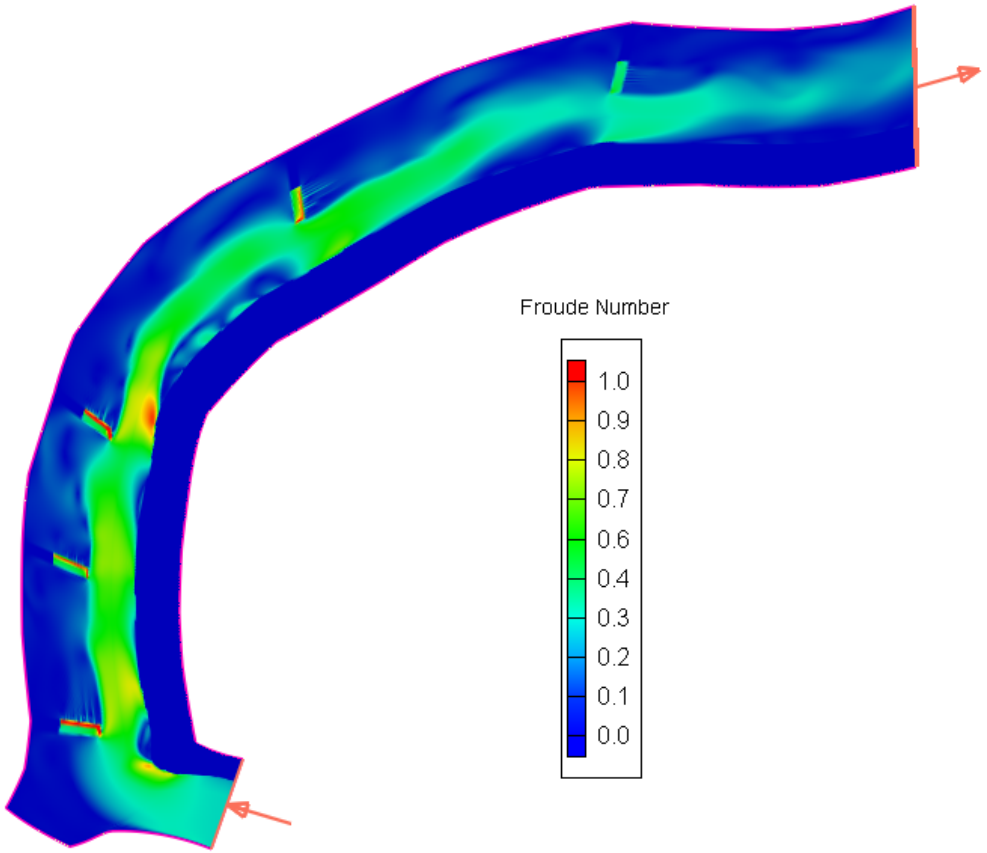


5 Barbs

# Total Shear Stress (N/m^2)
# Discharge: 40 m^3/s, Initial Water Height: 1.5 m

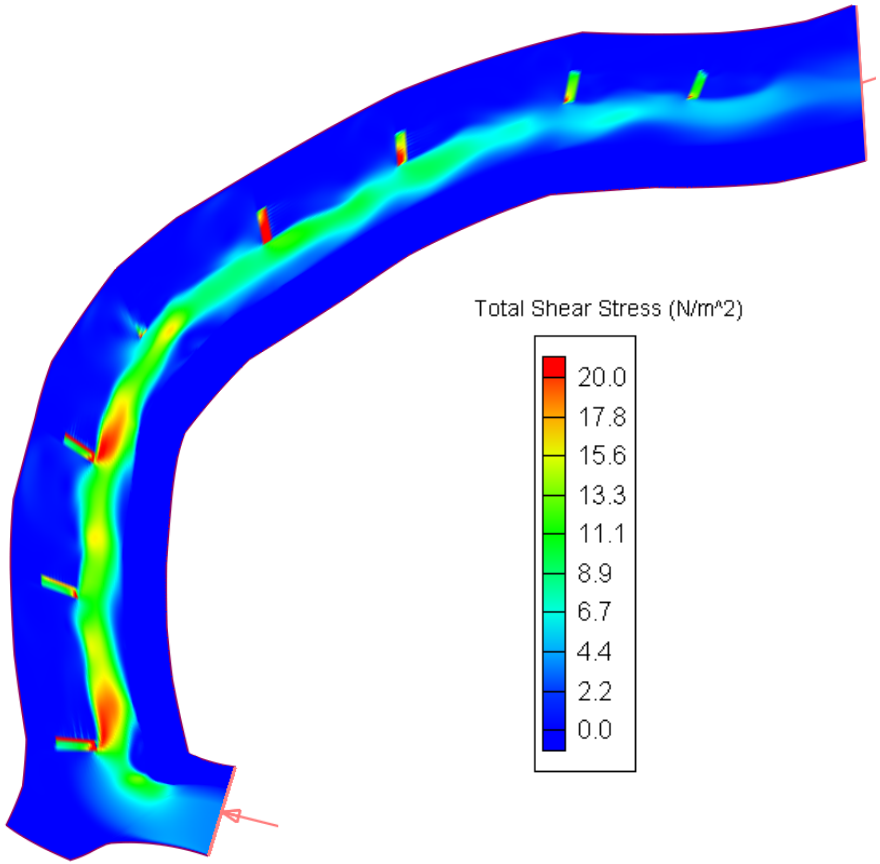


As built

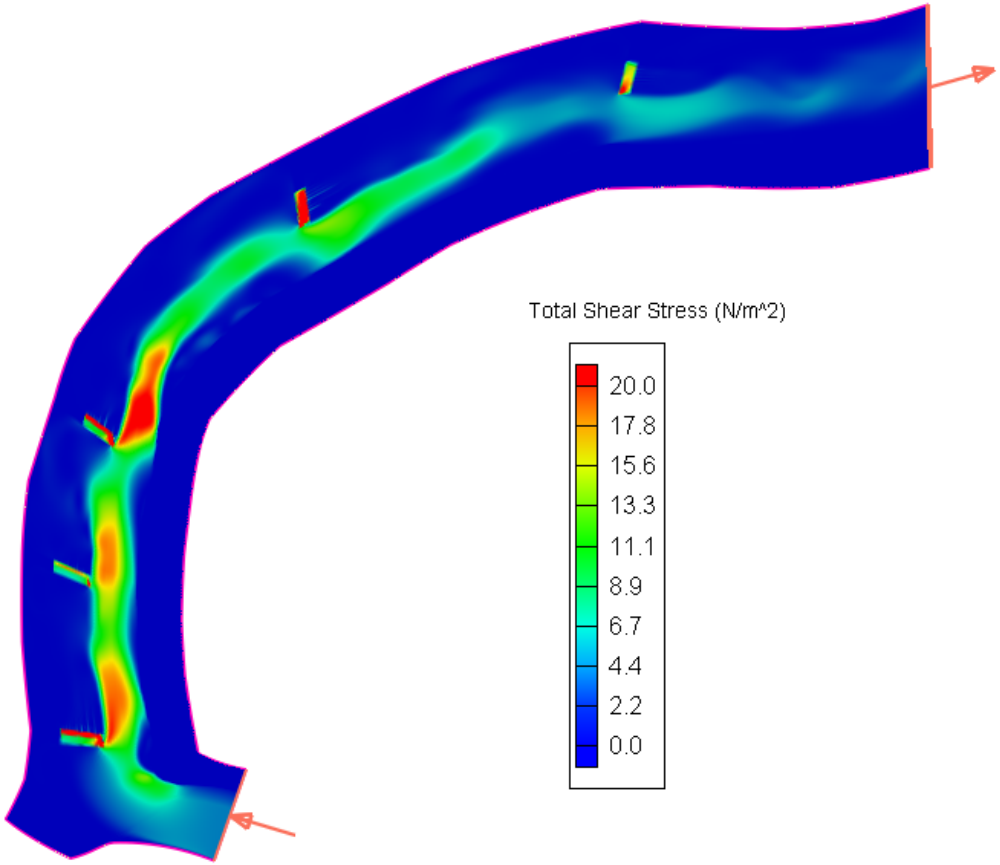


5 Barbs

Bed sediment transport is initiated
when Total Shear Stress > 19 N/m^2

# Study to Compare the Performance of Two Designs to Prevent River Bend Erosion in Arctic Environments

Sag River

7, 5, and 4 barbs simulations

$Q = 300\ m^3/s$

# 7 Barbs - No 1st Barb

Discharge: 300 m^3/s, Initial Water Height: 3.3 m

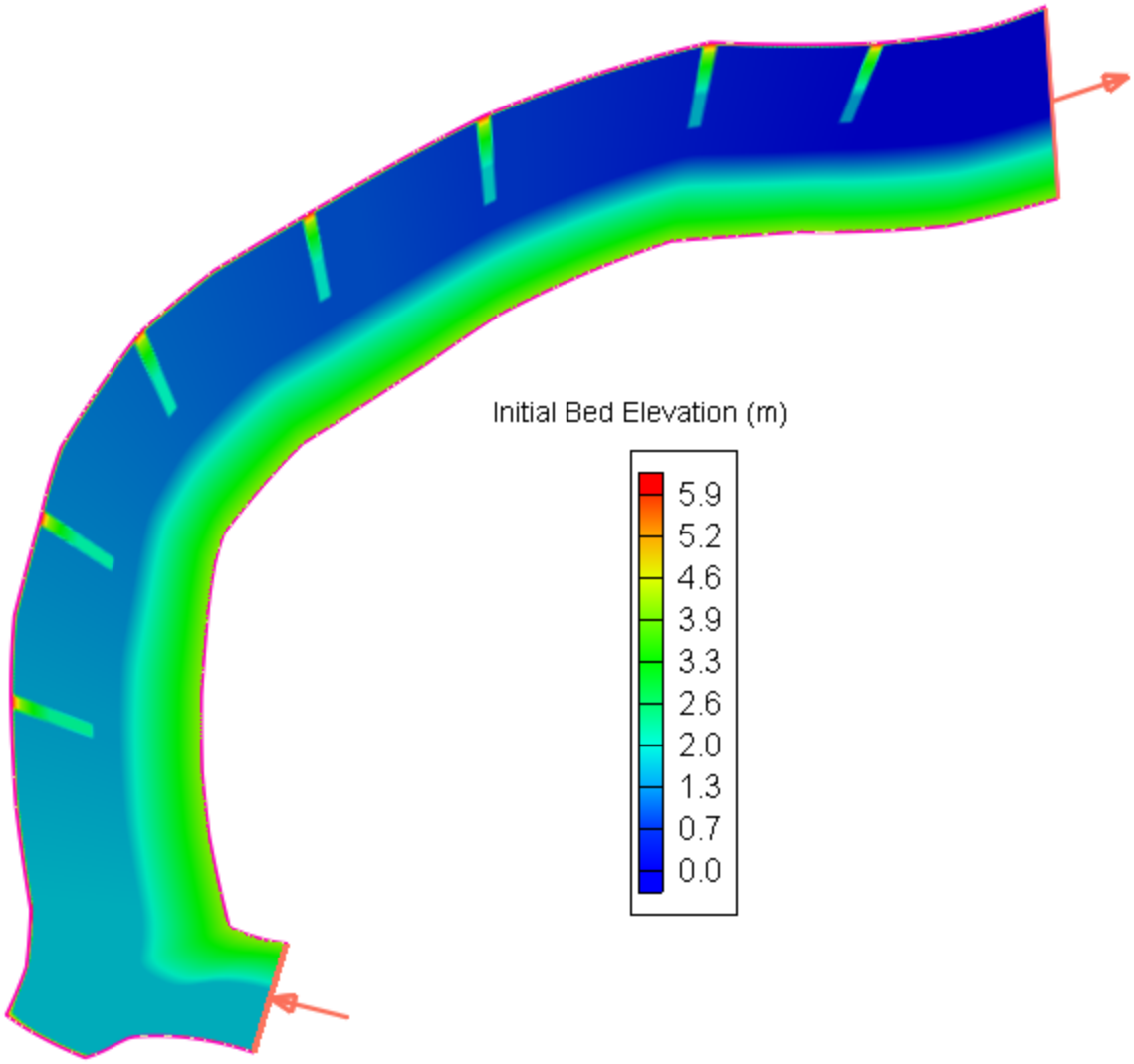

# Velocity Magnitude (m/s)

## Discharge: 300 m^3/s, Initial Water Height: 3.3 m

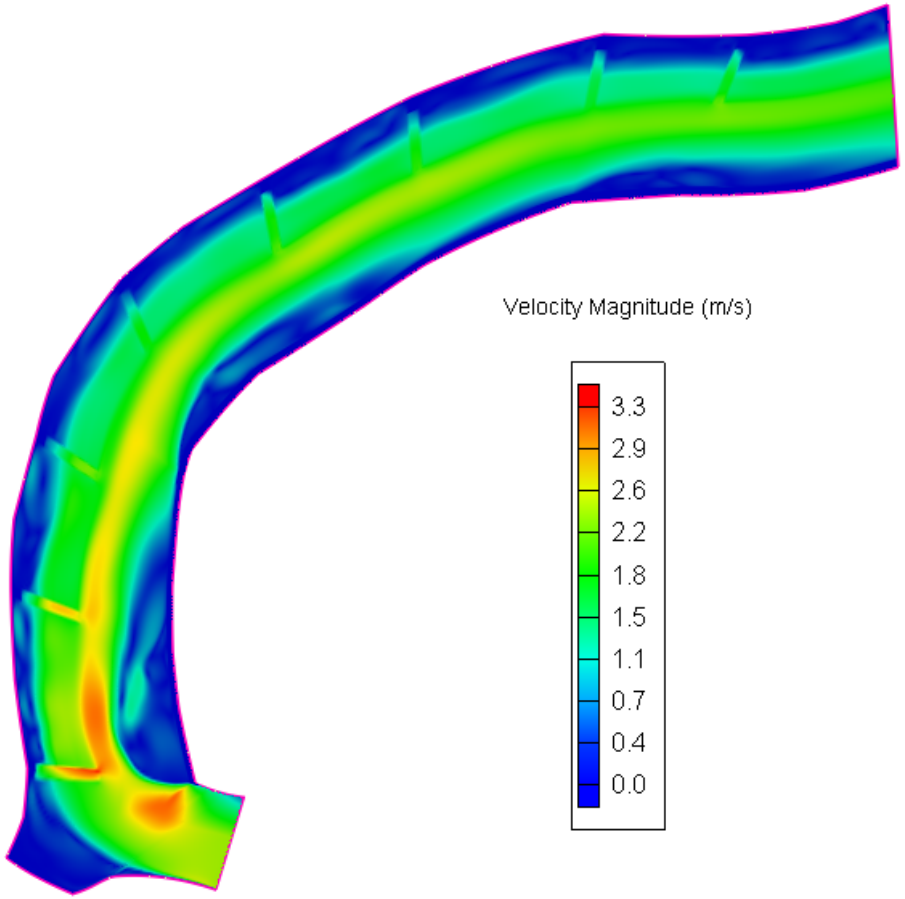


As built

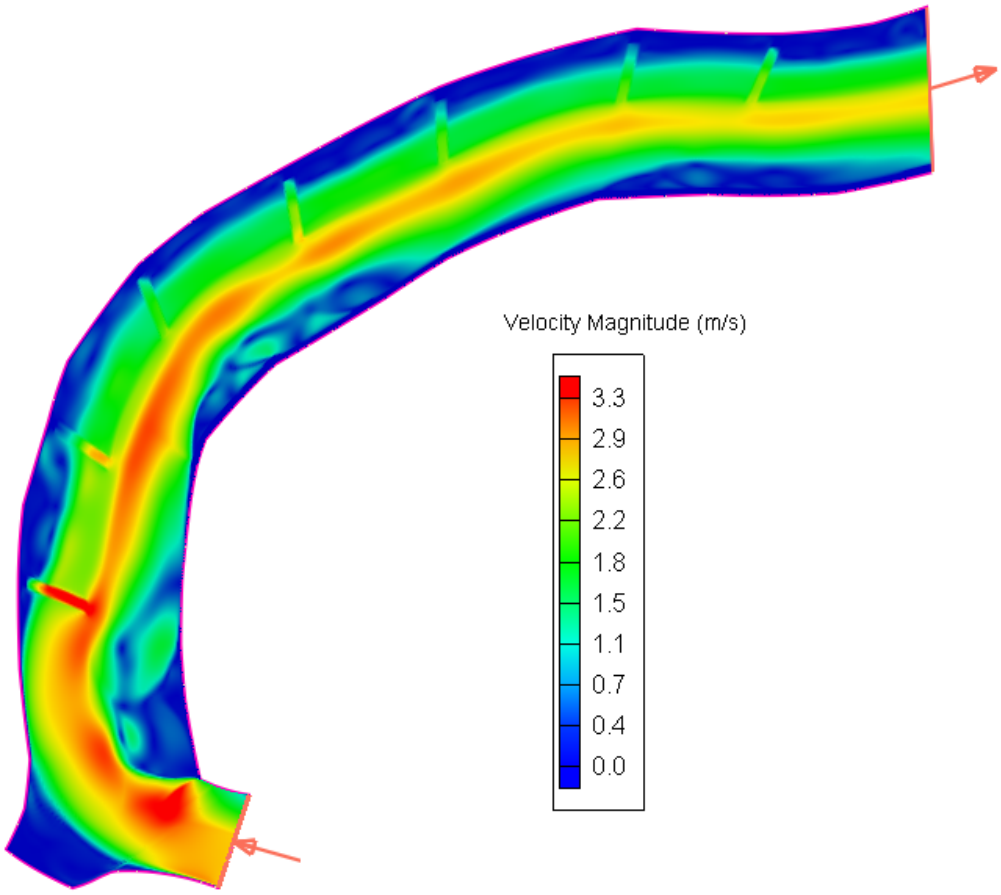


7 Barbs (no 1st barb)

# Total Specific Discharge (m^2/s)

## Discharge: 300 m^3/s, Initial Water Height: 3.3 m

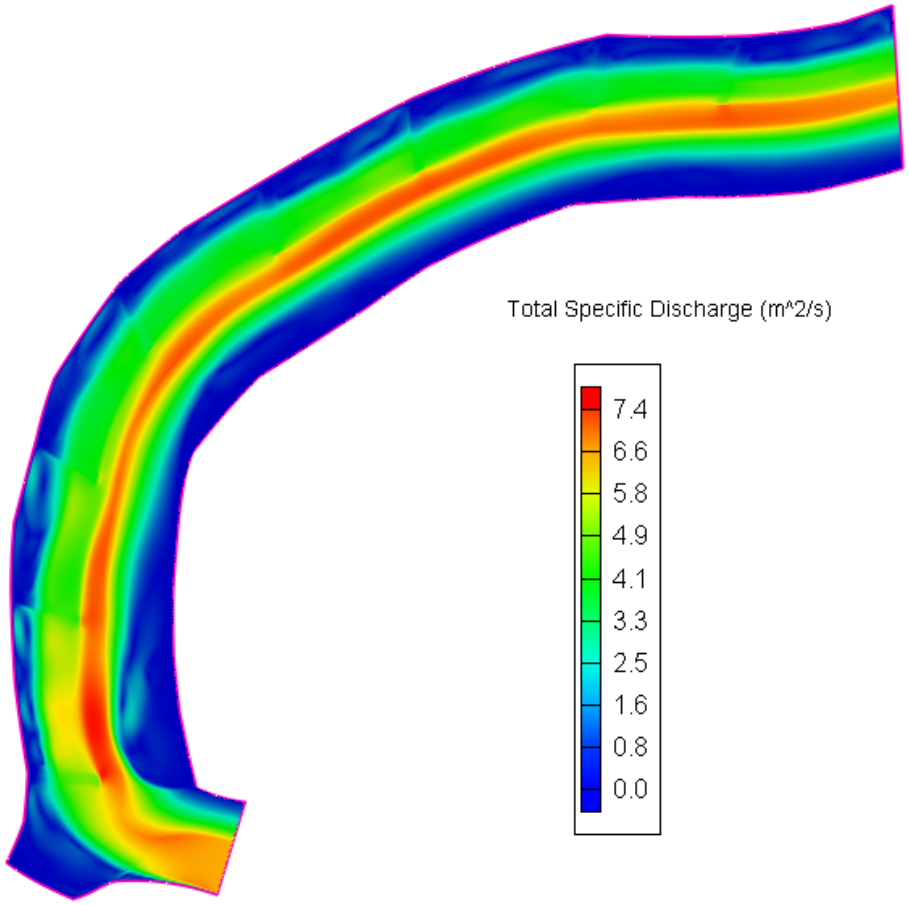


As built

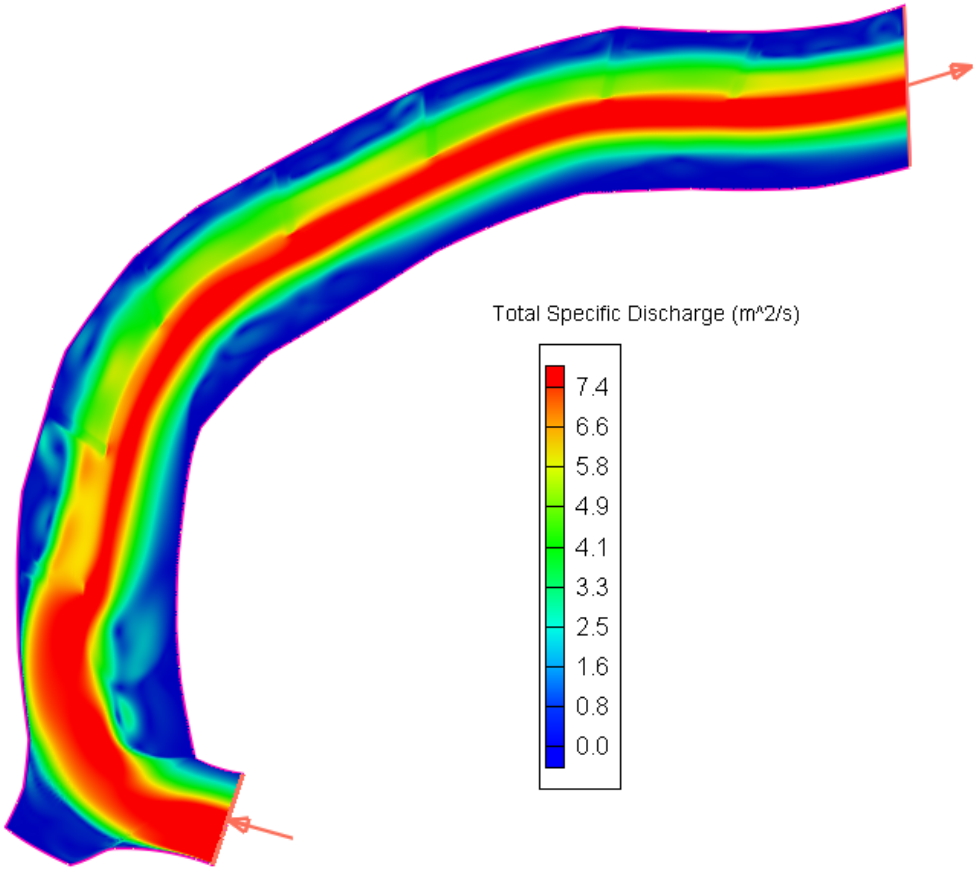


7 Barbs (no 1st barb)

# Froude Number

## Discharge: 300 m^3/s, Initial Water Height: 3.3 m

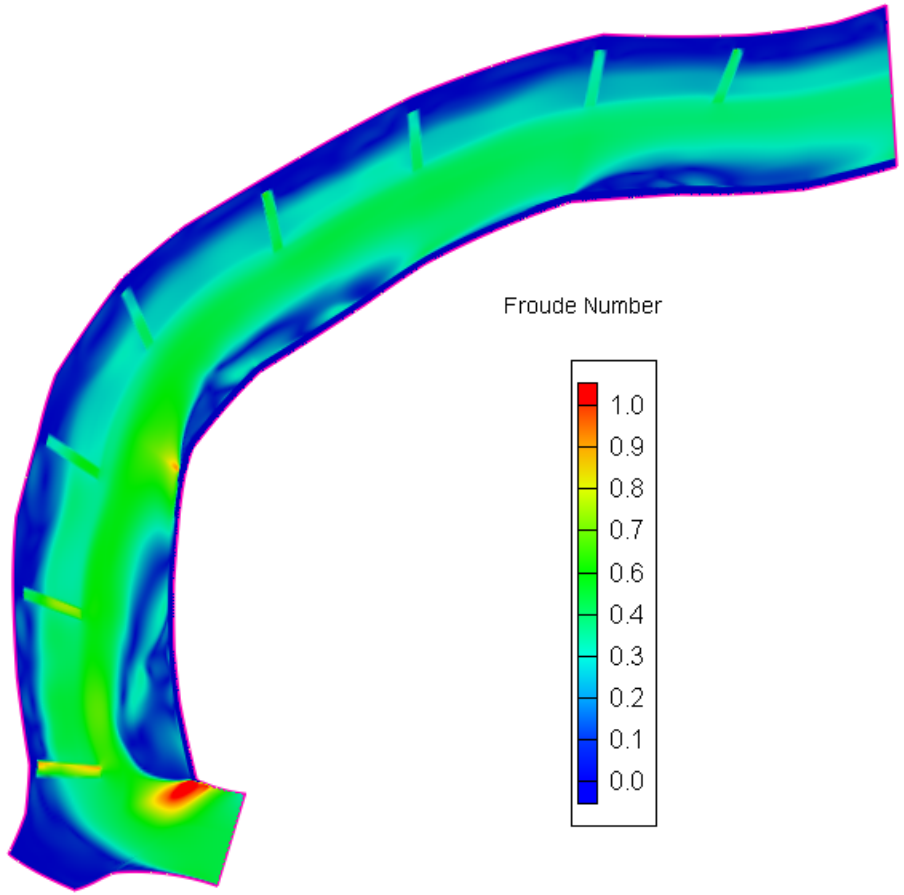


As built

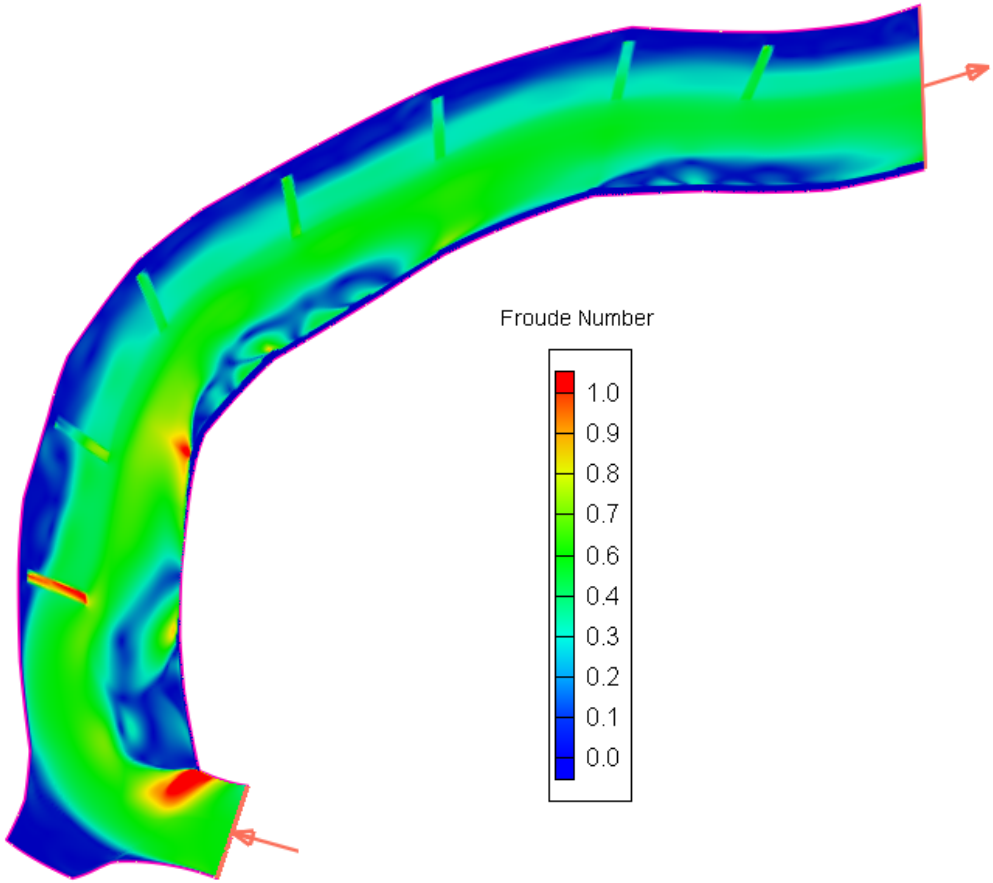


7 Barbs (no 1st barb)

# Total Shear Stress (N/m^2)

## Discharge: 300 m^3/s, Initial Water Height: 3.3 m

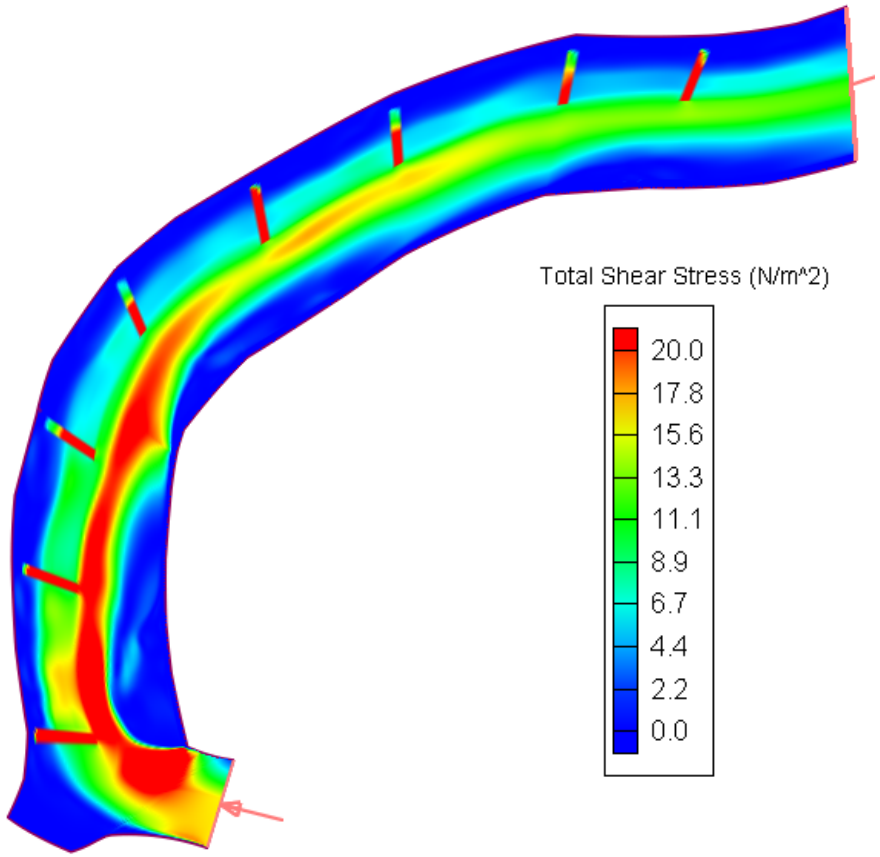


As built

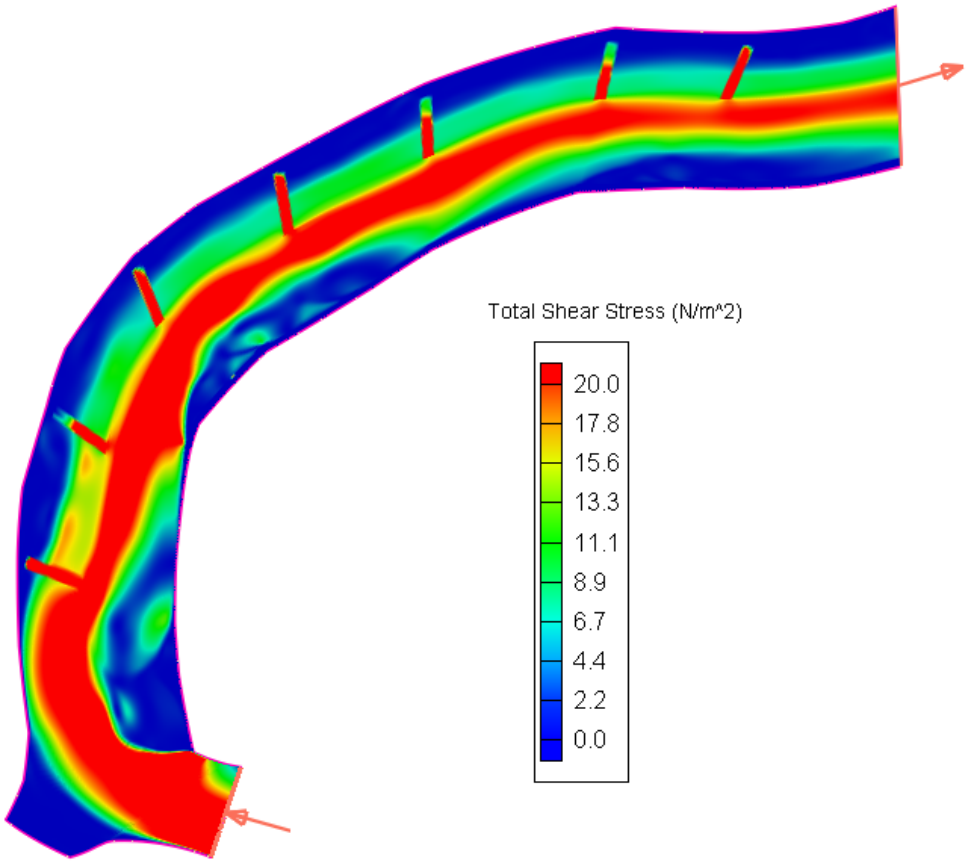


7 Barbs (no 1st barb)

Bed sediment transport is initiated
when Total Shear Stress > 19 N/m^2

# 7 Barbs - No 2nd Barb

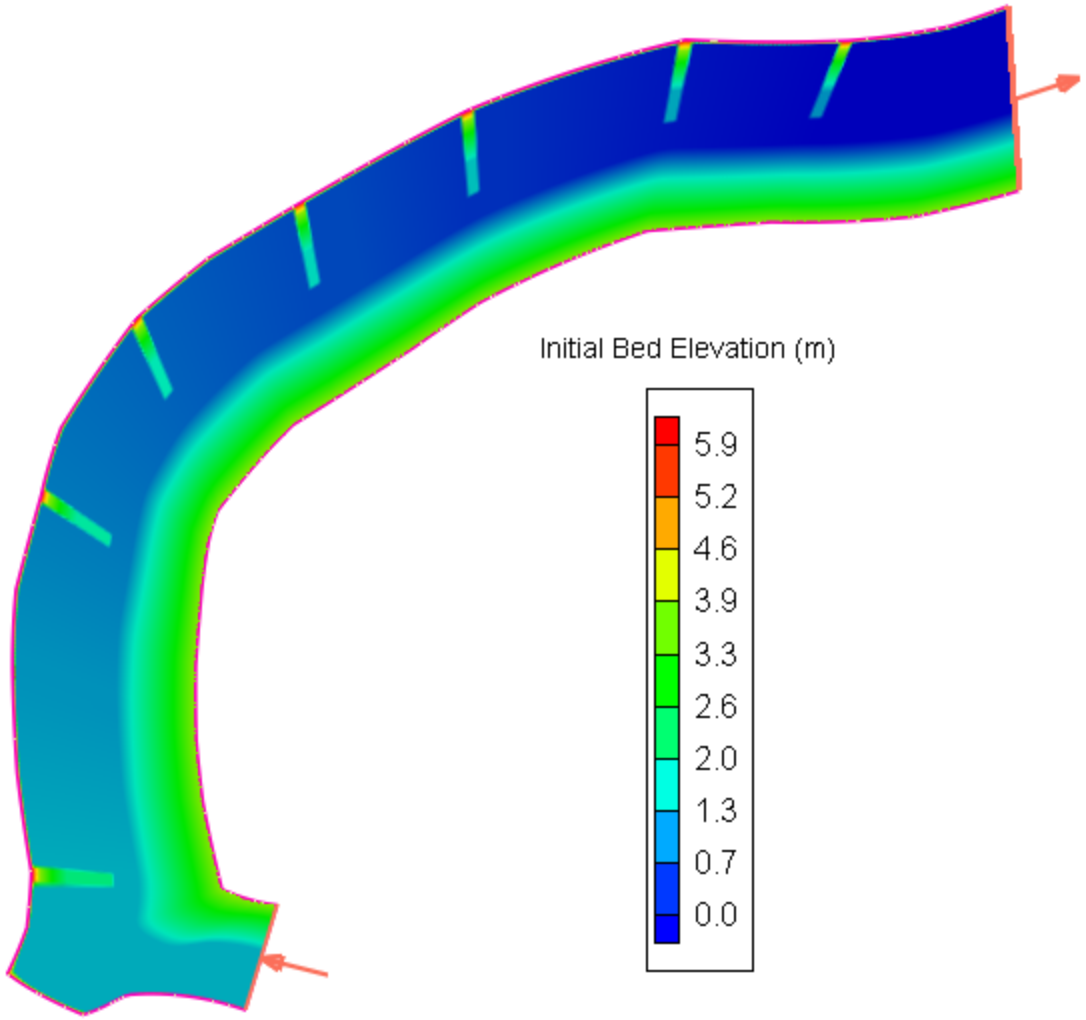

# Velocity Magnitude (m/s)

## Discharge: 300 m^3/s, Initial Water Height: 3.3 m

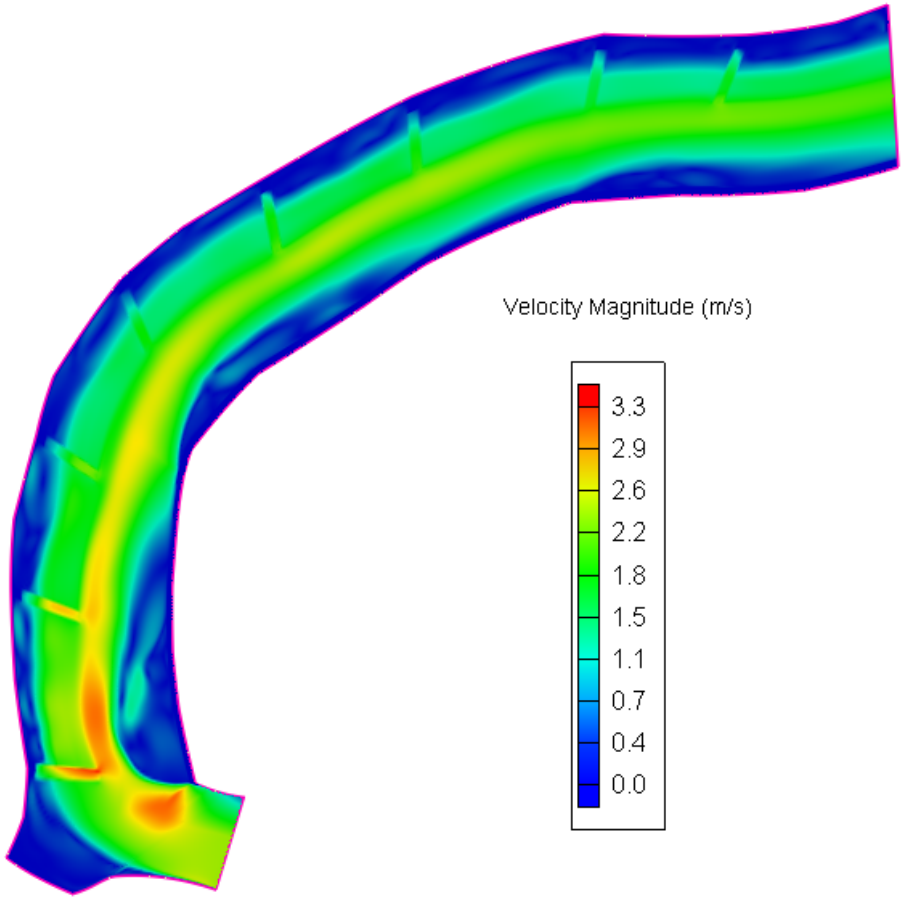


As built

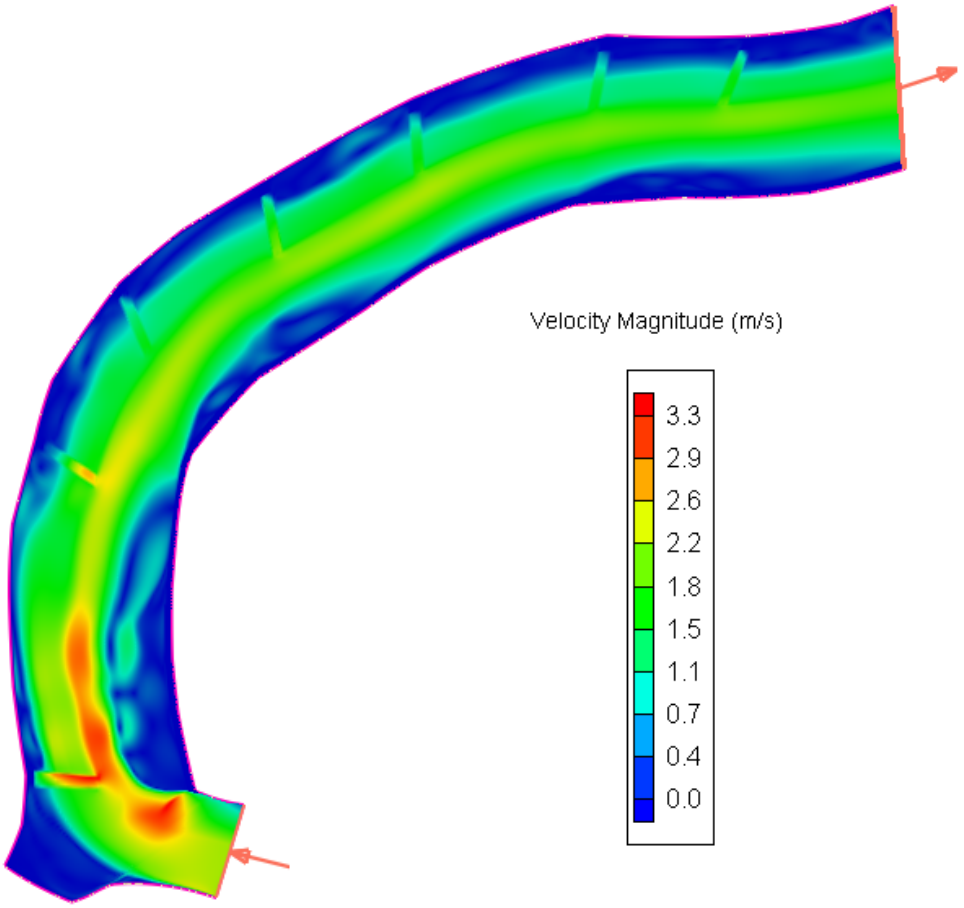


7 Barbs (no 2nd barb)

# Total Specific Discharge (m^2/s)

## Discharge: 300 m^3/s, Initial Water Height: 3.3 m

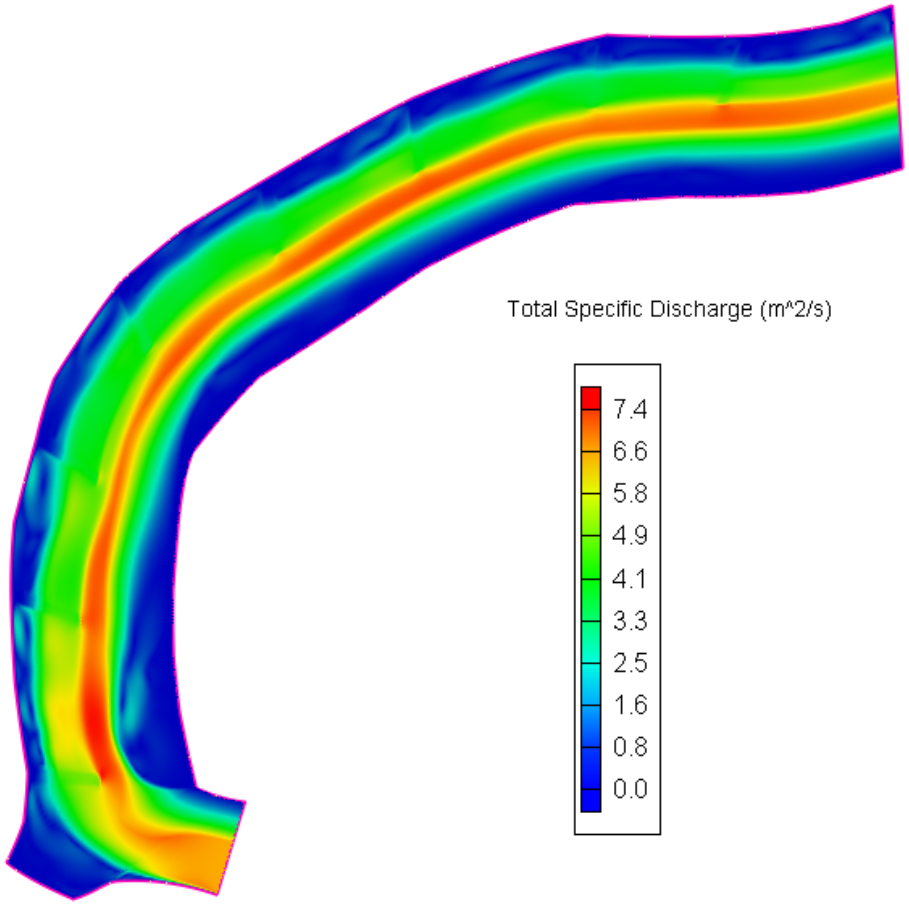


As built

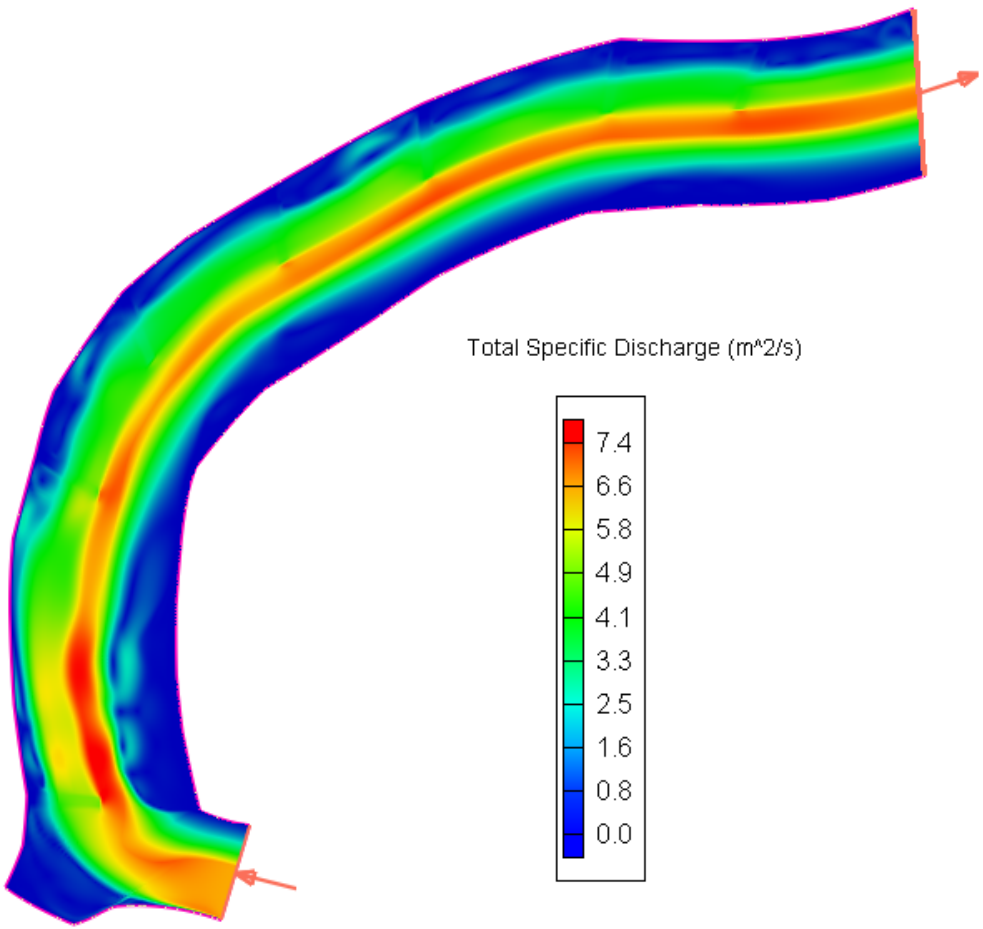


7 Barbs (no 2nd barb)

# Froude Number
## Discharge: 300 m^3/s, Initial Water Height: 3.3 m

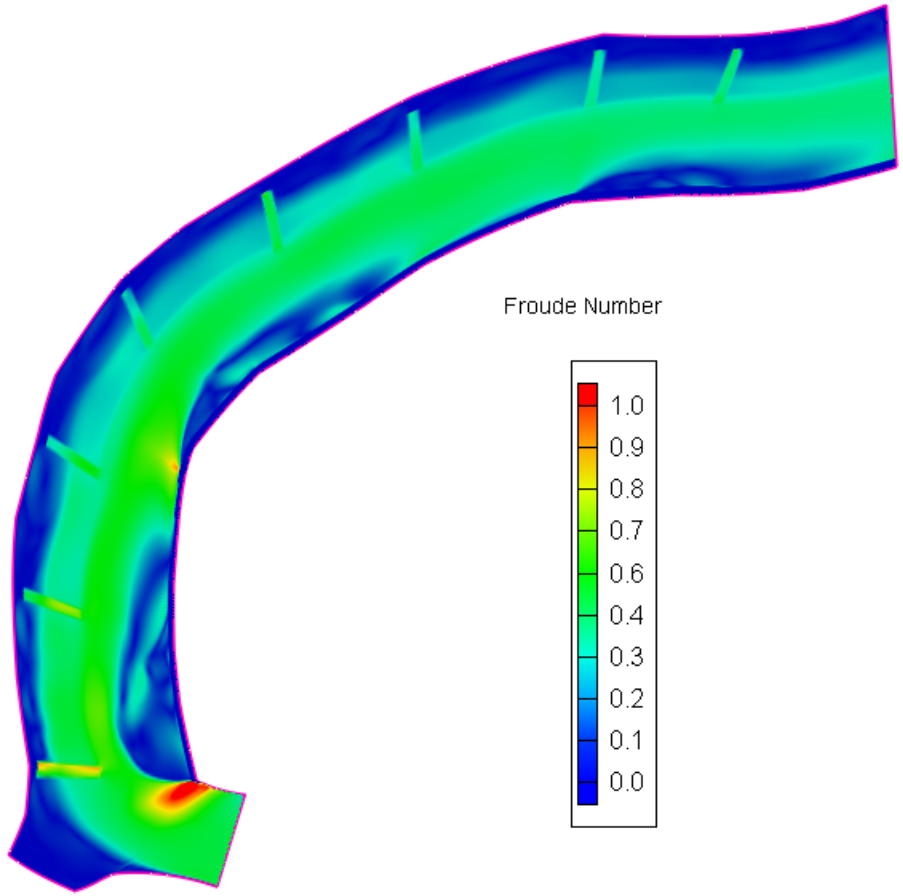


As built

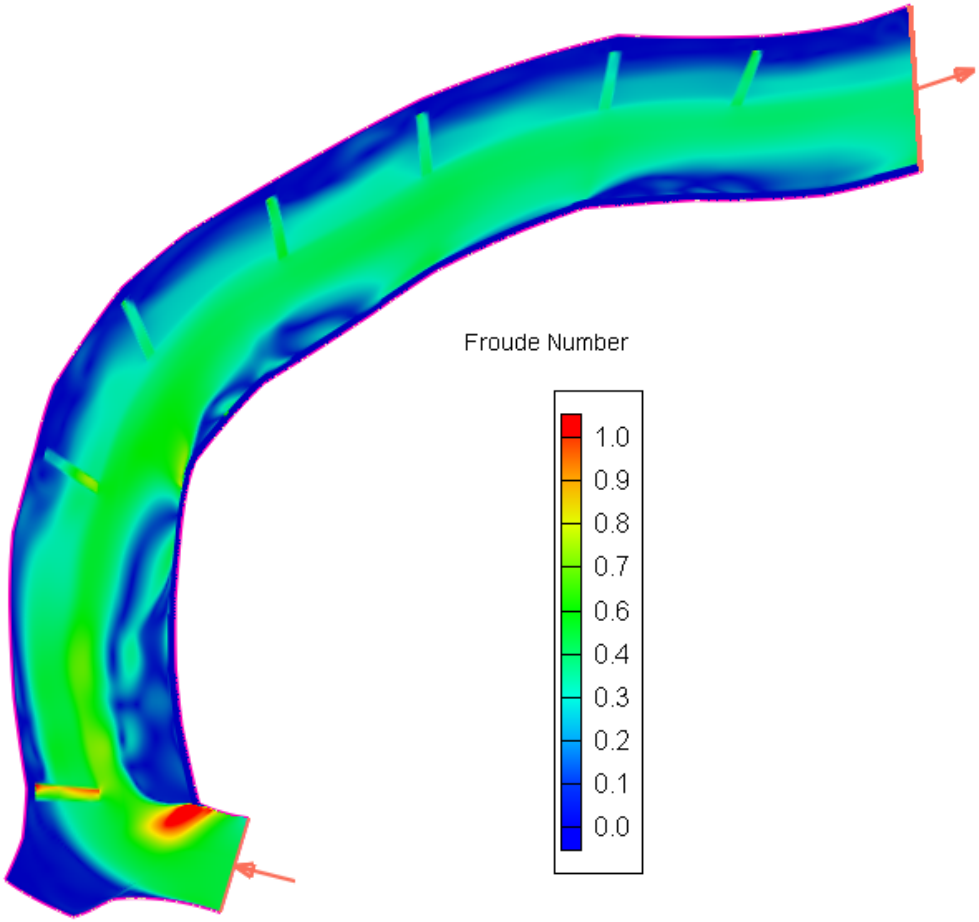


7 Barbs (no 2nd barb)

# Total Shear Stress (N/m^2)
# Discharge: 300 m^3/s, Initial Water Height: 3.3 m

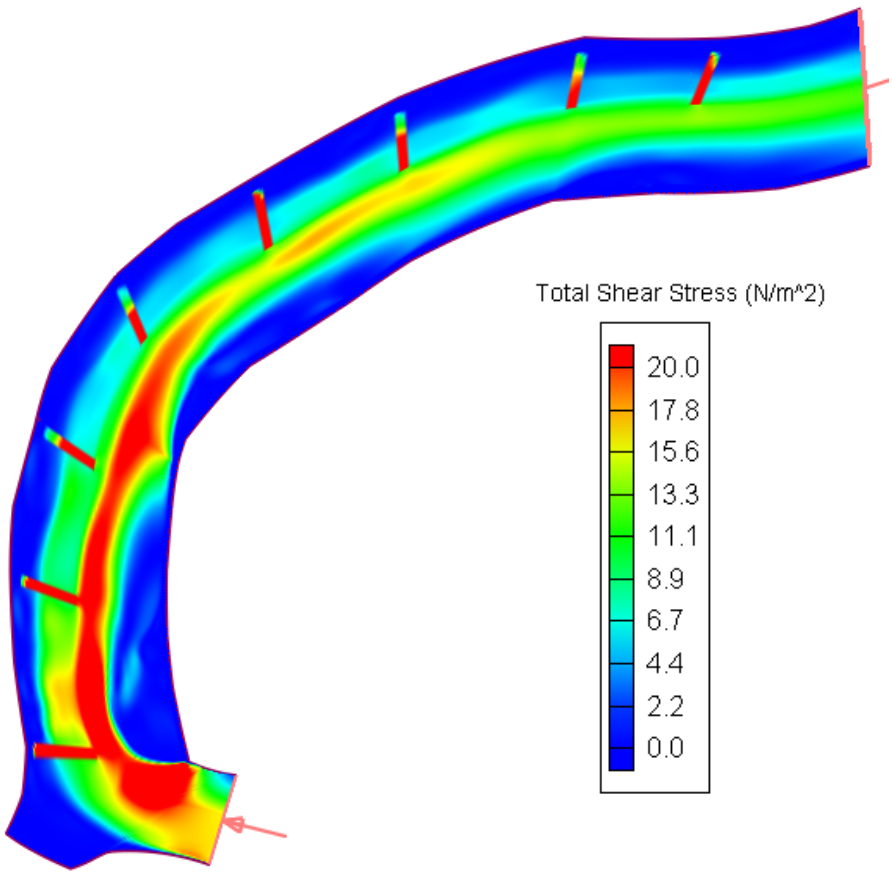


As built

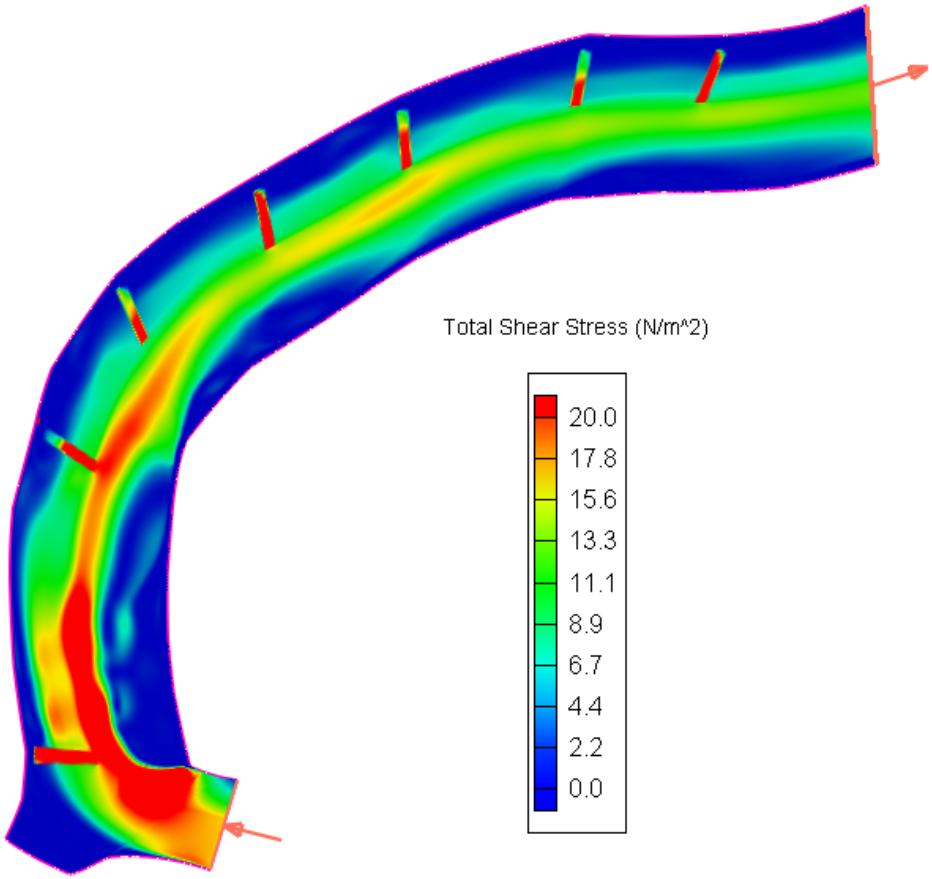


7 Barbs (no 2nd barb)

Bed sediment transport is initiated
when Total Shear Stress > 19 N/m^2

# 7 Barbs - No 3rd Barb

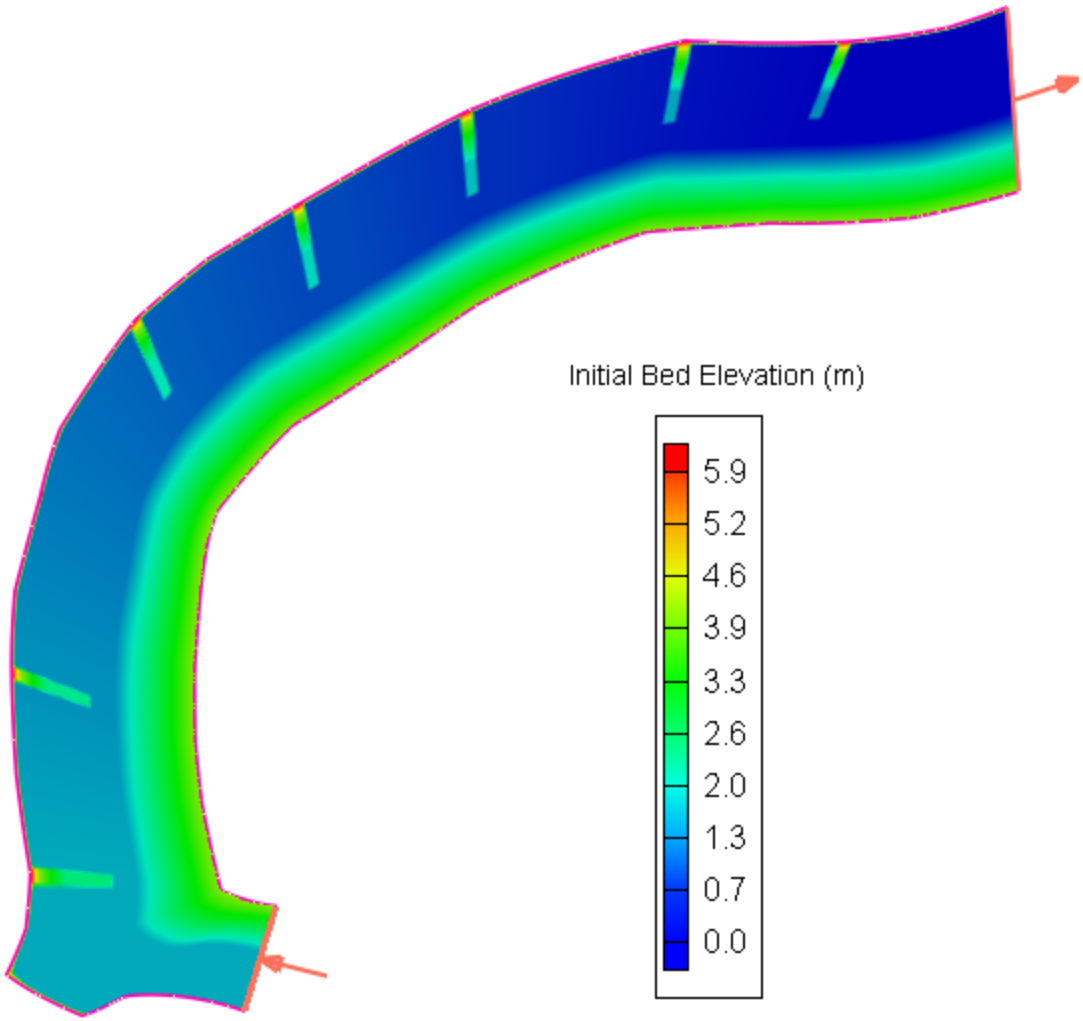

# Velocity Magnitude (m/s)

## Discharge: 300 m^3/s, Initial Water Height: 3.3 m

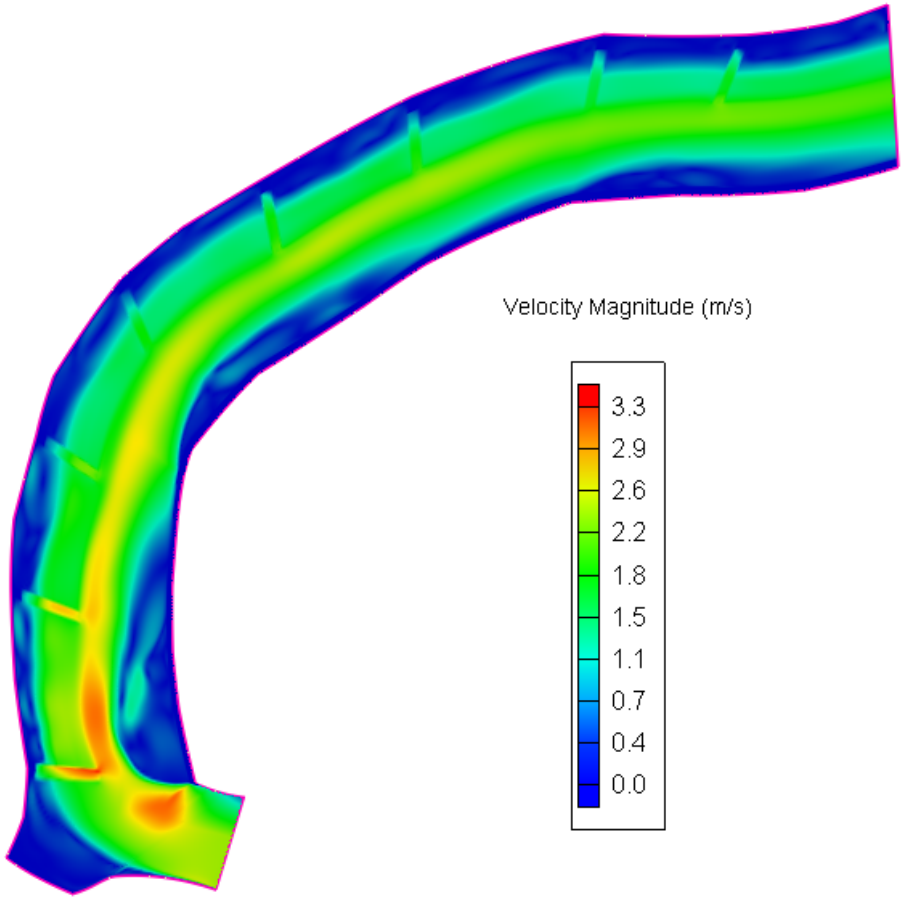


As built

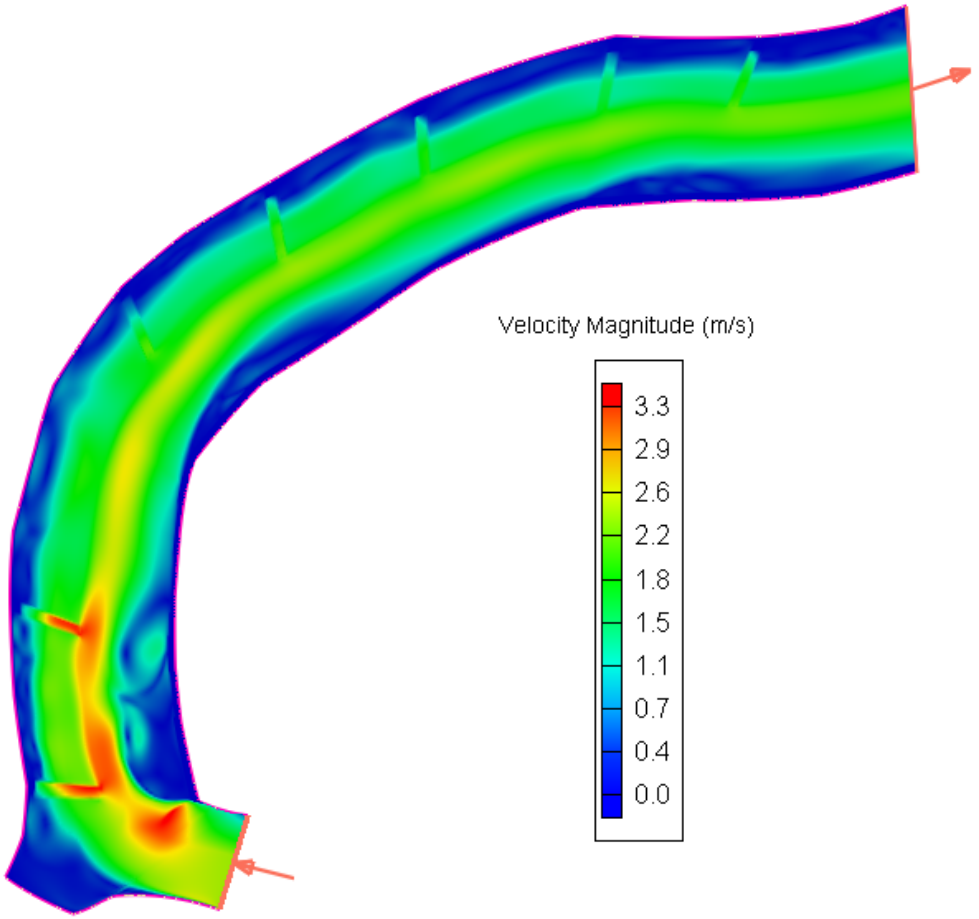


7 Barbs (no 3rd barb)

# Total Specific Discharge (m^2/s)

## Discharge: 300 m^3/s, Initial Water Height: 3.3 m

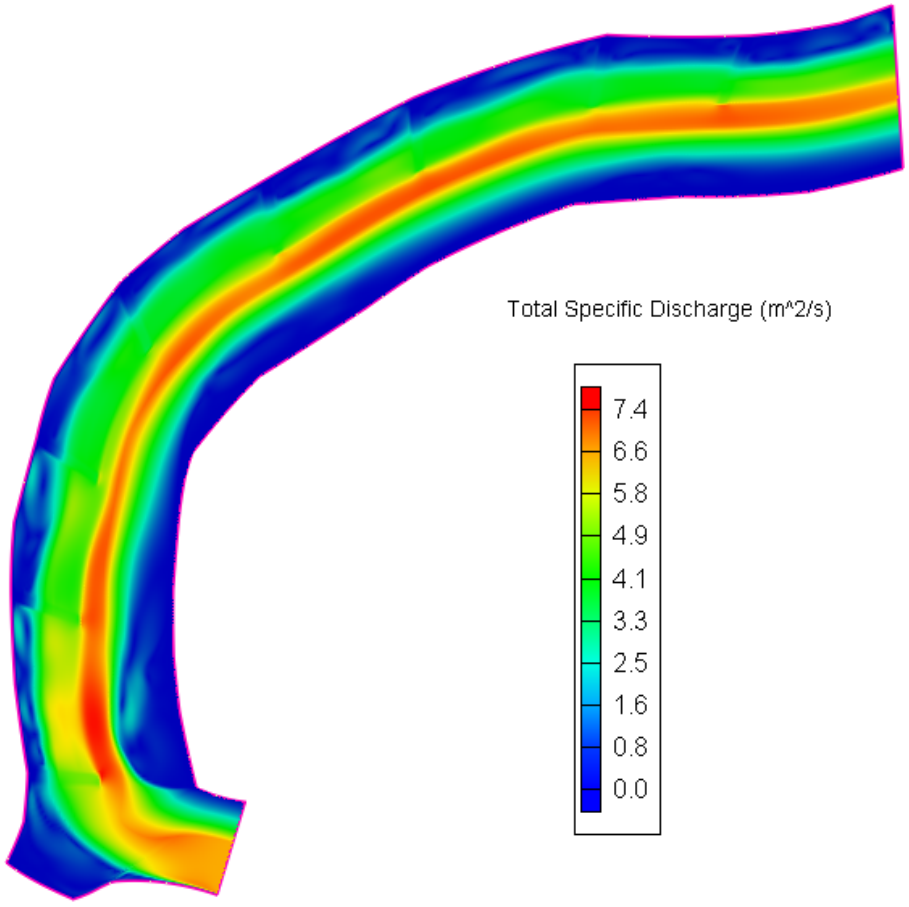


As built

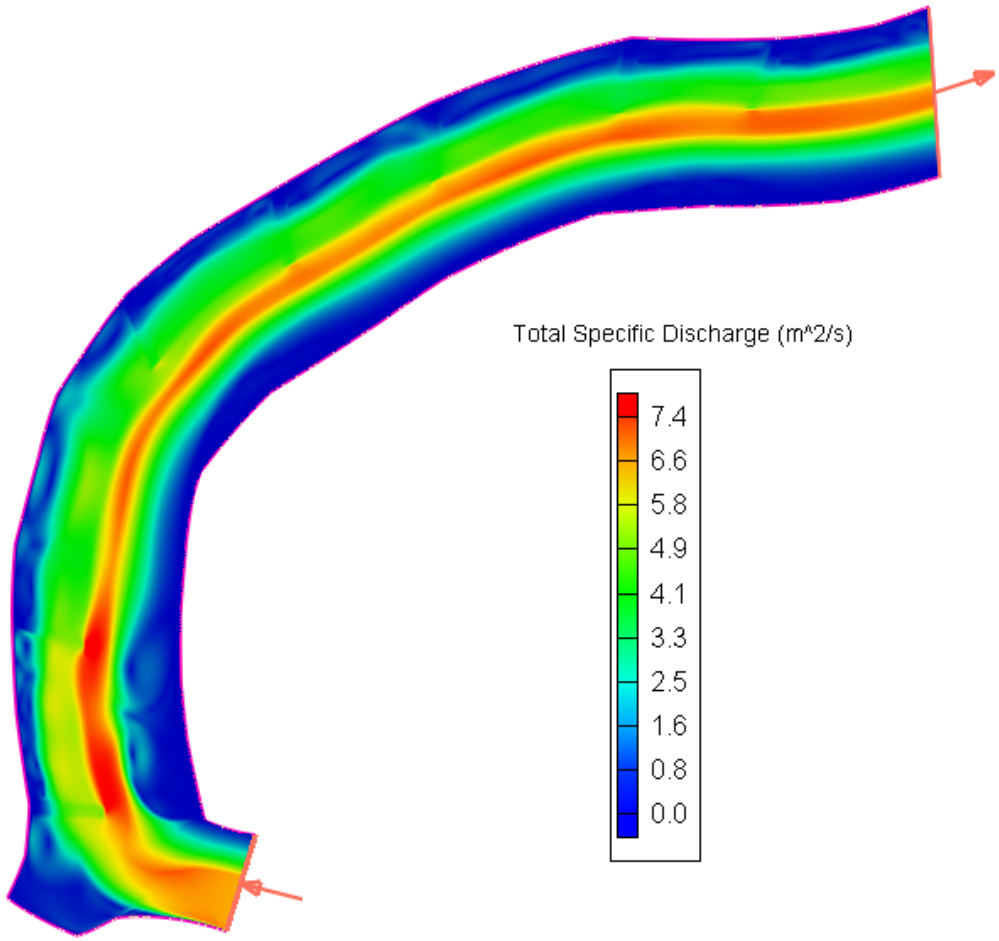


7 Barbs (no 3rd barb)

# Froude Number

## Discharge: 300 m^3/s, Initial Water Height: 3.3 m

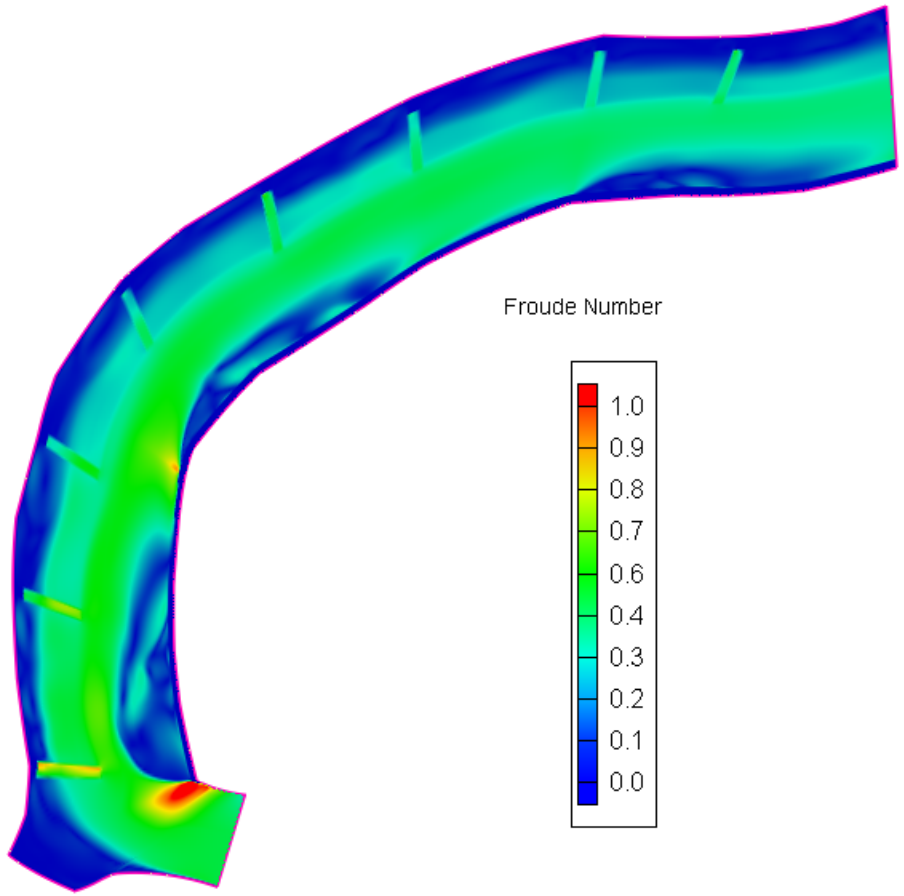


As built

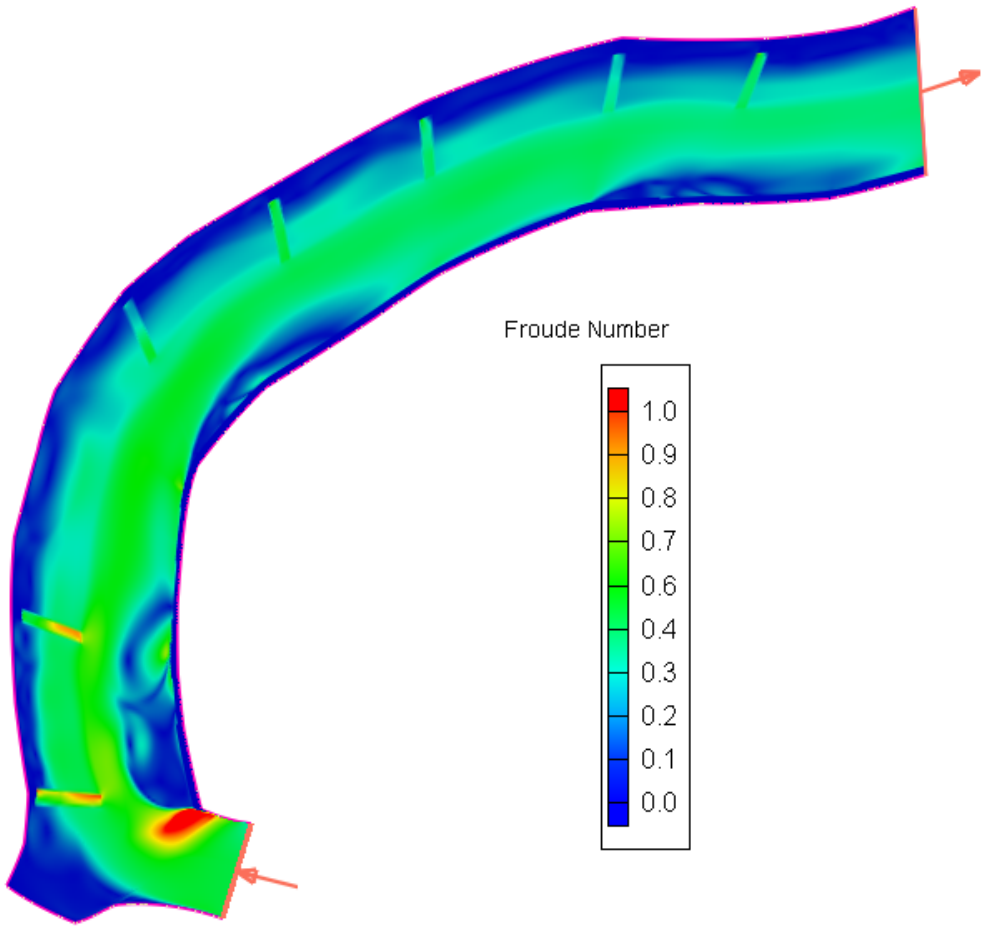


7 Barbs (no 3rd barb)

# Total Shear Stress (N/m^2)
# Discharge: 300 m^3/s, Initial Water Height: 3.3 m

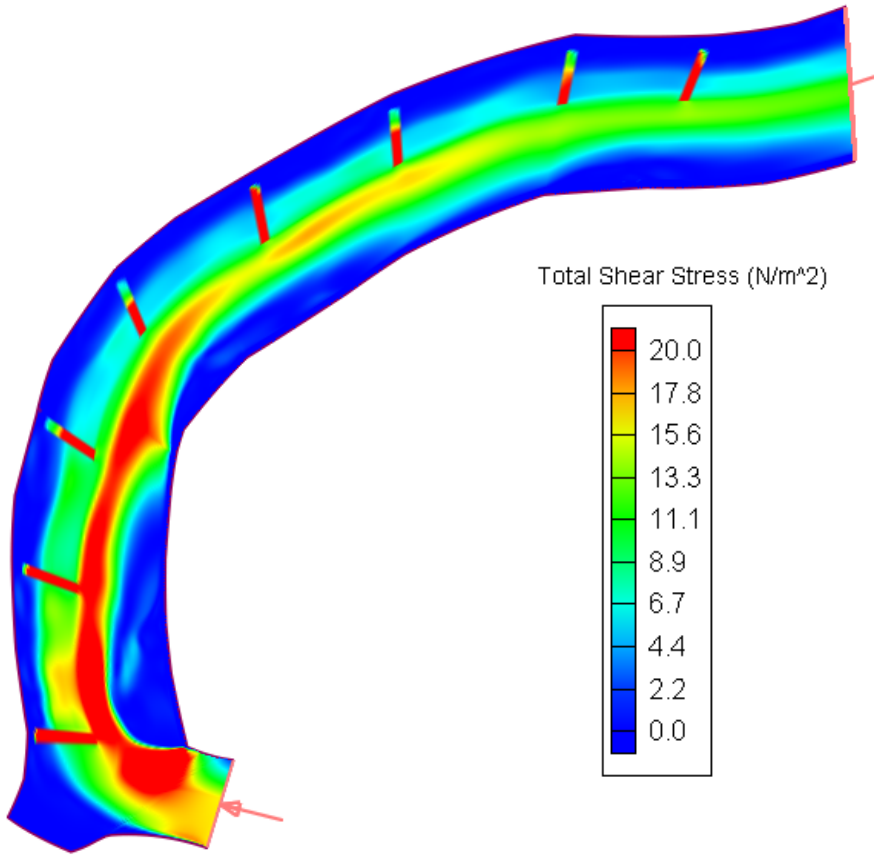


As built

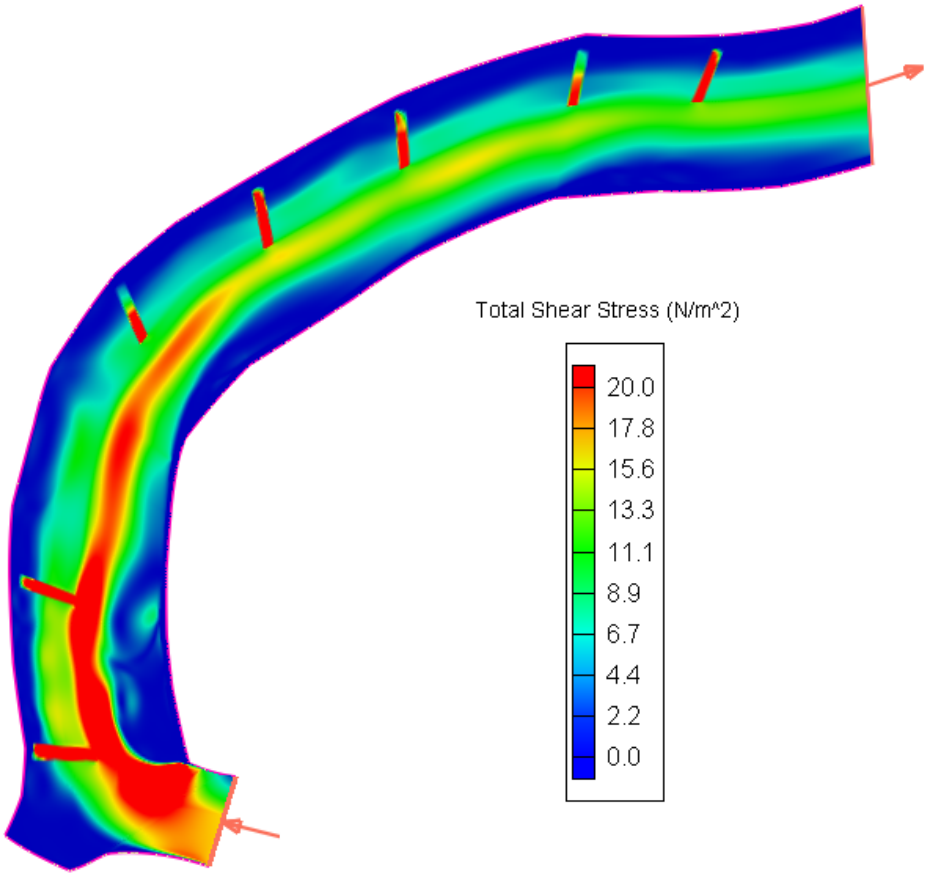


7 Barbs (no 3rd barb)

Bed sediment transport is initiated
when Total Shear Stress > 19 N/m^2

# 7 Barbs - No 4th Barb

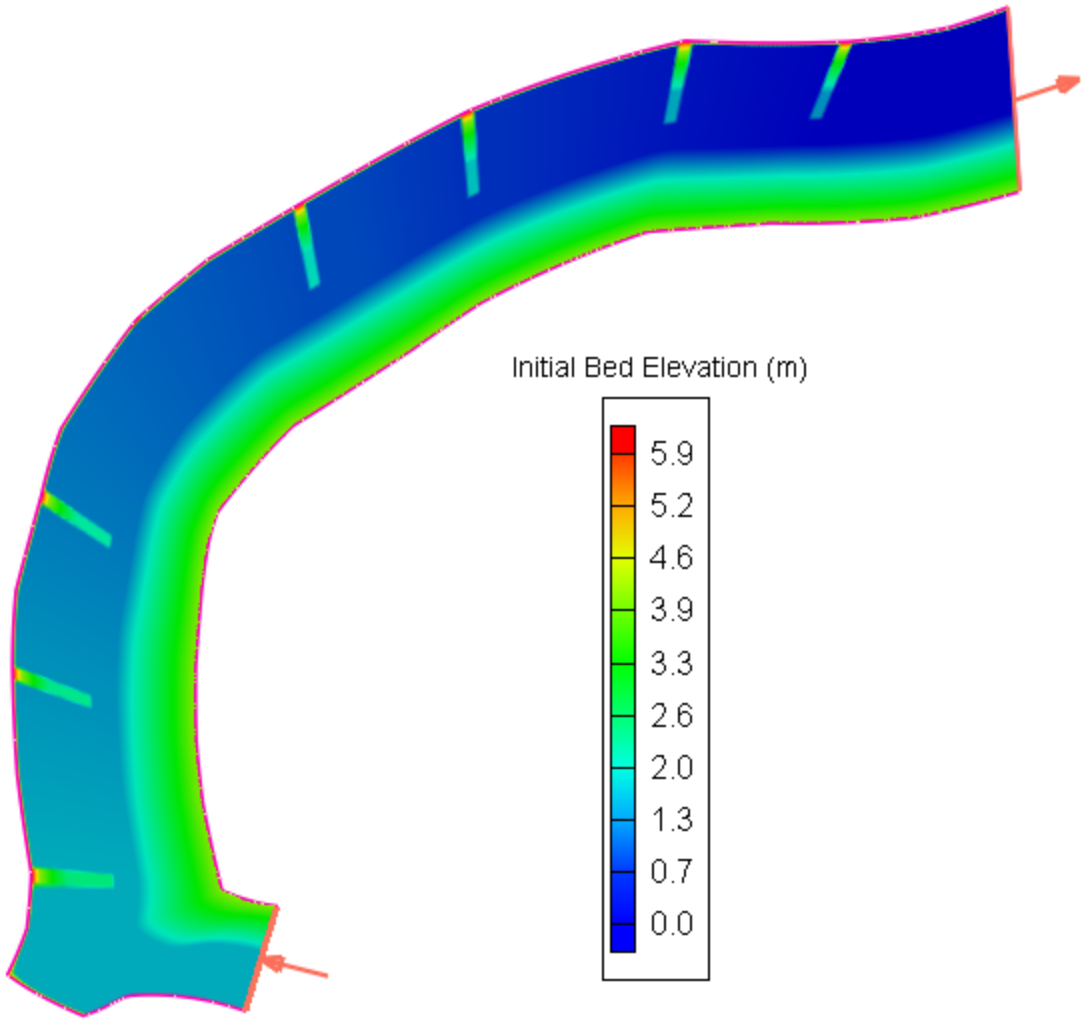

# Velocity Magnitude (m/s)

## Discharge: 300 m^3/s, Initial Water Height: 3.3 m

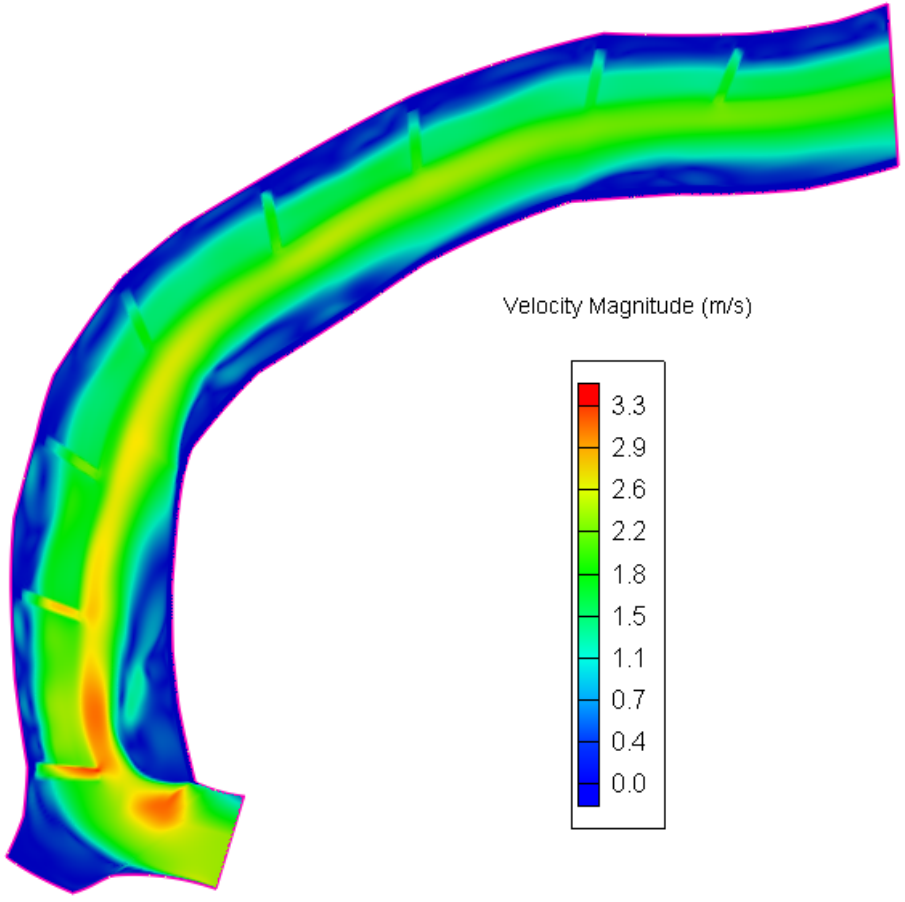


As built

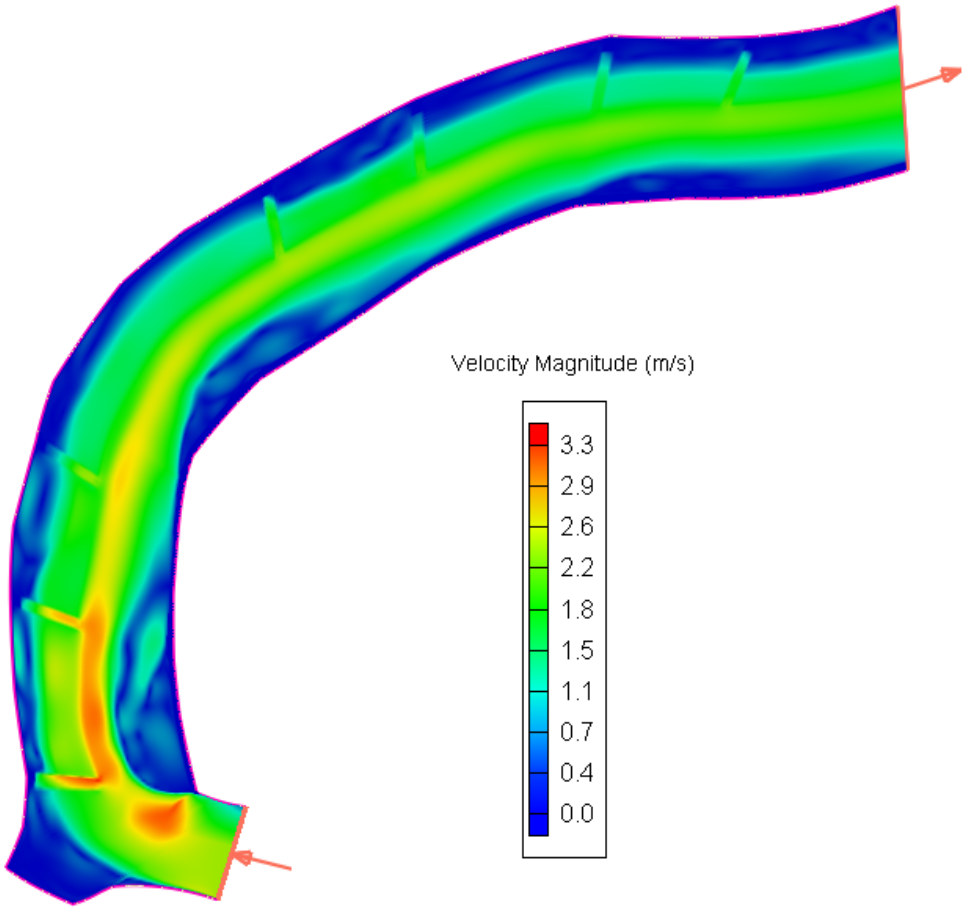


7 Barbs (no 4th barb)

# Total Specific Discharge (m^2/s)

## Discharge: 300 m^3/s, Initial Water Height: 3.3 m

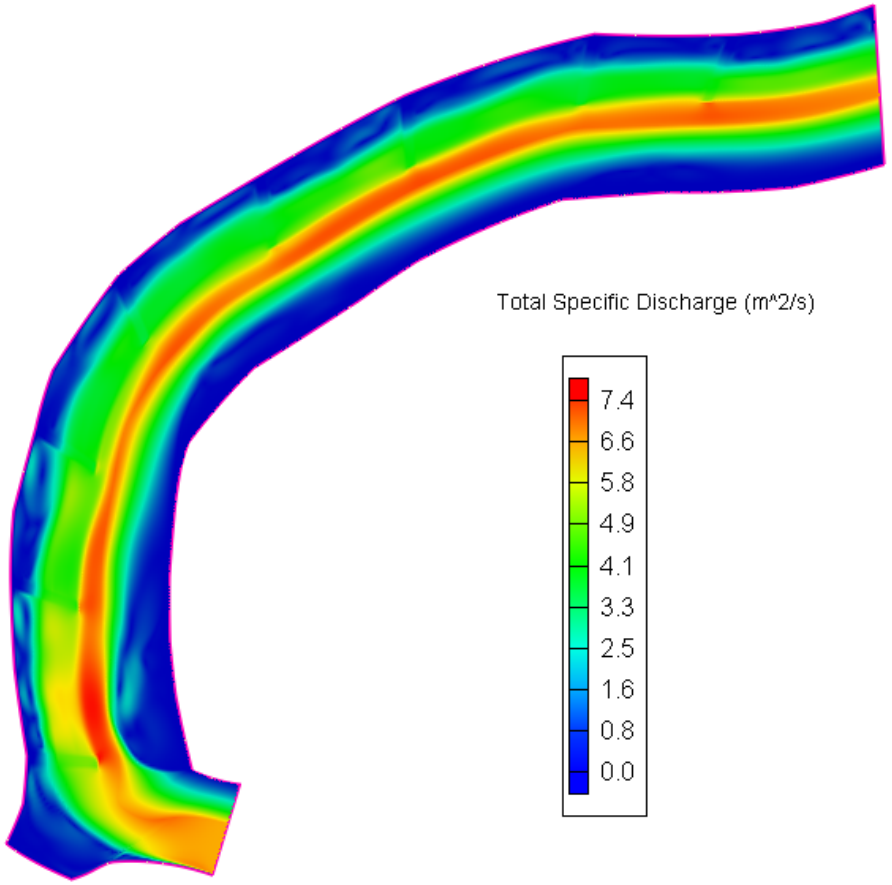


As built

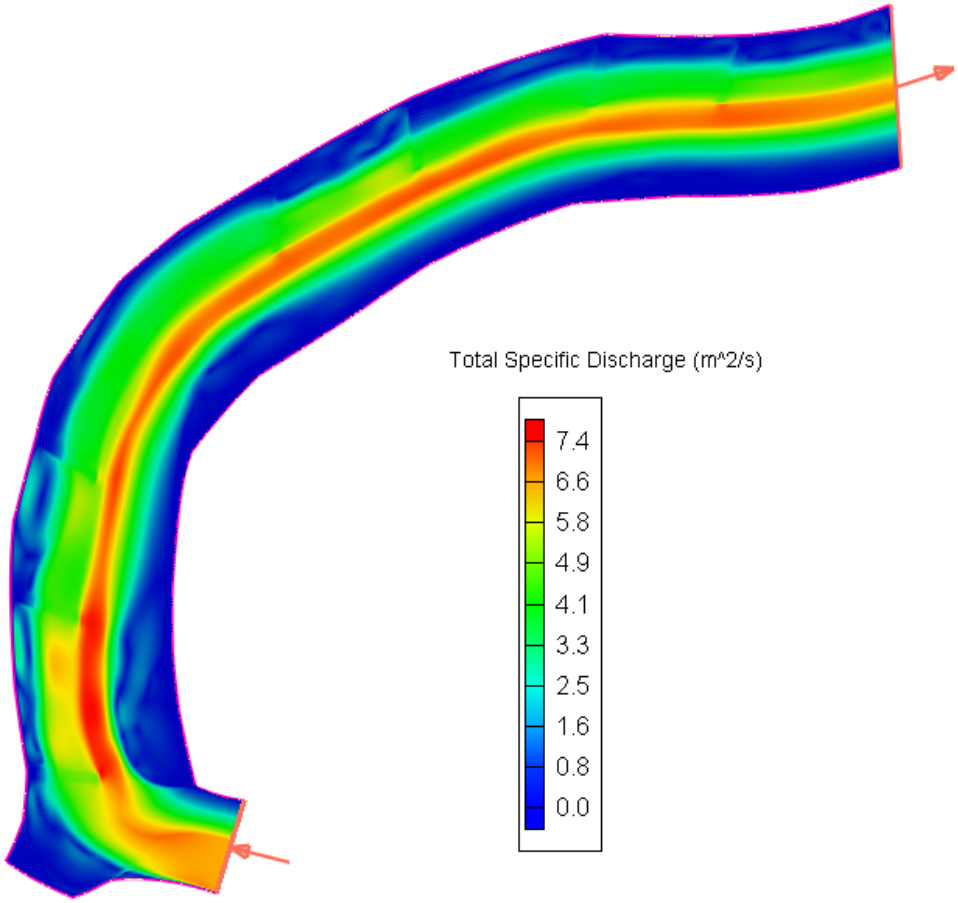


7 Barbs (no 4th barb)

# Froude Number
## Discharge: 300 m^3/s, Initial Water Height: 3.3 m

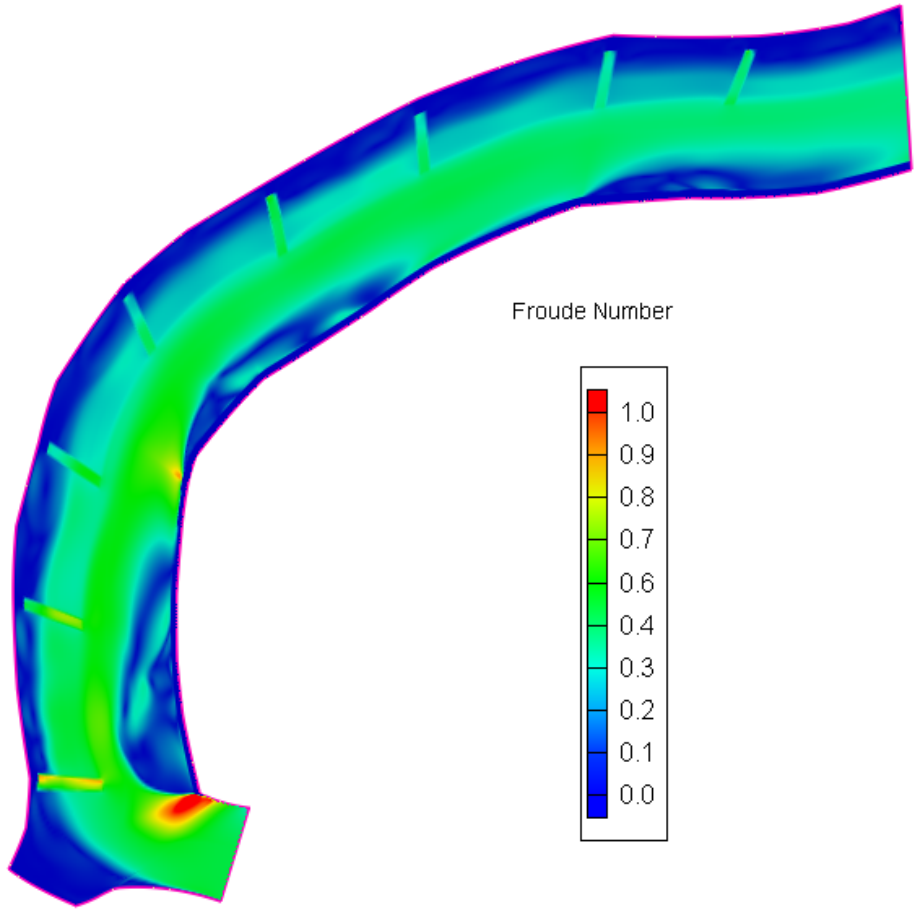


As built

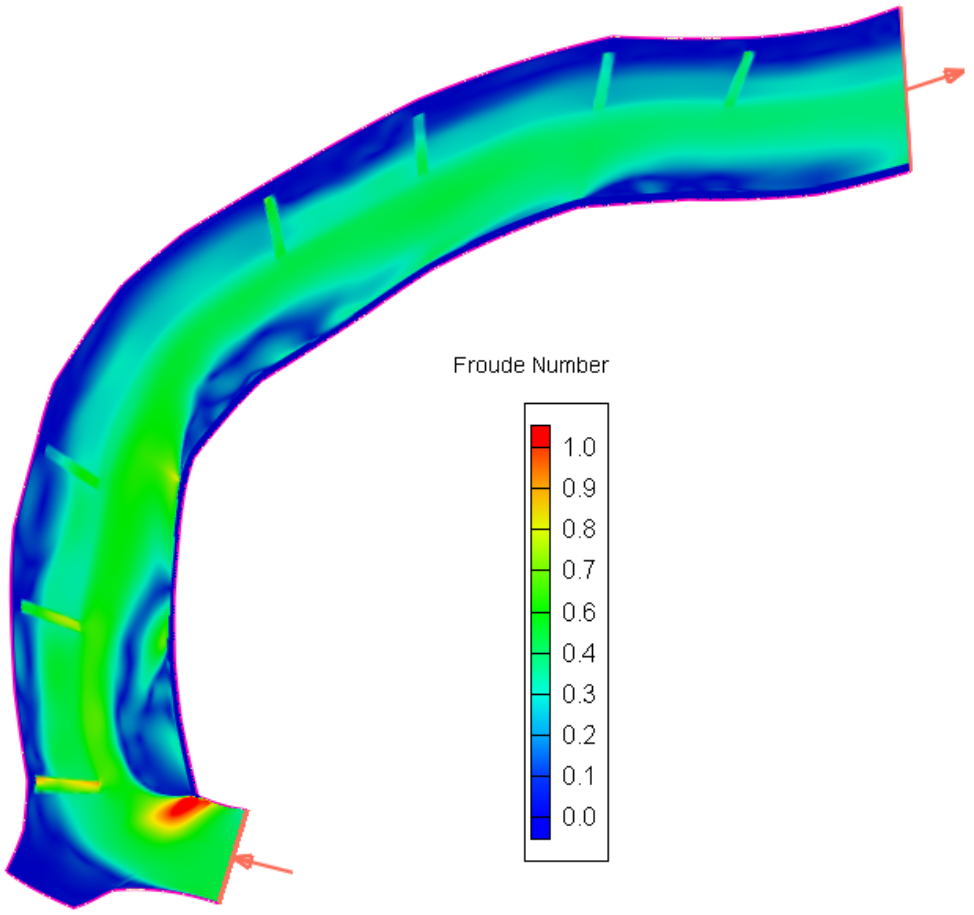


7 Barbs (no 4th barb)

# Total Shear Stress (N/m^2)
# Discharge: 300 m^3/s, Initial Water Height: 3.3 m

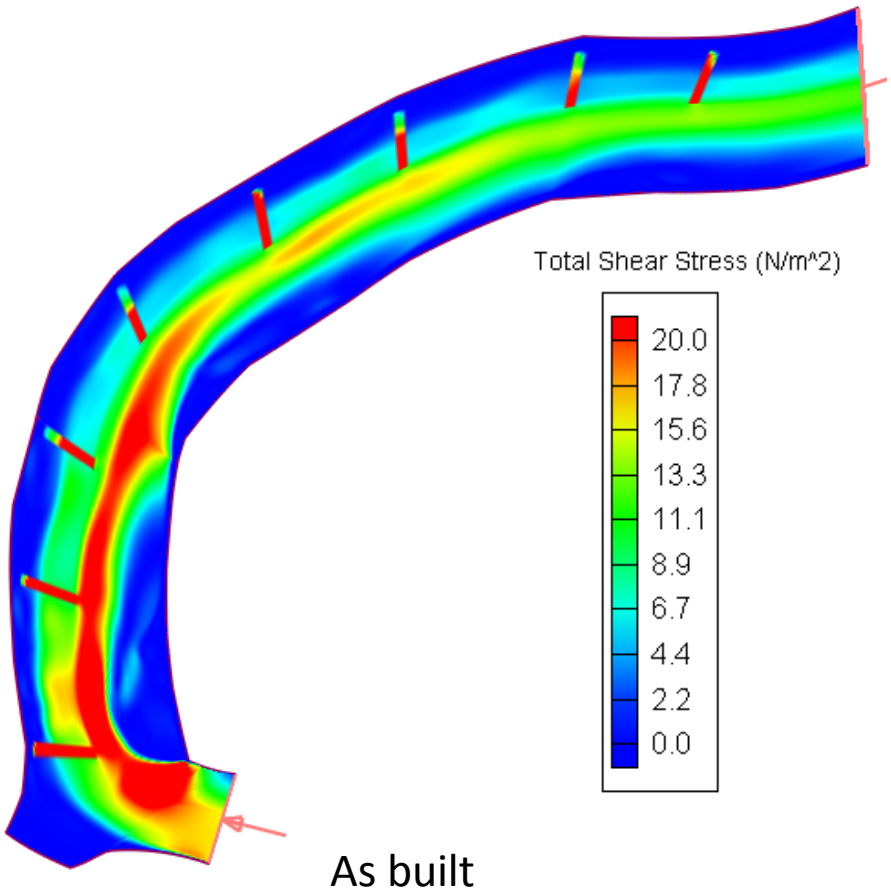


As built

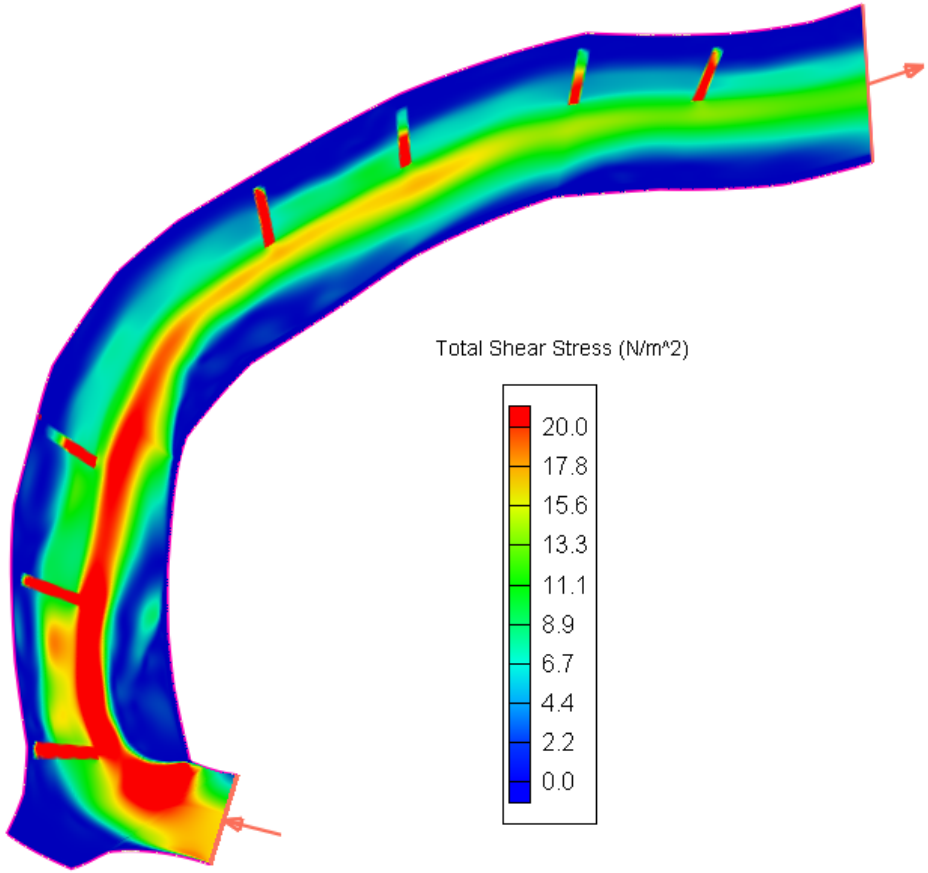


7 Barbs (no 4$^{tn}$ barb)

Bed sediment transport is initiated
when Total Shear Stress > 19 N/m^2

# 7 Barbs - No 5th Barb

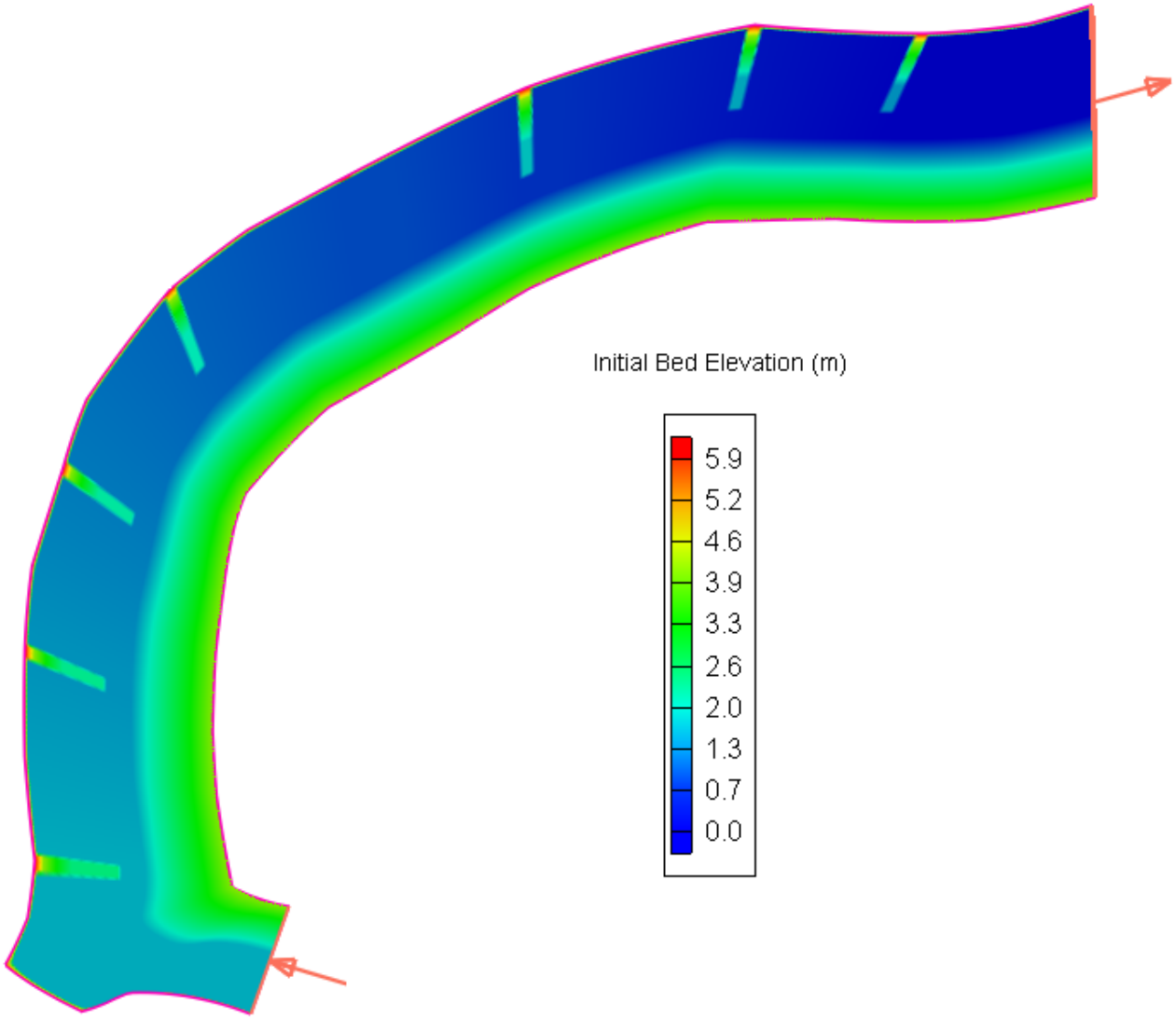

# Velocity Magnitude (m/s)

## Discharge: 300 m^3/s, Initial Water Height: 3.3 m

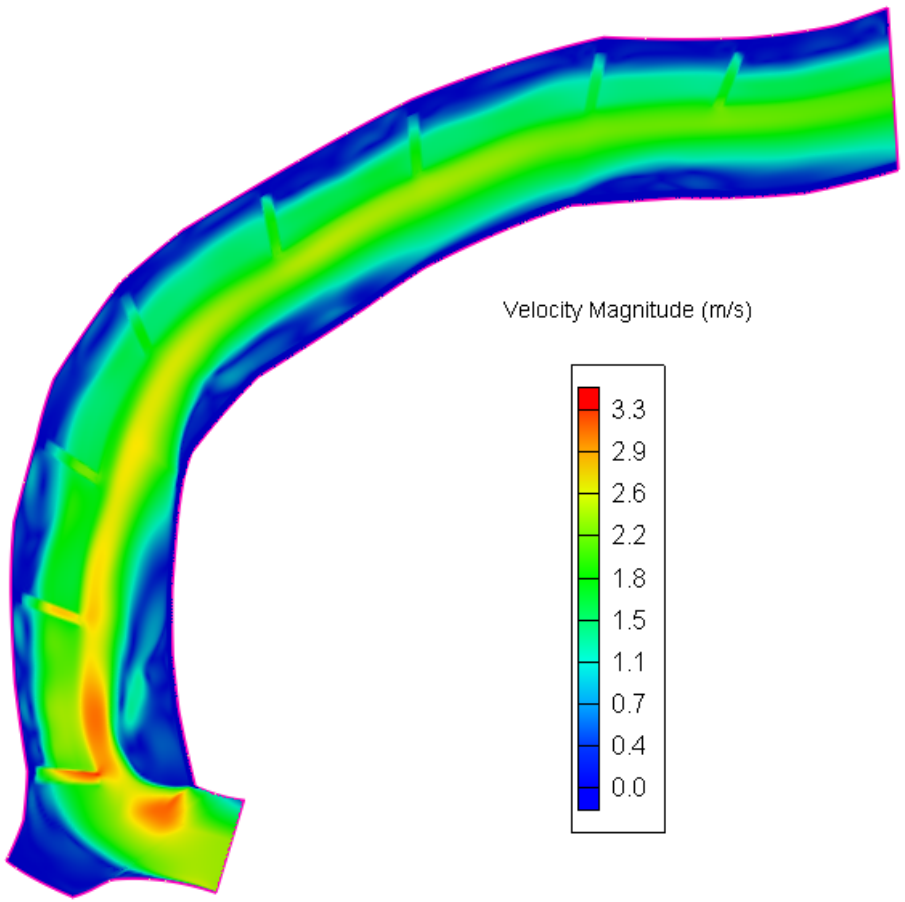


As built

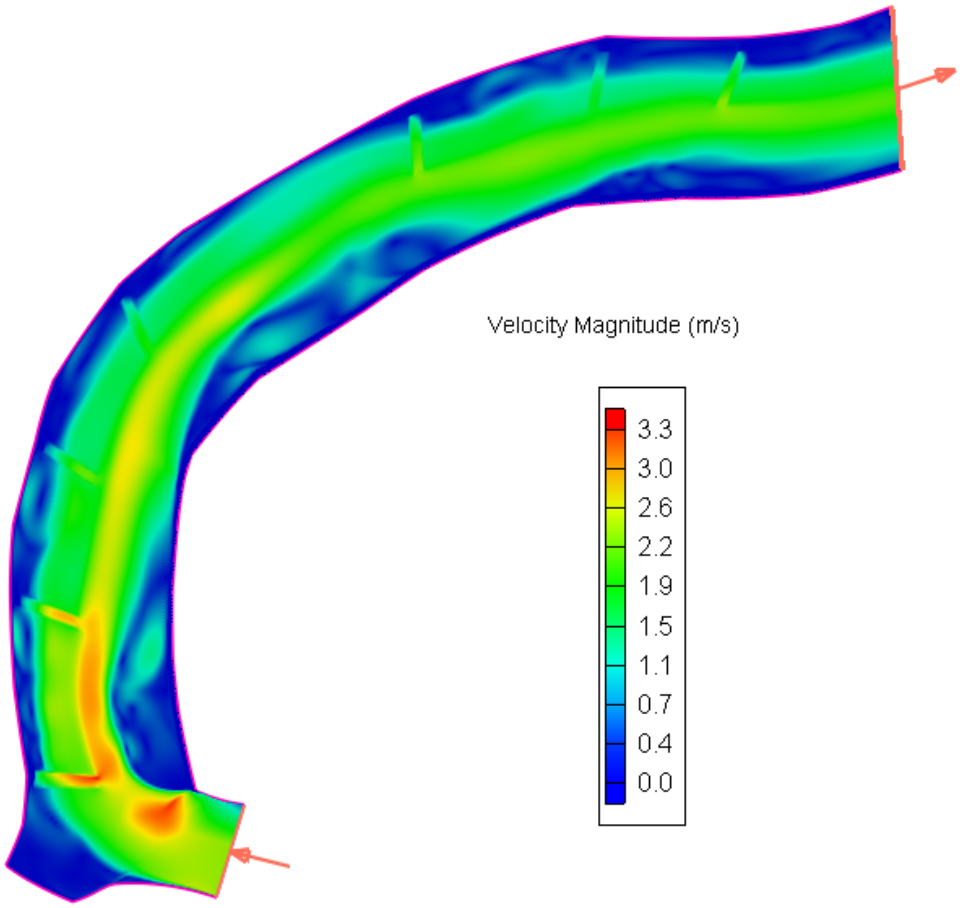


7 Barbs (no 5th barb)

# Total Specific Discharge (m^2/s)

## Discharge: 300 m^3/s, Initial Water Height: 3.3 m

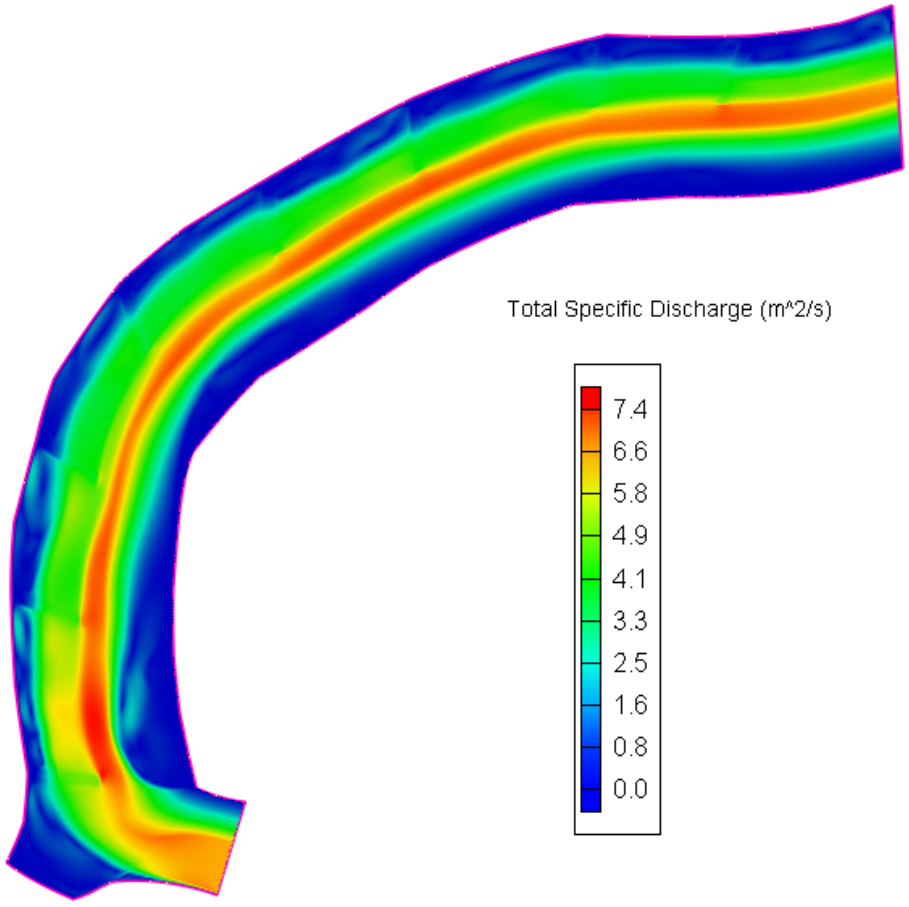


As built

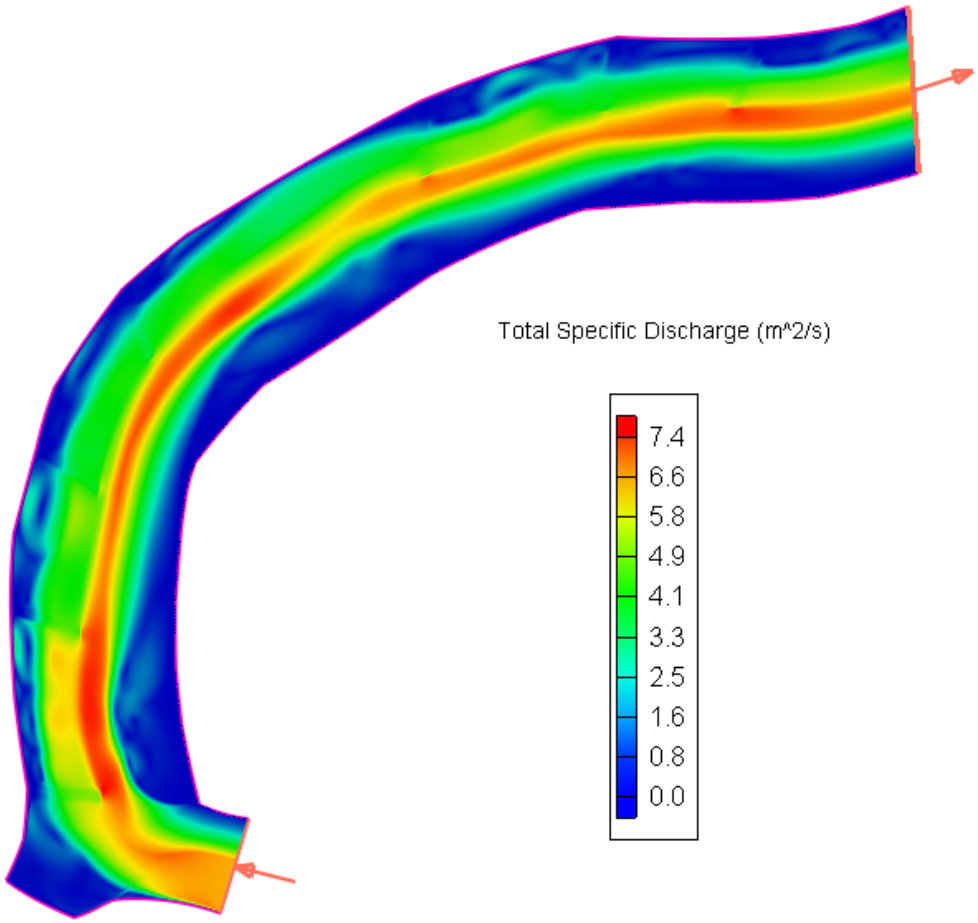


7 Barbs (no 5st barb)

# Froude Number
## Discharge: 300 m^3/s, Initial Water Height: 3.3 m

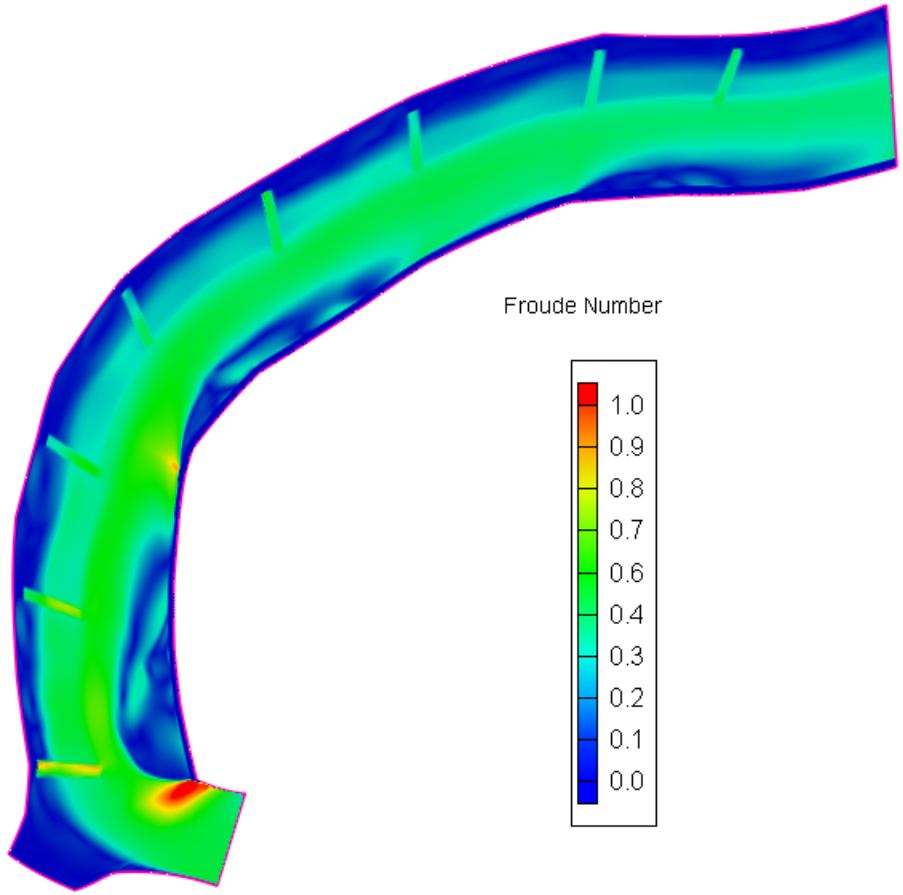


As built

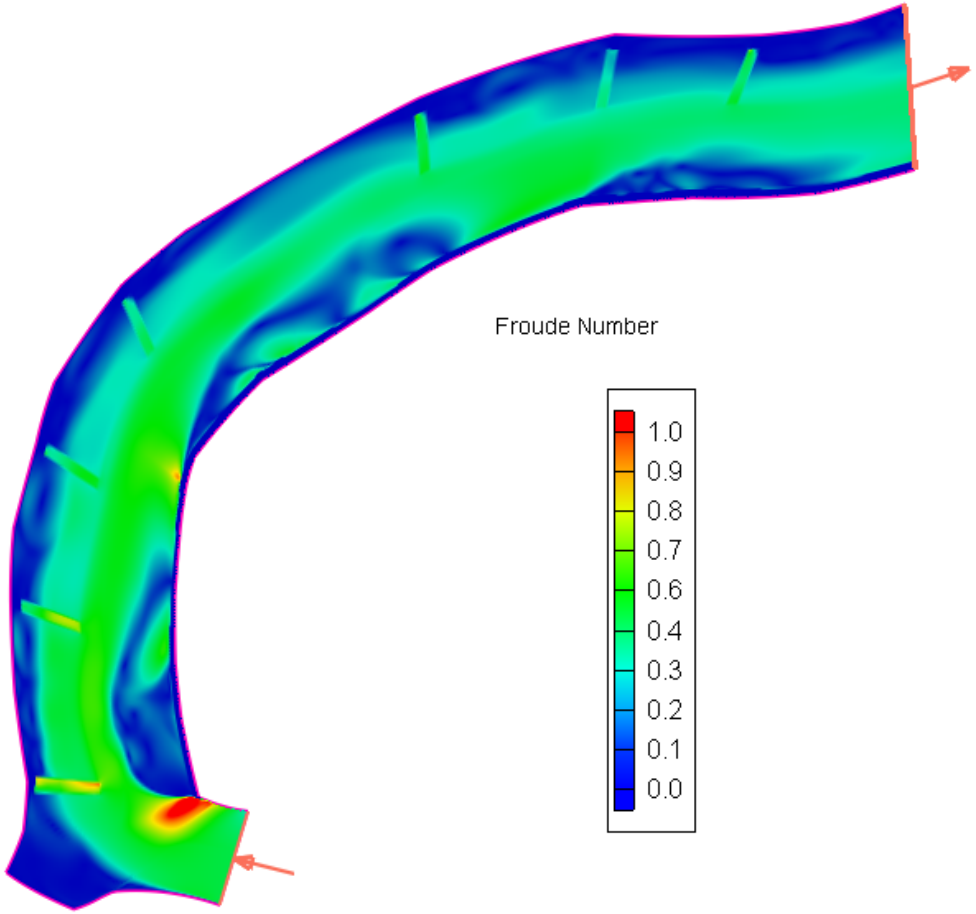


7 Barbs (no 5th barb)

# Total Shear Stress (N/m^2)
# Discharge: 300 m^3/s, Initial Water Height: 3.3 m

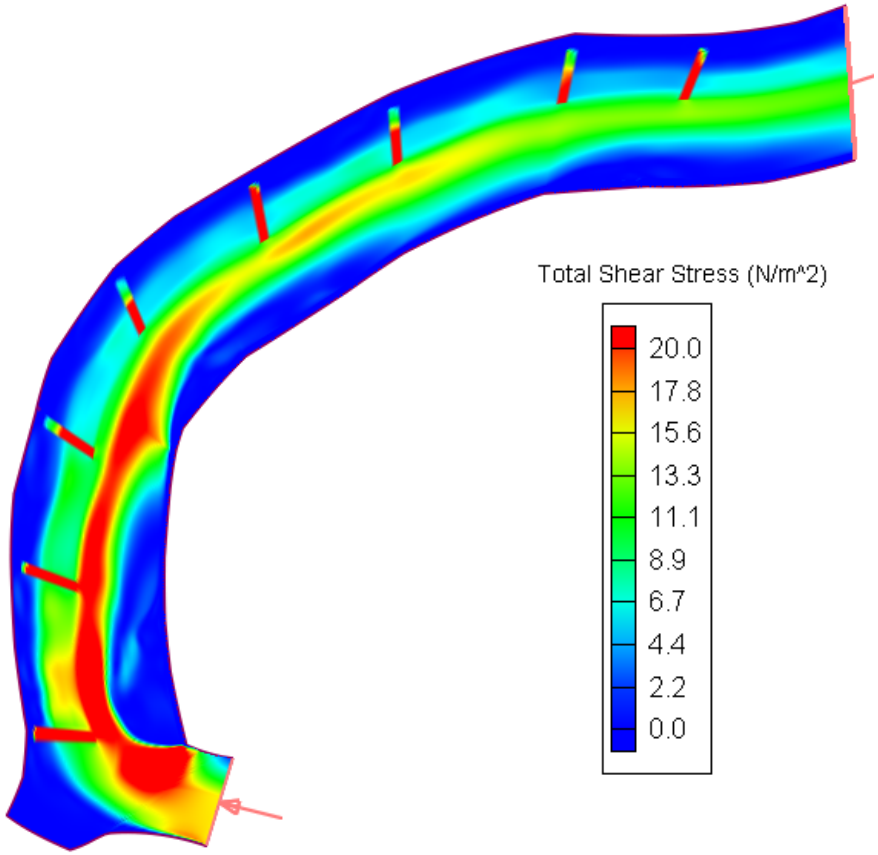


As built

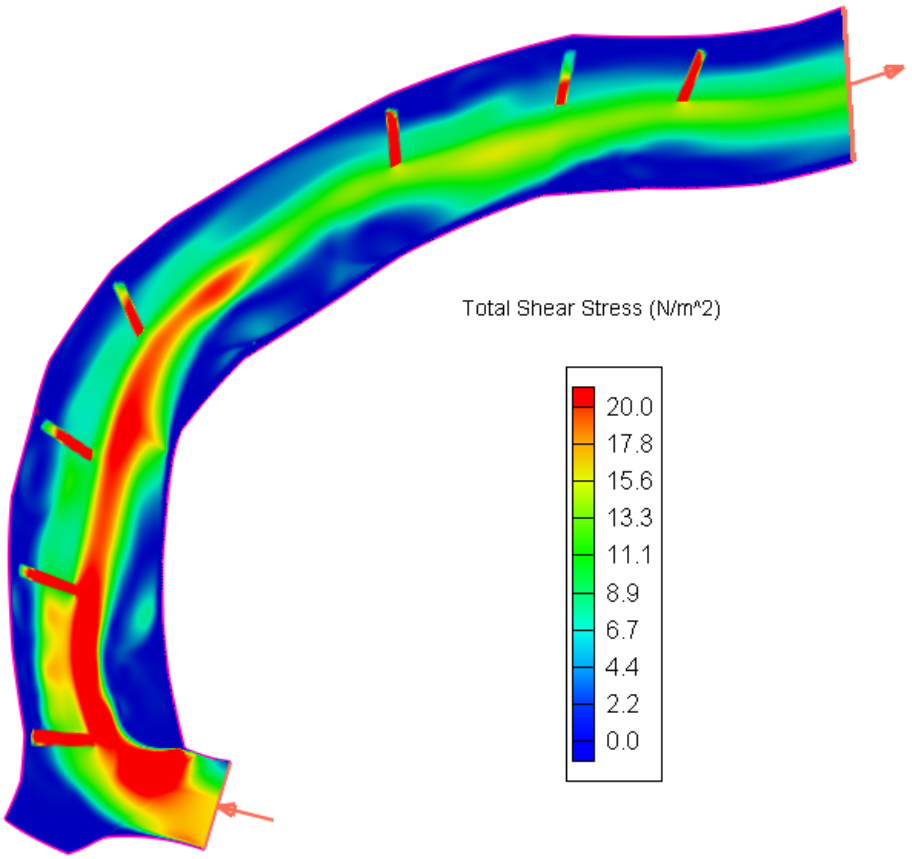


7 Barbs (no 5th barb)

Bed sediment transport is initiated
when Total Shear Stress > 19 N/m^2

# 7 Barbs - No 6th Barb

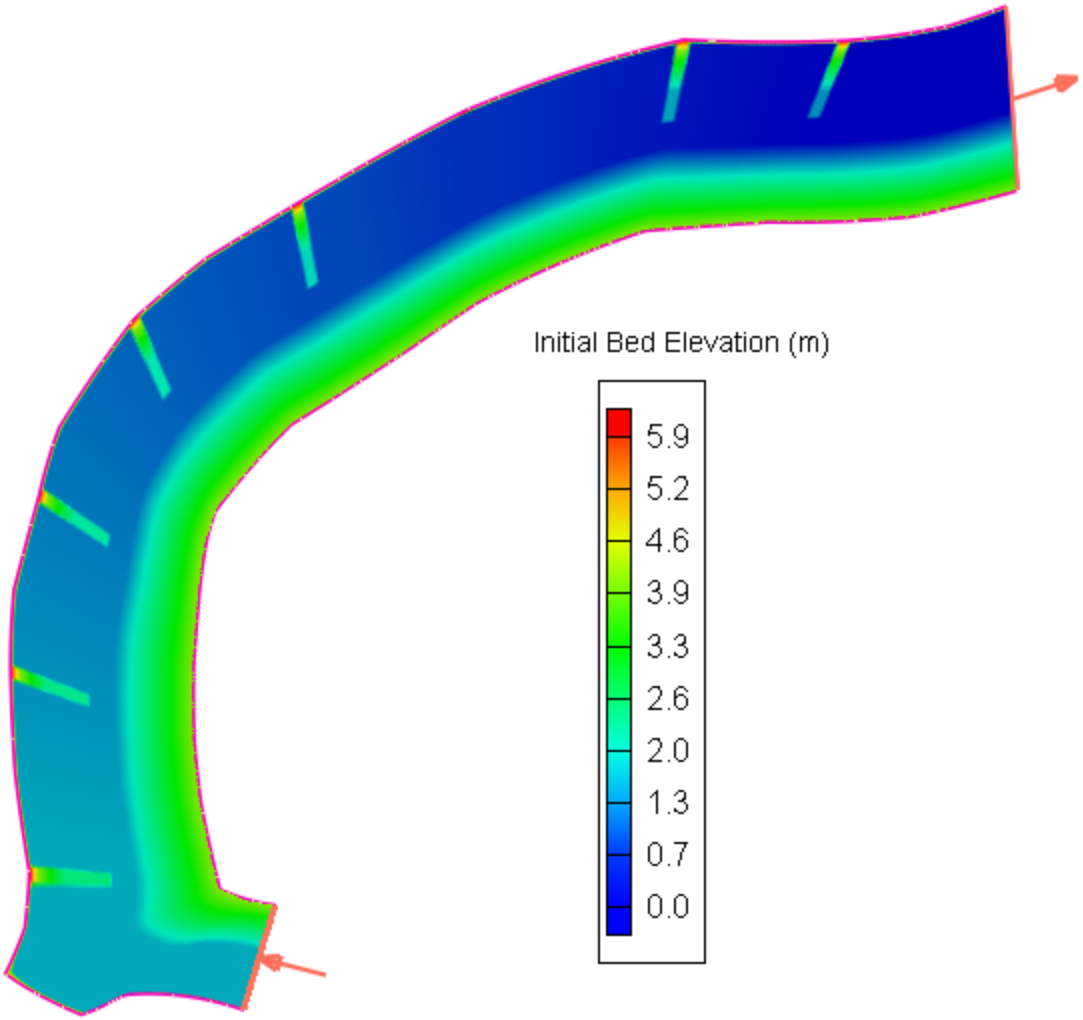

# Velocity Magnitude (m/s)

## Discharge: 300 m^3/s, Initial Water Height: 3.3 m

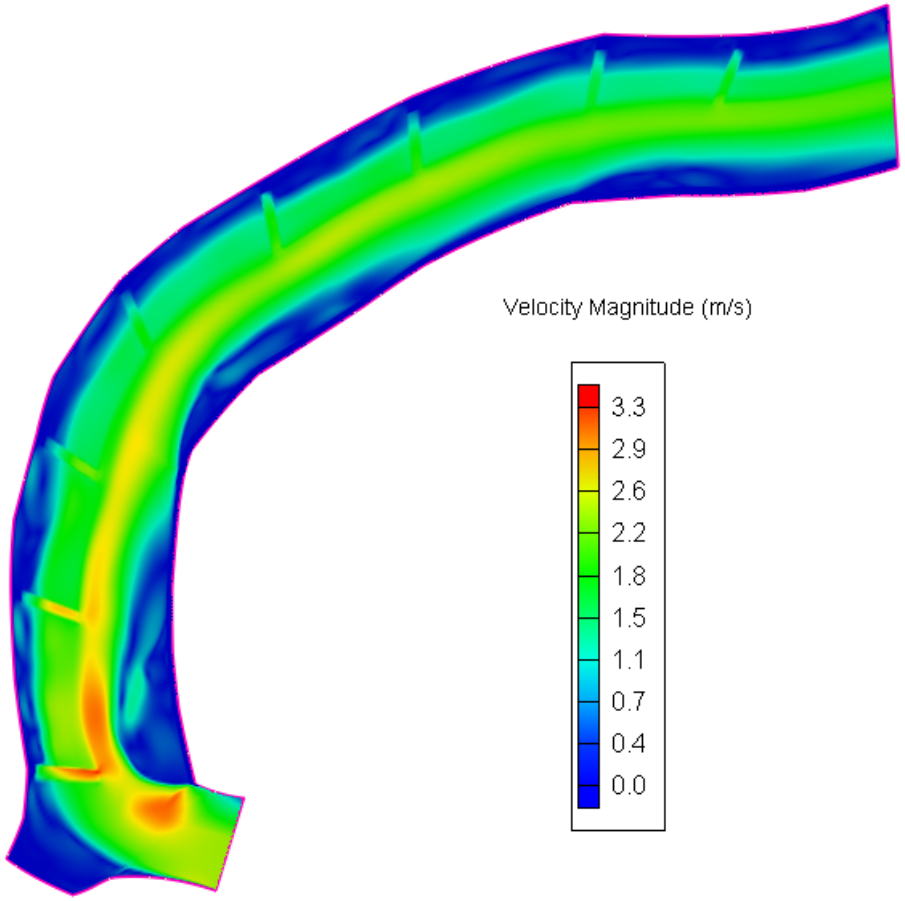


As built

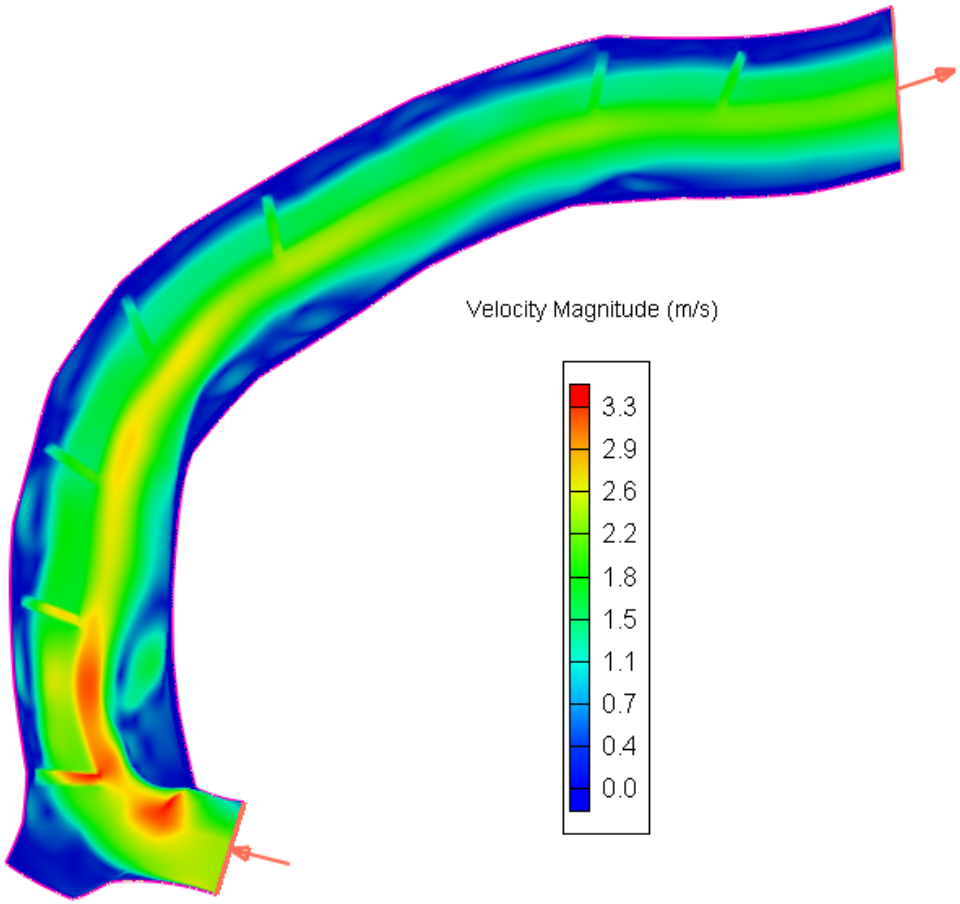


7 Barbs (no 6th barb)

# Total Specific Discharge (m^2/s)

## Discharge: 300 m^3/s, Initial Water Height: 3.3 m

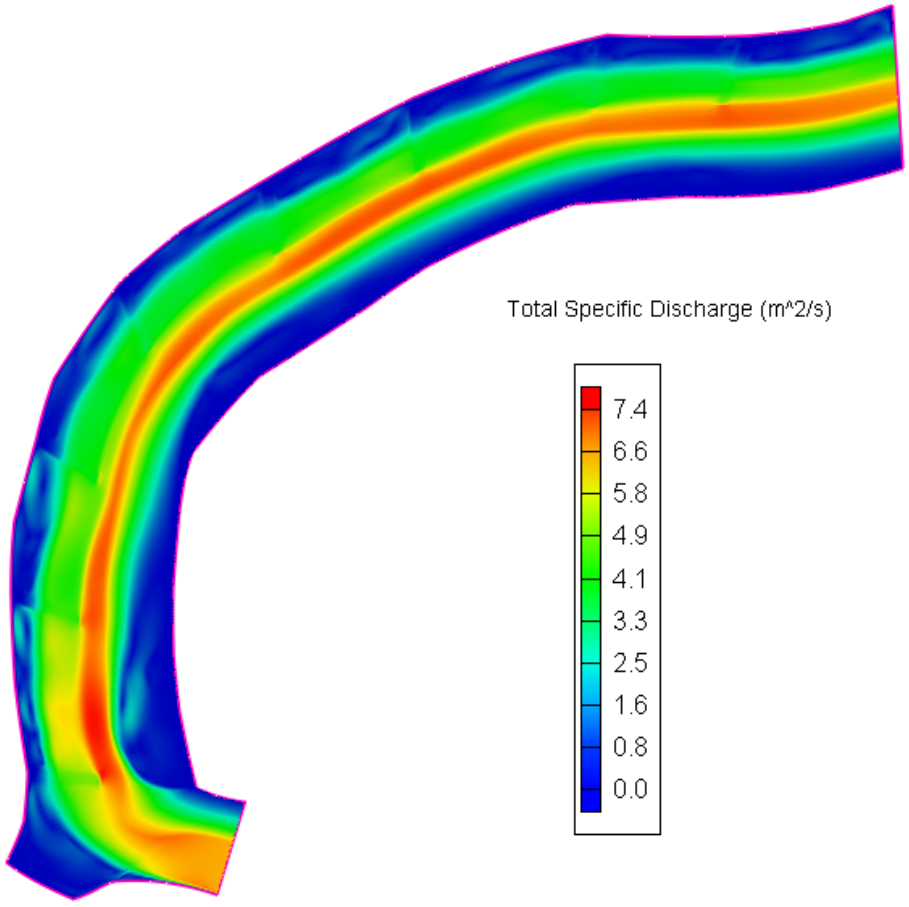


As built

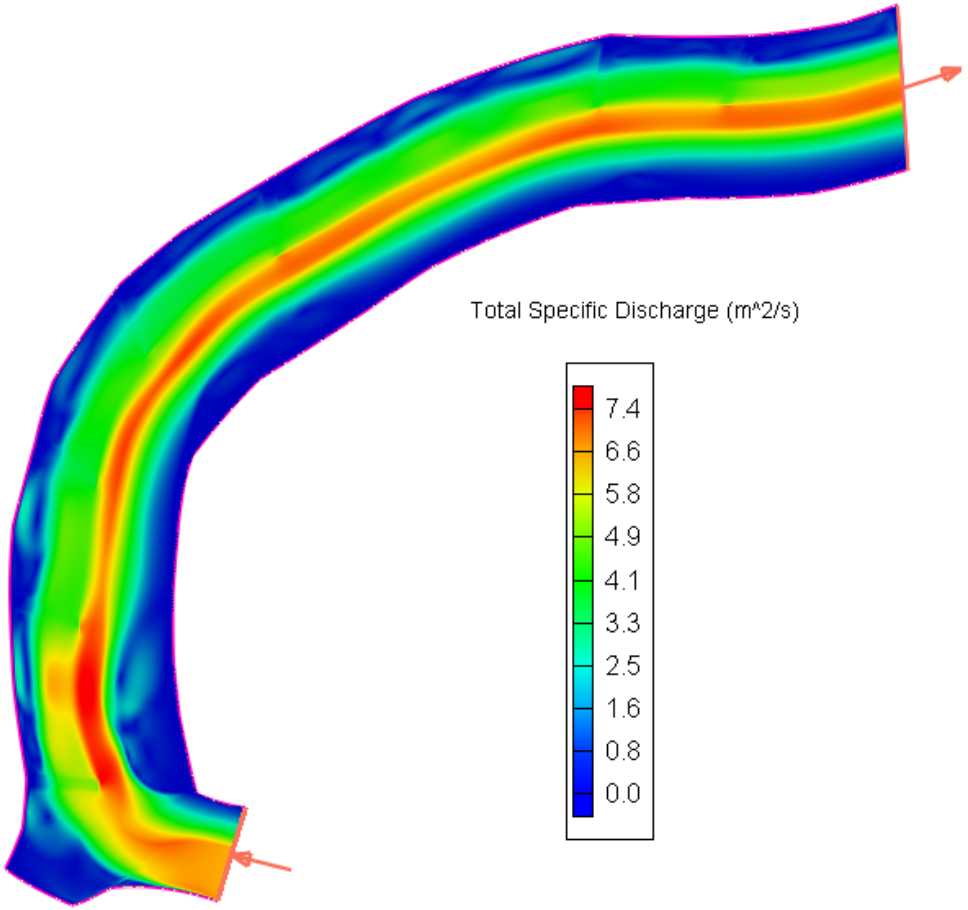


7 Barbs (no 6th barb)

# Froude Number
## Discharge: 300 m^3/s, Initial Water Height: 3.3 m

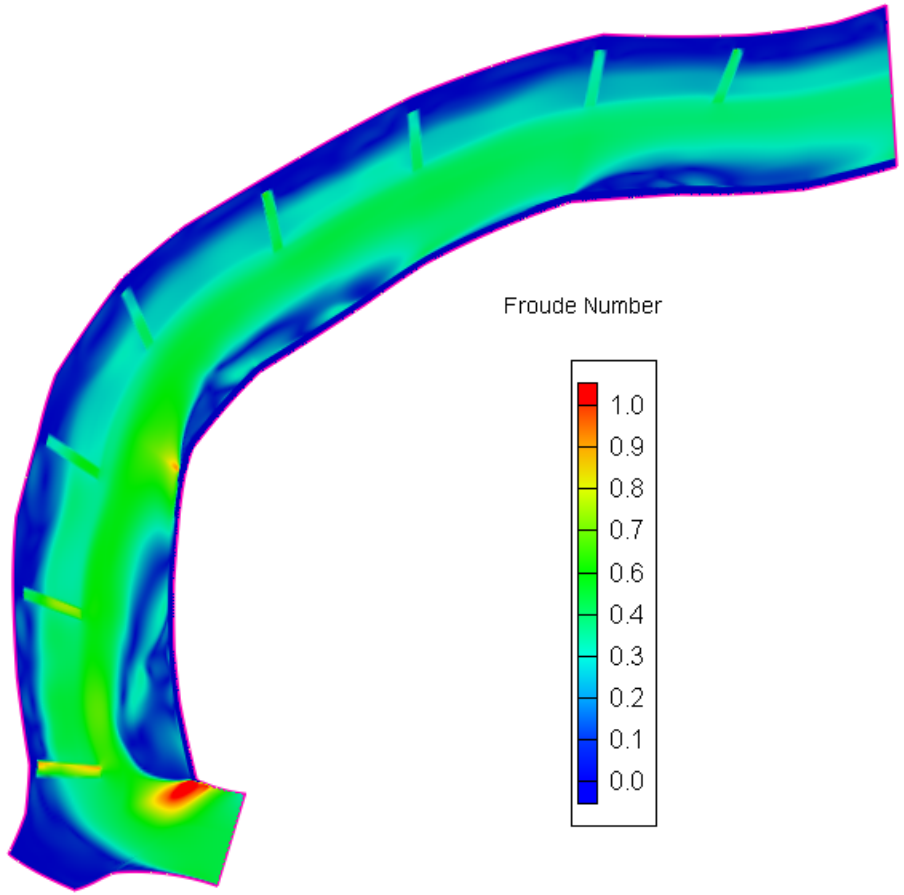


As built

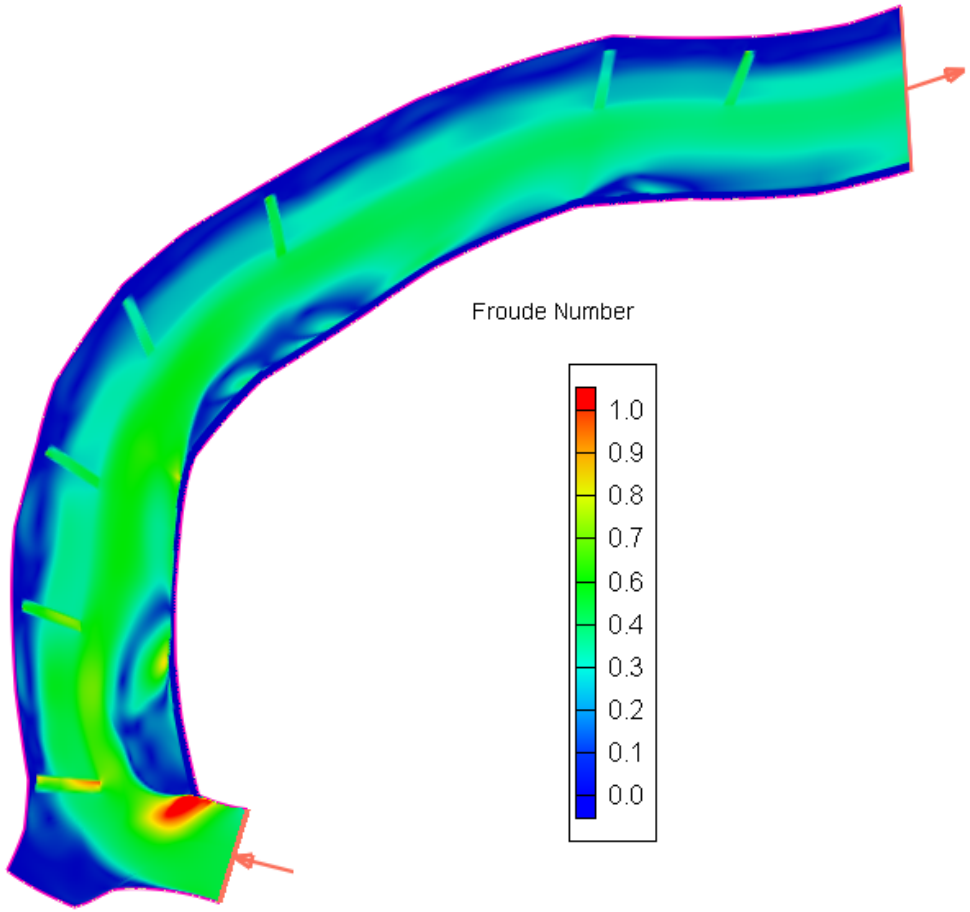


7 Barbs (no 6th barb)

# Total Shear Stress (N/m^2)
# Discharge: 300 m^3/s, Initial Water Height: 3.3 m

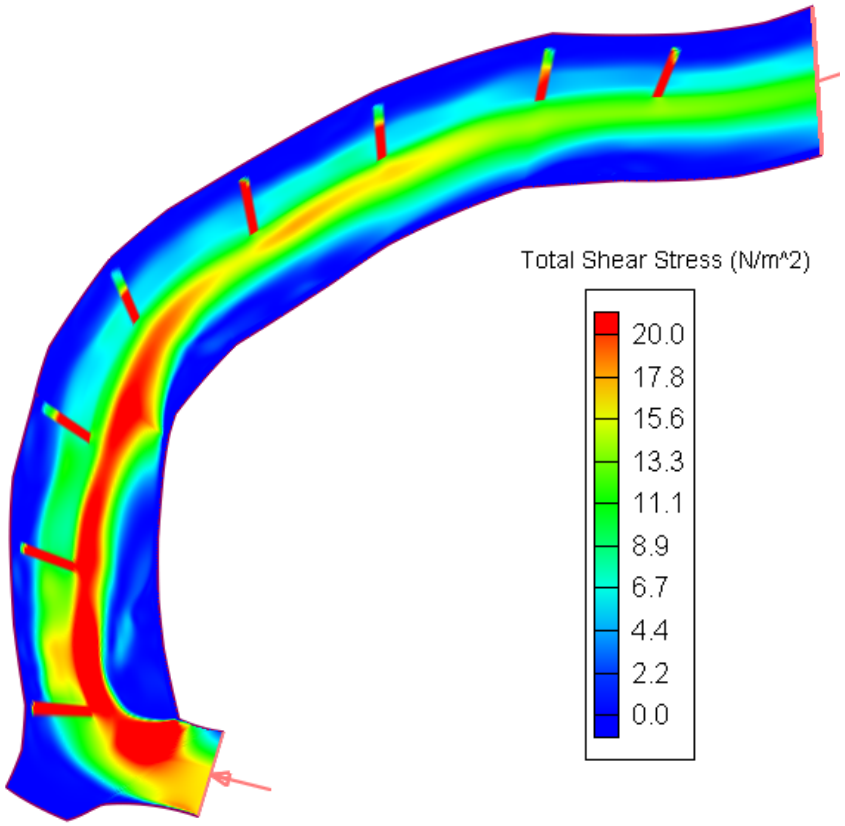


As built

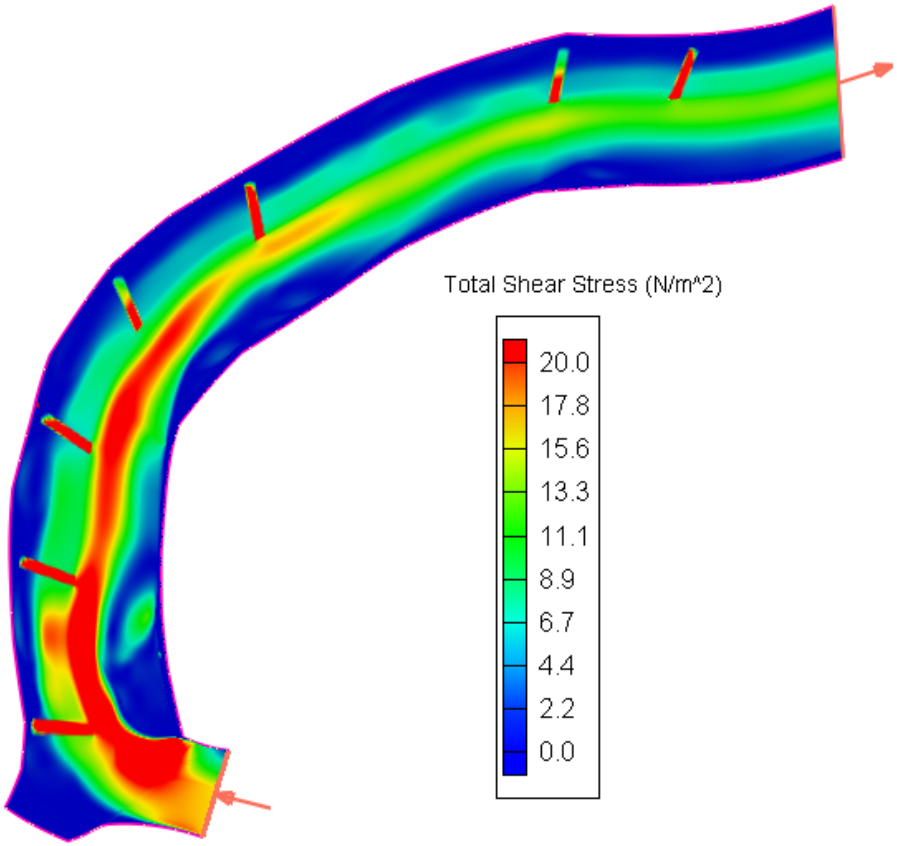


7 Barbs (no 6th barb)

Bed sediment transport is initiated
when Total Shear Stress > 19 N/m^2

# 7 Barbs - No 7th Barb

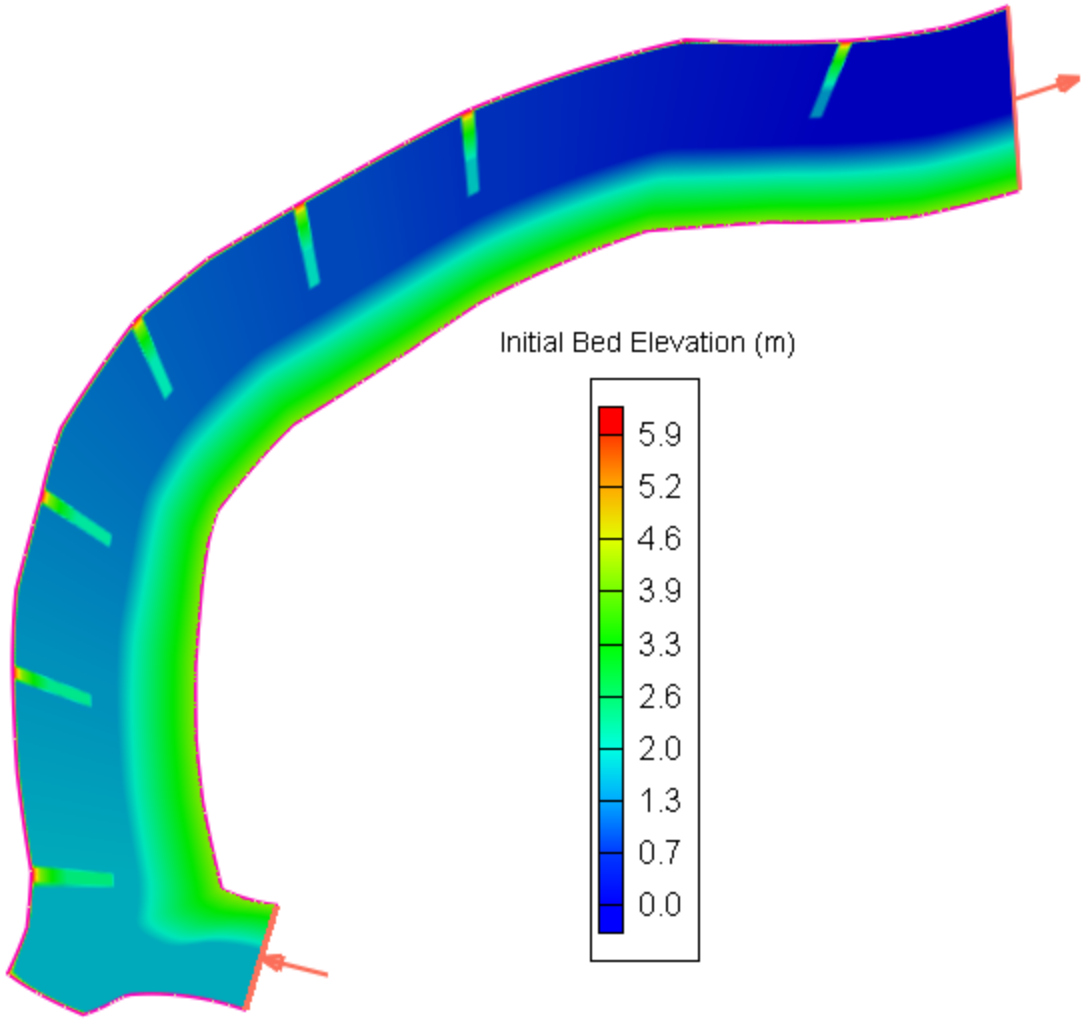

# Velocity Magnitude (m/s)

## Discharge: 300 m^3/s, Initial Water Height: 3.3 m

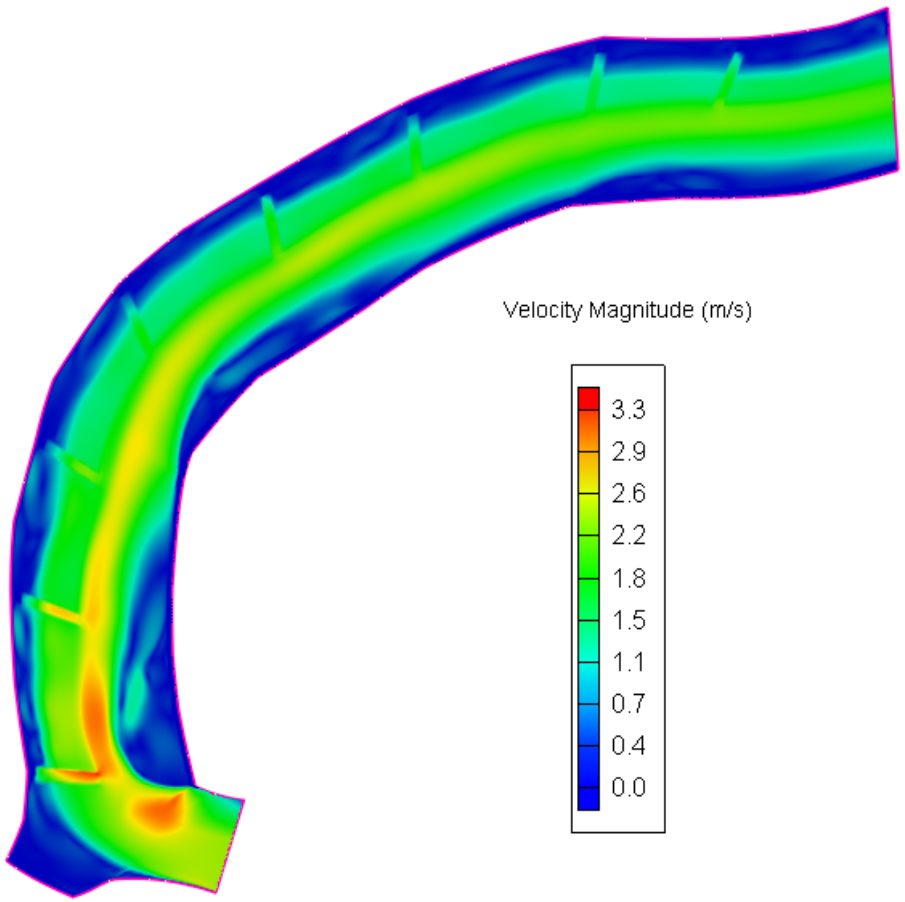


As built

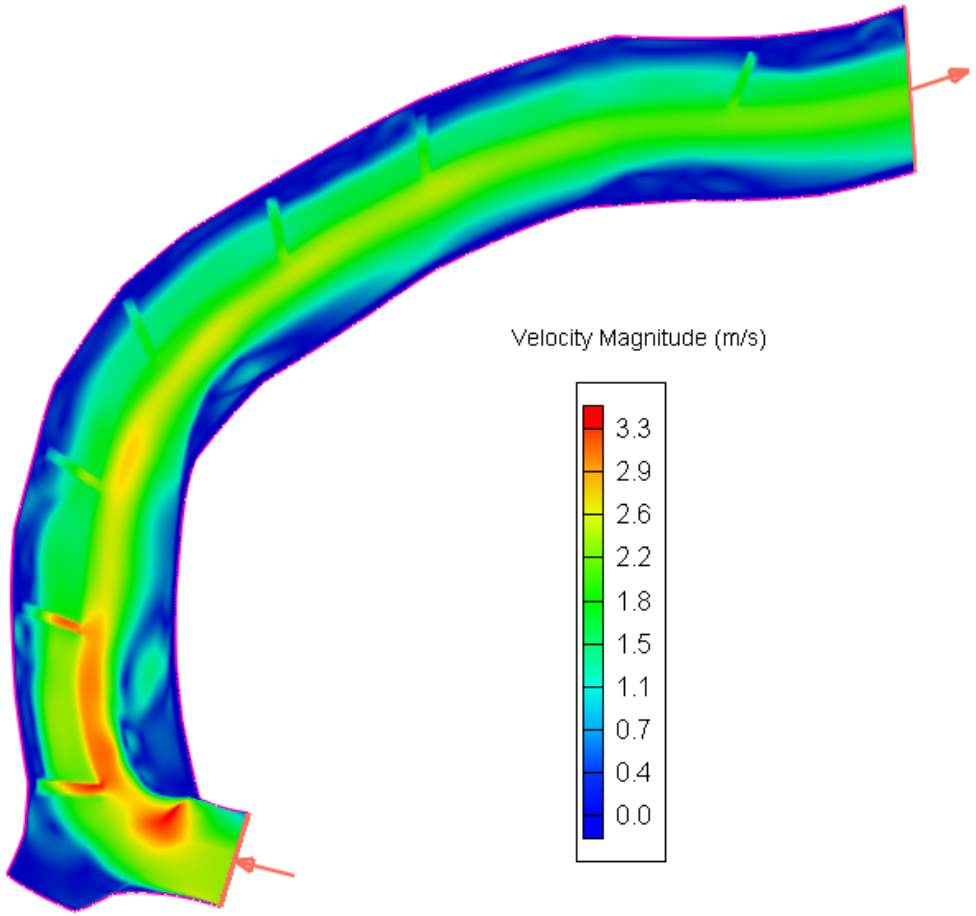


7 Barbs (no 7th barb)

# Total Specific Discharge (m^2/s)

## Discharge: 300 m^3/s, Initial Water Height: 3.3 m

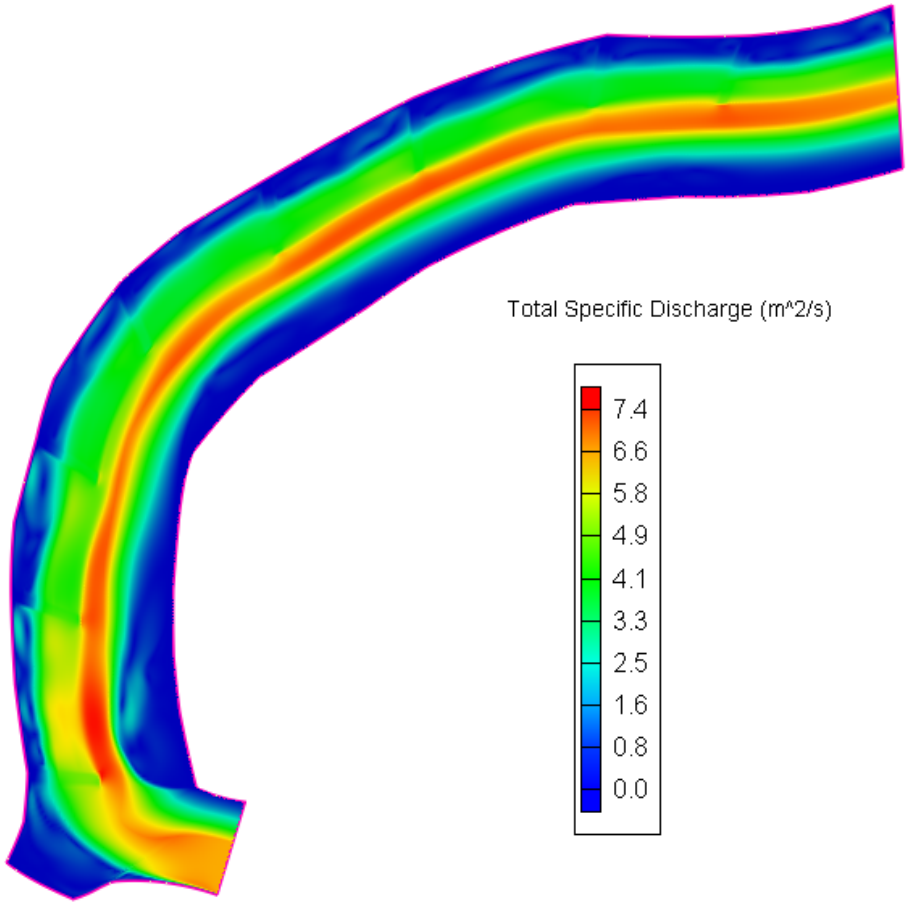


As built

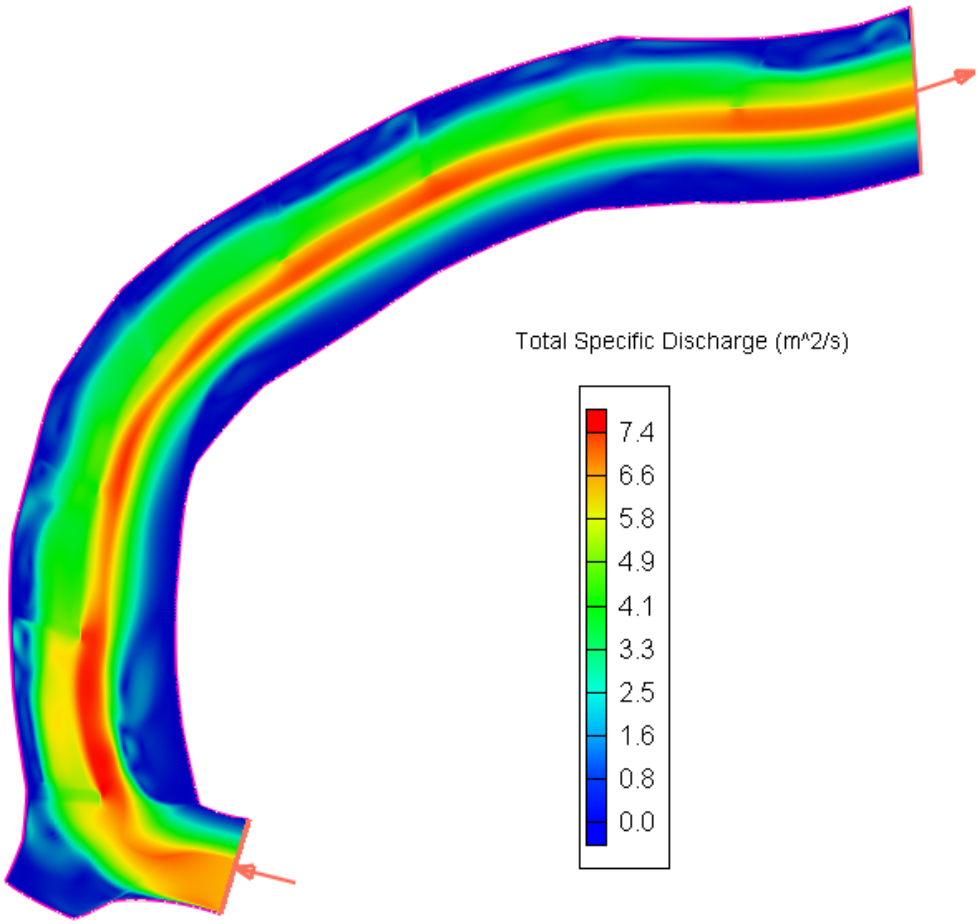


7 Barbs (no 7th barb)

# Froude Number
## Discharge: 300 m^3/s, Initial Water Height: 3.3 m

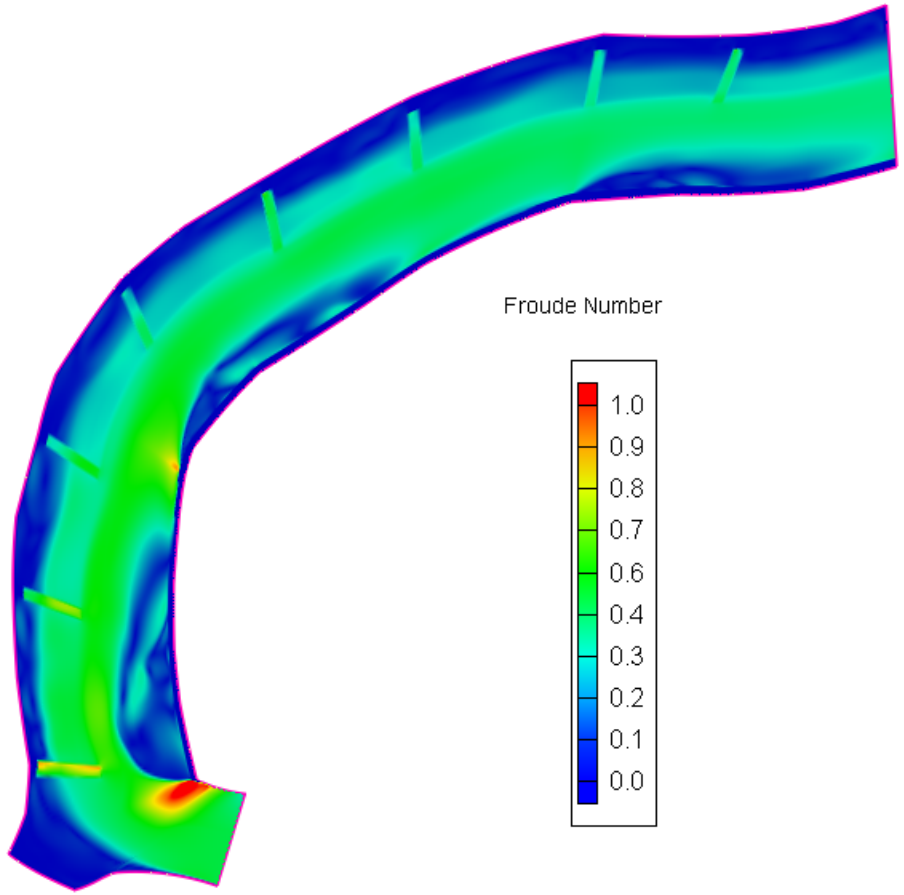


As built

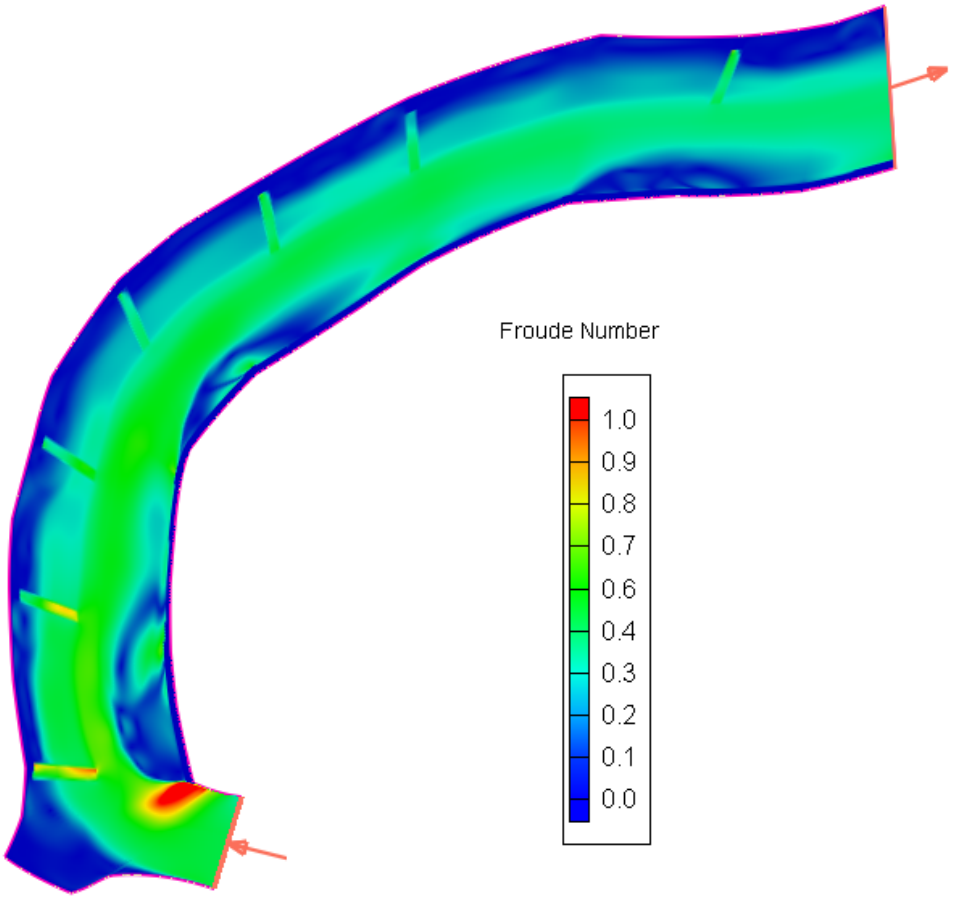


7 Barbs (no 7th barb)

# Total Shear Stress (N/m^2)
# Discharge: 300 m^3/s, Initial Water Height: 3.3 m

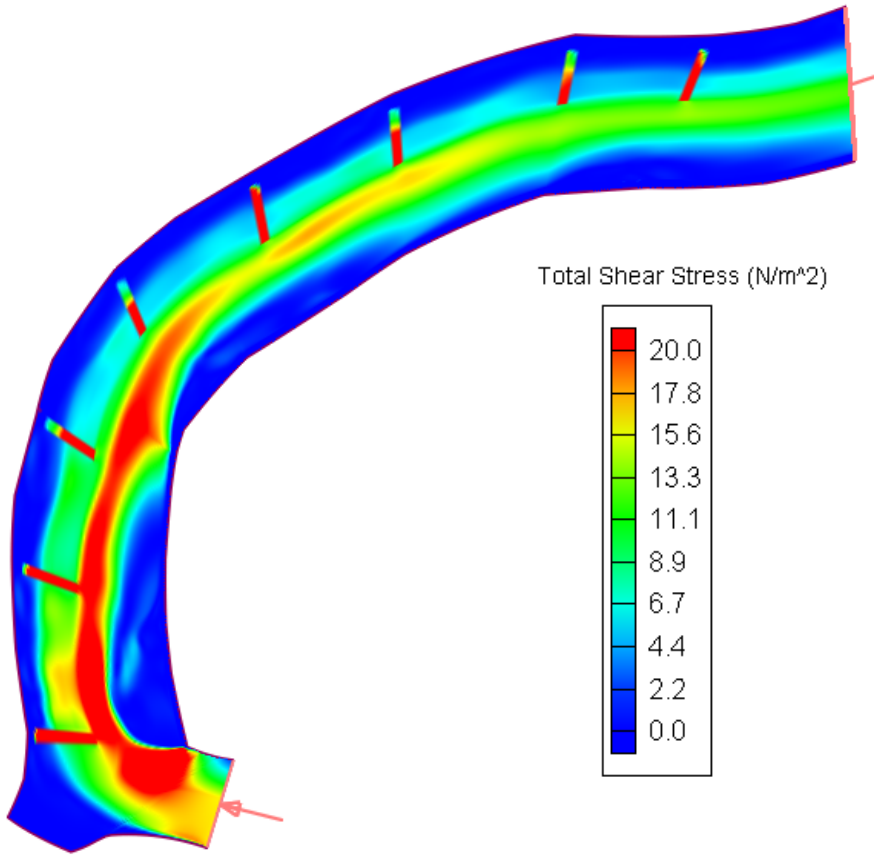


As built

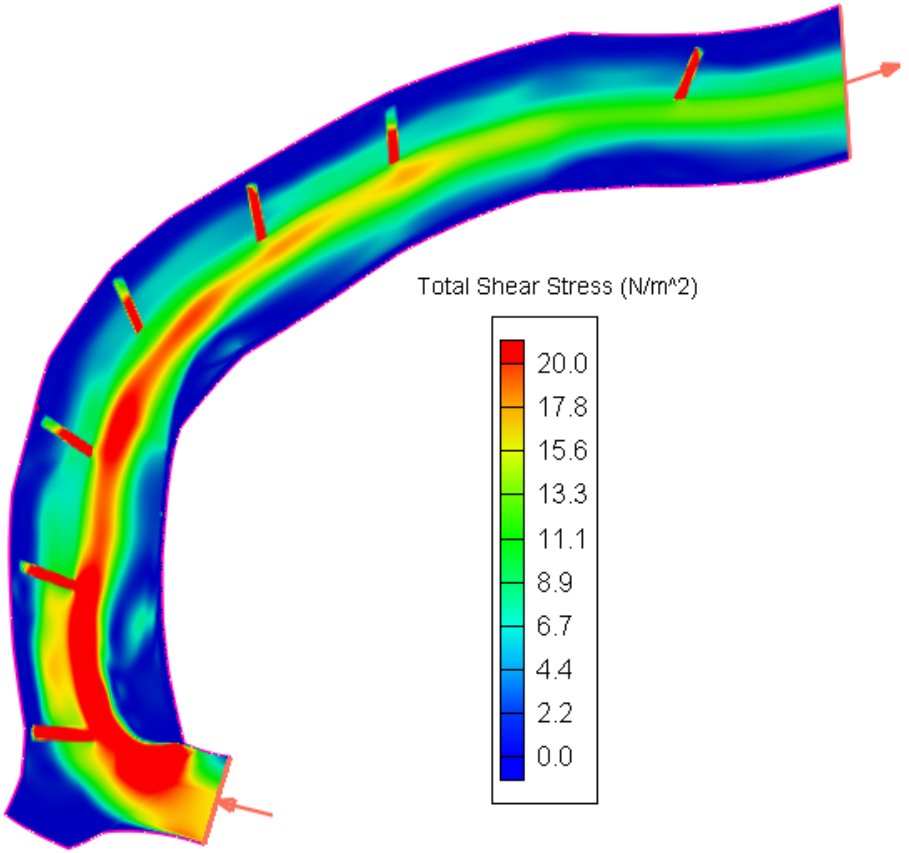


7 Barbs (no 7th barb)

Bed sediment transport is initiated
when Total Shear Stress > 19 N/m^2

# 7 Barbs - No 8th Barb

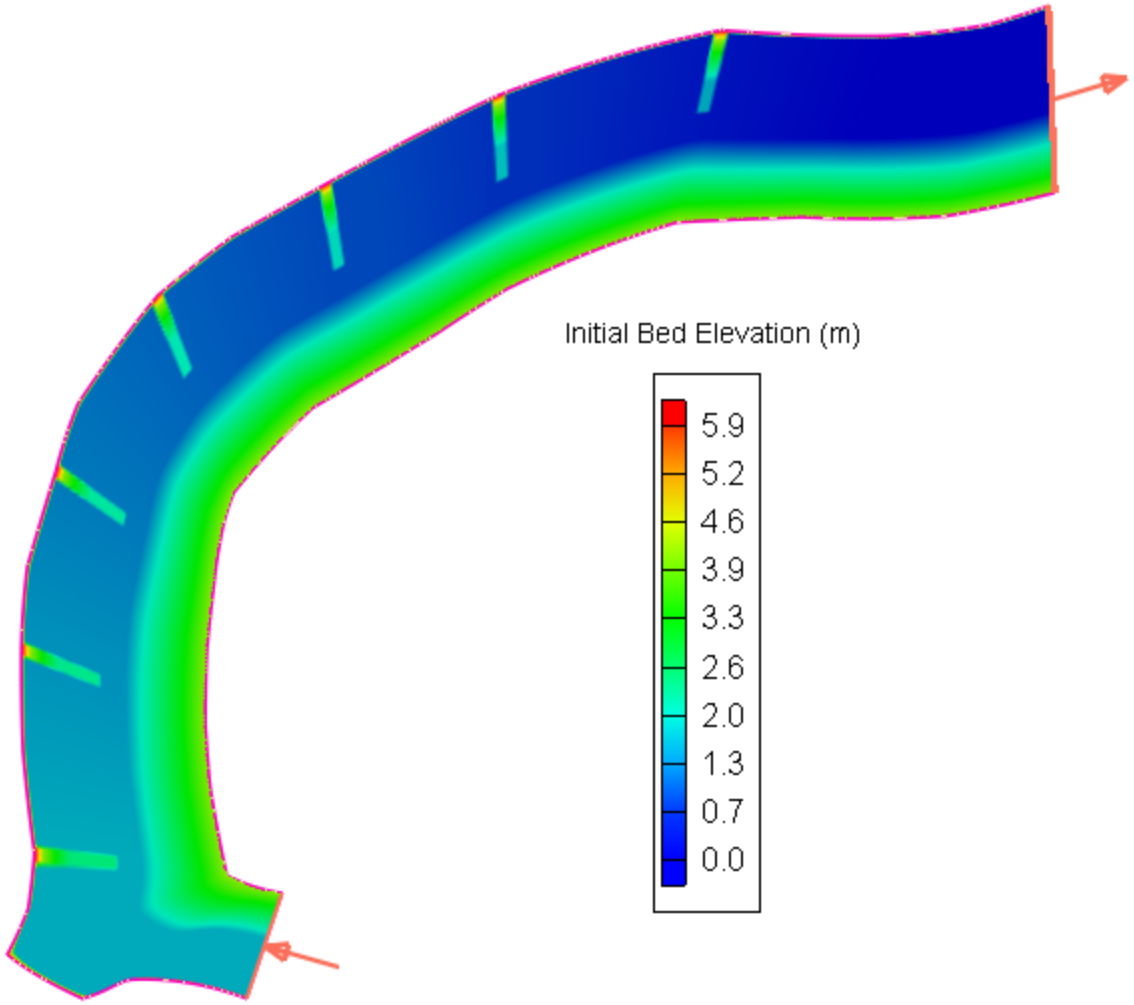

# Velocity Magnitude (m/s)

## Discharge: 300 m^3/s, Initial Water Height: 3.3 m

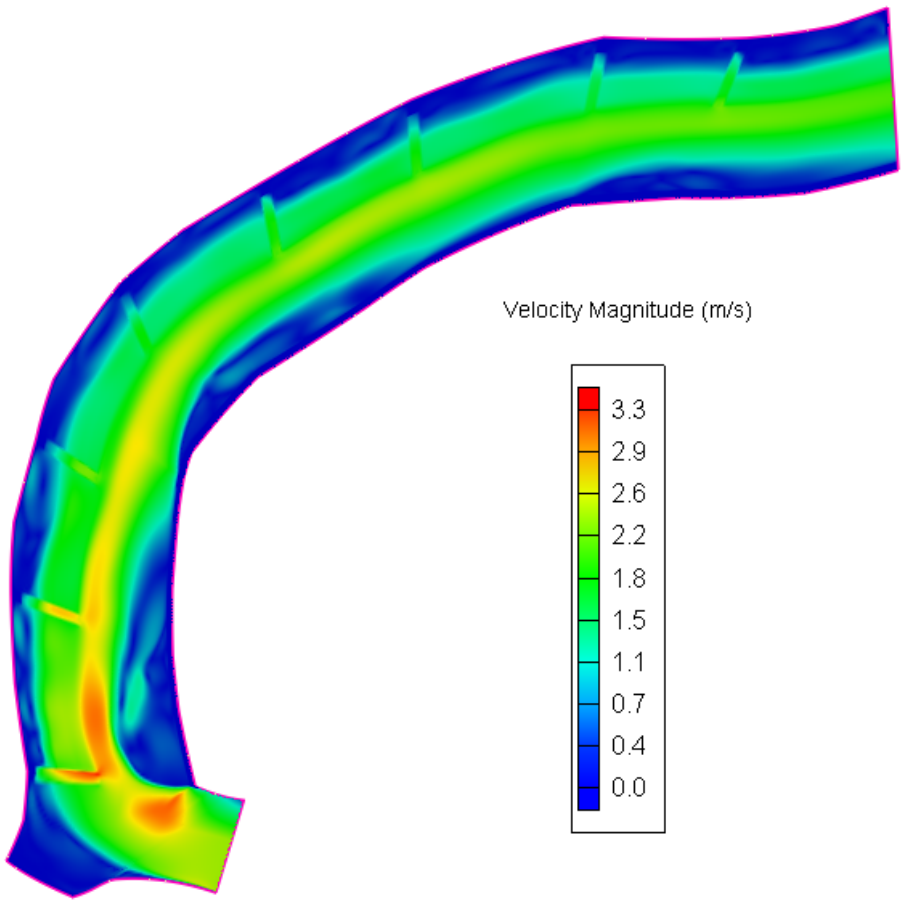


As built

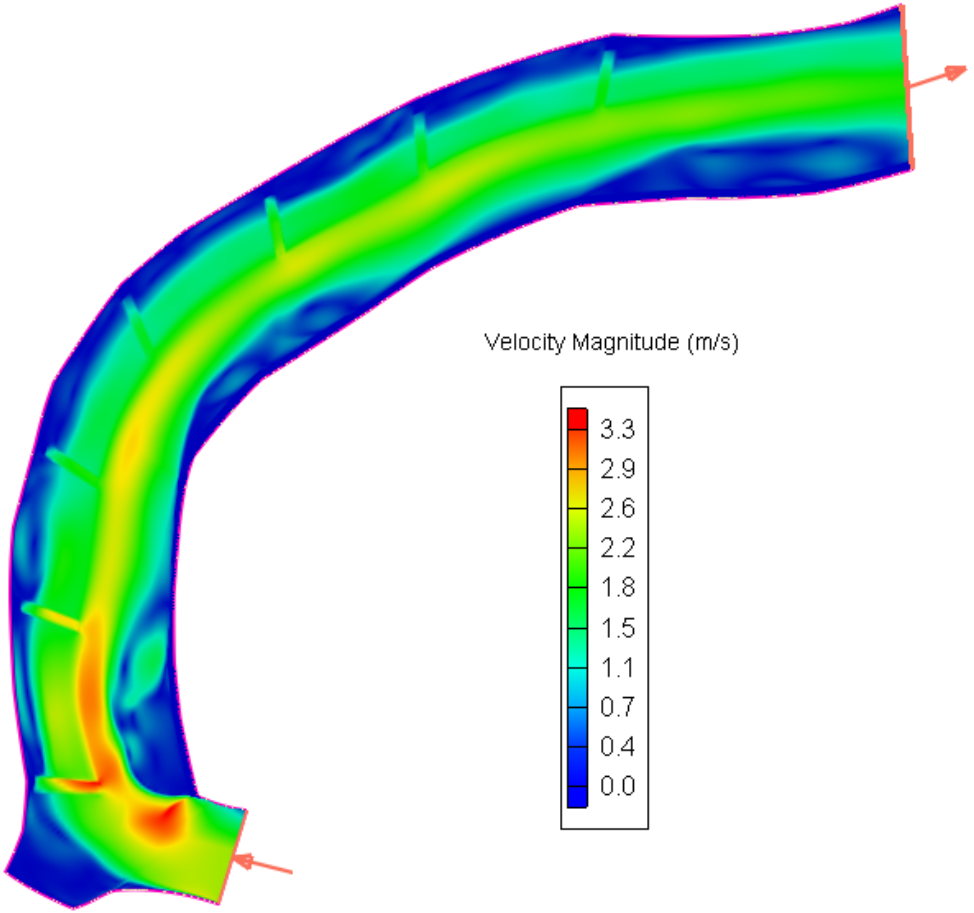


7 Barbs (no 8th barb)

# Total Specific Discharge (m^2/s)

## Discharge: 300 m^3/s, Initial Water Height: 3.3 m

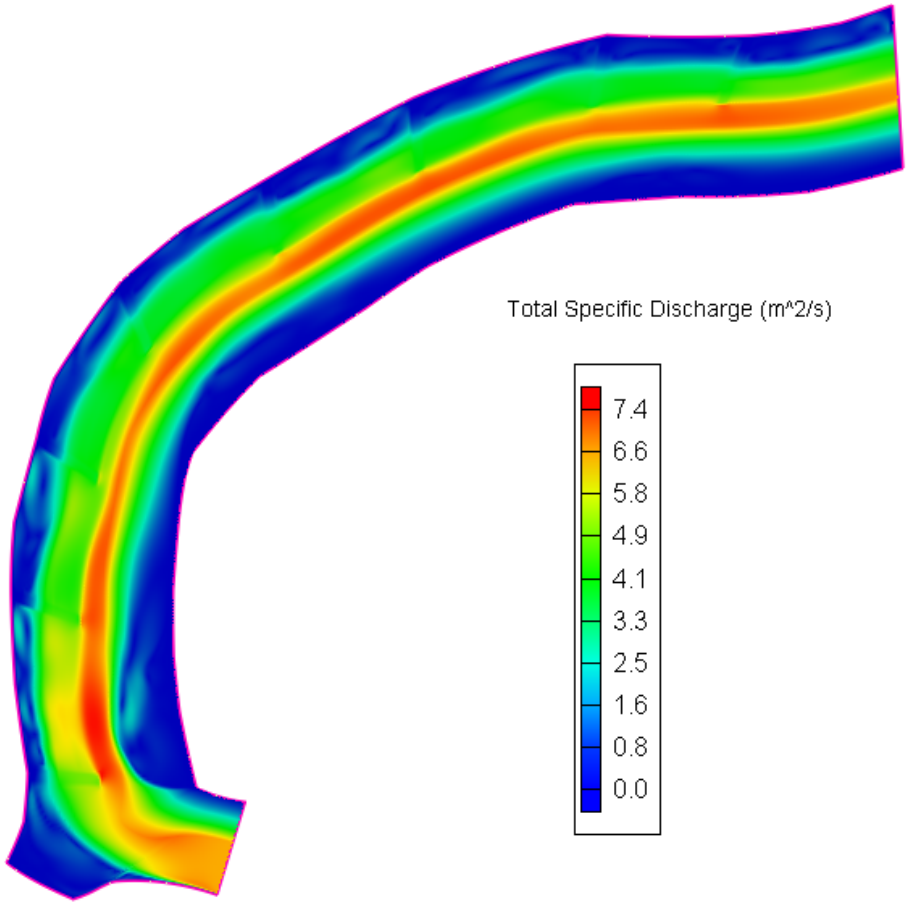


As built

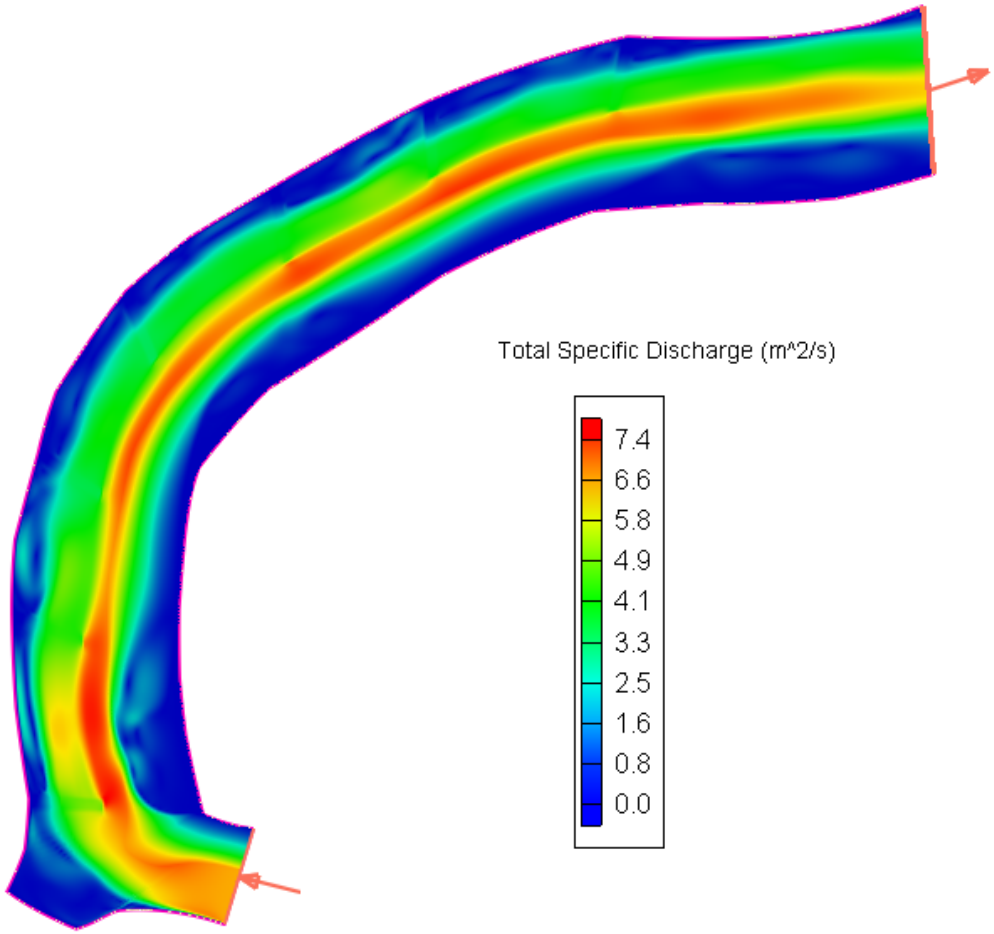


7 Barbs (no 8th barb)

# Froude Number
## Discharge: 300 m^3/s, Initial Water Height: 3.3 m

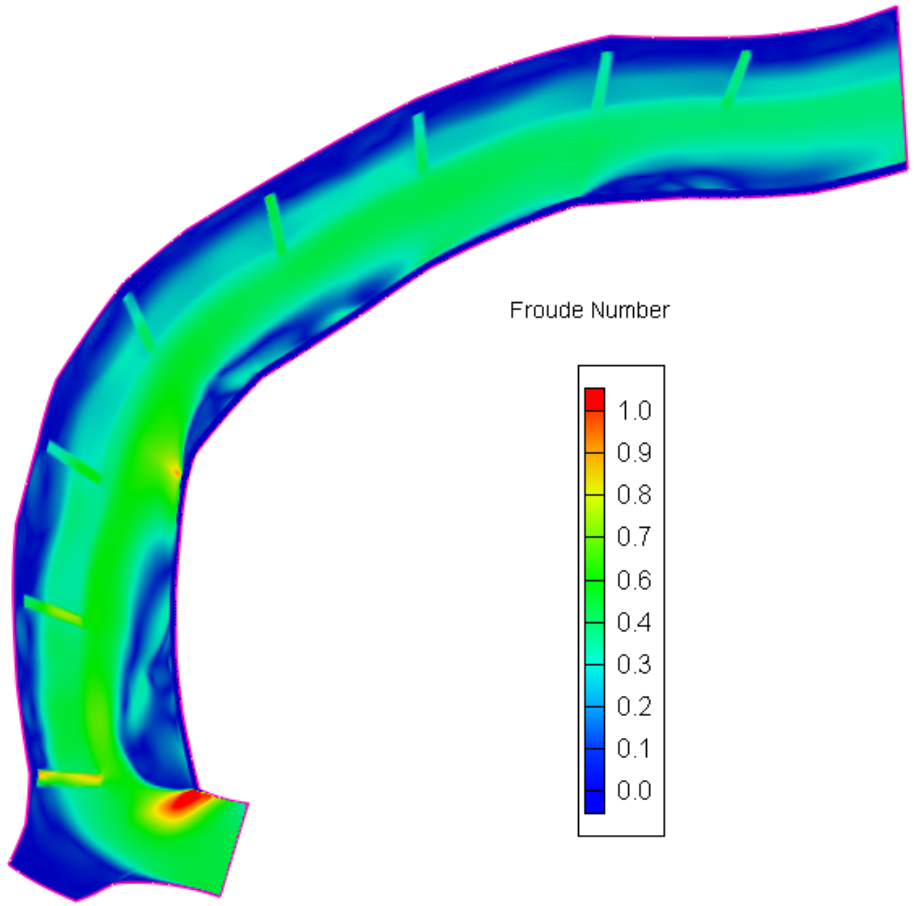


As built

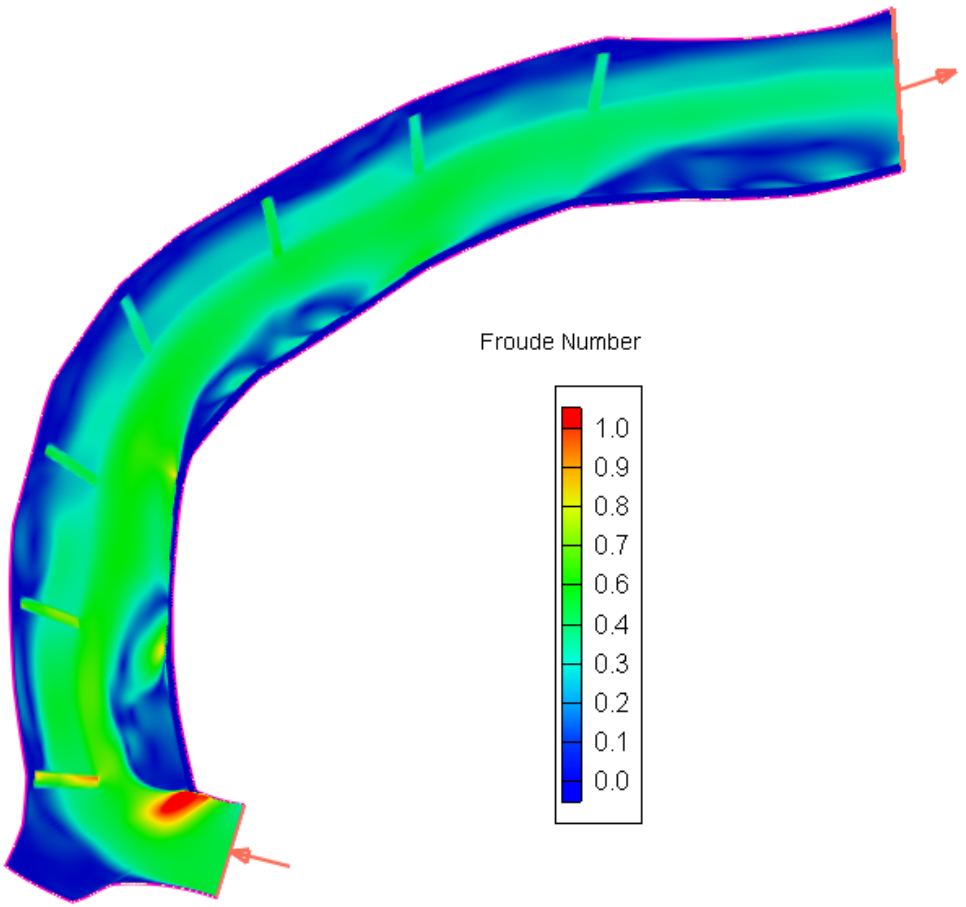


7 Barbs (no 8th barb)

# Total Shear Stress (N/m^2)
# Discharge: 300 m^3/s, Initial Water Height: 3.3 m

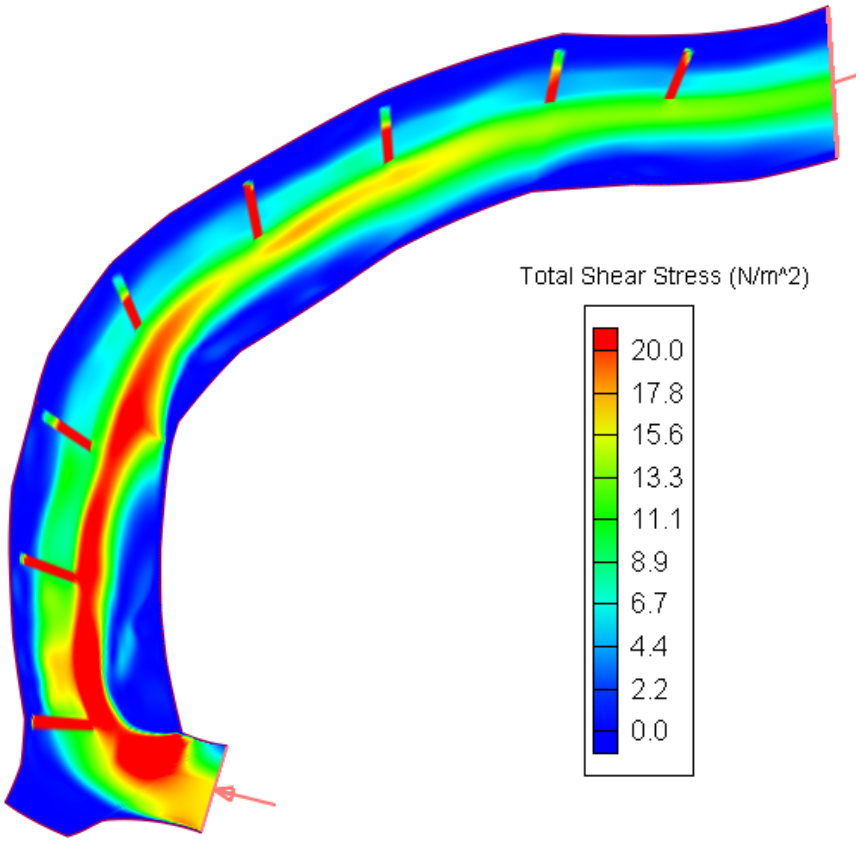


As built

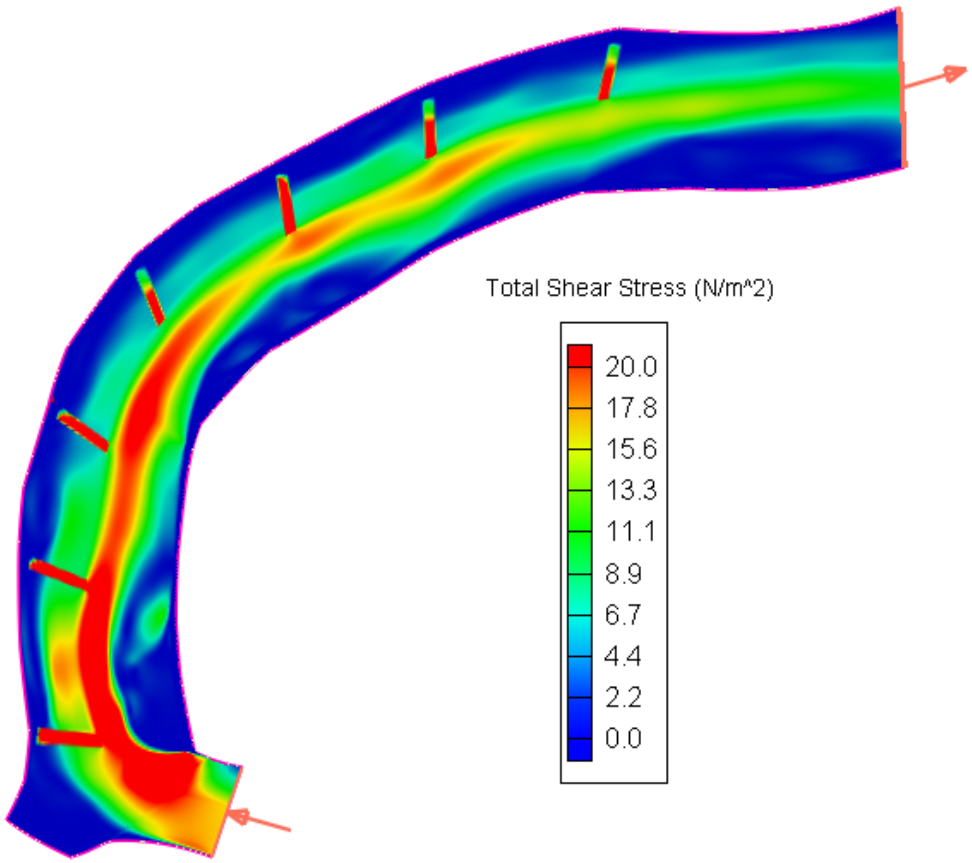


7 Barbs (no 8th barb)

Bed sediment transport is initiated
when Total Shear Stress > 19 N/m^2

# 4 Barbs - No 2nd, 4th, 6th, & 8th Barbs

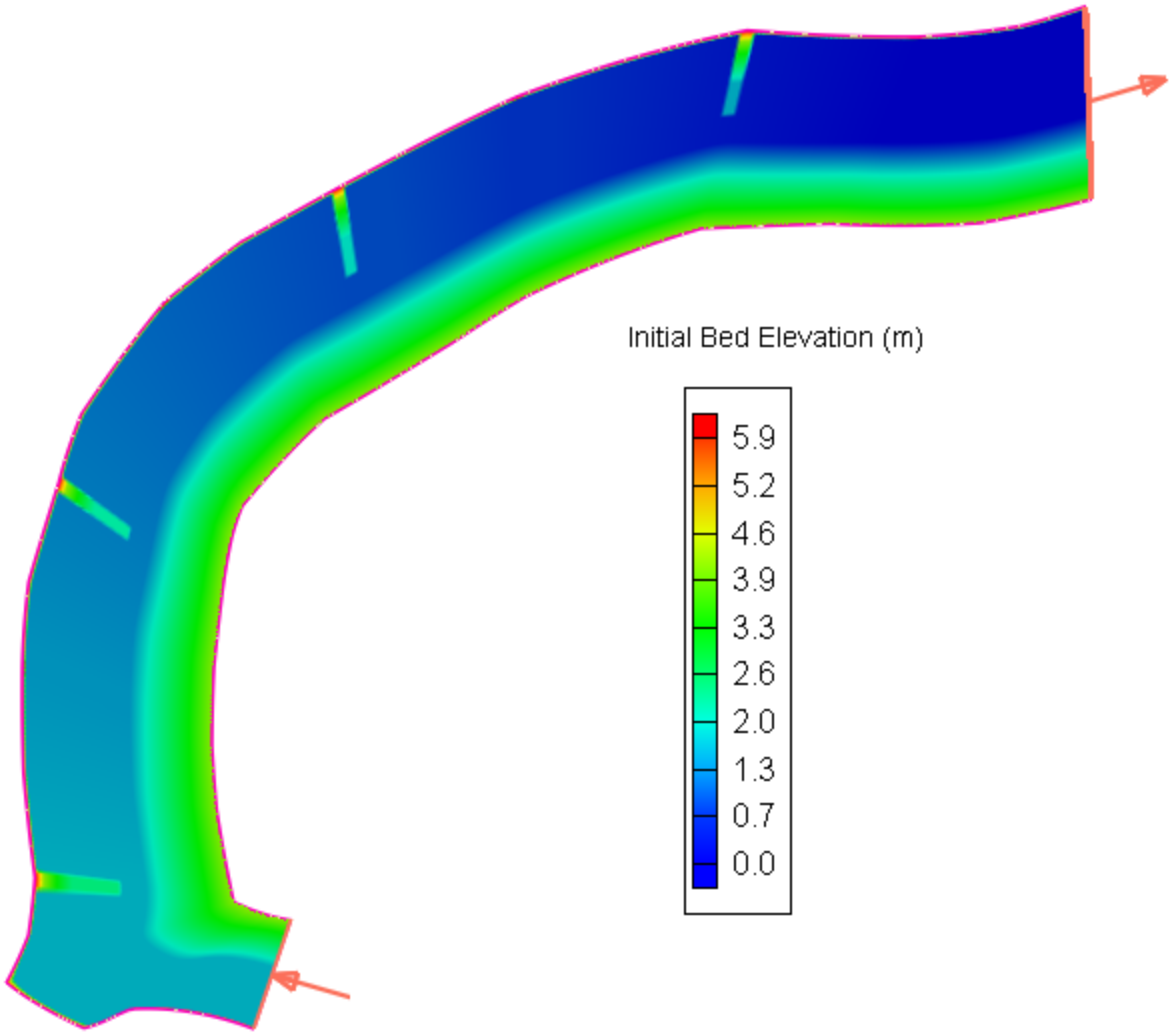

# Velocity Magnitude (m/s)

## Discharge: 300 m^3/s, Initial Water Height: 3.3 m

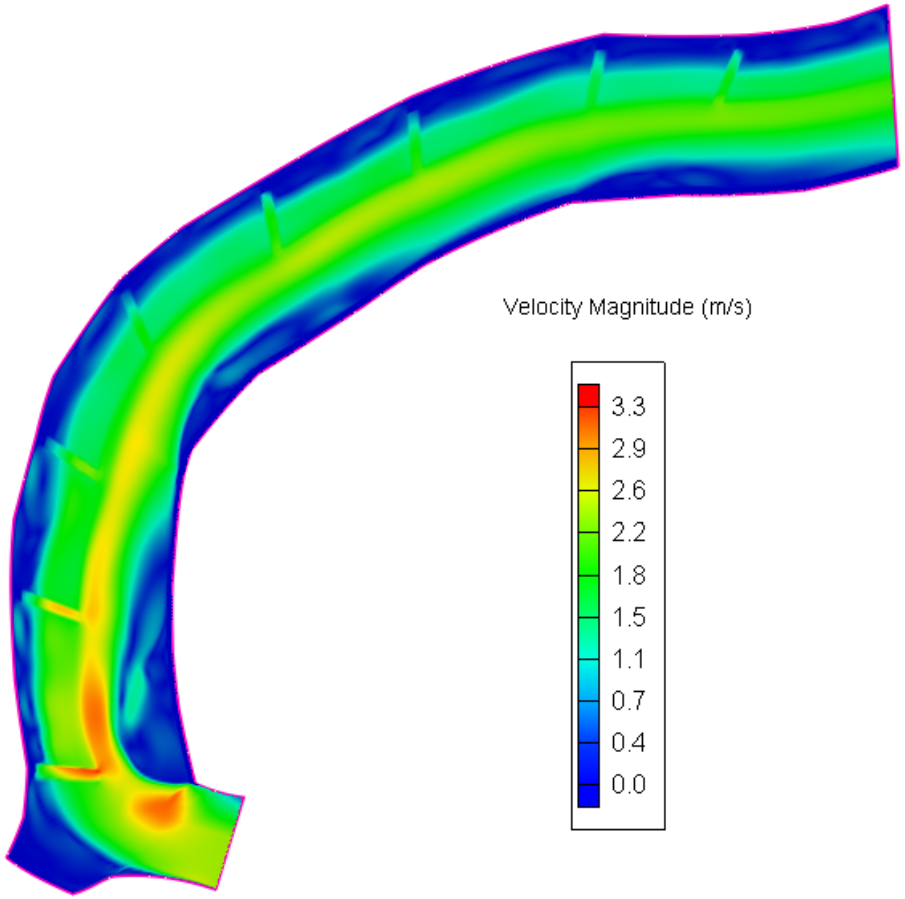


As built

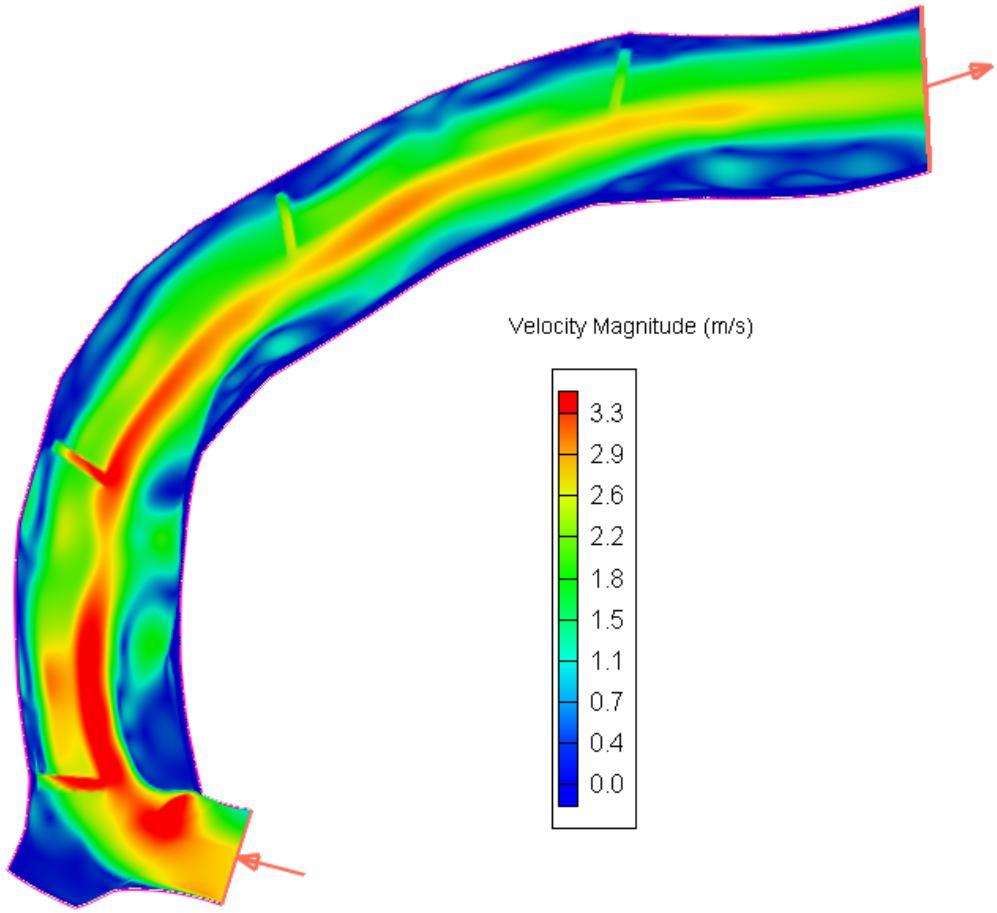


4 Barbs

# Total Specific Discharge (m^2/s)

## Discharge: 300 m^3/s, Initial Water Height: 3.3 m

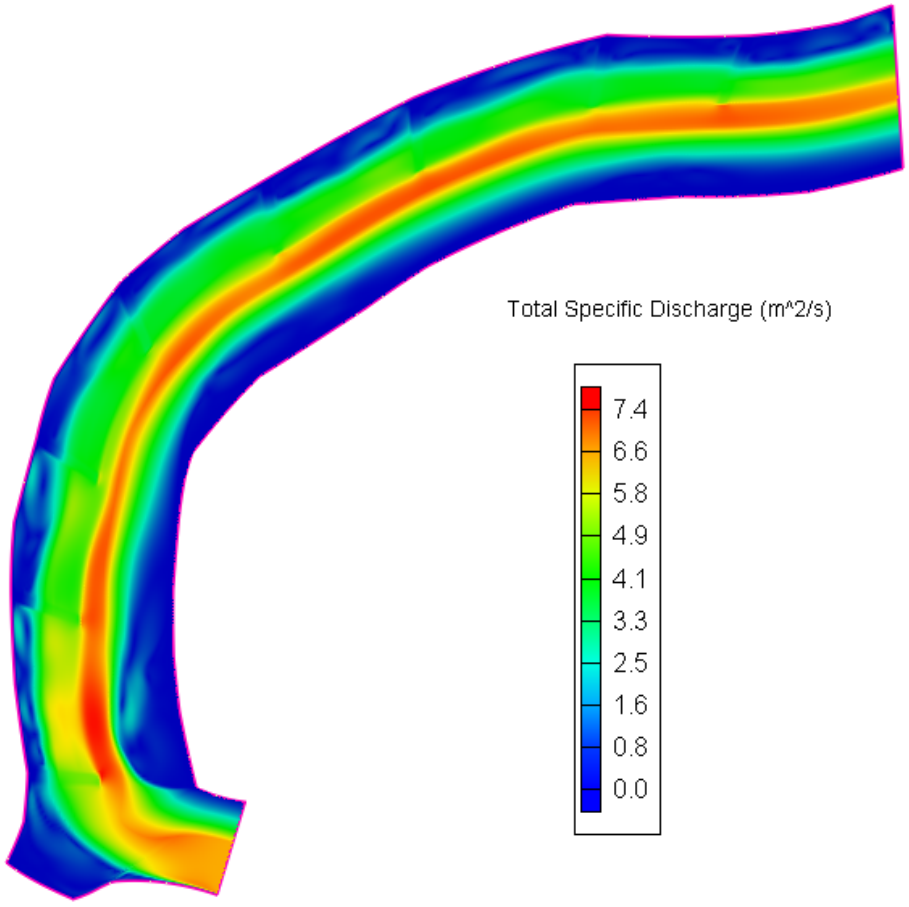


As built

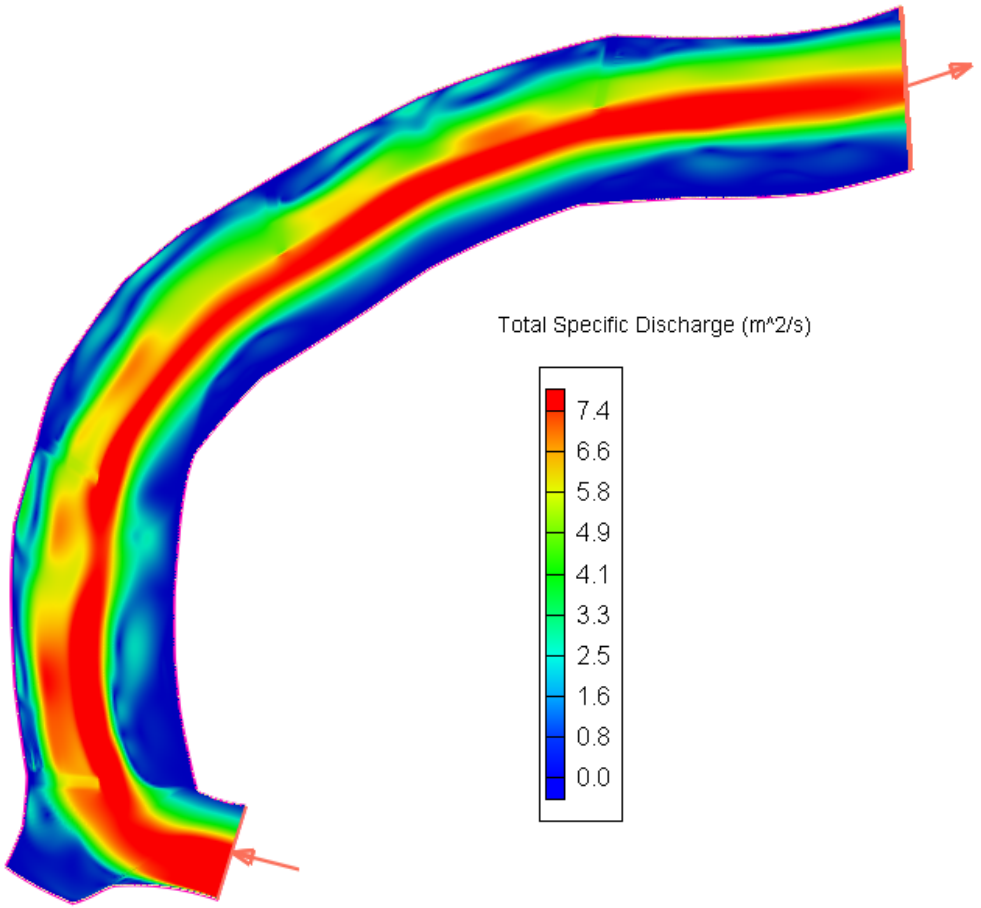


4 Barbs

# Froude Number
## Discharge: 300 m^3/s, Initial Water Height: 3.3 m

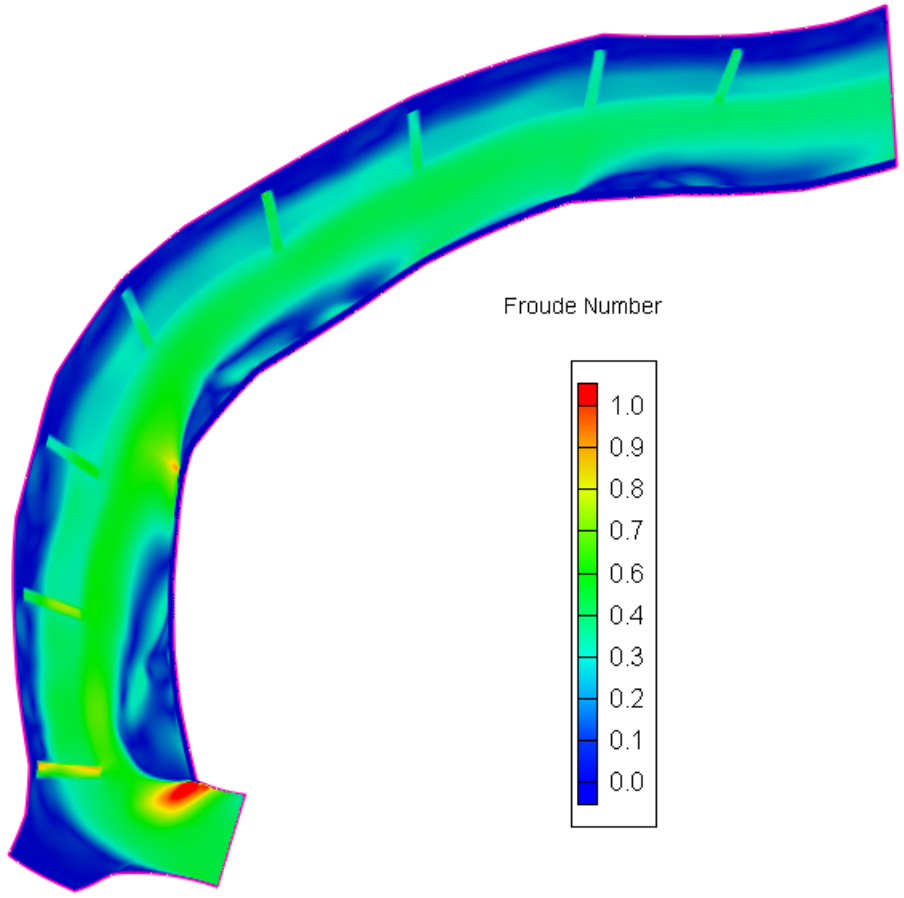


As built

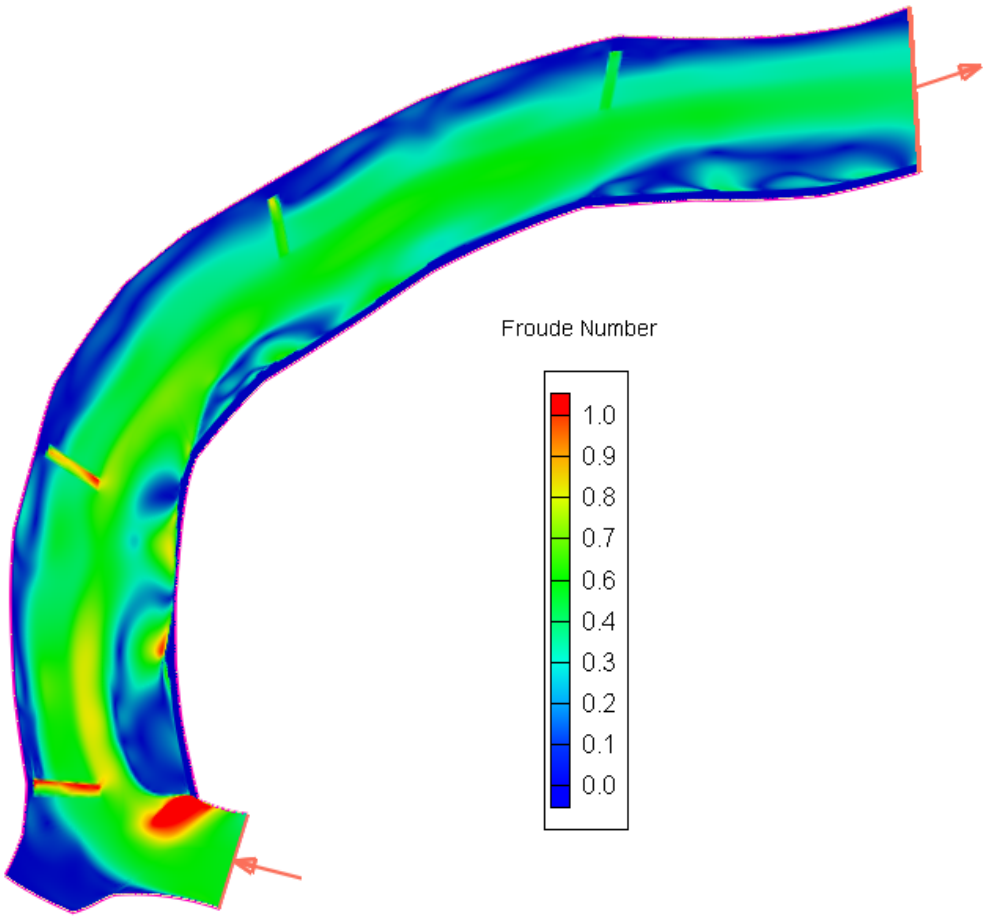


4 Barbs

# Total Shear Stress (N/m^2)
# Discharge: 300 m^3/s, Initial Water Height: 3.3 m

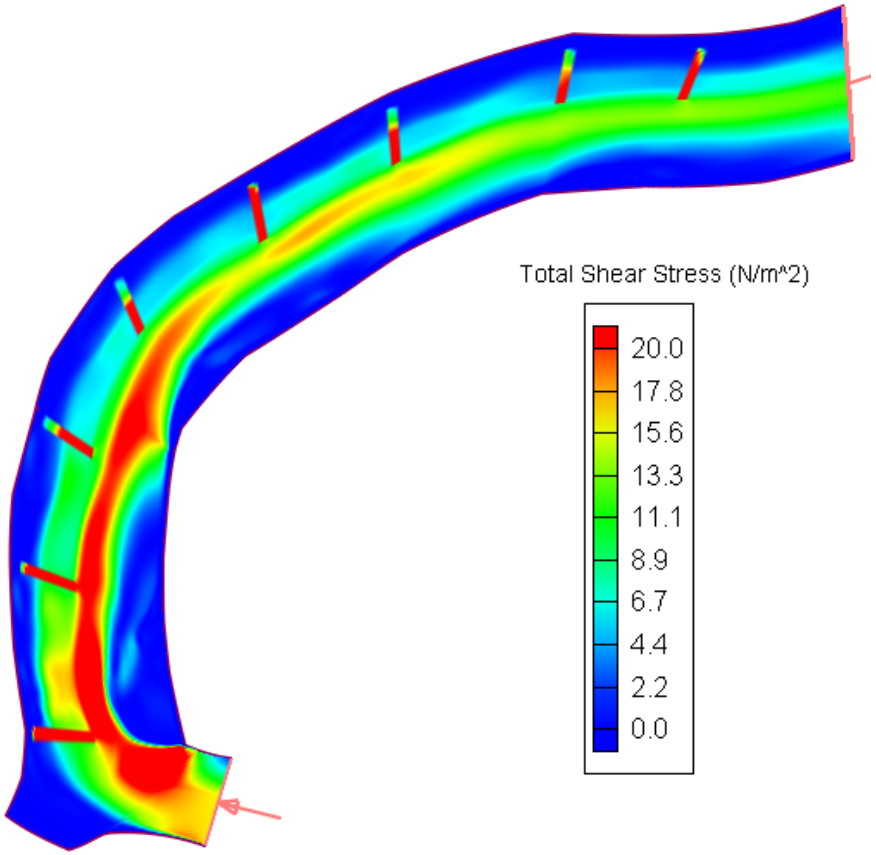


As built

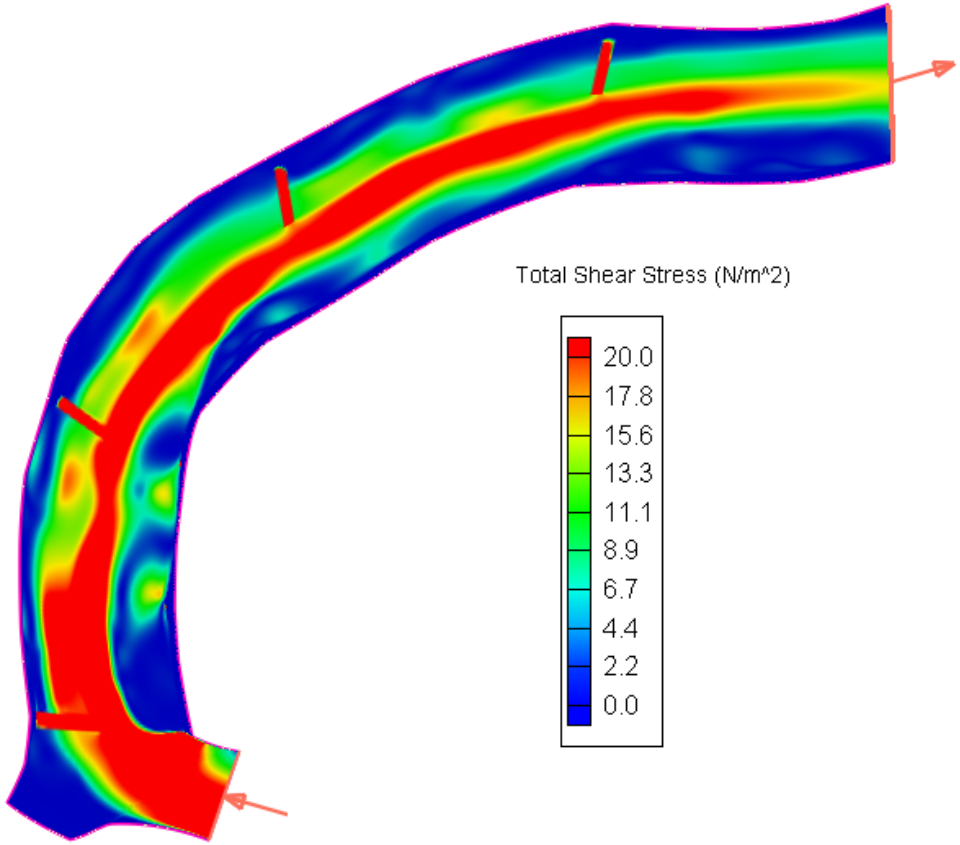


4 Barbs

Bed sediment transport is initiated
when Total Shear Stress > 19 N/m^2

# 5 Barbs - No 4th, 6th, & 8th Barbs

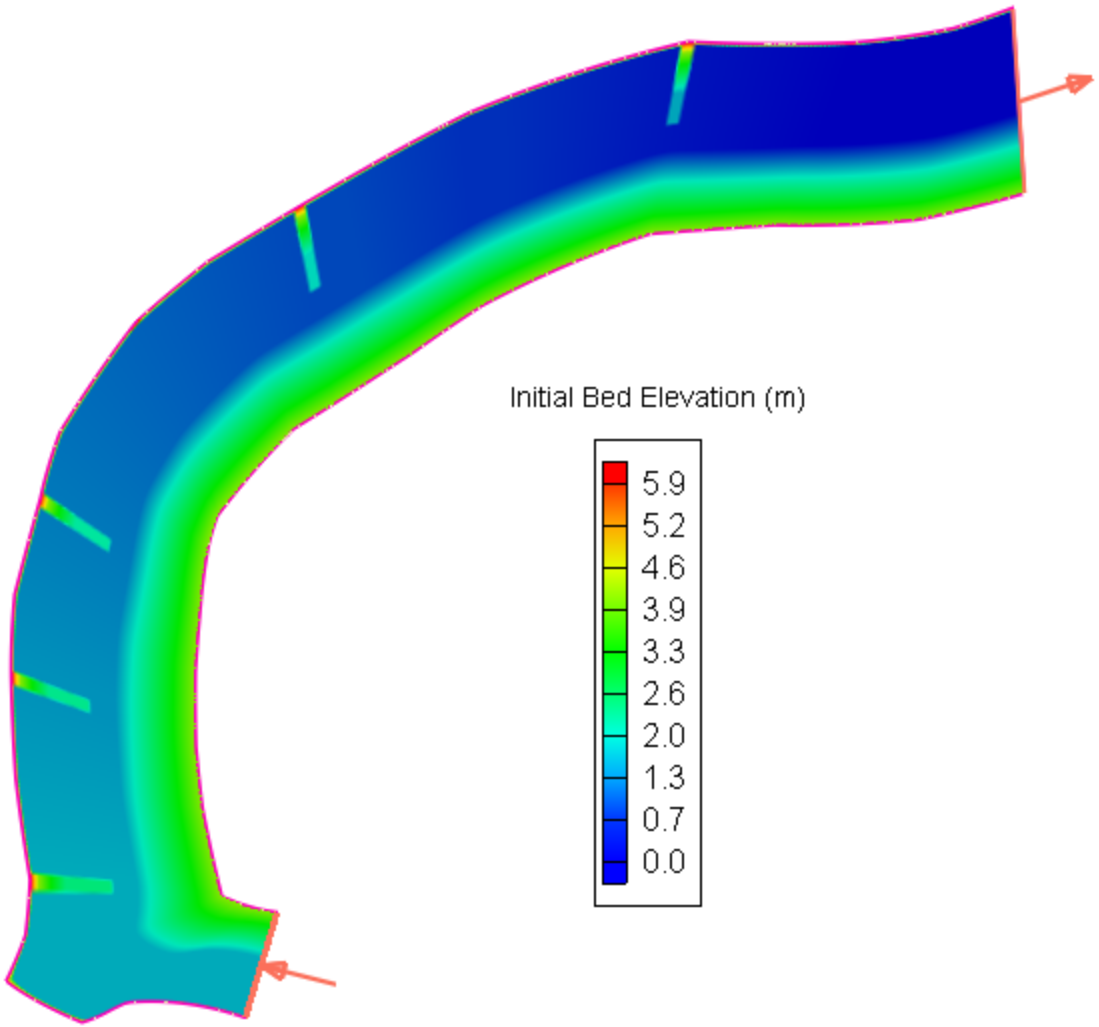

# Velocity Magnitude (m/s)

## Discharge: 300 m^3/s, Initial Water Height: 3.3 m

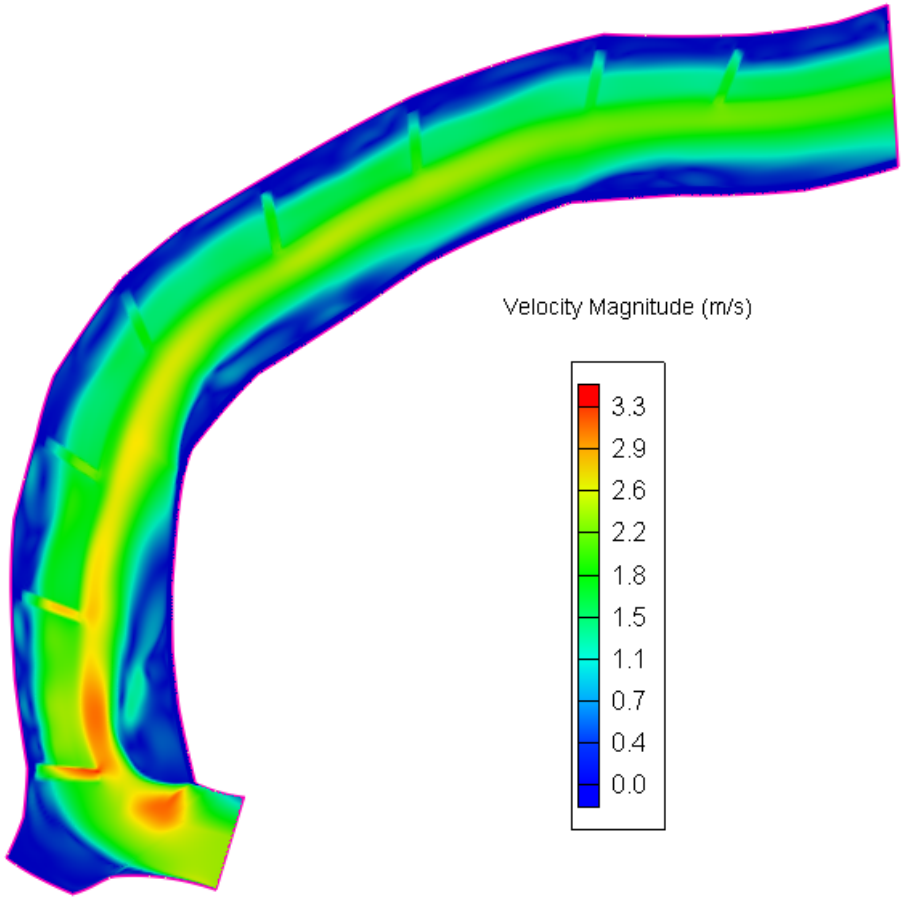


As built

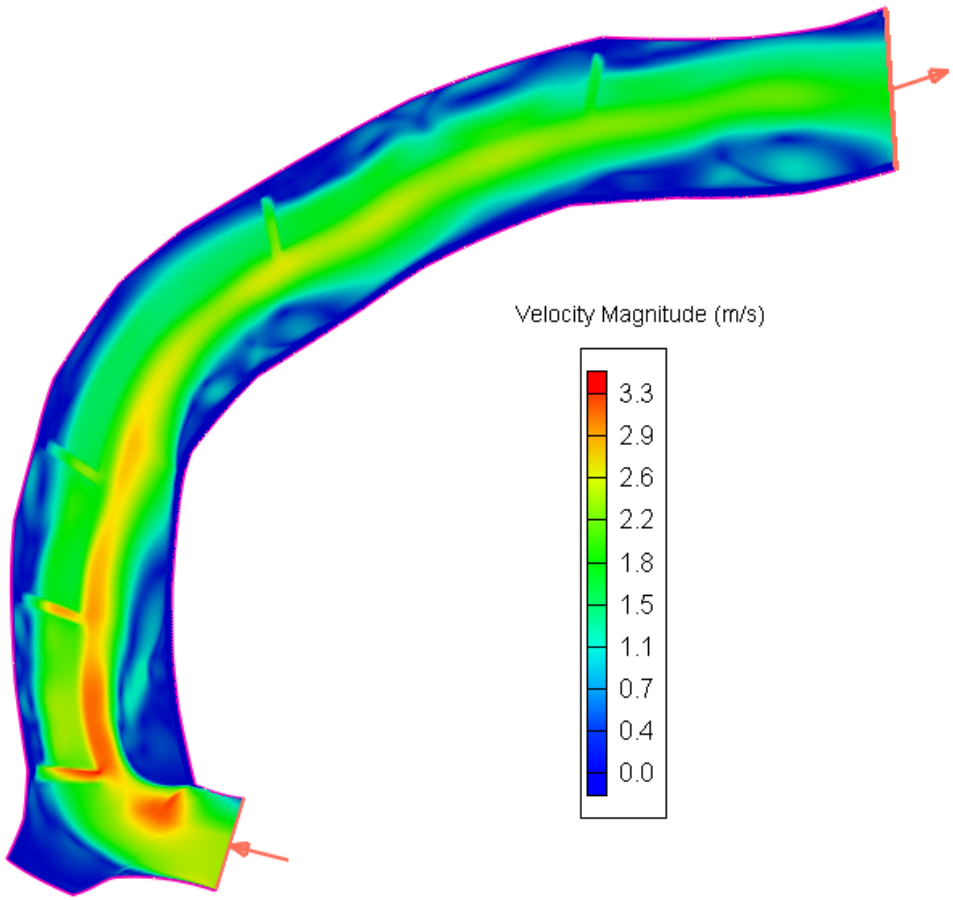


5 Barbs

# Total Specific Discharge (m^2/s)

## Discharge: 300 m^3/s, Initial Water Height: 3.3 m

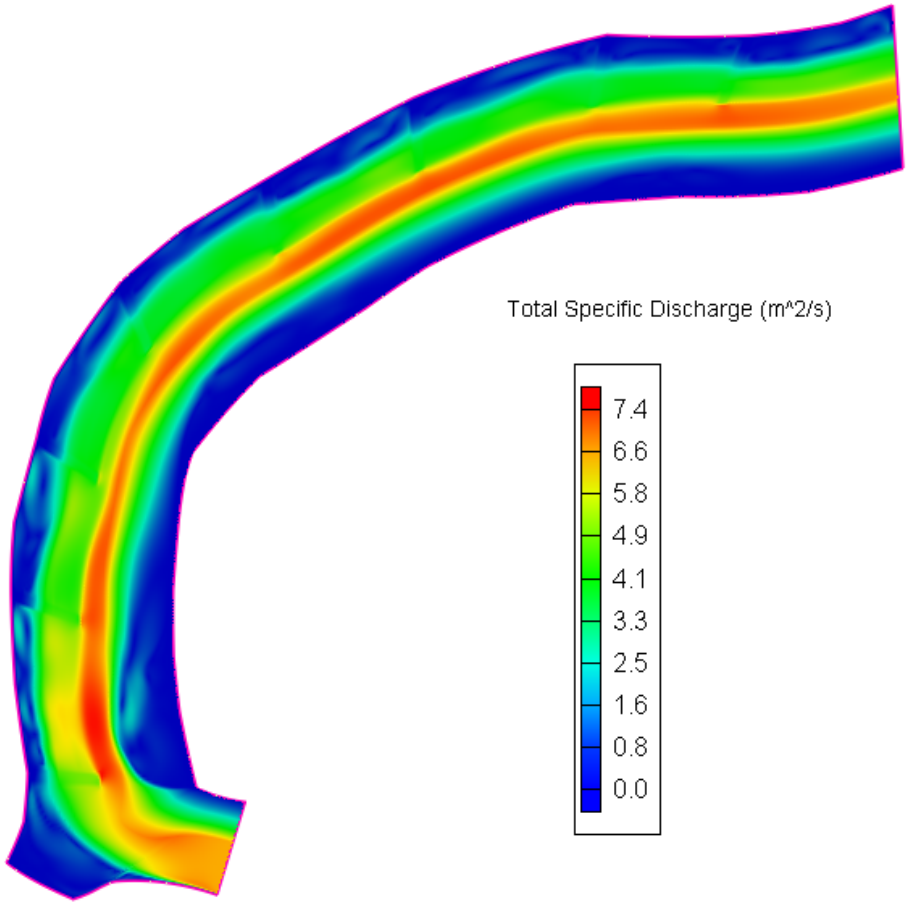


As built

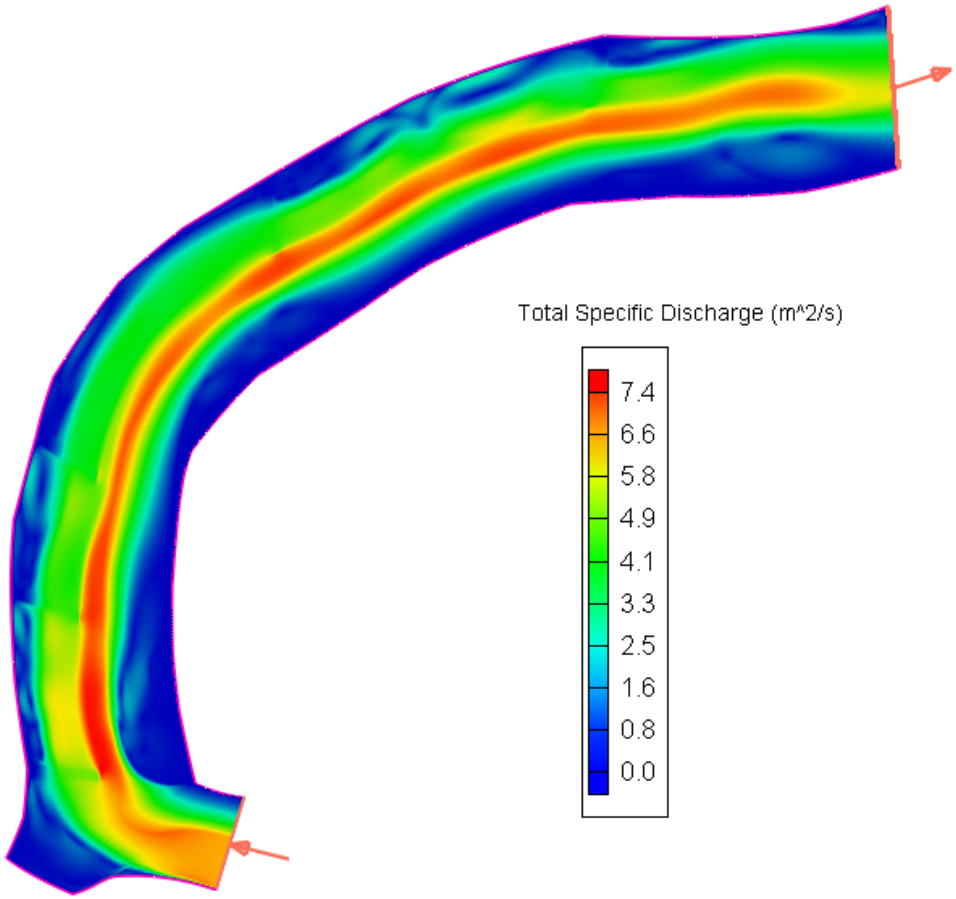


5 Barbs

# Froude Number
## Discharge: 300 m^3/s, Initial Water Height: 3.3 m

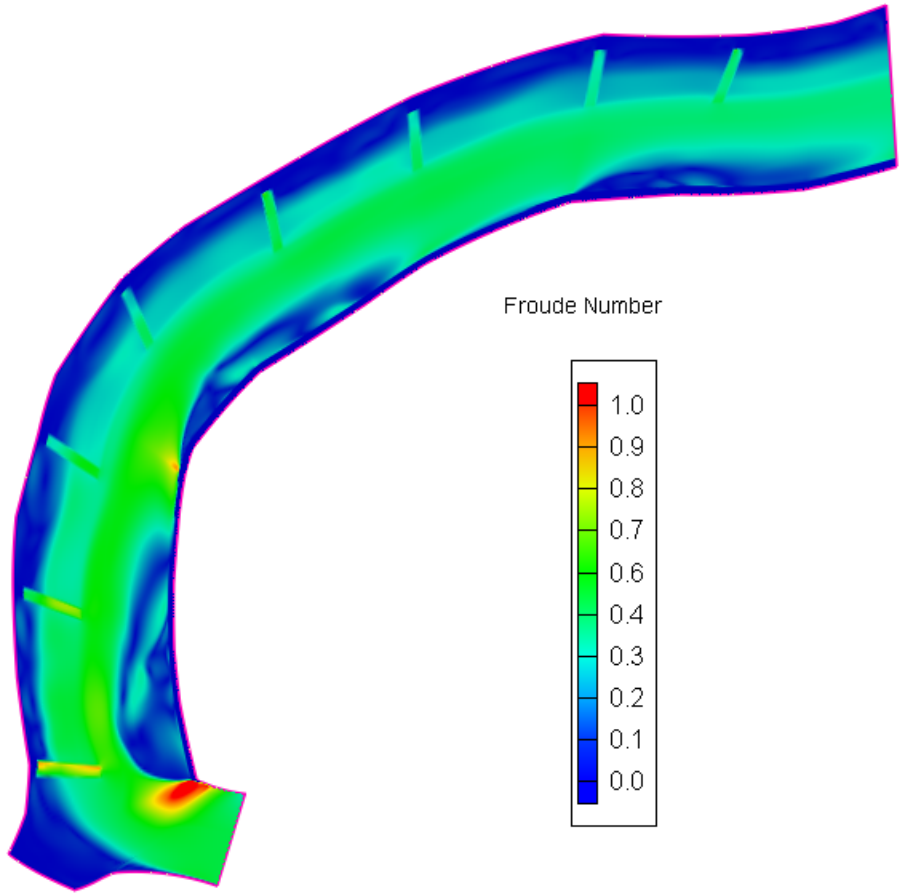


As built

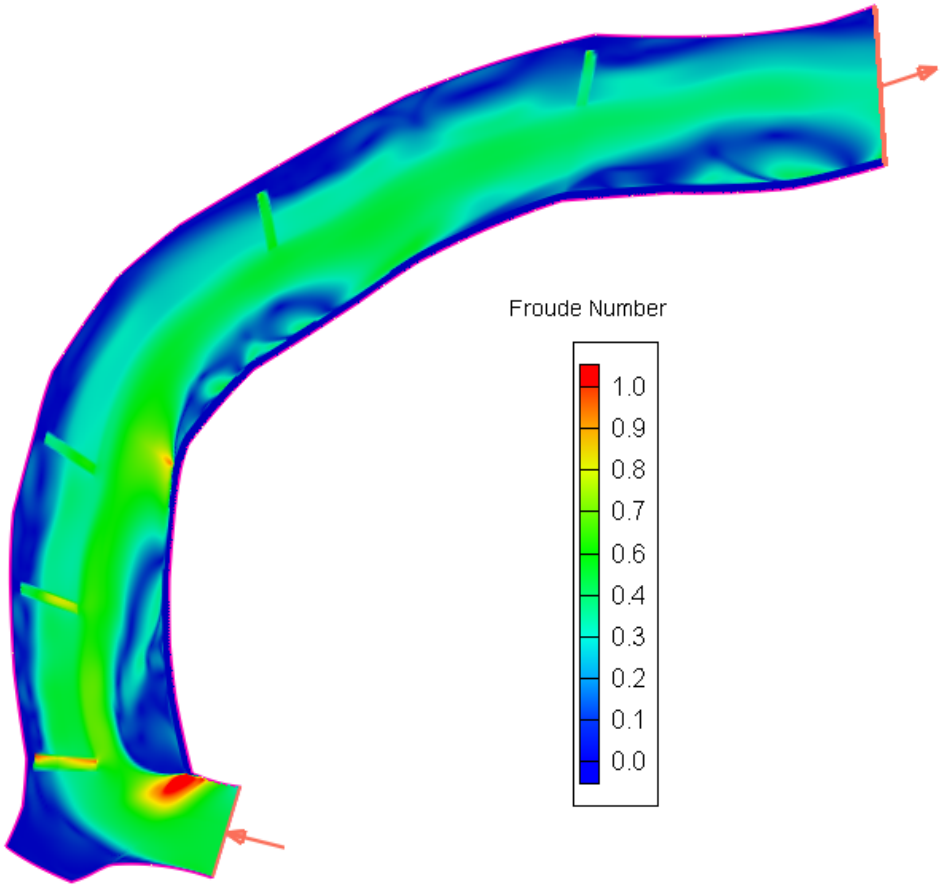


5 Barbs

# Total Shear Stress (N/m^2)
# Discharge: 300 m^3/s, Initial Water Height: 3.3 m

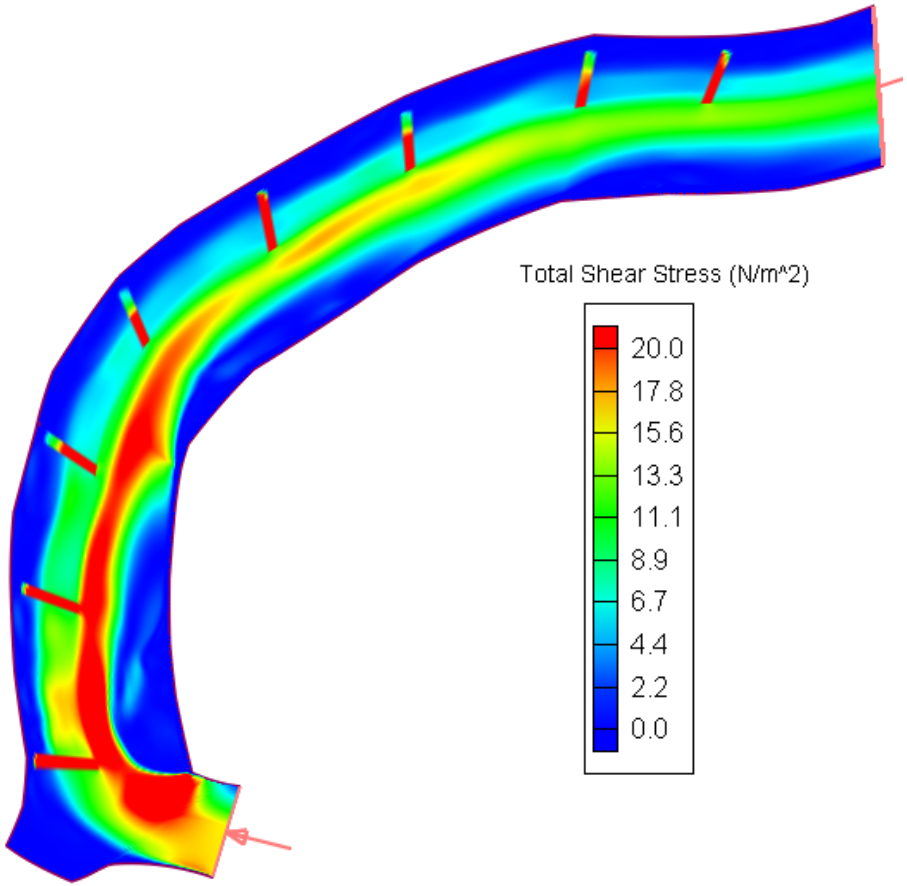


As built

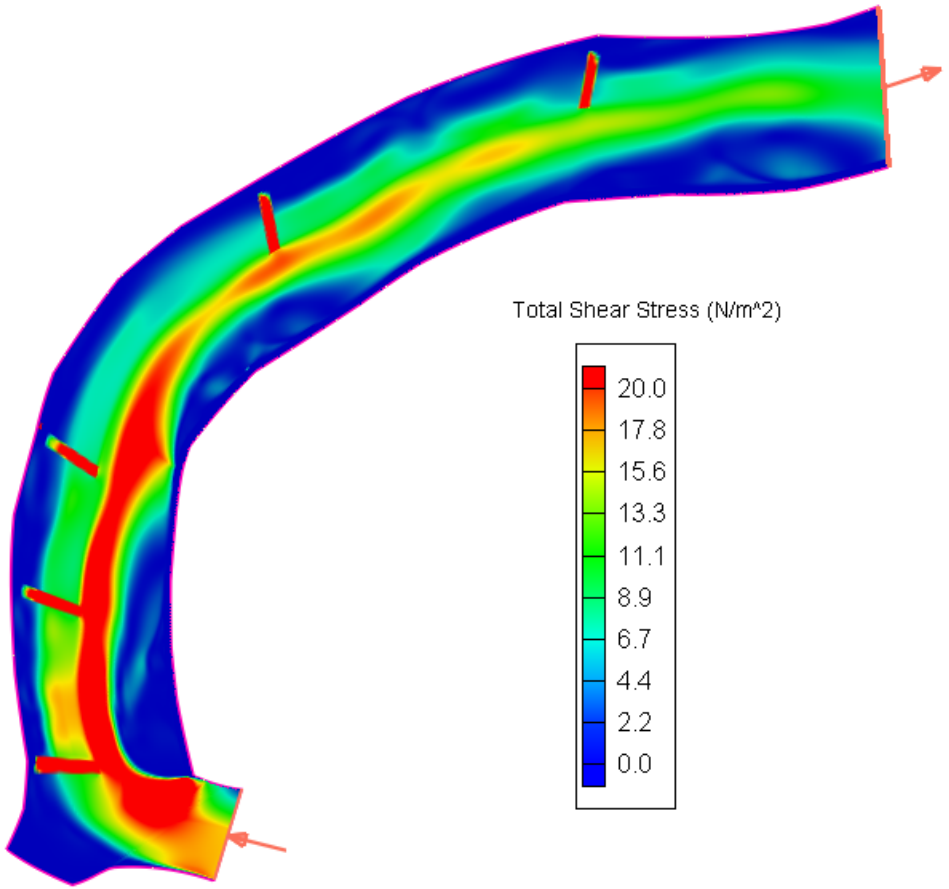


5 Barbs

Bed sediment transport is initiated
when Total Shear Stress > 19 N/m^2

# Study to Compare the Performance of Two Designs to Prevent River Bend Erosion in Arctic Environments

Hess Creek
2006 and 2009 simulations

# Initial Bed Elevation (m)

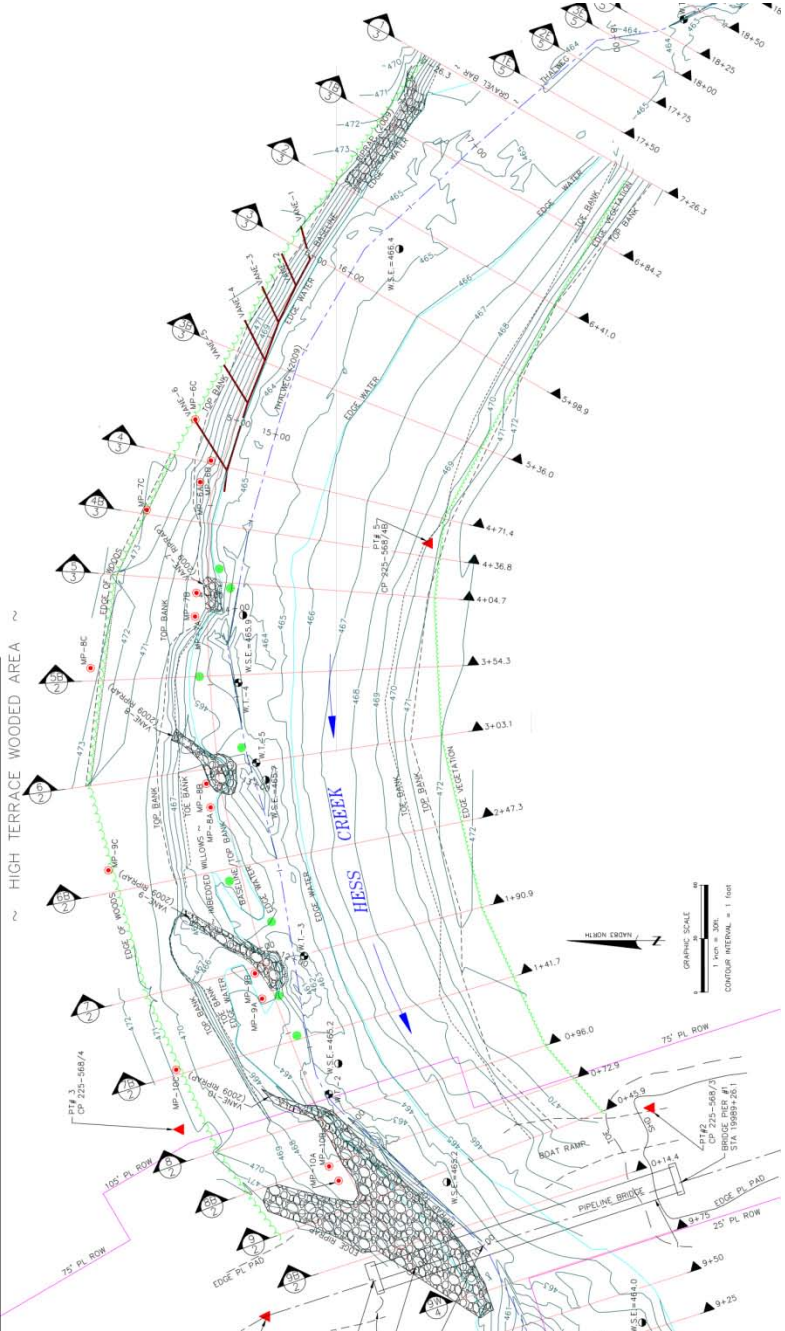


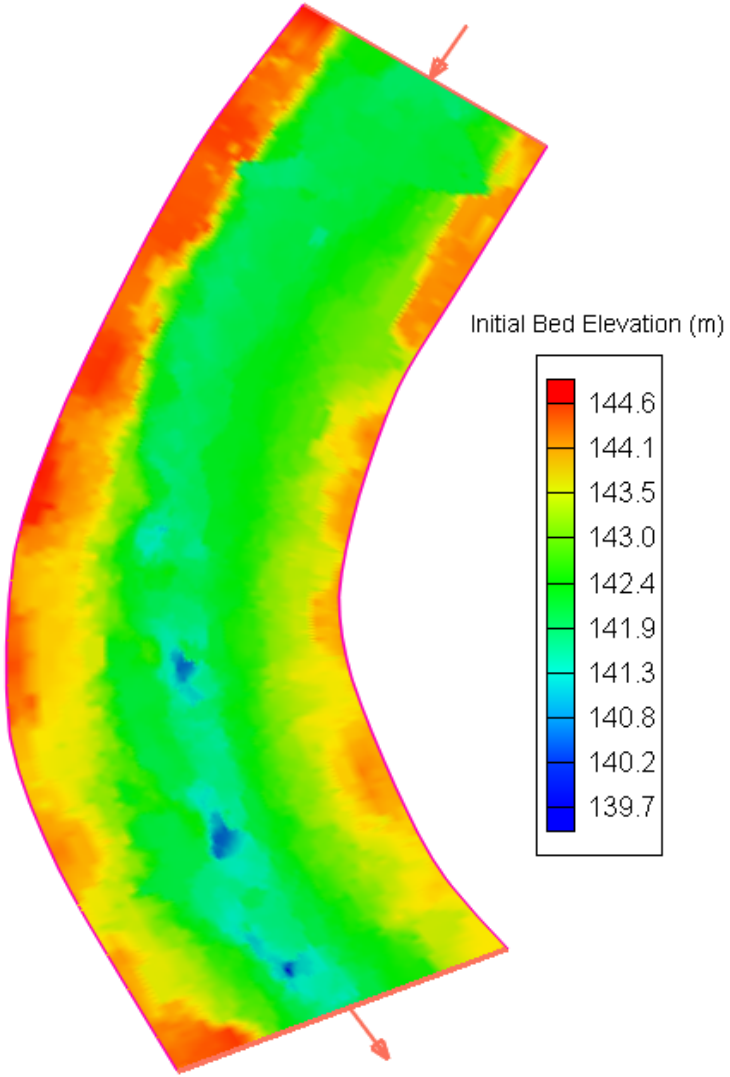


2009

# Initial Bed Elevation (m)

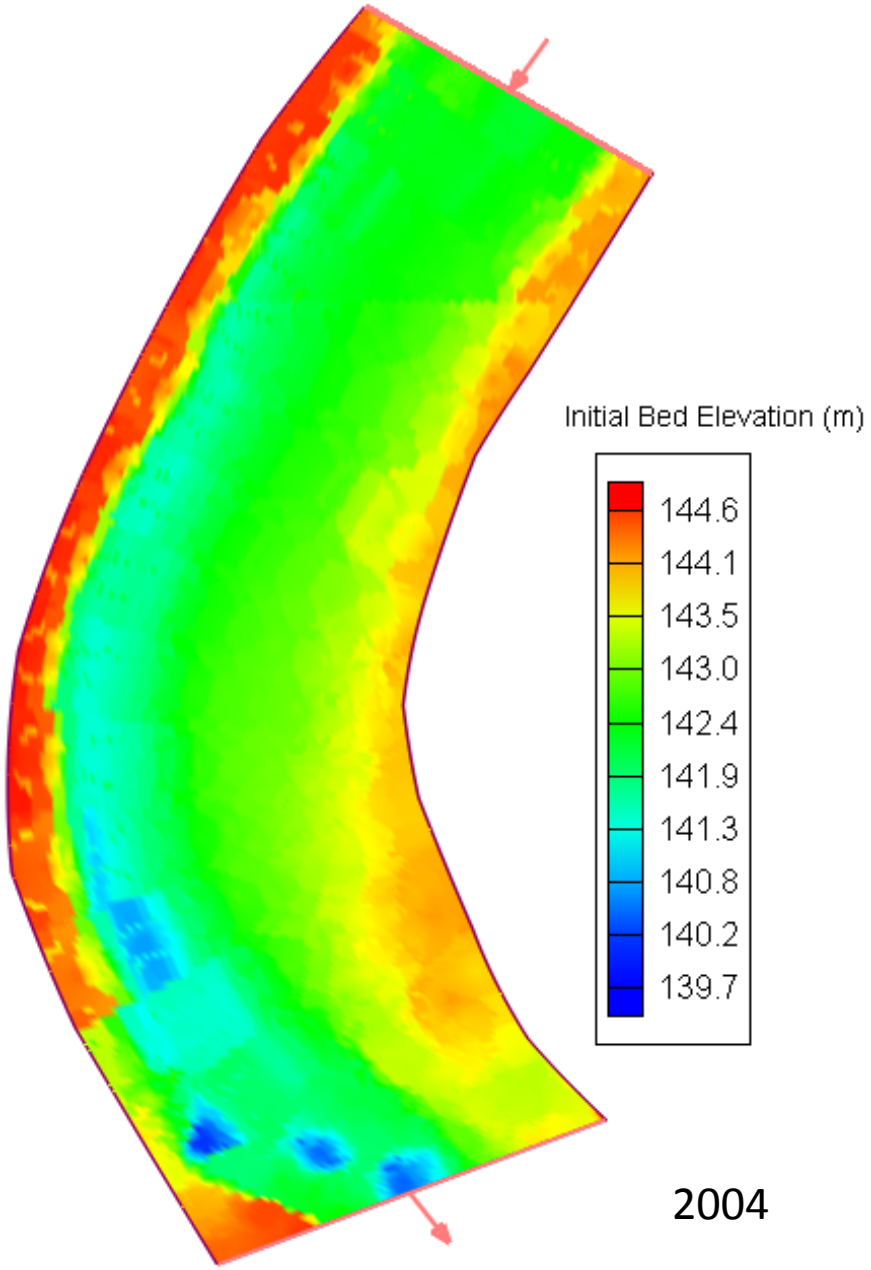


2004

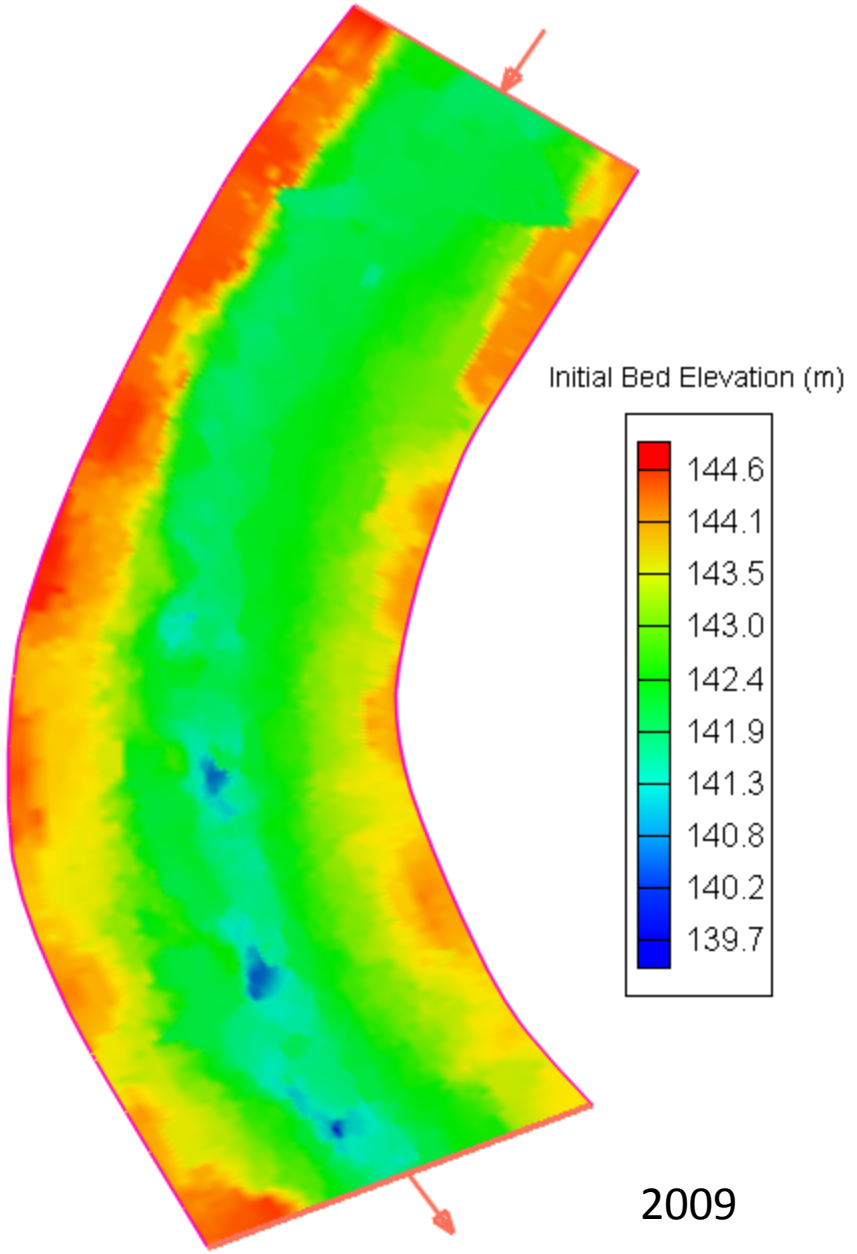


2009

# Water Depth (m)

Discharge: 95.57 m^3/s (3,375 cfs), Initial Water Height: 142.9 m (468.8 ft NAVD88)
(bankfull conditions)

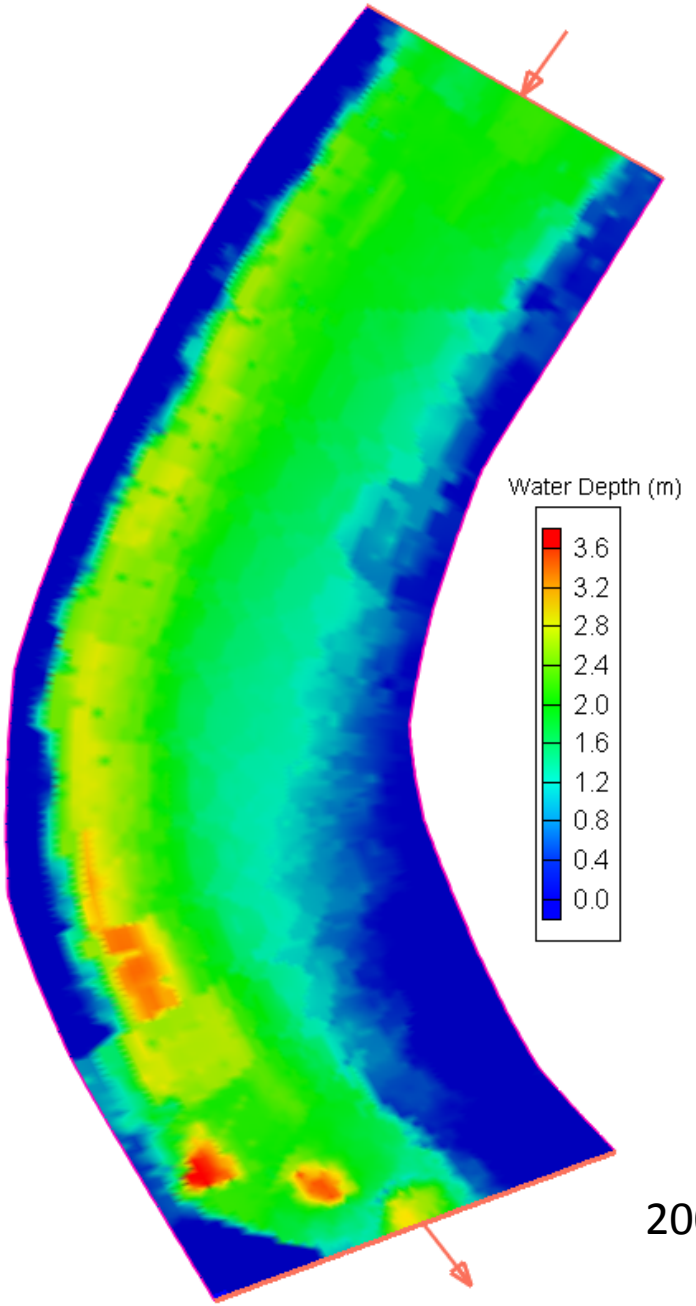


2004

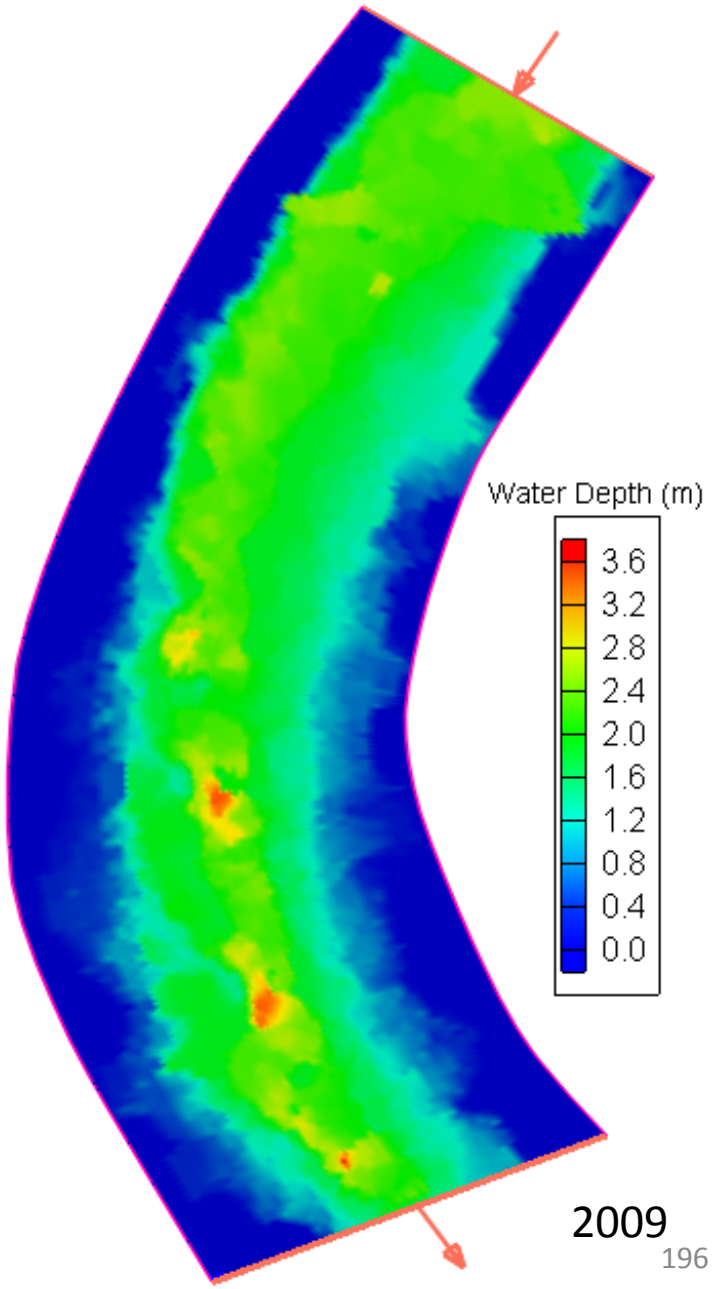


2009

# Velocity Magnitude (m/s)

Discharge: 95.57 m^3/s (3,375 cfs), Initial Water Height: 142.9 m (468.8 ft NAVD88)
(bankfull conditions)

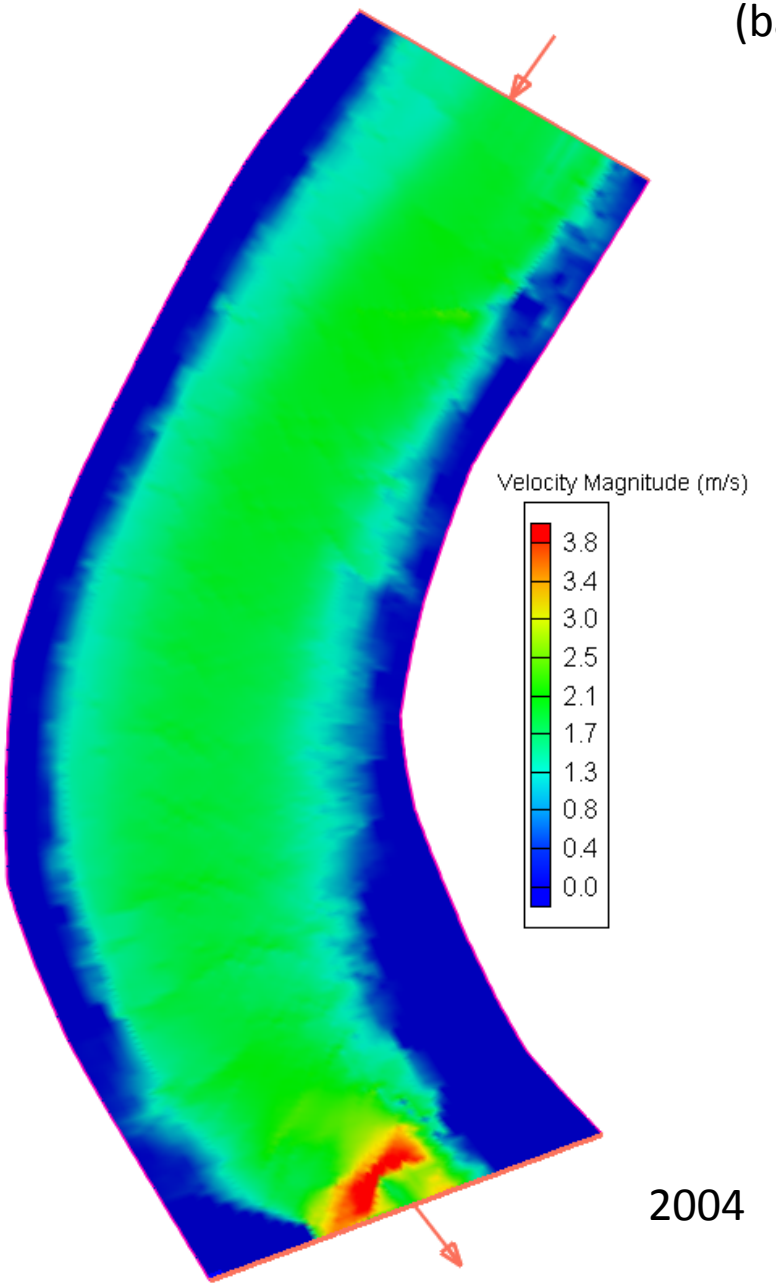


2004

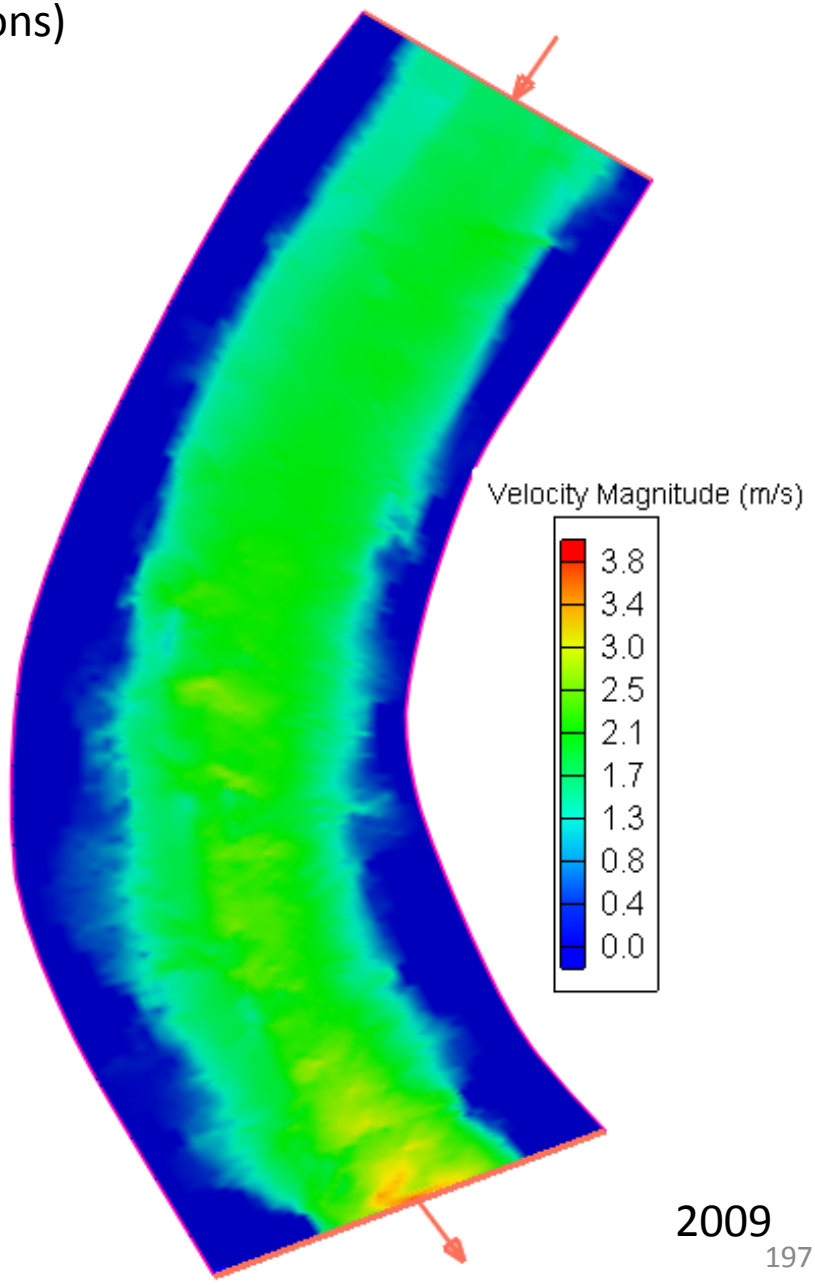


2009

# Specific Discharge (m^2/s)

Discharge: 95.57 m^3/s (3,375 cfs), Initial Water Height: 142.9 m (468.8 ft NAVD88)
(bankfull conditions)

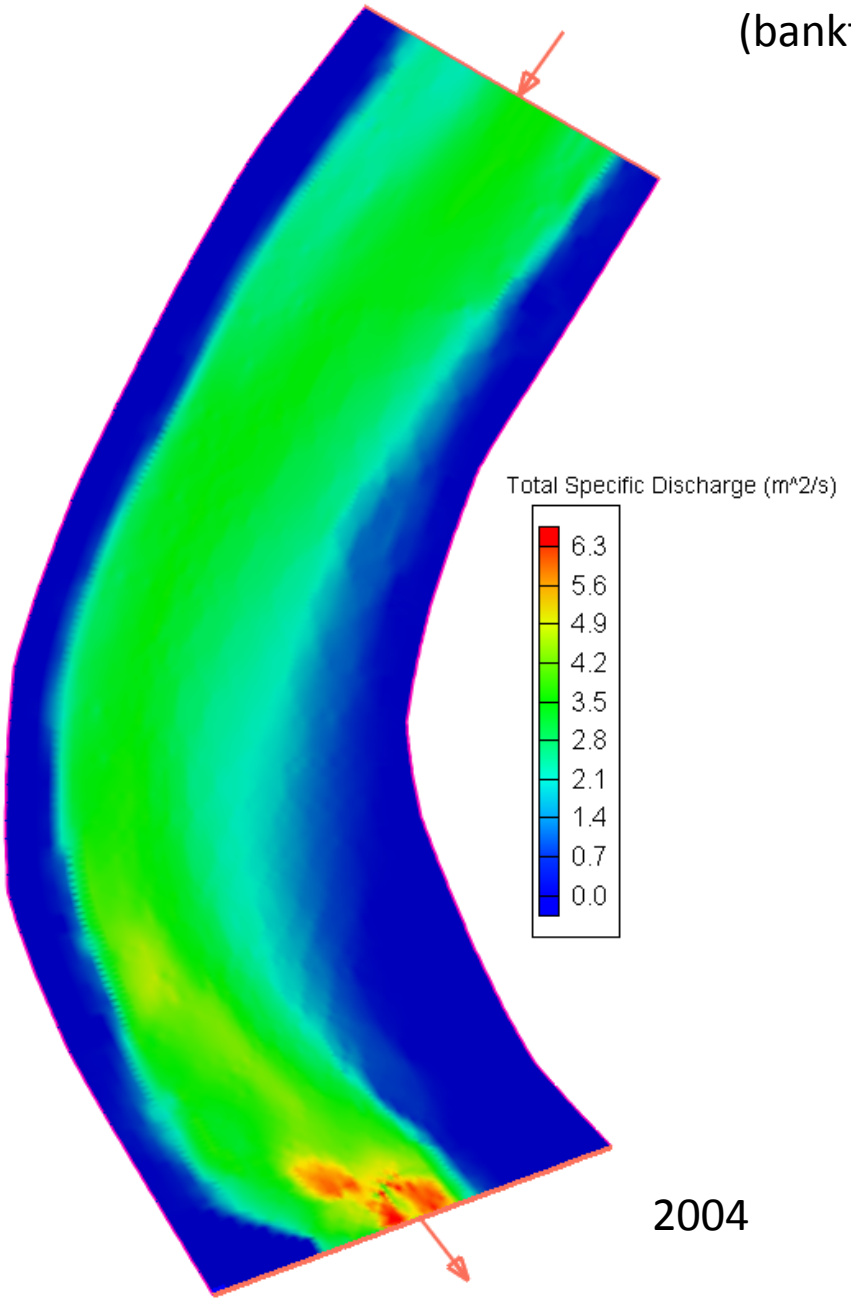


2004

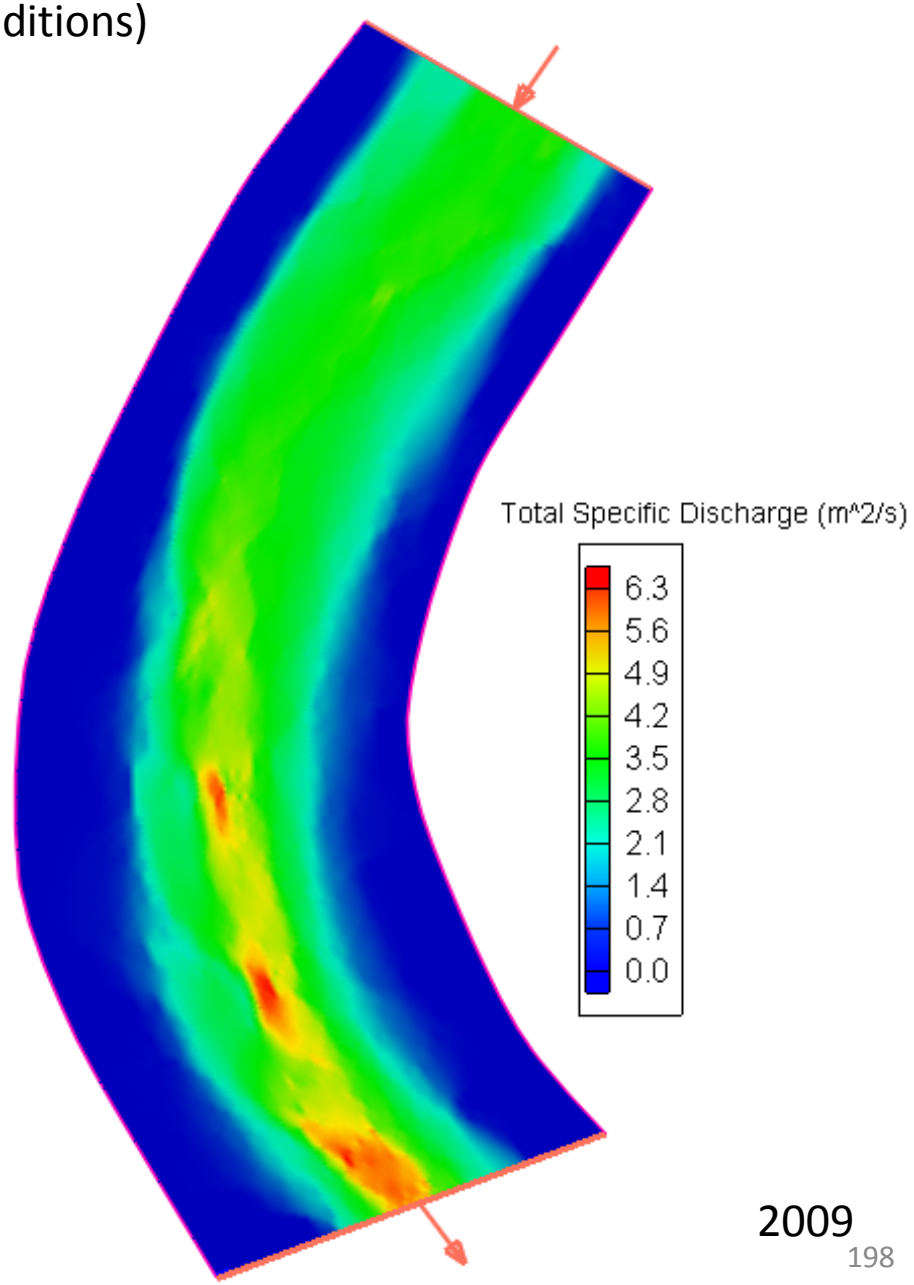


2009

# Total Shear Stress (N/m^2)

Discharge: 95.57 m^3/s (3,375 cfs), Initial Water Height: 142.9 m (468.8 ft NAVD88)
(bankfull conditions)

Bed sediment transport is
initiated when
Total Shear Stress >= 33 N/m^2

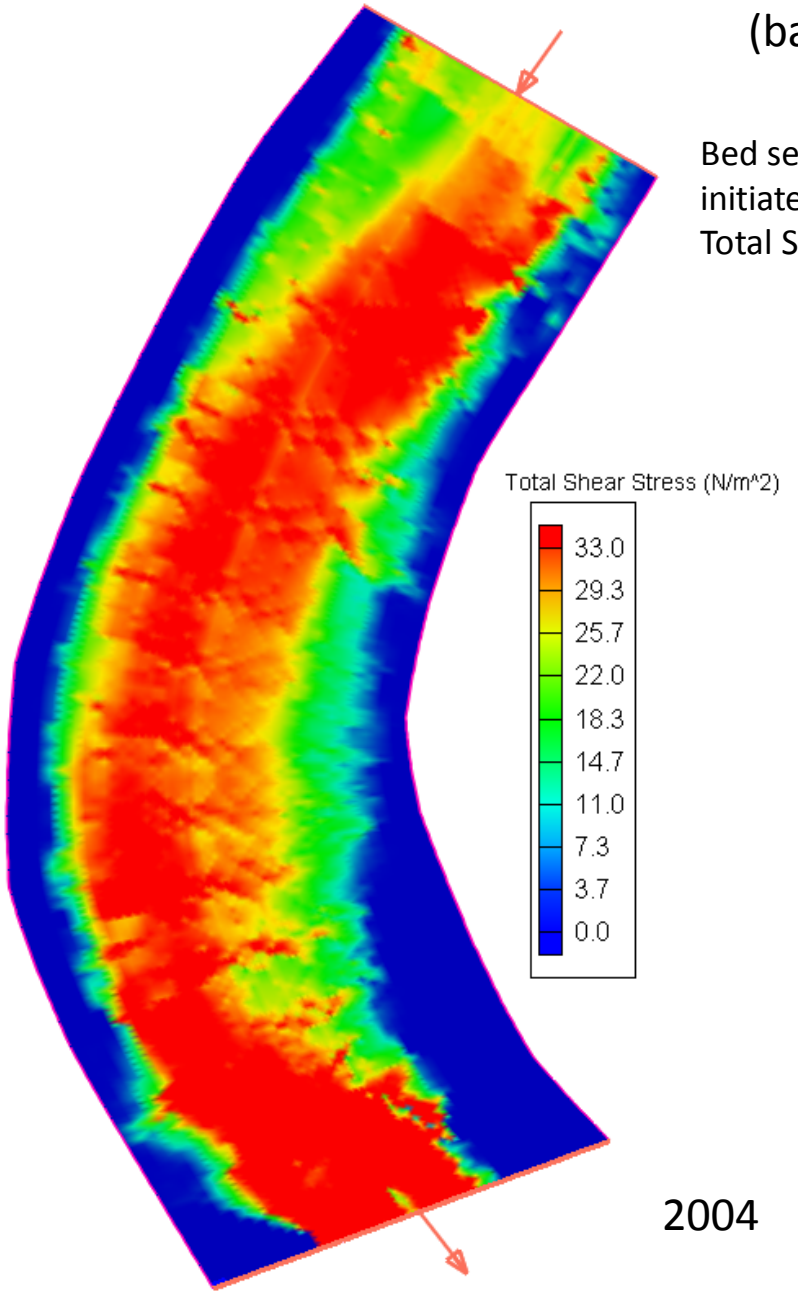


2004

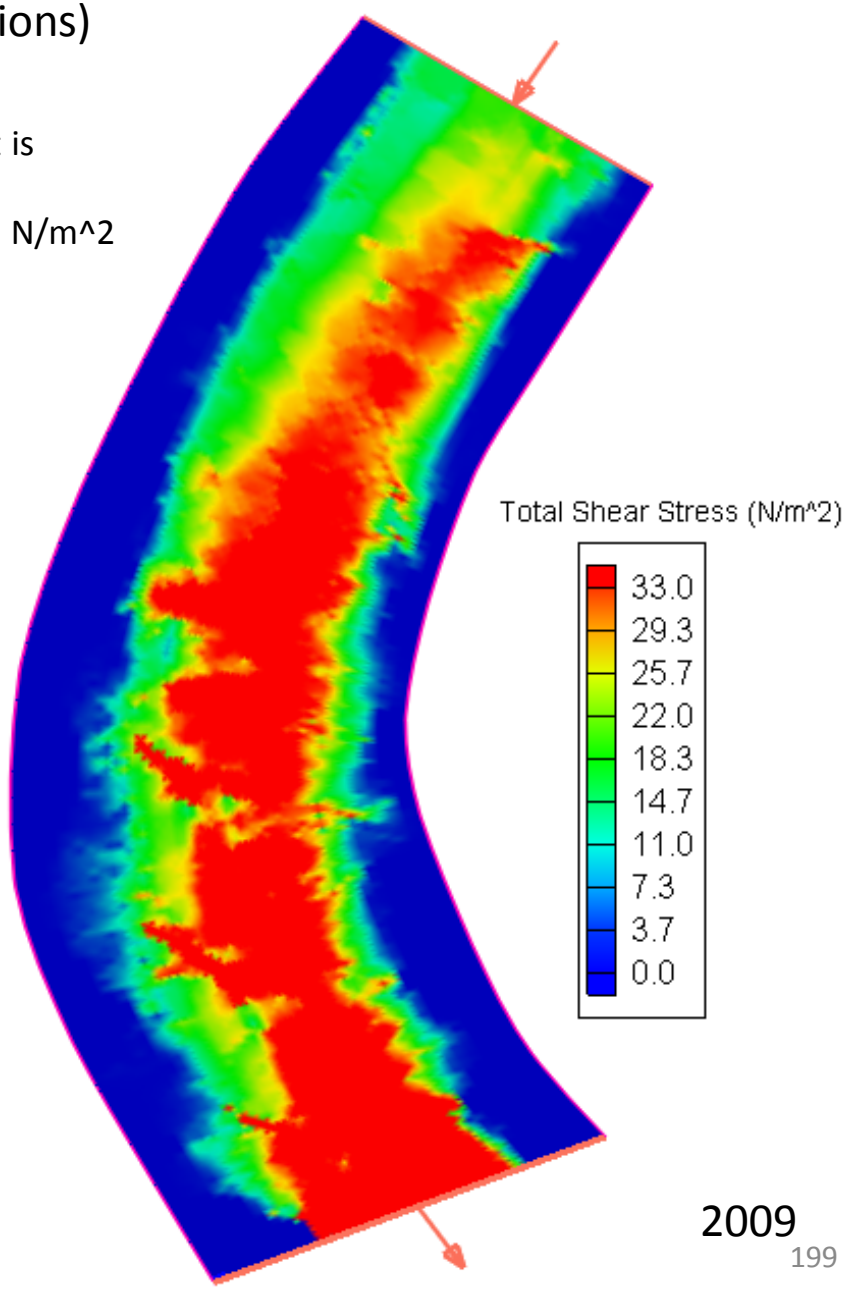


2009

# Total Shear Stress (N/m^2)

Discharge: 95.57 m^3/s (3,375 cfs), Initial Water Height: 142.9 m (468.8 ft NAVD88)
(bankfull conditions)

Vanes erosion is initiated when
Total Shear Stress >= 232 N/m^2

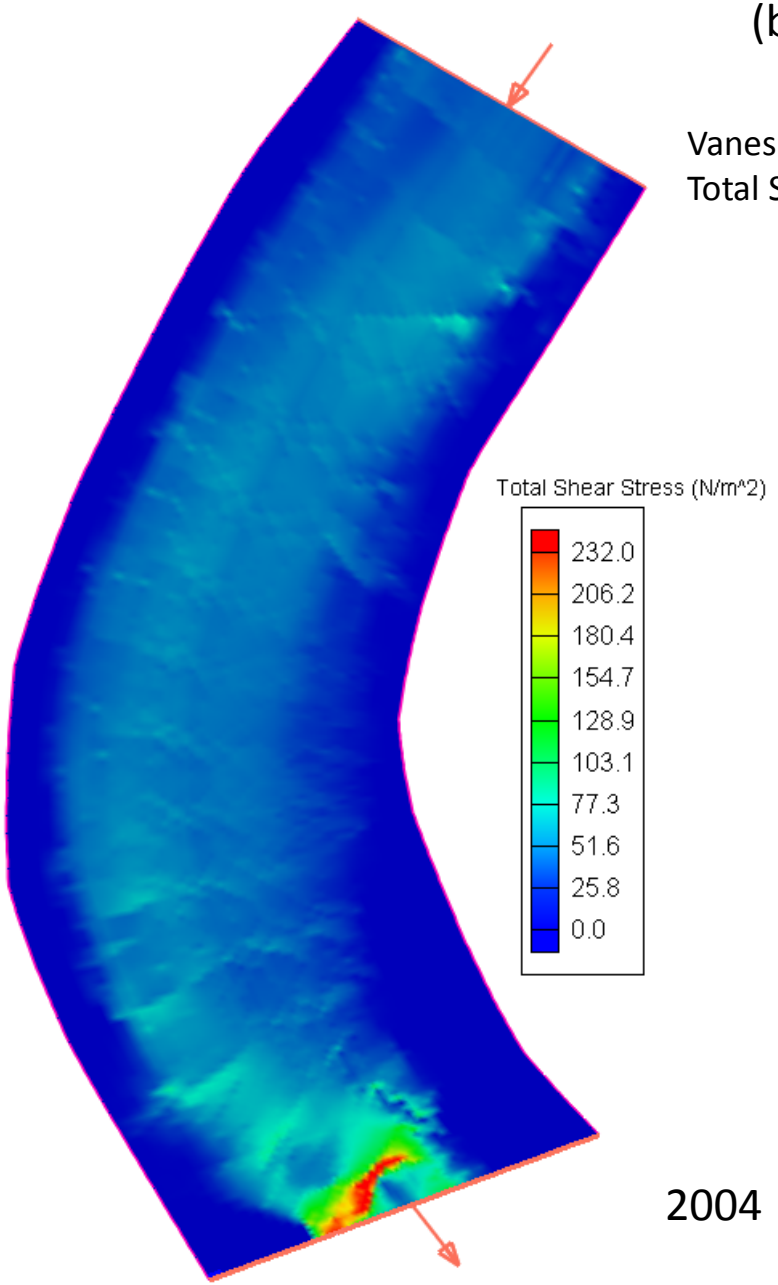


2004

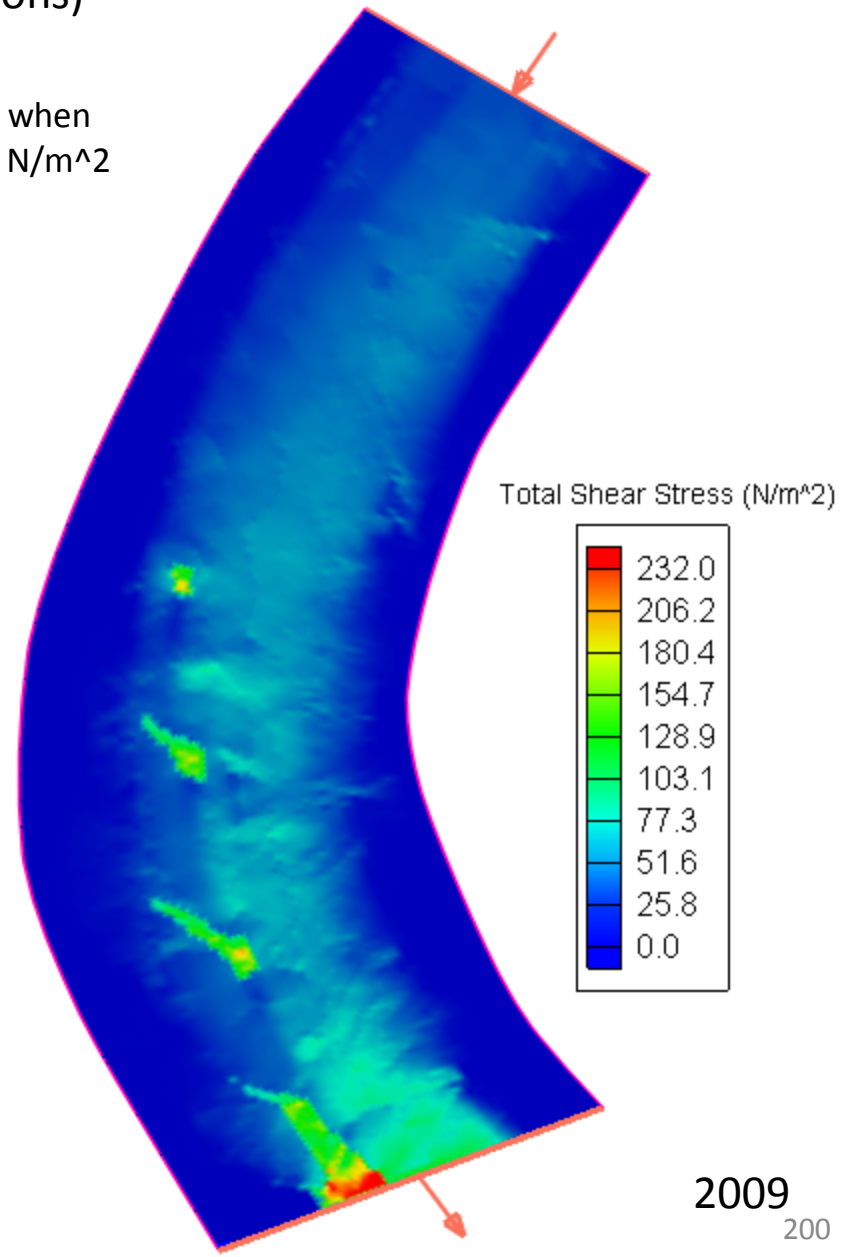


2009